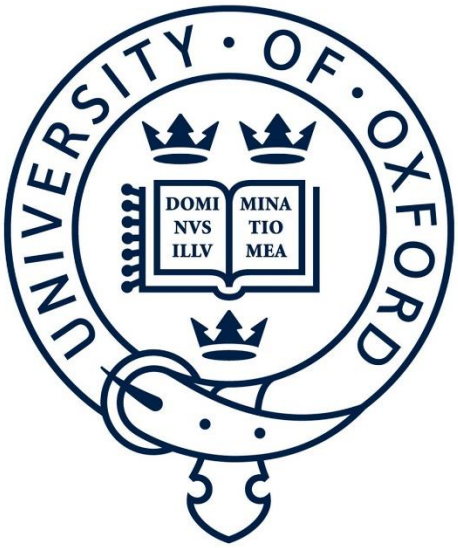
Approaches to Developing Novel Bioengineered Skin Substitutes



Xuxin Lim

February 2019

St Edmund Hall

This thesis is submitted for the degree of Doctor of Philosophy

at the University of Oxford

Contents

Abstract iv
Acknowledgements v
Abbreviations vi
List of Figures x
List of Tables xv
Publications, Presentations and Patents xvi
Chapter 1 Introduction 1
1.1. Background 1
1.2. Aims and Objectives 9
1.3. Scope of Thesis 11
Chapter 2 Literature Review 14
2.1. Systematic Review of Skin Substitutes for Acute and Chronic Wounds 14
2.1.1. Skin Substitutes for Burns 14
2.1.2. Skin Substitutes for Diabetic Ulcers 36
2.2. Rheological and Interfacial Chemistry of Emulsions: Key Concepts 64
2.2.1. Emulsions 64
2.2.2. Interfacial Chemistry of Emulsions 66
2.2.3. Surface Rheology of Emulsion 68
2.2.4. The Role of Surfactants for Emulsion Stability 69
2.2.5. Protein Surfactant Interaction – The Adsorption Problem 70
2.2.6. Forces of Interaction between Emulsion Droplets 72
2.2.7. Emulsion-Templating and PolyHIPEs 73
2.3. Principles of Lyophilization 75
2.4. Summary 76
Chapter 3 Formulation of an Emulsion-Templated Scaffold 77
3.1. Characterization of a Biocompatible Emulsion System 77
3.1.1. Introduction 77
3.1.2. Materials and Methods 79
3.1.3. Results 85
3.1.4. Discussion 98
3.1.5. Summary 103
3.2. Optimization of EmDerm Fabrication: Key Parameters 103
3.2.1. Introduction 103
3.2.2. Materials and Methods 105

3.2.3. Results 110
3.2.4. Discussion 125
3.2.5. Summary 129
Chapter 4 Biocompatibility of Emulsion-templated Bio-intelligent Scaffolds 130
4.1. Introduction 130
4.2. Materials and Methods 132
4.3. Results and Discussion 139
4.3.1. Cell Proliferation on EmDerm Scaffolds 139
4.3.2. Co-culture of Cells on EmDerm Scaffolds 145
4.3.3. Analysis of Proteome and Secretome of Cellularized EmDerm Scaffolds 161
4.4. Summary 181
Chapter 5 In Vivo Assessment of Emulsion Templated Scaffolds 182
5.1. Introduction 182
5.2. Materials and Methods 183
5.3. Results 189
5.4. Discussion 199
5.5. Summary 203
Chapter 6 Electrospun Membranes as Epidermal Skin Substitute 204
6.1. Introduction 204
6.2. Materials and Methods 206
6.3. Results 211
6.4. Discussion 217
6.5. Summary 220
Chapter 7 Conclusion and Future Work 221
7.1. Conclusions 221
7.2. Future Work 223
7.3. Contributions to the Field 227
References 229

Approaches to Developing Novel Bioengineered Skin Substitutes

Xuxin Lim, St Edmund Hall, Hilary Term 2019

Submitted for the degree of Doctor of Philosophy

Abstract

In this body of work, a new method of creating a tunable porous scaffold - emulsion templating - to reconstitute the dermal layer of skin was explored. This method has traditionally been used to create polymeric high internal phase emulsions (polyHIPEs). The challenge of using emulsions for templating protein hydrogel networks is the preservation of native protein conformation in an emulsion system.

In this instance, a non-ionic surfactant blend was used to create a metastable biocompatible emulsion system for templating collagen, collagen-fibrin and fibrin polymeric hydrogels. This method of manufacture has the added advantage of ease of control of pore size and formation of nanofibrous filaments within the scaffold itself. Parameters for control of pore size such as hydrophile-lipophile balance (HLB) values of surfactant mixes, surfactant concentration, excipient concentration, temperature and mixing rate were explored.

Protein-surfactant interaction was investigated using confocal fluorescence microscopy, tryptophan fluorescence, Fourier Transform Infrared Spectroscopy (FTIR), circular dichroism and enzymatic assays. Using Fluorescein Isothiocyanate Conjugate Bovine Serum Albumin (FITC-BSA) as a model protein, it was demonstrated that non-ionic surfactants competitively adsorbed at interfaces, allowing FITC-BSA to remain in the aqueous phase and retaining its native conformation. Using a decane emulsion system, a biocompatible emulsion system was formulated, and emulsion droplets were used to create a hierarchical microporous scaffold (EmDerm). The mechanical properties and degradation profile of EmDerm scaffolds were also characterized.

Three different cell types (human dermal fibroblasts, human dermal endothelial cells, mesenchymal stem cells) were seeded onto EmDerm scaffolds and cell proliferation was quantified as well as compared to commercial scaffolds Matriderm and Integra. The EmDerm scaffolds were shown to be highly biocompatible and comparable to commercial scaffolds. Co-cultures of various cell types were also performed to investigate the interaction of different cell types of the emulsion templated scaffolds.

The proteome and secretome for both monoculture and co-cultures were also extracted and characterized to investigate effect of EmDerm scaffolds on secretion of degradative enzymes, structural proteins and growth factors as an indicator for in vivo activity of such scaffolds. EmDerm scaffolds implanted in rat wound healing models demonstrated no systemic inflammatory response. However, there was mild to moderate localized inflammatory response at implantation site at Day 7. This was associated with increased vascularization of the wound site at Day 14.

Electrospinning of gelatin-polymer blends was also performed to create a pseudo-basement membrane as an epidermal carrier delivery system. The aim is to create an epidermal skin substitute to graft onto the neodermis when the EmDerm scaffolds have integrated into the wounds. Keratinocytes were shown to proliferate well on such membranes and the mechanical properties and degradation of the membranes were also characterized.

In conclusion, emulsion-templated scaffolds are biocompatible and promote wound vascularization and integration in murine wound healing models. This work has potentially beneficial implications in the field of tissue engineering and regenerative medicine, particularly for burns and chronic wounds.

Acknowledgements

I would like to express my deepest gratitude for my supervisors Prof Zhanfeng Cui, Dr Julian Dye and Mr Matthew Potter for their assistance and support during my DPhil. Throughout my studies in Oxford, I would especially like to thank Dr Dye for his expert technical advice and encouragement to complete my thesis.

I would also like to thank members from the Engineering Science Department, in particular Julian George, Linh Nguyen, Bas Brinkhof, Naresh Kasoju, Marzena Tkaczyk, Kalin Dragnevski, Igor Dyson, Marcus Green and Robert Jacobs for their time in training me how to use the various equipment needed for my project and for their assistance in providing expert advice. I would also like to thank staff at the Northwick Park Institute of Medical Research for their expertise and assistance with the animal work.

I would also like to thank my family and friends for their unwavering support throughout my DPhil. In particular, I would like to thank my parents and sister whose words of encouragement and never-ending patience motivated me to complete this thesis.

I would also like to express my gratitude to all the post-docs and lab mates, who have in one way or another contributed to this dissertation. I would also like to take this opportunity to thank my sponsors - A*STAR Graduate Academy (AGA) and the Chinese Regenerative Medicine Institute (CRMI), without which the work would not have been possible.

Lastly, I would like to dedicate this dissertation to my parents who have taught me to value patience, hard work, and focus, without which I would not have been able to complete this thesis.

Abbreviations

Ang-1	Angiopoetin-1
ANOVA	Analysis of Variance
ATR-FTIR	Attenuated Total Reflection- Fourier Transform Infrared Spectroscopy
AWERB	Animal Welfare and Ethical Review Bodies
BSA	Bovine Serum Albumin
CAK	Cultured Autologous Keratinocytes
CCK-8	Cell Counting Kit-8
CD	Circular Dichroism
CD31	Cluster of Differentiation 31 (aka Platelet endothelial cell adhesion molecule (PECAM-1)
CI	Confidence Interval
CEA	Cultured Epithelial Allografts
CMFDA	5-chloromethylfluorescein diacetate
CMC	Critical Micelle Concentration
CRP	C-Reactive Protein
CO_2	Carbon dioxide
Col1	Collagen Type 1
Col4	Collagen Type 4
CSS	Cultured Skin Substitutes
DFU	Diabetic Foot Ulcer
DSC	Differential Scanning Calorimetry
DMEM	Dulbecco's Modified Eagle's Medium
DPBS	Dulbecco's Phosphate Buffered Saline
DLVO	Derjaguin, Landau, Verwey, Overbeek theory
DMSO	Dimethyl sulfoxide
ECM	Extracellular matrix
EDC	1-Ethyl-3-(3-dimethylaminopropyl) carbodiimide
EDTA	Ethylenediaminetetraacetic acid
ELISA	Enzyme-Linked Immunosorbent Assay
EmDerm	Emulsion-templated scaffolds
FBS	Fetal Bovine Serum
FDA	Food and Drug Administration (USA)

FITC-BSA	Fluorescein Isothiocyanate Conjugate Bovine Serum Albumin
FTIR	Fourier Transform Infrared Spectroscopy
FTSG	Full Thickness Skin Graft
GFP	Green Fluorescent Protein
Hb	Haemoglobin
Hct	Haematocrit
HEPES	(4-(2-hydroxyethyl)-1-piperazineethanesulfonic acid)
HEK	Human Epidermal Keratinocytes
HDF	Human Dermal Fibroblasts
HDE	Human Dermal Endothelial cells (Microvascular)
HFIP	Hexafluoroisopropanol
HGF	Hepatocyte Growth Factor
HLB	Hydrophile-Lipophile Balance
HKGS	Human Keratinocyte Growth Serum
HSS	Hamilton Scar Scale
hTERT	Human Telomerase Reverse Transcriptase
H&E	Hematoxylin and Eosin
IL-8	Interleukin-8
LAL	Limulus Amebocyte Lysate
LDH	Lactate Dehydrogenase
MCH	Mean Cell Haemoglobin
MCV	Mean Cell Volume
MCHC	Mean Cell Haemoglobin Concentration
MHRA	Medicine and Healthcare Regulatory Agency
MPV	Mean Platelet Volume
MES	2-(N-Morpholino) ethanesulfonic acid buffer
MMP1	Matrix Metalloproteinase 1
MMP2	Matrix Metalloproteinase 2
MSC	Mesenchymal stem cells
MTT	(3-(4,5-dimethylthiazol-2-yl)-2,5-diphenyltetrazolium bromide
MW	Molecular Weight
NAD/NADH	Nicotinamide adenine dinucleotide
NBF	Neutral Buffered Formalin
NIH	National Institutes of Health

NCES	Noncultured Epidermal Cell Suspension
NHS	N-hydroxysuccinimide
NR	Not Reported
NaCl	Sodium Chloride
NaOH	Sodium Hydroxide
Na_2CO_3	Sodium Bicarbonate
OD	Optical Density
O-W	Oil-in-Water Emulsions
O-W-O	Oil-in-Water-in-Oil Mixed Emulsion
P68	Pluronic F68
PBS	Phosphate Buffered Saline
PCL	Polycaprolactone
PEG	Polyethylene glycol
pI	Isoelectric Point
PLGA	Poly(lactic-co-glycolic acid)
PLLA	Poly-L-lactic acid
PLT	Platelet count
PVA	Poly(vinyl alcohol)
PTFE	Polytetrafluoroethylene
PVP	Polyvinylpyrrolidone
polyHIPE	Polymeric High Internal Phase Emulsions
POSAS	Patient and Observer Scar Assessment Scale
PLLA	Poly-L-lactic Acid
PLGA	Poly-L-glycolic Acid
POSAS	Patient and Observer Scar Scale
PRISMA	Preferred Reporting Items for Systematic Reviews and Meta-Analyses
RBC	Red Blood Cell Count
RCT	Randomized Clinical Trials
rhVEGF	Recombinant Human Vascular Endothelial Growth Factor
rhEGF	Recombinant Human Epidermal Growth Factor
rhFGF	Recombinant Human Fibroblast Growth Factor
rhIGF-1	Recombinant Human Insulin-like Growth Factor-1
RR	Risk Ratio
SEM	Scanning Electron Microscopy

SBEG	Suction Blister Epidermal Grafting
SDS	Sodium Dodecyl Sulfate
SD	Standard Deviation
STSG	Split Thickness Skin Graft
Sulfa-NHS	sulfa- N-hydroxysuccinimide
Tg	Glass Transition Temperature
TGF-β	Transforming Growth Factor-β
TBSA	Total Burn Surface Area
TIMP1	Tissue Inhibitor of Matrix Metalloproteinase 1
VAS	Visual Analogue Scale
VEGF	Vascular Endothelial Growth Factor
VLU	Venous Leg Ulcer
VSS	Vancouver Scar Scale
vWF	von Willibrand Factor
WBC	White Blood Cell Count
WMD	Weighted Mean Difference
W-O	Water-in-Oil Emulsions
W-O-W	Water-in-Oil-in-Water Mixed Emulsions
UTS	Ultimate Tensile Strength
UV	Ultraviolet
UV-Vis	Ultraviolet–visible spectroscopy

List of Figures

Figure 1-1 Diagram of skin layers and structures. Reproduced with permission from © Elsevier.(4)... 2
Figure 1-2 Classification system for skin substitutes.... 8
Figure 2-1 PRISMA Flowchart for study selection for burns.... 18
Figure 2-2 Diagrammatic representation of overall study quality for burns.... 19
Figure 2-3 Risk of bias summary for studies on burns. 20
Figure 2-4 Forest plot of number of wounds healed comparing skin substitute vs standard care for burns. 22
Figure 2-5 Forest plot of mean time to healing comparing skin substitute vs standard care for burns. 23
Figure 2-6 Forest plot for percentage graft take comparing skin substitute vs standard care for burns. 24
Figure 2-7 Forest plot for percentage wound healed/epithelialized comparing skin substitute vs standard care for burns. 24
Figure 2-8 Forest plot for Vancouver Scar Scale comparing skin substitute vs standard care for burns. 25
Figure 2-9 Forest plot for pain assessment as per visual analogue scale (VAS) comparing skin substitute vs standard care for burns. 26
Figure 2-10 Forest plot for need for further surgery comparing skin substitute vs standard care for burns. 27
Figure 2-11 Forest plot for length of hospital stay comparing skin substitute vs standard care for burns. 28
Figure 2-12 Forest plot for infection rate comparing skin substitute vs standard care for burns.... 28
Figure 2-13 Forest plot for hypertrophic scarring comparing skin substitute vs standard care for burns. 29
Figure 2-14 Flowchart for study selection for skin substitutes for diabetic foot ulcers.... 41
Figure 2-15 Risk of bias graph for studies on diabetic foot ulcers. 42
Figure 2-16 Risk of bias summary for studies on diabetic foot ulcers.... 43
Figure 2-17 Forest plot of number of ulcers healed comparing skin substitutes vs standard care for diabetic foot ulcers.... 46
Figure 2-18 Forest plot of mean time to healing comparing skin substitutes and standard care for diabetic foot ulcers.... 46
Figure 2-19 Forest plot of mean area healed/epithelialized comparing skin substitutes vs control for diabetic foot ulcers.... 47
Figure 2-20 Forest plot of rate of infection comparing skin substitutes and control for diabetic foot ulcers.... 48
Figure 2-21 Forest plot of incidence of osteomyelitis comparing skin substitutes and controls in diabetic foot ulcers.... 49
Figure 2-22 Forest plot of incidence of cellulitis comparing skin substitutes vs control in diabetic foot ulcers.... 50
Figure 2-23 Forest plot of rate of ulcer recurrence comparing skin substitutes and standard care for diabetic foot ulcers.... 50
Figure 2-24 Forest plot of amputation comparing skin substitutes vs control for diabetic foot ulcers. 51
Figure 2-25 Forest plot of rate of hospitalization comparing skin substitutes vs control in diabetic foot ulcers.... 52
Figure 2-26 Forest plot of presence of pain comparing skin substitutes vs control in diabetic foot ulcers. 52

Figure 2-27 Forest plot of number of ulcers healed comparing different skin substitutes for diabetic foot ulcers. 53
Figure 2-28 Forest plot of mean time to closure comparing different skin substitutes for diabetic foot ulcer. 54
Figure 2-29 Forest plot of rate of infection comparing different skin substitutes for diabetic foot ulcers. 54
Figure 2-30 Forest plot of ulcer recurrence comparing different skin substitutes for diabetic foot ulcers. 55
Figure 2-31 Types of surfactants as categorized by type of head group. 66
Figure 2-32 Diagrammatic representation of Gibbs dividing line. 66
Figure 2-33 HLB values of surfactants and their uses. Reprinted with permission © Churchill Livingston. (98) 69
Figure 2-34 Diagram illustrating DLVO theory. 73
Figure 3-1 Light microscopy of Oil Red O stained emulsions showing phase transition of the emulsions as HLB value increases (Magnification 10x). Mean droplet diameter decreased significantly as HLB values increased ($p<0.05$). 85
Figure 3-2 Light microscopy of Oil Red O stained emulsions showing decrease in mean droplet diameter as surfactant concentration increased ($p<0.05$). 86
Figure 3-3 Light microscopy of Oil Red O stained emulsions showing decrease in mean droplet diameter as PVP concentration increased ($p<0.05$). 86
Figure 3-4 Light microscopy of Oil Red O stained emulsions showing no change in mean droplet diameter as temperature is increased ($p>0.05$). 87
Figure 3-5 Effect of increasing shear rate and surfactant concentration on mean droplet diameter of emulsions. Mean droplet size decreased as shear rate increased from 1500 rpm to 3000 rpm and as surfactant concentration increased from 0.25% to 1.5%. 88
Figure 3-6 Turbiscan emulsion stability profile over time for emulsions at different HLB values, PVP concentration and surfactant concentration. As HLB, PVP and surfactant concentration increased, change in light transmission and backscatter decreased. Coloured bar on the right represents timepoints of measurement indicating stability over time. 89
Figure 3-7 Viscoelastic properties of each emulsions system as represented by: (A) viscosity, (B) storage moduli and (C) loss moduli of each emulsion as angular frequency increases. (D) Storage and loss moduli are graphed together in logarithmic scale showing that storage moduli of the HLB 10 emulsion was highly variable indicating emulsion instability. 91
Figure 3-8 Confocal microscopy images showing 'coating-effect' as FITC-BSA and surfactant interact close to interfacial oil-aqeuous regions using emulsions with differing HLB values, PVP concentration and surfactant concentration. (10x magnification) 92
Figure 3-9 Quantification of relative fluorescence intensity of FITC-BSA in aqueous phase vs oil phase demonstrating that most of the protein remains in concentrated in the aqueous phase while the amount of protein in the oil phase is too low to be reliably quantified. 93
Figure 3-10 Second derivative of subtracted FTIR spectra of cream phase of the emulsions with BSA at different HLB, surfactant and PVP concentrations, showing only water peaks with no protein signals, compared with the four peaks in BSA. 94
Figure 3-11 Near-UV circular dichroism to assess conformation of BSA. Both emulsion only and denatured BSA did not show significant changes in CD value while buffered BSA solution and BSA incubated in HLB 13 demonstrated changes in CD value, indicating that the BSA molecules retained their folded state. 95
Figure 3-12 Tryptophan assay to assess conformation of fibrinogen. Denatured fibrinogen demonstrated left-shift whilst fibrinogen incubated in various surfactant and PVP concentrations retained their folded state. 96

Figure 3-13 LDH assay to assess enzyme function on exposure to emulsion mix. LDH enzyme activity is largely preserved regardless of surfactant concentration and is minimally affected by PVP concentration. 97
Figure 3-14 Mean droplet diameter of decane emulsions did not change significantly between HLB values of 12 to 14. 111
Figure 3-15 Mean droplet diameter for decane emulsion according to shear rate and surfactant concentration. Mean droplet diameter decreased as shear rate increased from 1000 to 3000 rpm and as surfactant concentration increased from 0.3% to 0.7%. At 0.1% there is minimal change in mean droplet diameter due to the fragmentation limit. 112
Figure 3-16 Turbiscan emulsion stability profile. Increase in (A) HLB value, (B) surfactant concentration and (C) PVP concentration resulted in increasing stability of the resulting emulsion. Coloured bars on the right represent the different time points measurements were taken. 113
Figure 3-17 Viscosity of decane emulsions remains relatively stable regardless of (A) HLB value and (B) surfactant concentration. 114
Figure 3-18 Storage and loss moduli values for decane emulsions by (A) HLB value and (B) surfactant concentration. The emulsions remain relatively stable across a range of HLB values and surfactant concentration. 116
Figure 3-19 Mean droplet diameter for collagen protein-emulsion hydrogels gradually decrease with increasing surfactant concentration. 117
Figure 3-20 Mean droplet diameter for fibrin protein-emulsion hydrogels decrease with increasing surfactant concentration. 117
Figure 3-21 Mean droplet diameter for collagen-fibrin protein-emulsion hydrogels decrease with increasing surfactant concentration. 118
Figure 3-22 SEM images of emulsion-templated collagen, collagen-fibrin and fibrin scaffolds and mean pore size of each scaffold by percentage surfactant. 119
Figure 3-23 Hydrolytic and enzymatic degradation of emulsion-templated collagen, collagen-fibrin and fibrin scaffolds. Fibrin scaffolds degraded much more rapidly compared to collagen and collagen-fibrin scaffolds. Percentage decrease in mass is significant after Day 1 due to initial dissolution of excipients. 121
Figure 3-24 Addition of excipients into protein-hydrogels did not significantly affect mean droplet diameter. 124
Figure 3-25 DSC profile of collagen (A), fibrin (B) and collagen-fibrin (C) scaffolds. Note glass transition temperature (Tg) of fibrin scaffolds was around -28°C. 125
Figure 4-1 Cell proliferation results by type of excipient. HDE and MSC had significantly higher proliferation rate in collagen scaffolds with P68 and mannitol as excipients. HDF had significantly lower proliferation rate in collagen-fibrin scaffolds with PEG as excipient and fibrin scaffolds with mannitol as excipient. 141
Figure 4-2 Cell proliferation outcome by concentration of surfactant. All three cell lines (HDF, HDE, MSC) had significantly higher proliferation rate in scaffolds made with 0.1% surfactant concentration indicating a surfactant concentration effect. 142
Figure 4-3 Cell proliferation outcome comparing EmDerm and controls. HDFs in EmDerm-C proliferated at a comparable rate to Matriderm and Integra. HDEs proliferated significantly better in EmDerm-CF and EmDerm-F. Meanwhile, MSCs in EmDerm-C and EmDerm-CF had higher proliferation rates compared to the other scaffolds. 143
Figure 4-4 Confocal microscopy of HDF, HDE and MSC seeded on EmDerm scaffolds. (Magnification 20x) 144
Figure 4-5 Cell proliferation outcome of co-cultures comparing EmDerm and controls. HEK/HDF in EmDerm-CF and EmDerm-F had significantly lower cell proliferation rate compared to other scaffolds. 146

Figure 4-6 Co-culture of cells on EmDerm-C scaffolds. (A) HDF/HDE – HDEs appear to form vascular networks with HDFs growing around these vessel-like structures. (B) MSC/HDE – MSCs retained their elongated morphology while the HDEs are interspersed between MSCs. (C) HEK/HDF - HEK grew in a sheet-like manner with HDFs scattered in between. 148
Figure 4-7 Co-culture of cells on EmDerm-CF scaffolds. (A) HDF/HDE - HDEs.and HDFs appear to grow in an inter-dispersed manner around each other. (B) MSC/HDE – MSCs retain their elongated morphology and HDEs were scattered around the scaffold. (C) HEK/HDF – HEKs grew in sheets while HDFs grew in clusters..... 151
Figure 4-8 Co-culture of cells on EmDerm-F scaffolds. (A) HDF/HDE – HDEs grew in a network-like manner with HDFs growing in between. (B) MSC/HDE – MSCs retained their elongated morphology with HDEs scattered amongst the MSCs. 153
Figure 4-9 Co-culture of cells on Integra scaffolds. (A) HDF/HDE co-culture – HDFs grew in sheets with HDEs forming network-like structures. (B) MSC/HDE – MSCs grew in clusters with HDEs interspersed in between. (C) HEK/HDF - HEK and HDFs grew in a sheet-like manner. 155
Figure 4-10 Co-culture of cells on Matriderm. (A) HDF/HDE – HDFs grew in a sheet-like manner while HDEs formed vessel-like structures. (B) MSC/HDE – MSCs grew in a haphazard manner with HDEs scattered in between. (C) HEK/HDF – HEKs and HDFs grew in a sheet-like manner. 158
Figure 4-11 Keratinocytes seeded on EmDerm-C (A), EmDerm-CF (B), Integra (C) and Matriderm (D) showing a flattened, stretched out morphology and partial stratification. 159
Figure 4-12 Secretome profile of HEK monoculture on scaffolds. Keratinocytes seeded on Integra secreted higher amounts ECM remodelling proteins and vascular growth factors e.g. MMP1, FGF-B, IL-8 and TIMP-1..... 162
Figure 4-13 Proteome profile of HEK monoculture on scaffolds. Keratinocytes seeded on Integra scaffolds produced higher amounts of ECM remodelling proteins and vasculogenic factors e.g. MMP1, FGF-B, IL-8 and TIMP-1. 163
Figure 4-14 Secretome profile of HDF monoculture on scaffolds. Fibroblasts seeded on Integra scaffolds secreted higher amounts of collagen and vasculogenic factors e.g. IL-8 and fibronectin compared to EmDerm scaffolds..... 164
Figure 4-15 Proteome profile of HDF monoculture on scaffolds. HDF seeded on EmDerm-F scaffolds produced higher amounds of collagen and ECM remodelling proteins e.g. MMP1, MMP2 and TIMP-1 as well as vasculogenic proteins e.g. IL-8 and fibronectin. 165
Figure 4-16 Secretome profile of HDE monoculture on scaffolds. Endothelial cells seeded on Integra secreted the highest amount of collagen, IL-8 and TIMP-1. Endothelial cells seeded on EmDerm-C secreted the highest amount of FGF-B, while endothelial cells seeded on EmDerm-F secreted highest amount of fibronectin and endothelial cells on EmDerm-CF secreted highest amount of VEGF..... 166
Figure 4-17 Proteome profile of HDE monoculture on scaffolds. Endothelial cells seeded on EmDerm-C produce the highest levels of collagen 1, collagen 4, MMP1, MMP2, TIMP1 and vasculogenic factors e.g.FGF-B, IL-8, fibronectin..... 167
Figure 4-18 Secretome profile of MSC monoculture on scaffolds. MSCs seeded on Integra secreted highest amount of collagen, MMP1, MMP2, TIMP1 and vasculogenic factors e.g. VEGF-A, IL-8, fibronectin, ang-1 and HGF. 168
Figure 4-19 Proteome profile of MSC monoculture on scaffolds. MSC seeded on EmDerm-F produced the highest levels of collagen, MMP1, and fibronectin while MSC seeded on EmDerm-CF produced highest levels of MMP2 and IL-8. FGF-B and TIMP1 levels were highest in Integra scaffolds seeded with MSC..... 169
Figure 4-20 Secretome profile of HEK/HDF co-culture on scaffolds. HEK/HDF seeded on EmDerm-C secreted highest levels of MMP1, MMP2 and vasculogenic factors e.g. VEGF-A, fibronectin while HEK/HDF seeded on EmDerm-CF secreted highest amounts of collagen, IL-8 and HGF..... 170

Figure 4-21 Proteome profile of HEK/HDF co-culture on scaffolds.HEK/HDF seeded on EmDerm-C produced the highest amount of collagen, MMP2, TIMP1 and vasculogenic factors FGF-B, HGF. HEK/HDF seeded on EmDerm-F produced highest amount of MMP1 and IL-8. 171
Figure 4-22 Secretome profile of HDF/HDE co-culture on scaffolds. HDF/HDE seeded on EmDerm-C secreted highest amounts of collagen and vasculogenic factors VEGF-A, Il-8, fibronectin and HGF. 172
Figure 4-23 Proteome profile of HDF/HDE co-culture on scaffolds. HDF/HDE seeded on EmDerm-C scaffolds produced highest amounts of collagen 4, MMP1, MMP2 and VEGF-A. HDF/HDE seeded on Integra produced highest amounts of FGF-B and HGF. 173
Figure 4-24 Secretome profile of MSC/HDE co-culture on scaffolds. MSC/HDE seeded on EmDerm-C secreted highest amounts of collagen, FGF-B and HGF. 174
Figure 4-25 Proteome profile of MSC/HDE co-culture on scaffolds. MSC/HDE seeded on EmDerm-C produced highest amounts of collagen and HGF. MSC/HDE seeded on EmDerm-CF scaffolds produced highest amounds of FGF-B, IL-8 and fibronectin..... 175
Figure 5-1 Schematic representation of in vivo experimental plan. 3 rats were used for the study and each rat was implanted with 4 scaffold discs. Wounds on one side were abraded to remove part of dermis while the other side was not. Biopsies were taken on Day 7 and Day 14. Blood sampling was done on Day 0, Day 7 and Day 14. 185
Figure 5-2 4 subcutaneous pockets containing scaffolds on either side of the rat's flank were created. At Day 7, wound biopsies were taken (one each from the abraded and non-abraded sides). Finally, on Day 14, full-thickness excision of the wounds was performed on termination. 186
Figure 5-3 Endotoxin assay with lines representing levels of endotoxin concentrations in each of the scaffold..... 190
Figure 5-4 Hematological analysis of inflammatory markers. There was no significant change from baseline of any of the white cell, neutrophil, lymphocyte or platelet counts. 191
Figure 5-5 Biochemical analysis (CRP levels) of inflammation. There was no significant change from baseline for CRP levels. 191
Figure 5-6 Day 7 biopsy of EmDerm-C. Left (abraded) and right (non-abraded). Both show minimal local inflammatory changes and partly degraded scaffolds. 192
Figure 5-7 Day 7 biopsy of EmDerm-CF. Left (abraded) and right (non-abraded). The abraded wound showed minimal inflammatory reaction compared to the non-abraded wound where there is a mild to moderate inflammatory reaction around the scaffold. In both cases, scaffolds were partly degraded. 192
Figure 5-8 Day 7 biopsy of EmDerm-F. Left (abraded) and right (non-abraded). In both scaffolds, there is mild to moderate inflammatory reaction within and around the partially degraded scaffolds. 193
Figure 5-9 Day 14 biopsy of EmDerm-C. There is increased vascularization of the wound site as shown by the arrows and scaffolds have been remodelled/integrated into the wounds. 194
Figure 5-10 Day 14 biopsy of EmDerm-CF. There is increased vascularization of the wound site as shown by the arrows and scaffolds have been remodelled/integrated into the wounds. However, there is some residual inflammatory response and increased deposition of ECM in the dermal layer. 194
Figure 5-11 Day 14 biopsy of EmDerm-F. There is increased vascularization of the wound (as shown by arrows) and significant deposition of ECM material within the wound site and dermal layer. 195
Figure 5-12 Day 14 biopsy of EmDerm-C (non-abraded). There is minimal inflammatory response and most of the scaffold has been remodelled with ingrowth of vascular structure (see arrows). 196
Figure 5-13 Day 14 biopsy of EmDerm-CF (non-abraded). There is minimal inflammatory response and most of the scaffold has been remodelled with ingrowth of vascular structure (see arrows)..... 196
Figure 5-14 Day 14 biopsy of EmDerm-F (non-abraded). There is minimal inflammatory response and most of the scaffold has been remodelled with ingrowth of vascular structure (see arrows). There is significant deposition of ECM as well. 197

Figure 5-15 Mean number of blood vessels in biopsies. In both the abraded and non-abraded wounds, there is higher mean number of vascular structures in wounds treated with EmDerm-C. 198
Figure 5-16 Mean grade of inflammation in biopsies. In both the abraded and non-abraded wounds, there is significantly higher degree of inflammation in EmDerm-F scaffolds, followed by EmDerm-CF then EmDerm-C. 198
Figure 6-1 Scanning electron microscopy (SEM) images of all electrospun scaffolds. 211
Figure 6-2 Degradation profiles of electrospun membranes showing greatest reduction in percentage original mass of PLLA/gelatin over 7 days. 214
Figure 6-3 Reduction in mean area of electrospun scaffolds were greatest for PLGA and PLGA/gelatin scaffolds and least for PCL and PLLA scaffolds. 215
Figure 6-4 Live/Dead assay showing high cell viability (>70%) for all electrospun scaffolds. Hybrid scaffolds had higher mean percentage cell viability compared to pure polymer scaffolds but was not statistically significant ($p>0.05$). 216
Figure 6-5 Cell proliferation (MTT) assay showing significant increase cell proliferation in all electrospun membranes by Day 14. The effect is more pronounced in hybrid scaffolds compared to pure polymer scaffolds but was not statistically significant ($p>0.05$). 216
Figure 6-6 Confocal microscopy of keratinocytes on electrospun membranes stained with Phalloidin and Hoescht. Keratinocytes on hybrid membranes appear to have a more flattened, spread-out morphology (especially on PLLA-G) compared to polymer only membranes. (10x magnification) . 217

List of Tables

Table 1-1 List of available commercial skin substitutes. Note: this list is non-exhaustive. 9
Table 2-1 Summary of outcomes from studies involving skin substitutes for burns. 33
Table 2-2 Summary of outcomes from meta-analysis by type of skin substitute for burns. 33
Table 2-3 Summary of studies included in this systematic review for diabetic foot ulcers. 60
Table 2-4 Summary of meta-analysis outcomes by skin substitutes for diabetic foot ulcers. 61
Table 3-1 Tween 20 and Span 20 mixing volume ratio. 79
Table 3-2 A summary of mechanical properties of each scaffold. 122
Table 3-3 Mean gelation time for each protein hydrogel. 122
Table 6-1 Summary of fibre diameter of all electrospun membranes. 212
Table 6-2 Summary of porosity results of all electrospun membranes. 212
Table 6-3 Summary of mechanical properties of all electrospun membranes by tensile testing. 213

Publications, Presentations and Patents

Publications

1. Lim, X., Potter, M., Cui, Z. and Dye, J.F., 2018. Manufacture and characterisation of EmDerm—novel hierarchically structured bio-active scaffolds for tissue regeneration. Journal of Materials Science: Materials in Medicine, 29(6), p.79.

Manuscript in preparation

1. Lim, X., Potter, M., Cui, Z. and Dye, J.F., 2019. Systematic Review of Skin Substitutes for Burns.
2. Lim, X., Potter, M., Cui, Z. and Dye, J.F., 2019. Systematic Review of Skin Substitutes for Chronic Wounds.
3. Lim, X., Potter, M., Cui, Z. and Dye, J.F., 2019. Characterization of a Biocompatible Emulsion System.
4. Lim, X., Potter, M., Cui, Z. and Dye, J.F., 2019. Co-culture and In Vitro Assessment of EmDerm scaffolds.
5. Lim, X., Potter, M., Cui, Z. and Dye, J.F., 2018. In Vivo Assessment of EmDerm Scaffolds in a Murine Wound Healing Model.
6. Lim, X., Potter, M., Cui, Z. and Dye, J.F., 2018. Electrospun Membrane as an Epidermal Skin Substitute.

Presentations and Published Abstracts

1. Evaluation of Electrospun Scaffolds as Biocompatible Epidermal Carrier Delivery System. Xuxin Lim, Julian Dye, Hua Ye, Zhanfeng Cui. eCM Meeting Abstracts 2016, Collection 5, TCES (page 68).
2. Smart scaffolds: Utilizing a microfluidic hydrogel platform to synthesize gelatin-based microchannel dermal scaffolds to enhance vascularization. Xuxin Lim, Julian Dye, Hua Ye, Zhanfeng Cui. eCM Meeting Abstracts 2016, Collection 5, TCES (page 65).
3. Development and characterization of a composite skin construct with electrospun membrane and microchannel hydrogel. Xuxin Lim, Julian Dye, Hua Ye, Zhanfeng Cui. eCM Meeting Abstracts 2017, Collection 2, TERMIS EU (page 383).

Patent

1. Manufacture and characterisation of EmDerm—novel hierarchically structured bio-active scaffolds for tissue regeneration. Xuxin Lim, Julian Dye, Zhanfeng Cui. Patented file on March 2018 by Oxford University Innovations.

Chapter 1 Introduction

1.1. Background

Burns and chronic wounds contribute to a significant portion of co-morbidities to patients around the world. In 2004, the incidence of severe burns was around 11 million and accounts for 300,000 deaths globally. (1) Significant improvements have been made to enhance the wound healing and recovery process of these patients using dressings and skin substitutes. Numerous commercial skin substitutes have been developed since the 1960s with the aim of facilitating the healing process of chronic wounds and burns. However, the efficacy of these skin substitutes remains debatable. (2)

The ideal skin substitute would be one that has all the following criteria (3): (a) infection resistant, (b) prevents heat and water loss, (c) good tensile strength, (d) cost-effective, (e) easily stored and available, (f) non-toxic and biocompatible, (g) easily applied, (h) derived from autologous cells, (i) integrates well into wounds, and (j) resistant to shear.

To date, there are no skin substitutes which meet all the criteria listed above. There is still a need to develop better tissue-engineered scaffolds to promote wound healing in acute and chronic wounds.

Anatomy of the skin

The skin can be divided into 2 layers – the epidermis and dermis (see Figure 1-1). The basement membrane separates the dermal and epidermal layer, although there are interactions between the keratinocytes and fibroblasts within the skin.

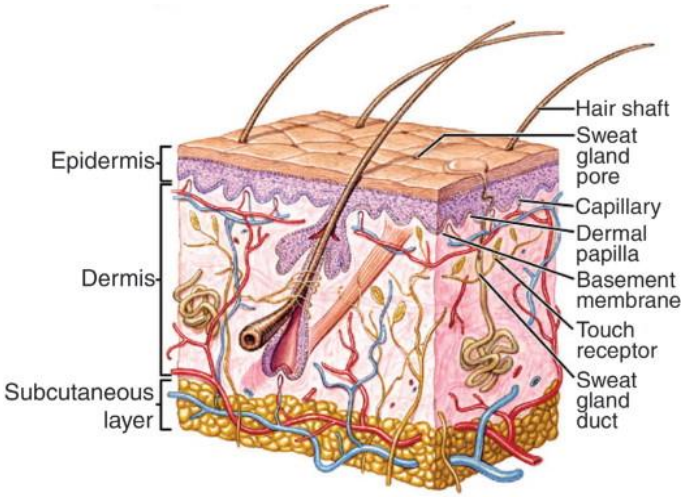


Figure 1-1 Diagram of skin layers and structures. The upper most layer is the epidermis, followed by the dermis and subcutaneous layer. The dermal layer contains numerous skin appendages and neurovascular networks. Reproduced with permission from © Elsevier.(4)

The average epidermal layer is 100 to 300 microns thick and is made up of stratified squamous epithelium, comprising of differentiated keratinocytes. (5,6) The epidermal layer acts as a semi-permeable layer which prevents loss of heat and water as well as providing a mechanical barrier to protect against pathogens in the environment. It can be further divided into five layers: stratum basale, stratum spinosum, stratum granulosum, stratum lucidum, and stratum corneum. (7) The stratum basale contains stem cells which differentiate into keratinocytes which make up the upper layers. (7)

The dermal layer can be subdivided into the superficial papillary and deep reticular dermis. It contains the vascular plexus, nerve endings and sweat glands which help with homeostasis and provides tactile sensation of the environment. It also houses the innate immune cells which guard against pathogens from the environment. The presence of vascular networks within the dermal layer also supports the epidermal layer and allows for healing and regeneration to occur. There is cross-talk between the dermal fibroblasts and epidermal keratinocytes which regulates the stratification and differentiation of basal keratinocytes into the stratum corneum. (8)

Wound healing process

Acute wounds are often traumatic injuries which heal by primary or secondary intention. Meanwhile, chronic wounds are defined as wounds which have not healed within six weeks. These wounds often have high bacterial load colonising the wound and poor vascular supply to the surrounding tissue.

Wounds can also be divided based on the depth of skin area involved – superficial, partial thickness (superficial, mid or deep dermal) and full-thickness injury. Superficial wounds such as sunburns and grazes often heal very well on their own as only the epidermal layer is involved. Partial thickness and full thickness wounds often require the application of skin substitutes or dressings or surgical intervention to promote wound healing and prevent scarring. Early wound closure results in better healing and less scarring. (9)

Wound healing can be divided into primary, secondary and tertiary intention healing. (10) Primary wound healing occurs when wound edges can be approximated together for example using staples and sutures. This is often achieved in acute wounds such as cuts and lacerations.

Secondary wound healing occurs when wounds are too wide to achieve close approximation. Thus, the wound heals from the base and is left to granulate. This tends to occur in chronic wounds such as diabetic foot ulcers or venous leg ulcers where the wound area is too large to close. There is a need for a skin substitute or skin grafting to promote healing in such wounds.

Finally, tertiary intention healing is where the wound is left open for a period of time before delayed approximation of wound edges (i.e. a combination of primary and secondary intention healing). This can sometimes occur in grossly contaminated wounds whereby there is a need for serial debridement of

the wound bed down to healthy tissue, to ensure that when the wound is definitively closed, there is a lower risk of infection and necrosis.

Occasionally, there is a need to provide immediate coverage of large surface area acute wounds such as burns. In these instances, there is a need for tangential excision to remove the unhealthy parts of the wound bed down to a well-vascularized wound bed and apply a skin graft or skin substitute to provide immediate coverage.

Skin grafting is a three-stage process involving plasmatic inbibition where the graft absorbs nutrients and plasma from the wound bed itself. The next step is inosculation whereby vessels in the graft connects with vessels from the host tissue. Finally, there is neovascular ingrowth where blood capillaries grow into the graft itself from the wound bed and the graft becomes integrated into the circulatory system of the host. (11)

Types of skin substitutes

A skin substitute can be defined as a material which replaces a skin component (e.g. dermis or epidermis) which stimulates regenerative wound healing. One example of a skin substitute is Integra which is a dermal regeneration template made up of cross-linked microporous bovine collagen and shark chondroitin sulfate while another is Matriderm which is a non-crosslinked collagen-elastin scaffold. Integra is used for two-staged reconstructions as it requires a split-thickness skin graft at 14 days while Matriderm is used for single-staged reconstructions which can support a split-thickness skin graft at the same time.

In contrast, a wound dressing is a material which provides temporary wound protection by providing a physical barrier from bacteria and which keeps the wound moist. Some hydrocolloid dressings have

anti-microbial properties which reduces risk of infection while others are highly absorbant and adhere to the wound until re-epithelialization occurs.

Skin substitutes can be categorized based on several criteria such as cellularity, area replaced, materials used (natural, synthetic or biosynthetic) and permanence. (12) As there are so many types of skin substitutes, the classification of skin substitutes can be difficult.

Cellularity

Skin scaffolds can be categorized as cellular or acellular. Cellular scaffolds have a much higher cost of production, are more difficult to manufacture, transport and store, as well as carry the risk of disease transmission. (12) Cellular scaffolds can be further subdivided into whether they are autologous or allogenic. Examples of autologous epidermal substitutes include Epicel, EpiDex, EpiBase, MySkin, LaserSkin and Bioseed-S. CellSpray or ReCell are cell suspensions which can be directly sprayed onto wounds. Meanwhile cellular dermal substitutes include Dermagraft-TC (Transcyte), Hyalograft 3D and Activ-Derm which are derived from allogenic fibroblasts. Bilayer cellular skin substitutes include Karoskin, Apligraf, Orcel, PolyActive and TissueTech.

Acellular scaffolds, on the other hand, are much easier to manufacture, have lower costs of production and can be lyophilized for long-term storage and availability. (12) They tend to come in the form of decellularized dermis or amniotic membrane or intestinal mucosa/organs from bovine/porcine sources. There is also a growing number of bioengineered collagen/ECM-derived products which have been processed in some way to create a porous scaffold for cellular ingress. Examples of allogenic acellular scaffolds include AlloDerm, KaroDerm, SureDerm and GraftJacket while xenografts include Permacol and OASIS (derived from porcine subintestinal mucosa). Bioengineered acellular scaffolds include Integra, Matriderm, EZ Derm, Pelnac, Biobrane and Hyalomatrix.

Area replaced

Skin substitutes can also be classified based on the area replaced. Monolayer scaffolds can be designed to replace the epidermal layer or dermal layer. Meanwhile, bilayer scaffolds are often for dermo-epidermal replacement simultaneously.

Epidermal skin substitutes are often autologous where a small area of the patient's skin is harvested and grown into confluent or sub-confluent sheets in vitro. However, these cellular sheets are rather fragile and can often tear or blister when applied due to lack of a supporting structure when grafted. (5) The process of culturing autologous keratinocytes and stratification could take up to 30-days and thus, these skin substitutes are not ideal for immediate application. Moreover, confluent keratinocyte sheets tend to proliferate slowly when grafted which is an added challenge in providing permanent epidermal coverage. (5)

Dermal substitutes have a role to play in partial and full thickness wounds where there is a need to promote revascularization of the wound bed and result in less scarring. Some dermal substitutes come with a silicone backing which acts as a temporary barrier to prevent heat and water loss, as well as infection. Acellular dermal substitutes act by encouraging angiogenesis and providing immediate coverage in the wound area. While cellular dermal substitutes have biologically active fibroblasts which secrete growth factors and extracellular matrix proteins to promote wound healing. The cells themselves do not permanently engraft as they are allogenic. These dermal replacements require split thickness skin grafting at a later stage when the dermis has integrated into the wound and the silicone layer can be removed.

True bilayer scaffolds are skin substitutes with both cellular dermal and epidermal layer which do not require further skin grafting at a later stage. Allograft bi-layers from preserved cadaveric skin can be

obtained from Skin Banks but only act as a temporary dressing as they cause immunorejection. Scaffolds with keratinocyte and fibroblast co-culture from autologous sources can act as a permanent skin substitute but take a long time to subculture, are very costly and require immediate grafting. (3)

Materials used

The type of material used to manufacture skin substitutes can have a significant impact on the biocompatibility of scaffolds. Scaffolds made up of natural polymers such as collagen, gelatin, fibrin, hyaluronic acid and decellularized dermis (xenograft or allograft) are much more biocompatible and able to integrate well into wounds.

Biosynthetic scaffolds such as those made of biodegradable polymers (polyglactin, polycaprolactone, poly-glycolic acid and poly-lactic acid) are often combined with native proteins to increase mechanical strength and for better control of degradation rate since these polymers have predictable degradation times. An example is Dermagraft which is a cellular scaffold made up of neonatal fibroblasts seeded onto a bioabsorbable polyglactin mesh which stays on wounds for up to 6 weeks.

Synthetic scaffolds e.g. those made up of silicone, polyurethane or nylon do not degrade, and thus do not integrate into the wounds well. They are often used as dressings or as the backing of dermal substitutes which are later removed. An example of skin scaffolds in this category is Suprathel – an absorbable, synthetic co-polymer made by phase-inversion and lyophilization which mimics the properties of the epithelium.

Permanence

Most skin substitutes made up of biodegradable polymers or native extracellular matrix (ECM) proteins such as collagen, hyaluronic acid or fibrin do not stay permanently in the wound itself. Rather, they

undergo a process of degradation and remodelling by the cells which migrate into the scaffolds. This results in less scarring and fibrosis. As they are derived from animal and human sources, they do not have to be removed once applied.

The degree of degradation and remodelling also depends on whether the scaffold is made up of cross-linked proteins or not. Cross-linking slows down the rate of degradation and confers better mechanical stability. (13) Synthetic materials such as nylon do not integrate and often provoke an inflammatory response which results in fibrosis. They are often used as a covering which needs to be removed once dermal engraftment has taken place.

A simplified classification system and a diagrammatic representation of various skin substitutes is shown in Figure 1-2. A non-exhaustive list of currently available skin substitutes is also compiled in Table 1-1. Research into bioengineered skin substitutes has grown exponentially over the past decade and thus, it is difficult to collate a comprehensive list of available skin substitutes as the field is ever changing. The general consensus from research into skin substitutes is that these materials are safe, however the efficacy of skin substitutes itself is dependent on various factors including wound environment, host factors, infection, pressure/shear forces, vascularity and time from injury to application of skin substitute.

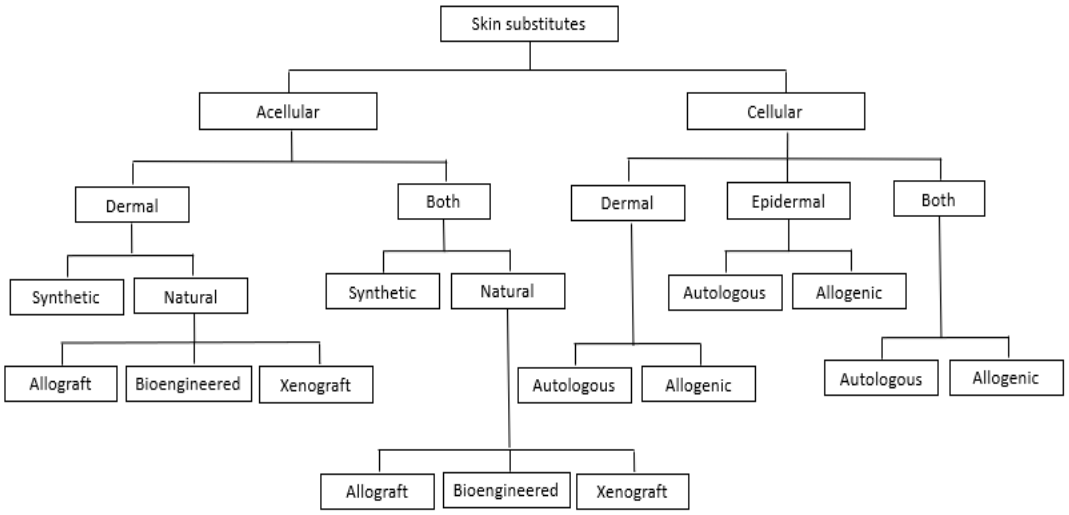


Figure 1-2 Classification system for skin substitutes.

Skin substitute	Description
Epidermal replacement	
Myskin	Autologous cell seeded scaffold (silicone)
Epicel	Autologous cell sheet
Epidex	Autologous cell sheet
EPIBASE	Autologous cell sheet
Laserskin	Autologous cell seeded scaffold (hyaluronic acid)
Bioseed	Autologous cell seeded scaffold (fibrin)
Celaderm	Allogenic cell sheet
Dermal replacement	
Alloderm	Allogenic human acellular dermis
Biobrane	Xenogenic porcine acellular dermis (nylon, collagen)
Dermagraft	Allogenic neonatal fibroblast in synthetic ECM (polyglactin)
Integra	Xenogenic bovine acellular dermis with silicone backing
Transcyte (Dermagraft-TC)	Allogenic neonatal fibroblast in porcine dermis with nylon and silicone cover
EZ Derm	Xenogenic porcine acellular dermis
Karoderm	Allogenic human acellular dermis
Permacol	Xenogenic porcine acellular dermis
Hyalomatrix	Allogenic acellular dermis with silicone backing
SureDerm	Allogenic human acellular dermis
Matriderm	Xenogenic bovine acellular dermis (collagen, elastin)
GraftJacket	Allogenic human acellular dermis
Oasis	Xenogenic porcine acellular dermis
Terudermis	Xenogenic bovine acellular dermis, silicone
Pelnac	Xenogenic porcine acellular dermis, silicone
Epidermal/dermal construct	
Apligraf	Allogenic cells in bovine dermis
Orcel	Autologous cells in allogenic dermis
Tissue Tech (Hyalograft 3D + Laserskin)	Autologous cells in hyaluronic acid dermis
PolyActive	Autologous cells in synthetic bilayer made up of PEO/PBT
StrataGraft	Allogenic stratified NIK cells on cultured fibroblasts

Table 1-1 List of available commercial skin substitutes. Note: this list is non-exhaustive.

1.2. Aims and Objectives

One of the main areas of clinical need is providing immediate coverage for patients with large surface area burns. In patients with >50% total burns surface area (TBSA), split thickness skin grafting (STSG) is challenging as there is insufficient donor area to harvest. (5) The aim is to reconstitute the dermal and epidermal layers as quickly as possible. However, ready-made dermal scaffolds are often acellular or made up of allogenic cells while epidermal skin substitutes which are autologous requires a long time for culturing.

One way to achieve the need for permanent dermal and epidermal reconstitution in partial to full thickness injuries using autologous cells is to simultaneously apply a dermal scaffold to restore the dermal layer and harvesting a small area of skin for culturing autologous keratinocytes on a carrier membrane.

Therefore, the aim of this thesis is to explore two manufacturing methods of creating a dermal and epidermal skin scaffolds using emulsion templating and electrospinning. The objective is to tackle the clinical problem of large surface area partial to full thickness burns and wounds where there is a need to replace both the dermal and epidermal layer, either concurrently or sequentially. Emulsion templating is used to develop a dermal skin substitutes which has microporous and nanofibrous architecture while electrospinning is used to create a pseudo-basement membrane as a carrier for cultured epidermal cells.

It is hypothesized that porous scaffolds with added nanostructure will facilitate cell migration and proliferation by providing biological cues to guide cell movement. (14) Emulsion templating is a process where emulsion droplets are used to template protein hydrogel networks to create a hierarchical microporous nanostructured scaffold which would encourage cellular ingress and diffusion of oxygen and nutrients. (15)

Although emulsion templating is commonly used for polymers, there is much progress to be made for templating proteins due to the problem of denaturation. (16) To ensure that protein scaffolds retain their native conformation, a biocompatible emulsion system is required where protein molecules are not denatured by the surfactants or adsorbed onto the interface irreversibly. The control of parameters influencing the mean droplet size of the biocompatible emulsion system is also investigated, which allows for tunability of porosity of the emulsion-templated scaffolds.

Three types of emulsion-templated scaffolds were developed – EmDerm-Collagen, EmDerm-Collagen/Fibrin and EmDerm-Fibrin. The manufacturing parameters, mechanical properties, degradation and biocompatibility of these emulsion templated scaffolds were tested in vitro and in vivo using a variety of assays and animal wound healing models. Electrospun membranes were also characterized and seeded with keratinocytes to investigate the feasibility of using such membranes as a carrier system for delivery of cultured epidermal substitutes.

This would allow a two-stage skin reconstruction process where the dermal layer is applied and allowed to vascularize while autologous skin cells are harvested and grown onto an electrospun membrane carrier and applied once the dermal layer has grafted successfully. Large surface area burns can be managed much more efficiently in this manner.

1.3. Scope of Thesis

In this thesis, a novel bi-layer construct is developed comprising of a dermal emulsion-templated scaffolds and an epidermal electrospun membrane layer. These constructs can be used jointly or independently of each other. The unique microporous nanofibrous architecture of the dermal layer facilitate cellular ingress, vascularization and thus integration of the scaffolds into the wound environment, while the fibrous electrospun membrane provides epidermal coverage for healing.

This thesis comprises of 7 chapters. The first chapter provides a general introduction of the clinical need for tissue scaffolds, introduces the anatomy of skin, physiology of wound healing and an overview of skin substitutes and outlines the aims and objectives of this thesis.

Chapter 2 is a literature review of the clinical use of existing commercially available skin substitutes in burns and diabetic foot ulcers. The efficacy of these skin substitutes was explored in detail with

objective outcome measures. This aim is to summarize all available evidence from clinical trials for skin substitutes. In the second half of this chapter, the fundamental concepts of emulsion-templating, including interfacial chemistry, surface rheology, role of surfactants, protein-surfactant interaction and a brief overview of the use of this technology in manufacture of polymeric high internal phase emulsions (polyHIPE) and lyophilization were explored as well.

Chapter 3 describes the formulation of a biocompatible emulsion system in which protein function is preserved. The key parameters for optimization of EmDerm manufacture including freeze drying parameters, excipient choice, duration of cross-linking, gelation time, rheological assessment of emulsion systems and mechanical properties of the scaffolds were also investigated.

In Chapter 4, the biocompatibility of each scaffold structure was characterized using cell proliferation assays by seeding each EmDerm scaffold with human dermal fibroblasts, human dermal endothelial cells and mesenchymal stem cells. The effects of co-culturing a combination of cell types (HEK/HDF, HDF/HDE and MSC/HDE) were also explored. In addition, a magnetic multiplex assay was used to investigate the proteome and secretome profile of cells seeded onto the scaffolds (mono-culture and co-culture). A panel of degradative enzymes, structural proteins and growth factors integral for extracellular matrix remodelling and angiogenesis were quantified using this assay.

In Chapter 5, the EmDerm scaffolds were tested for biocompatibility in a rat wound healing model. Markers for systemic inflammation were monitored via blood sampling and immunohistochemistry was done on tissue biopsies to examine for presence of localized inflammatory response and vasculogenesis.

In Chapter 6, electrospun membranes were manufactured and seeded with keratinocytes to explore their potential as epidermal substitutes. This would allow for dermal regeneration with EmDerm scaffolds and preparation of a cultured epidermal sheet in vitro for a two-stage full-thickness skin replacement.

Chapter 7 is a summary of conclusions drawn from preceeding chapters and potential areas to explore for future work are identified and discussed.

Chapter 2 Literature Review

2.1. Systematic Review of Skin Substitutes for Acute and Chronic Wounds

In this section, the effect of skin substitutes on acute wounds such as burns and chronic wounds such as diabetic foot ulcers are evaluated through a systematic review of all available randomized controlled clinical trials searched through various databases. A meta-analysis is also performed to quantify the efficacy and adverse effects of skin substitutes in such wounds.

2.1.1.Skin Substitutes for Burns

Introduction

Acute burns cause significant morbidity and mortality worldwide. In particular, adults with >60% total burn surface area (TBSA) and paediatric patients with >40% TBSA are at higher risk of mortality and morbidity even in specialized burns centres. (17) Partial and full thickness burns are often treated with split thickness skin grafts from normal healthy areas of the body, as it is the gold standard treatment for burns. However, in cases whereby large total burn surface areas are involved, there may be limited sites to harvest donor split thickness skin grafts.

Bioengineered skin substitutes provide an alternative means of providing coverage and facilitating wound healing in burn injuries and donor sites of split thickness skin grafts. Various types of skin substitutes have been developed over the years to replace the epidermal and/or dermal layer of native skin. These include but are not limited to acellular matrices, cellular matrices, cell suspensions, amniotic membranes, synthetic membranes, cultured epithelial autografts and allografts as well as preserved cadaveric allografts.

Previous systematic reviews of available clinical trials have been done. (2,18) However, due to increasing availability of various new types of artificial skin, a systematic review and meta-analysis of

all randomized controlled trials published to date to re-evaluate the updated evidence for bioengineered skin substitutes was performed. In this review, both skin substitutes and biological dressings have been included as some types of skin substitutes can also be considered as a biological dressing. Biological dressings such as amniotic membrane and Biobrane do not integrate into the wound as they merely prepare the wound bed for a second stage skin grafting whilst skin substitutes such as Integra and Matriderm engrafts into the wound as the neodermis prior to delayed skin grafting.

Methods

Search strategy

A literature search was performed on several electronic databases as listed below to identify relevant randomized controlled trials:

- The Cochrane Wound Specialist Register
- The Cochrane Central Register of Controlled Trials (CENTRAL)
- Ovid MEDLINE (1946 to 22 December 2015)
- Ovid MEDLINE (In-process & Other Non-Indexed Citations) (1946 to 22 December 2016)
- Ovid EMBASE (1974 to 22 December 2015)
- EBSCO CINAHL (1982 to 22 December 2015)

The search strategy comprised of the following keywords: (bioengineered OR synthetic OR artificial OR biosynthetic OR graft) AND (skin) AND (randomi?ed controlled trials OR RCT) AND (burn OR burns). Studies were limited to randomized clinical trials and humans only but no language or age limits were placed. Several relevant randomized controlled trials were further identified by bibliographic review and citation tracing of selected papers.

Selection criteria

The titles and abstracts of articles identified through the literature search were reviewed. The shortlisted articles were each evaluated to see if they met the pre-defined inclusion criteria:

- Studies must be a randomized controlled trial involving at least one skin substitute (including intra-patient studies) compared to standard wound care.
- Comparative studies between two or more skin substitutes are also included.
- Studies must include patients with burns.
- Studies must involve humans only.
- Studies must include a reproducible and objective method of reporting primary and/or secondary outcomes.

Studies were excluded if they were not randomized controlled trials (e.g. retrospective case studies), did not include any skin substitute (e.g. wound dressings only), do not involve burns or acute/traumatic wounds (e.g. diabetic foot ulcers, venous ulcers), were purely animal studies or only involved subjective outcome measures. The primary outcome of interest was the incidence of complete wound closure or re-epithelialization, percentage graft take and mean time to complete healing or closure of the wounds. Secondary outcomes include change in wound area, rate of wound healing and incidence of adverse effects such as infection, pain, scarring/contracture and length of hospital stay, need for further surgery and mortality.

Data collection and analysis

The full text of potentially relevant abstracts and citations were retrieved. Irrelevant or duplicate publications were excluded and the remaining studies were assessed for eligibility. Data from shortlisted studies was extracted using a standardized data collection proforma. Data extracted included: author, year of publication, type of skin defect (e.g. split thickness skin graft donor, depth of burns), mean

wound size, details of intervention and control, primary and secondary outcome data, duration of follow up and incidence of adverse outcomes (e.g. infection, cellulitis, mortality).

Assessment of methodological quality and reporting bias

Methodological quality of each study was assessed for risk of bias using the Cochrane tool for assessing risk of bias. Each study was evaluated for random sequence generation, allocation concealment, blinding of participants and personnel, blinding of outcome assessment, incomplete outcome data, selective reporting and other bias (e.g. sponsorship from companies).

Statistical analysis and data synthesis

Summary statistics including means, standard deviations, medians and ranges of primary and secondary outcomes were extracted from each study. For continuous variables, pooled means and standard deviations of each reported outcome was compiled into Forest plots and weighted mean difference was calculated. For dichotomous data, pooled risk ratios were calculated using the Mantel-Haenszel method. Where possible, subgroup analysis for similar studies was done. Statistical significance was set at $p<0.05$ and confidence intervals at 95% were determined. Each study was also assessed for degree of heterogeneity using the I^2 data statistic. A value of I^2 of more than 80% is considered to have significant heterogeneity. Statistical analysis was done on RevMan 5.3 Review Manager (The Nordic Cochrane Centre, Copenhagen, Denmark).

Results

Search outcomes

Initially, 1744 articles were identified using the search strategy as mentioned above. After title and abstract screening, 65 articles were selected for a more thorough full text review. A total of 30 articles were eligible for inclusion based on selection criteria of this review.

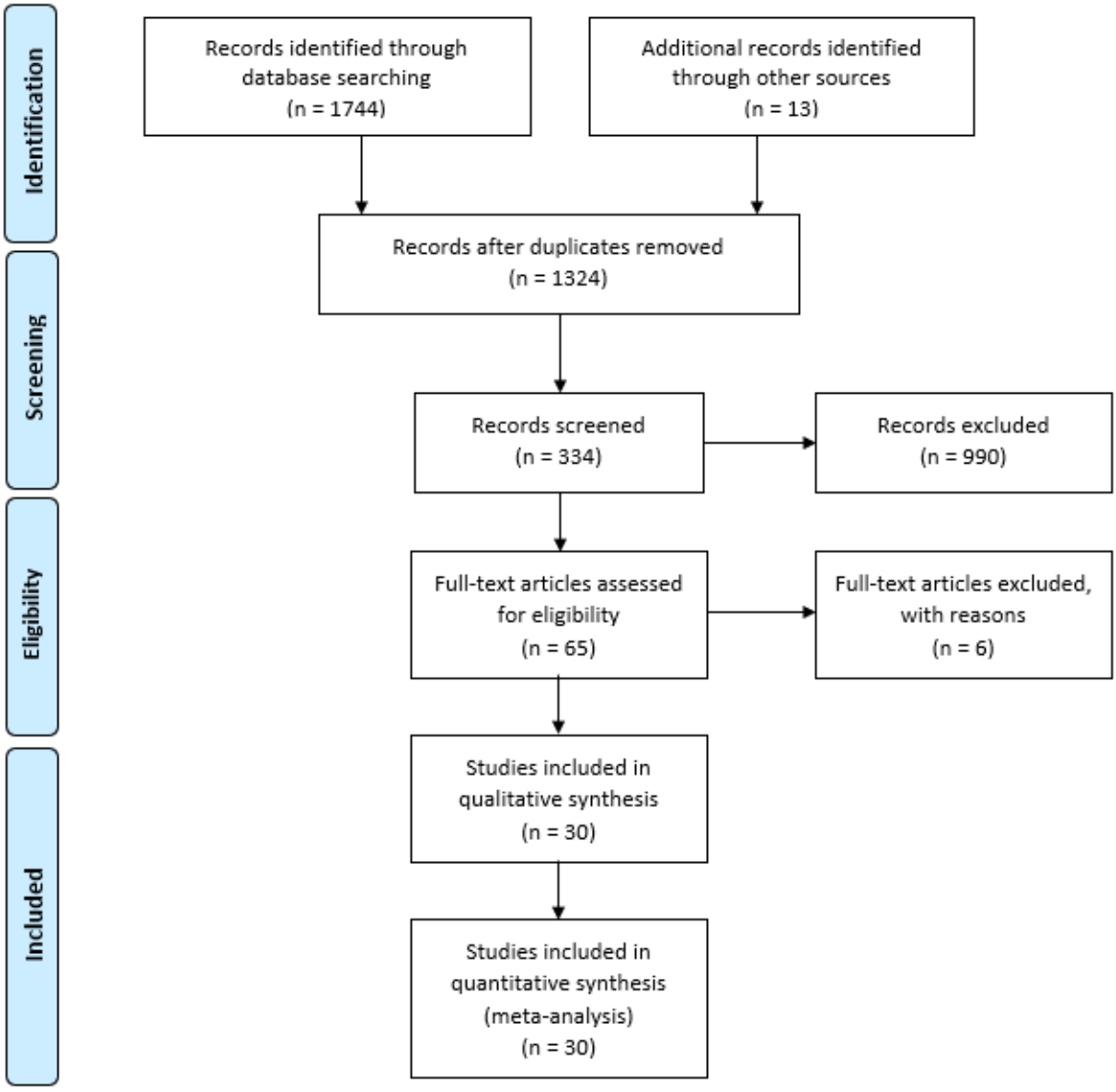


Figure 2-1 PRISMA Flowchart for study selection for burns.

Methodological quality of included studies

A large proportion of studies did not specify method of random sequence generation nor had any mention of allocation concealment. Blinding of participants and outcome assessment was also not done in many studies, as the nature of skin substitutes used made it difficult for blinding. Incomplete data reporting was encountered in several studies, as patients were lost to follow up. In addition, attrition bias was difficult to assess, as some studies did not report number of patients followed-up long term for assessment of quality of scarring. As far as possible, intention-to-treat analysis was done to limit risk of bias from incomplete data reporting. Selective reporting was minimal across studies analysed as most studies reported the pre-defined primary and secondary outcomes. However, several studies that focussed on histological analysis did not include complete clinical data, which limited the extractable data for downstream meta-analysis.

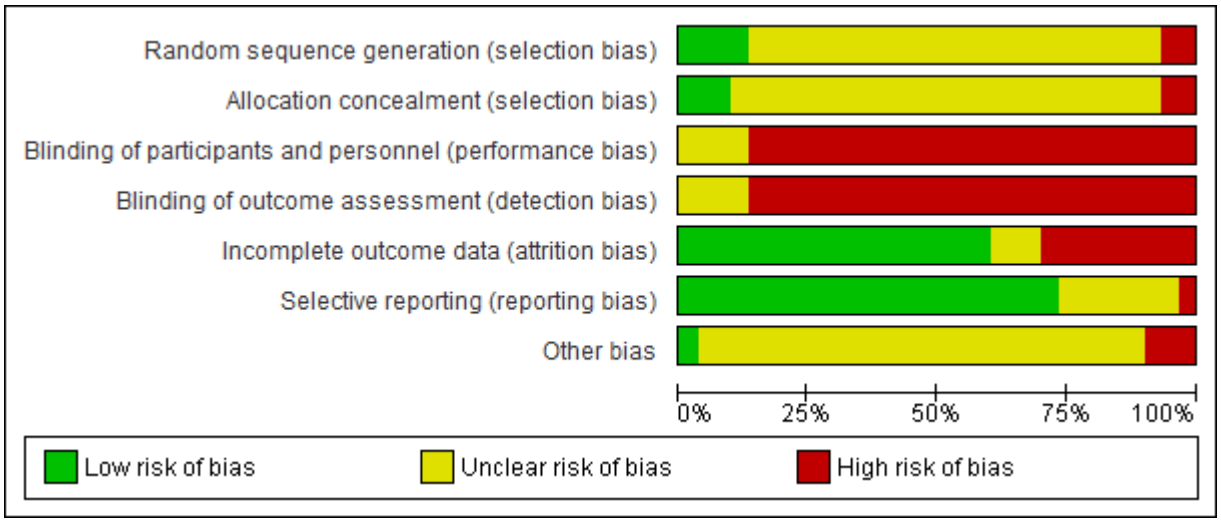


Figure 2-2 Diagrammatic representation of overall study quality for burns.



Figure 2-3 Risk of bias summary for studies on burns.

Primary and Secondary Outcomes

In total, 30 studies, comparing 12 different skin substitutes were included in the systematic review. These include amniotic membrane, Integra, Biobrane, Matriderm, Apligraf, Trancyte (Dermagraft TC), Suprathel, cadaveric allografts (e.g. Alloderm), Xenoderm, autologous cultured skin substitutes (CSS), cultured epithelial allografts (CEA), autologous keratinocyte suspensions (e.g. ReCell). Meta-analysis of outcomes was also performed to pool results from similar studies to compare outcomes of each skin substitute as well.

Number of wounds healed

Pooled risk ratio shows that skin substitutes do not significantly increase number of wounds healed (RR 0.93, CI 0.74, 1.19). Amniotic membrane appears to improve number of wounds healed but this was not statistically significant (RR 1.57, CI 1.01, 2.44). (19) Biobrane does not significantly improve number of burns healed (RR 0.98, CI 0.80, 1.19). (20) Integra did not significantly change number of wounds healed (RR 0.90, CI 0.69, 1.18). (21) Glycerol preserved allografts did not significantly improve number of wounds (RR 0.89, CI 0.64, 1.24). (22) Suprathel was shown to significantly reduce number of wounds healed compared to split-thickness skin grafts (RR 0.50, CI 0.29, 0.86). (23)

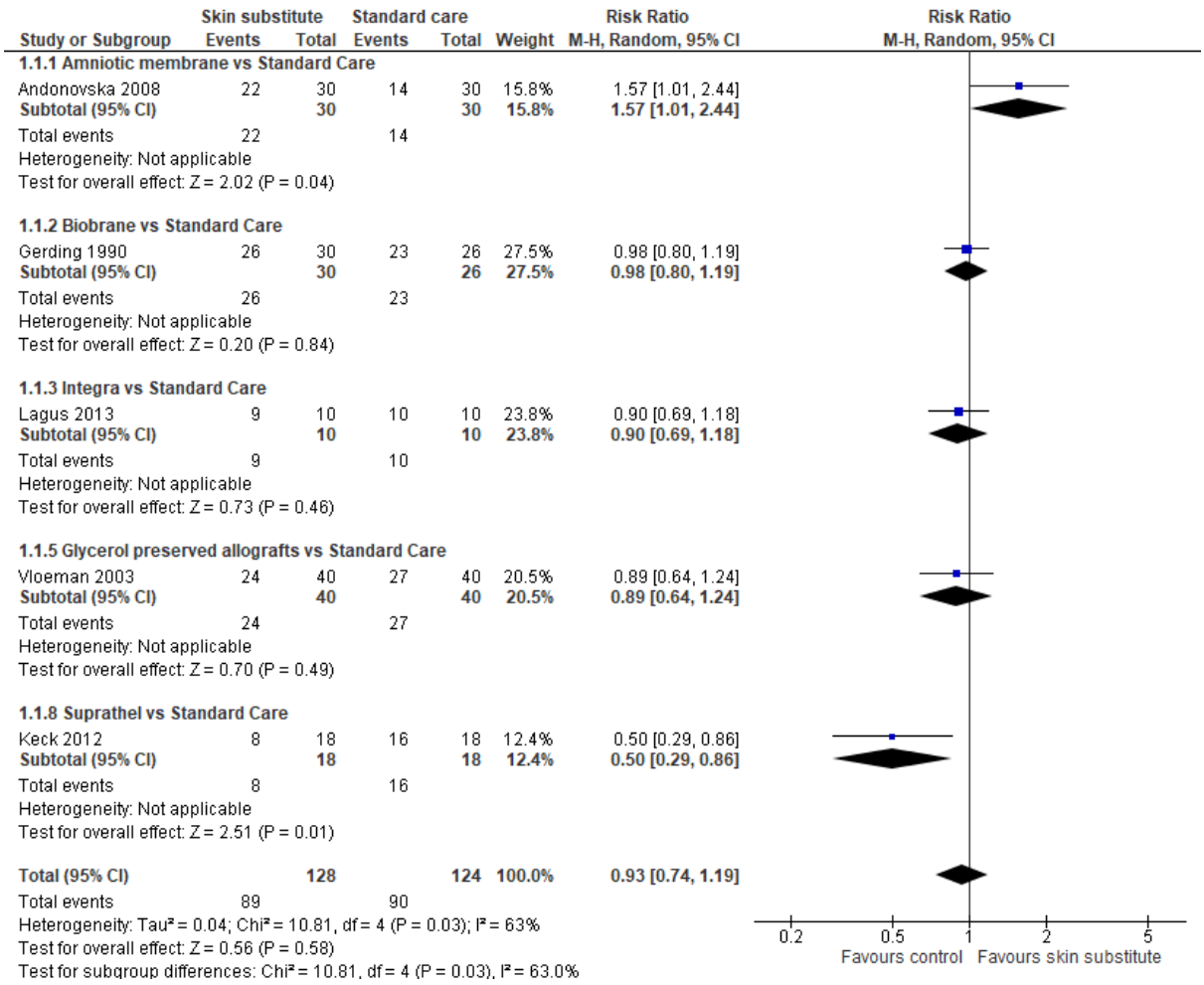


Figure 2-4 Forest plot of number of wounds healed comparing skin substitute vs standard care for burns.

Mean time to healing

Skin substitutes significantly reduced mean time to wound healing overall (WMD -3.79, CI -5.38, -2.20). Amniotic membrane significantly improved mean healing time (WMD -2.01, CI -2.77, -1.25). (24,25) Biobrane significantly reduced mean time to healing (WMD -3.68, CI -5.99, -1.37). (20,26,27) Transcyte also significantly reduced mean time to healing for burns compared to standard care (WMD -6.24, CI -8.44, -4.03). (28,29) Integra was also shown to reduce mean healing time (WMD -3.70, CI -5.21, -2.19). (30)

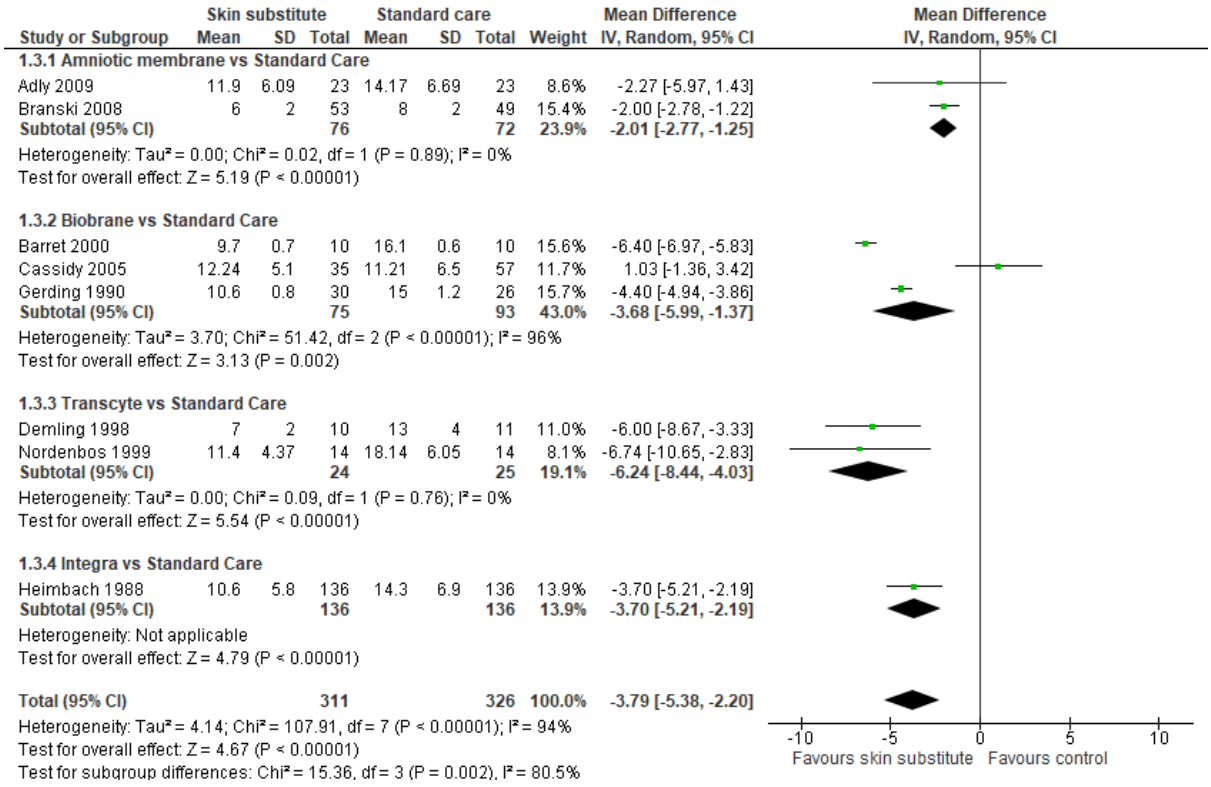


Figure 2-5 Forest plot of mean time to healing comparing skin substitute vs standard care for burns.

Percentage graft take

Skin substitutes did not significantly increase percentage of graft take overall (WMD 3.14, CI -16.12, 22.40). Amniotic membrane was the only skin substitute which significantly increased percentage of graft take (WMD 22.77, CI 19.72, 25.80). (31) Autologous cultured skin substitutes resulted in decreased percentage graft take (WMD -9.60, CI -10.50, -8.70). (32) Epithelial cells cultured on Matriderm did not significantly change percentage of graft take (RR -1.00, CI -7.50, 5.50). (33) Alloderm did not significantly improve percentage of graft take (RR 0.30, CI -6.77, 7.37). (34)

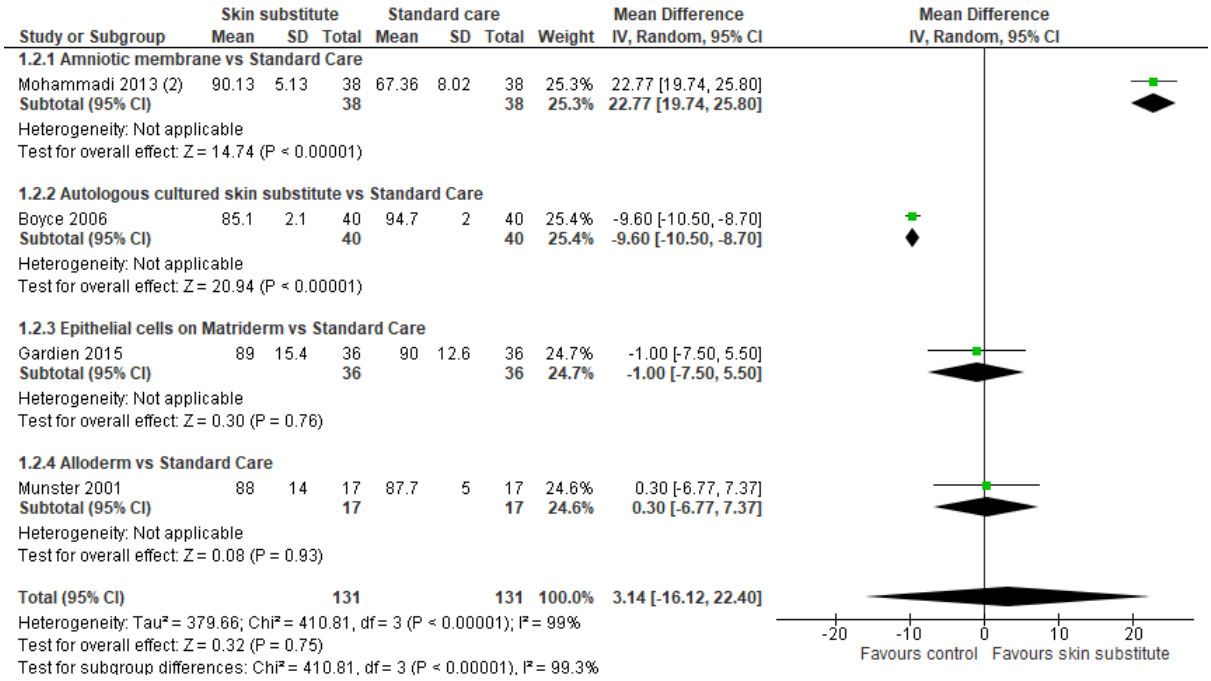


Figure 2-6 Forest plot for percentage graft take comparing skin substitute vs standard care for burns.

Percentage wound area healed

Mean percentage wound area epithelialized was not significantly higher in patients treated with skin substitutes (WMD -18.62, CI -45.34, 8.11). Autologous cultured skin substitute resulted in lower percentage wound area healed compared to STSG (WMD -31.60, CI -32.59, -30.61). (32) Meanwhile, Matriderm with epithelial cells did not significantly change percentage wound area healed compared to standard care (WMD -4.30, CI -16.16, 7.56). (33)

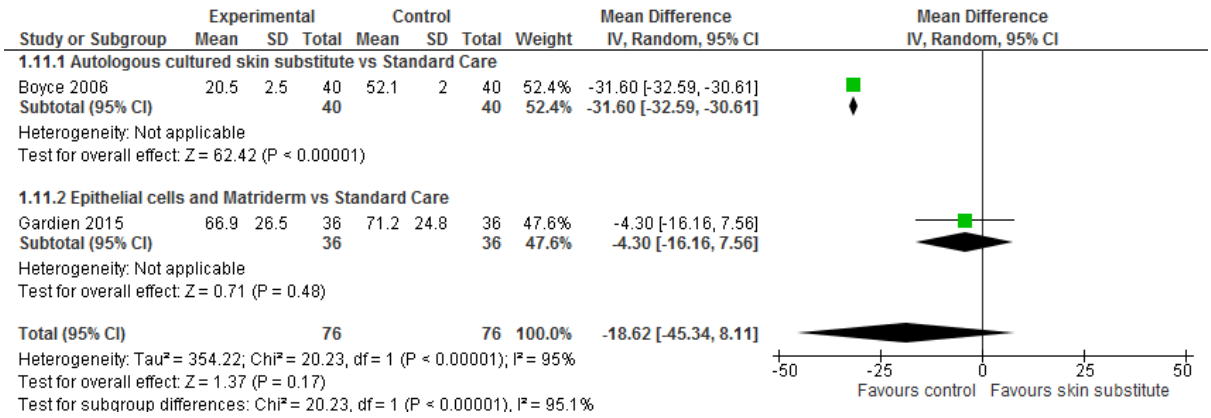


Figure 2-7 Forest plot for percentage wound healed/epithelialized comparing skin substitute vs standard care for burns.

Scarring (Vancouver Scar Scale)

Scarring outcomes as measured by the Vancouver Scar Scale (VSS) were better in patients treated with skin substitutes compared to controls overall (WMD -1.52, CI -2.43, -0.61). Integra appears to improve scaring outcomes (WMD -2.30, CI -3.52, -1.08). (35) Alloderm did not significantly result in better scarring outcomes compared to standard care. (WMD -0.66, CI -1.59, 0.27). (34) Transcyte also reduced VSS scores in patients with burns (WMD -1.75, CI -2.61, -0.89). (29)

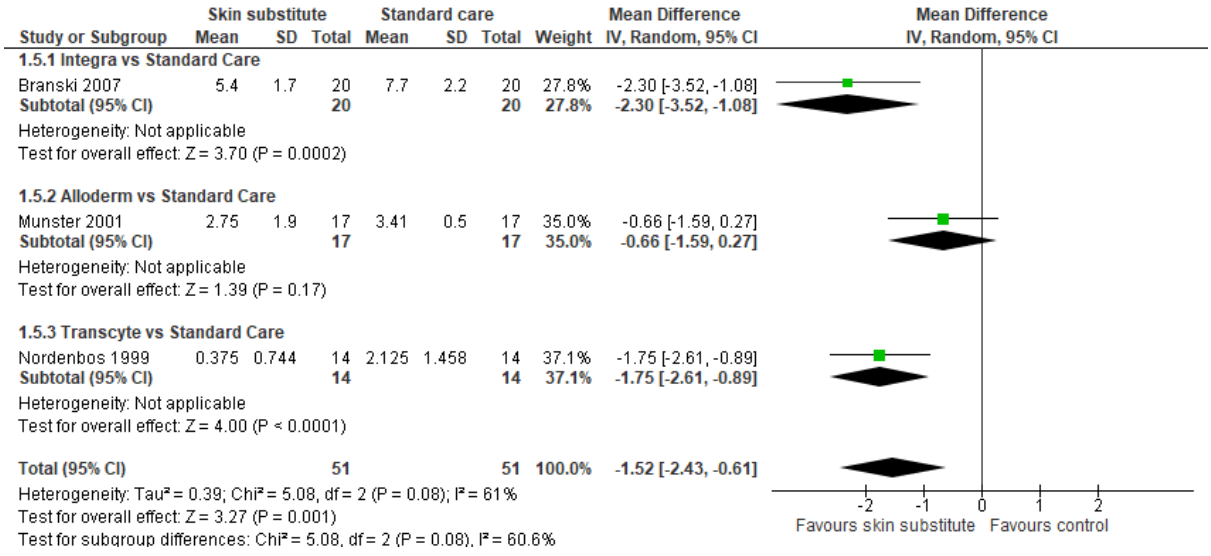


Figure 2-8 Forest plot for Vancouver Scar Scale comparing skin substitute vs standard care for burns.

Pain (VAS)

Pain as measured by Visual Analogue Scale (VAS) was reduced in patients treated with skin substitutes overall (WMD -2.19, CI -3.43, -0.94). Biobrane did not reduce pain scores in patients with burns (WMD -1.07, CI -3.01, 0.88) (20,27) while Transcyte improved pain scores in patients with burns (WMD -3.00, CI -3.86, -2.14). (28) ReCell improved pain scores as well (WMD -3.50, CI -4.11, -2.89). (36)

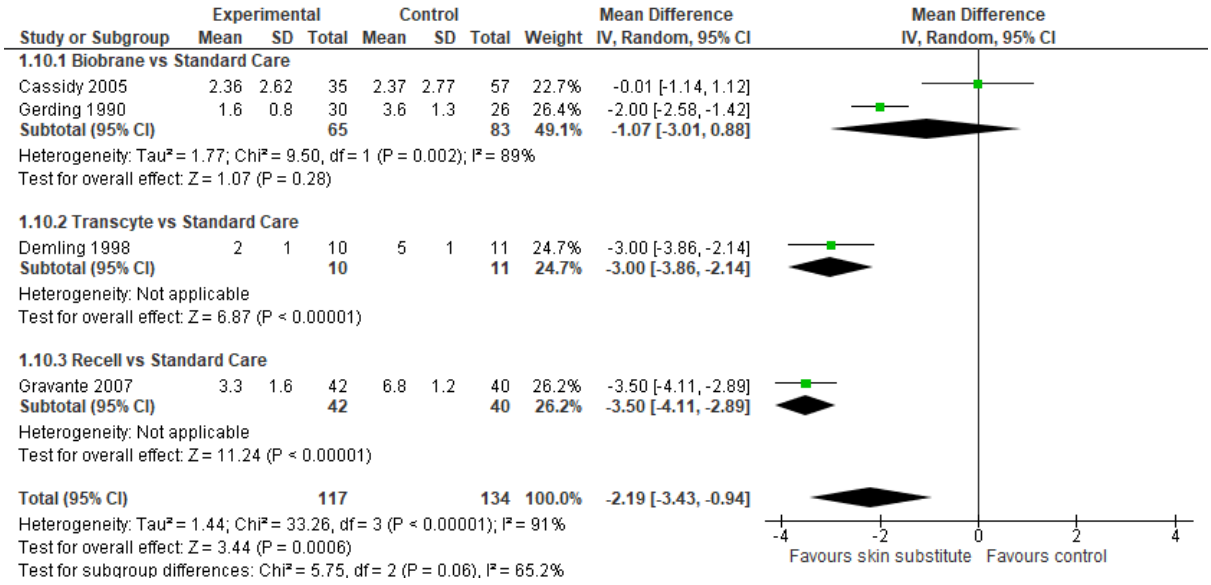


Figure 2-9 Forest plot for pain assessment as per visual analogue scale (VAS) comparing skin substitute vs standard care for burns.

Need for further surgery

The use of skin substitutes did not change the need for additional surgery for patients with burns overall (RR 0.35, CI 0.10, 1.23). However, Transcyte did significantly reduce need for further surgery in burns patients (RR 0.12, CI 0.03, 0.44) (29,37,38) and Euroskin reduce rate of further surgery in patients with burns as well (RR 0.33, CI 0.15, 0.75). (22) Meanwhile, Biobrane and ReCell did not significantly reduce need for additional surgery (RR0.87, CI 0.06, 13.18 and RR 0.12, CI 0.01, 1.80 respectively). (20,39) Autologous cultured skin substitutes appears to increase rate of further surgery (RR 27.00, CI 1.66, 439.27). (32)

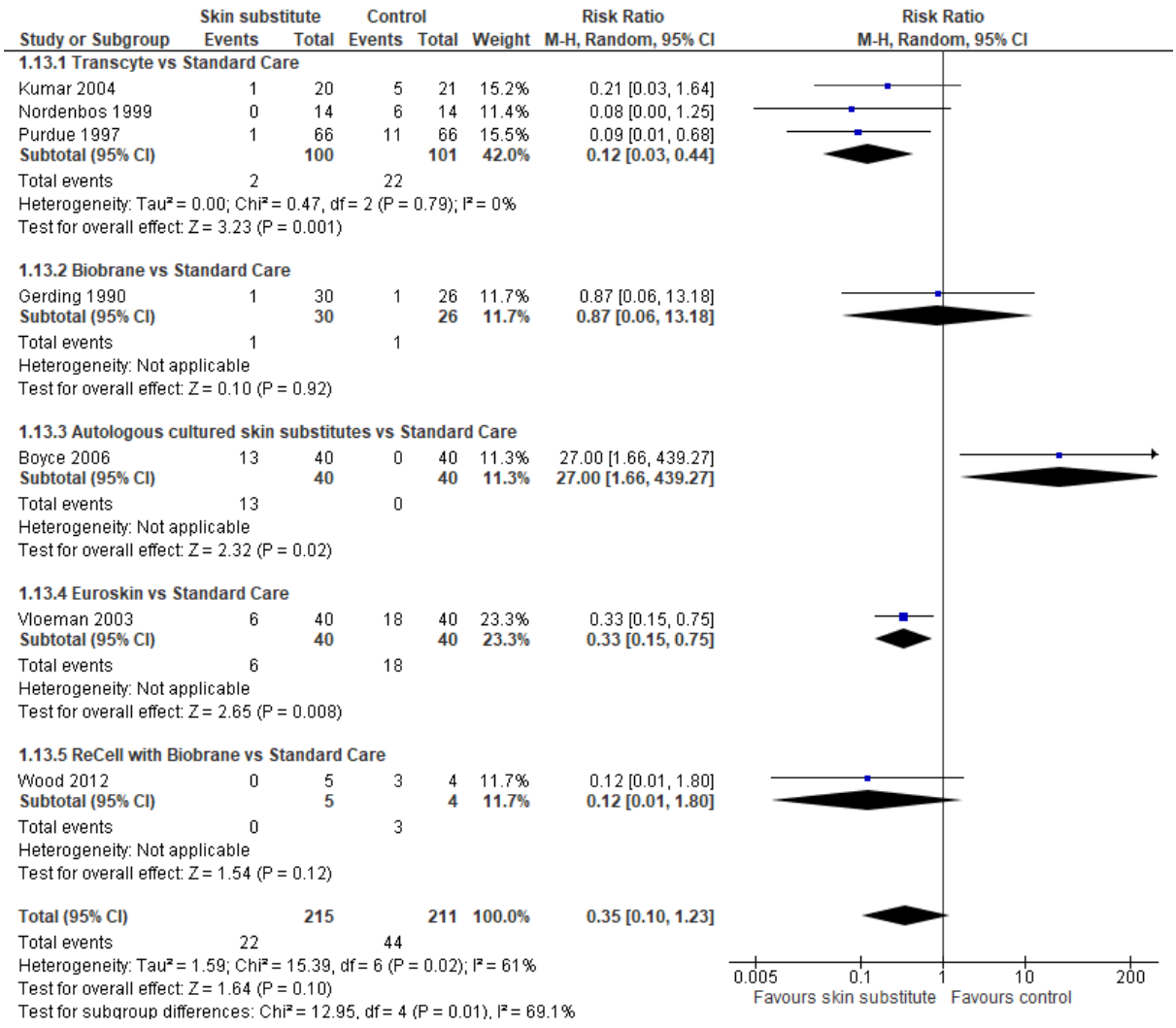


Figure 2-10 Forest plot for need for further surgery comparing skin substitute vs standard care for burns.

Length of hospital stay

The use of skin substitutes did not affect length of hospital stay in patients with burns overall (WMD -4.86, CI -14.71, 4.99). Biobrane significantly reduced length of hospital stay in burns patients (WMD -10.66, CI -13.64, -6.47) (26) while amniotic membrane did not affect duration of hospitalization (WMD 0.00, CI -0.39, 0.39). (25)

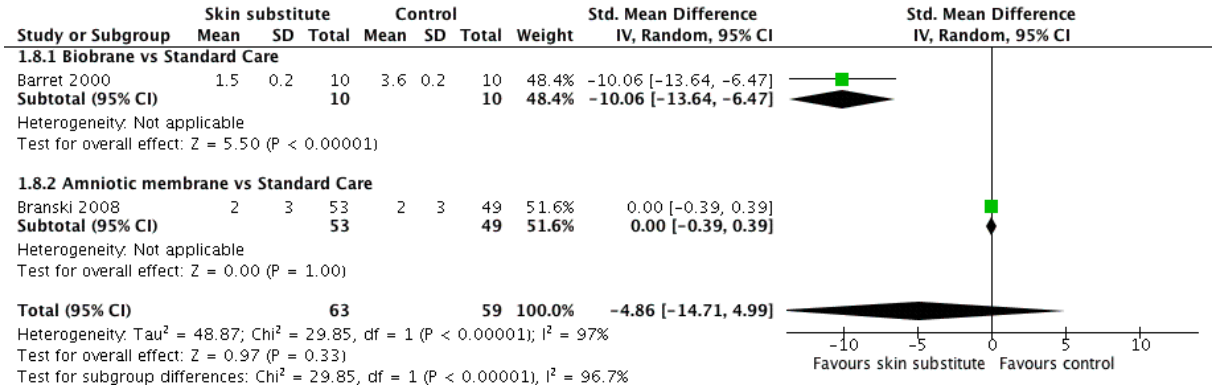


Figure 2-11 Forest plot for length of hospital stay comparing skin substitute vs standard care for burns.

Infection rate

Rate of infection was significantly reduced in patients treated with skin substitutes compared to controls (RR 0.53, CI 0.34, 0.83). Xenoderm appears to reduce rate of infection (RR 0.44, CI 0.20, 0.96). (40) Amniotic membrane marginally reduced rate of infection but this was not statistically significant (RR 0.55, CI 0.30, 1.01). (19,24) Biobrane and Transcyte did not significantly alter rate of infection in patients with burns (RR 1.31, CI 0.31, 5.57 and RR 0.08, CI 0.00, 1.25 respectively). (29,41)

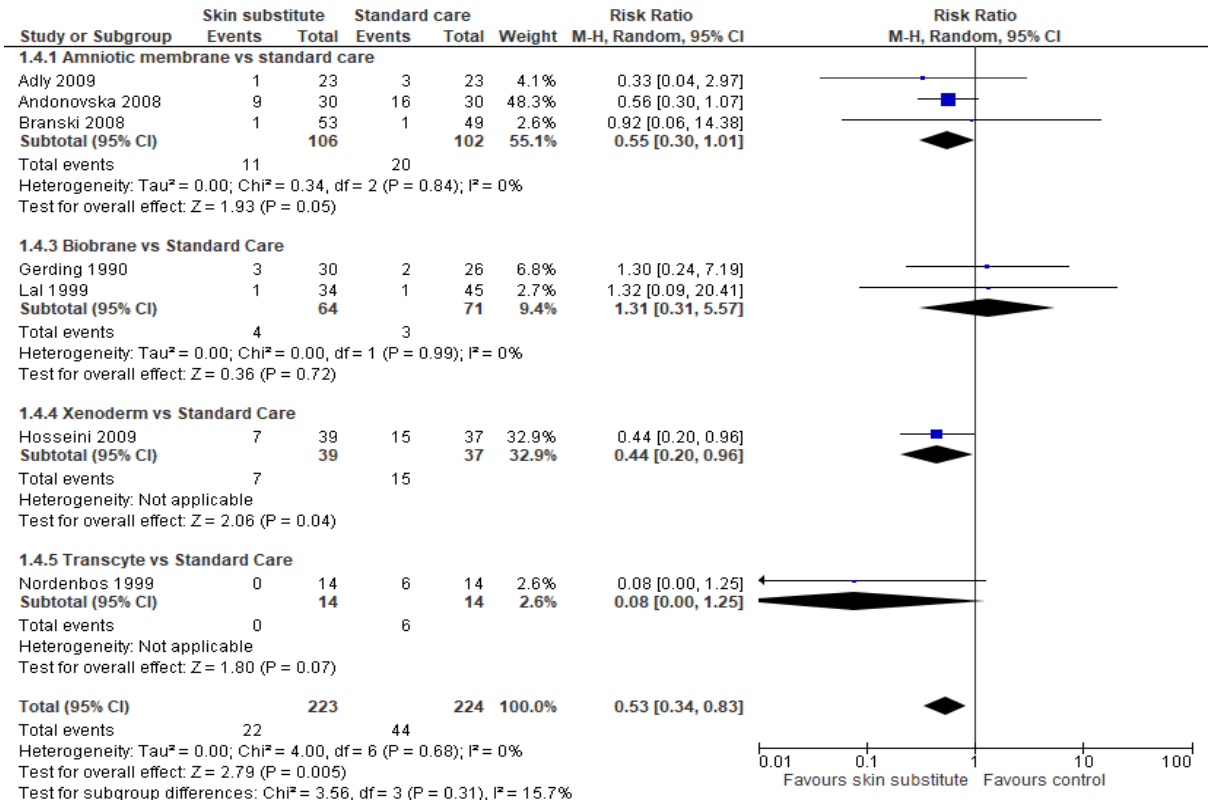


Figure 2-12 Forest plot for infection rate comparing skin substitute vs standard care for burns.

Hypertrophic scarring

Hypertrophic scarring was not significantly different in patients treated with skin substitutes overall (RR 0.80, CI 0.24, 2.65). Amniotic membrane and glycerol preserved allografts did not significantly result in difference in incidence of hypertrophic scarring in patients (RR 1.04, CI 0.44, 2.48 and RR 0.20, CI 0,01, 3.35 respectively). (25,42)

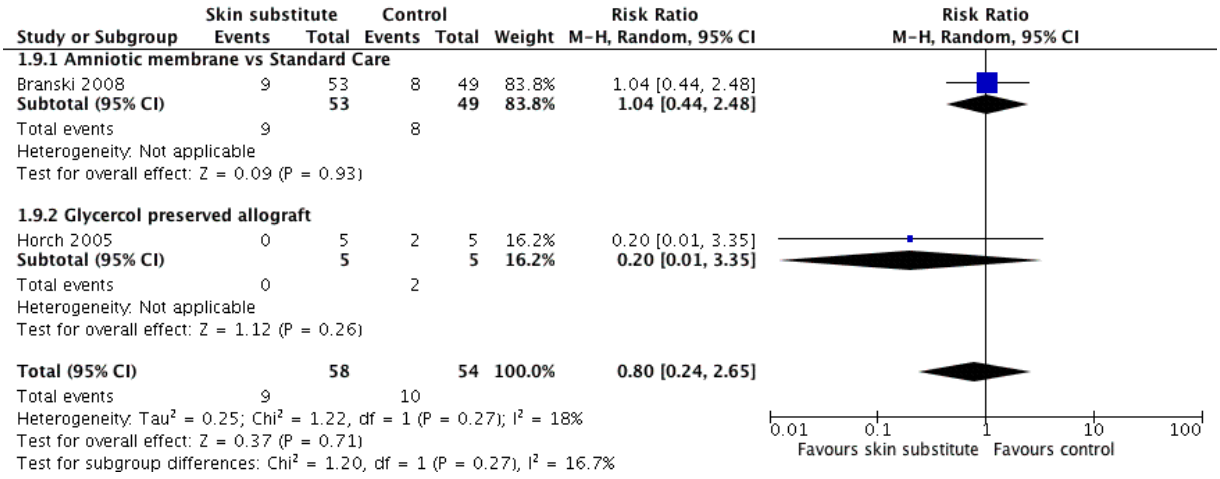


Figure 2-13 Forest plot for hypertrophic scarring comparing skin substitute vs standard care for burns.

Author (Year)	Treatment (number of patients)	Control (number of patients)	Number of wounds; Type of wounds; Mean TBSA (%) or wound size (cm^2)	Primary outcome (percentage wounds healed)		Secondary Outcome	Adverse Outcomes	Duration of follow up
				Treatment n/N (%)	Control n/N (%)			
Burns								
Adly 2009 (24)	Biomembrane (amnion) (23)	Polyurethane (23)	46 burns 2nd and 3rd degree burns Mean TBSA 7.7%	NR	NR	Mean time to healing: B: 11.9 ± 6.09 days Control: 14.17 ± 6.69 days	Infection: B: 1/23 Control: 3/23 Pain: B: 4/23 (17.4%) Control: 11/23 (47.8%)	21 days
Andonovska 2008 (19)	Amnion (30)	Vaselin gauze (30)	60 wounds Dermal and subdermal burns Mean TBSA unclear	22/30	14/30	NR	Infection: AM: 9/30 Control: 16/30	7 days
Barret 2000 (26)	Biobrane (10)	1% silver sulfadiazine (10)	20 wounds 2nd degree paediatric burns Mean TBSA 7.8-8.9%	NR	NR	Length of stay: B: 1.5 ± 0.2 days Control: 3.6 ± 0.2 days Time to healing: B: 9.7 ± 0.7 days Control: 16.1 ± 0.6 days	No infection in both groups	2-3 weeks
Branski 2007 (35)	Integra (20)	Meshed autograft with allograft overlay (20)	20 paired wounds Large surface area burns (>50% TBSA) Mean TBSA 73 ± 15%	NR	NR	Length of stay: I: 41 ± 4 days Control: 39 ± 4 days	Mortality: Integra: 40% Control: 30% Scarring (12 mth): Integra: 5.4 ± 1.7 Control: 7.7 ± 2.6	24 months
Branski 2008 (25)	Amnion (53)	Topical antimicrobials (49)	102 wounds Facial, head and neck partial thickness burns in paediatric patients Mean TBSA 11-12%	NR	NR	Length of hospital stay: AM: 2 ± 3 days Control: 2 ± 3 days Time to heal: AM: 6 ± 2 days Control: 8 ± 2 days	Infection: AM: 1/53 Control: 1/49 Hypertrophic scarring: AM: 9/53 Control: 8/49	1 year
Boyce 2002 (43)	Autologous cultured skin substitute (12)	STSG (12)	45 paired wounds Full thickness burns Mean TBSA 76.9% ± 2.76%	NR	NR	Percentage engraftment (Day 14): CSS: 89.2% ± 2.5% STSG: 94.9% ± 3.6% TBSA close at 28 days: CSS: 16.7% ± 2.6% STSG: 58.7% ± 1.8%	Regrafting: CSS: 2/12 STSG: 0/12	28 days
Boyce 2006 (32)	Autologous cultured skin substitutes (40)	STSG (40)	40 paired wounds Full thickness burns Mean TBSA 73.4%	NR	NR	Take rate at 14 days: CSS: 85.1 ± 2.1% STSG: 94.7 ± 2% % TBSA closed at 28 days: CSS: 20.5 ± 2.5% STSG: 52.1 ± 2%	Scarring (VSS): CSS: 2 STSG: 2.5 Regrafting rate: CSS: 13/40 STSG: 0/40	28 days
Cassidy 2005 (27)	Biobrane (35)	Duoderm (57)	92 wounds Intermediate thickness TBSA <10%	NR	NR	Mean time to healing: B: 12.24 ± 5.1 days D: 11.21 ± 6.5 days	Pain (VAS): B: 2.36 ± 2.62 D: 2.37 ± 2.77	2-3 weeks
Demling 1998 (28)	TranCyte (10)	Bacitracin (11)	21 wounds Partial thickness facial burns TBSA >50% facial area	NR	NR	Mean time to healing: T: 7 ± 2 days Control: 13 ± 4 days Wound care time: T: 0.35 ± 0.1 days	Pain (VAS): T: 2 ± 1 Control: 4 ± 2	2 weeks

						Control: 1.9 ± 0.5 days		
Gardien 2015 (33)	Autologous EC on Matriderm + STSG (36)	STSG only (36)	36 wounds Full thickness burns Mean TBSA 24%	NR	NR	Mean area epithelialized: Matriderm: 66.9 ± 26.5% Control: 71.2 ± 24.8% Graft take: Matriderm: 89 ± 15.4% Control: 90 ± 12.6%	Scarring POSAS (12 month): Matriderm: 18.2 ± 10.2 Control: 14.2 ± 7.2	12 months
Gerding 1988 (44)	Biobrane (27)	Silver sulfadiazine (23)	50 wounds Partial thickness burns Mean TBSA 6.3%	20/27	11/23	Mean healing time: B: 13.7 ± 1.3 days SSD: 21.3 ± 2.3 days	Pain: B: 2.4 ± 0.13 SSD: 3.8 ± 0.17 Need for surgery: B: 4/27 SSD: 5/23 Infection: B: 4/27 SSD: 4/23	3 weeks
Gerding 1990 (20)	Biobrane (30)	Silver sulfadiazine (26)	56 wounds Partial thickness burns TBSA 2.2%	26/30	23/26	Mean healing time: B: 10.6 ± 0.8 SSD: 15.0 ± 1.2	Pain: B: 1.6 ± 0.8 SSD: 3.6 ± 1.3 Infection: B: 3/30 SSD: 2/26 Need for surgery: B: 1/30 SSD: 1/26	2 weeks
Gravante 2007 (36)	ReCell (42)	STSG (40)	82 wounds Deep partial thickness burns Mean area 180-186 cm^2	NR	NR	Mean healing time: R: 13 days Control: 12 days	Contracture: R: 12/42 Control: 15/40 Pain: R: 3.3 ± 1.6 Control: 6.8 ± 1.2	2-3 weeks
Heimbach 1988 (30)	Integra	Control (dressing, autologous, allograft, xenograft)	139 wounds Mean burn area 46.5 ± 15% TBSA	86 ± 21 (Epidermal) 62 ± 4 (Integra)	66 ± 8	Mean healing time: I: 10.6 ± 5.8 Control: 14.3 ± 6.9	Hypertrophy: I: 42% Control: 57%	1 year
Hosseini 2009 (40)	Xenoderm (39)	Silver sulfadiazine (37)	78 wounds Partial thickness burns 10-60% TBSA	NR	NR	NR	Infection: X: 7/39 (17.9%) Control: 15/37 (40%) Hospital stay <1 wk: X: 31/29 Control: 15/37	5 weeks
Horch 2005 (42)	Glycerol preserved cadaver skin (5)	Silver sulfadiazine (5)	5 paired wounds Superficial/deep facial partial thickness burns Mean area unclear	NR	NR	% re-epithelialisation: G: 10.5% S: 12.4%	Hypertrophic scarring: G: 0/5 S: 2/5	6 months
Keck 2012 (23)	Suprathel (18)	STSG (18)	18 paired wounds Deep dermal burns Median 17.5% TBSA Wound size 100cm^2	8/18 (44.4%)	16/18 (88.9%)	NR	Scarring VSS (Day 90): Suprathel: 3 (0-9) STSG: 2 (2-5)	90 days
Kumar 2004 (37)	TransCyte (20) Biobrane (17)	Silver sulfadiazine (21)	Partial thickness burns Paediatric patients 5% TBSA	NR	NR	Mean time to healing: T: 9.5 days B: 9.5 days S: 11.2 days	Need for autografting: T: 1/20 B: 3/17 S: 5/21	Unclear
Lal 1999 (41)	Biobrane (41)	Topical treatment (48)	89 wounds	NR	NR	Time to heal/ % TBSA:	Infection:	21 days

			Superficial scalds Paediatric patients < 25% TBSA			B: 1.5 days Control: 2.3 days Length of hospital stay/ % TBSA: B: 0.3 days Control: 0.5 days	B: 1/34 Control: 1/45 Failure: B: 2/34 Control: NR	
Lagus 2013 (21)	Integra (10)	STSG (10) Cellonex (10)	30 wounds Deep 3rd degree burns Mean area 50cm^2	9/10	10/10	NR	Scarring (VSS) at 3 mths/12 mths: Integra 2.5/1.3 STSG 2.5/0.8 Cellonex 2.0/0.8	12 months
Mohammaddi 2013 (31)	STSG with amnion (54)	STSG with staples (54)	108 wounds 2nd to 3rd degree burns on extremities 4-15% TBSA	NR	NR	Take rate: AM: 96.76% Control: 88.79% Time to take: AM 6.98 ± 1.35 Control 13.9 ± 1.66	NR	21 days
Mohammaddi 2013 (45)	STSG with amnion (38)	STSG with vaselin gauze (38)	76 wounds Chronic burn wounds Mean TBSA 29%	NR	NR	Take rate: AM: 90.13 ± 5.13% Control: 67.36 ± 8.20%	NR	21 days
Munster 2000 (34)	A: Alloderm + STSG (17)	B: Alloderm ± delayed STSG (17) C: STSG only (17)	17 wounds Third degree burns Mean area 28.7cm^2	NR	NR	Graft take: A: 88 ± 14 % B: 75 ± 9 % C: 87.7 ± 5% Donor healing time: Alloderm: 8.4 ± 1.7 days STSG only: 12.7 ± 2.2 days	Scarring (VSS): Alloderm: 2.75 ± 1.9 STSG only: 3.41 ± 0.5	1 year
Noordenbos 1999 (29)	TransCyte (14)	Silver sulfadiazine (14)	14 paired wounds Partial thickness burns %TBSA 3.1-3.6 cm^2	NR	NR	Mean time to healing: T: 11.4 ± 4.37 days Control: 18.14 ± 6.05 days	Infection: T: 0/14 Control: 6/14 Need for surgery: T: 0/14 Control: 2/14 VSS (1 year): T: 0.375 ± 0.744 Control: 2.125 ± 1.458	1 year
Purdue 1997 (38)	Dermagraft TC (66)	Allograft (66)	66 paired wounds Partial to full thickness burns Mean TBSA 44%	NR	NR	Graft take (Day 14): D: 94.7% Control: 93.1%	Need for surgery: D: 1/66 Control: 11/66	28 days (post-autograft)
Ryssel 2007 (46)	Matriderm + STSG - sheet (3) - mesh (5)	STSG only - sheet (6) - mesh (7)	28 wounds (incomplete data) Partial to full thickness burns Mean TBSA 45.6%	83.4% (1 week)	82.5% (1 week)	NR	VSS (3 - 4 months): M: 3 Control: 6	3-4 months
Selig 2013 (47) (1 year follow up from Keck 2012)	Suprathel (11)	STSG (11)	11 paired wounds Deep dermal burns Median 17.5% TBSA Wound size 100cm^2	As below	As below	NR	Median VSS: Suprathel 2 (0-6) STSG 3 (1-3)	1 year
Uhlig 2006 (48)	A: Suprathel (22) B: Suprathel (24)	Paraffin gauze (22) Omniderm (24)	A: 22 paired wounds; B 24 paired wounds Partial thickness burns A: 380 cm^2; B: 479 cm^2	NR	NR	NR	Pain (VAS): Suprathel (A) 9 Paraffin gauze (A) 21.7 Omniderm (B) 10.5 Paraffin gauze (B) 16.3	3 months

Vloemans 2003 (22)	Glycerol preserved allografts (Euroskin) (40)	Aquacel (40)	89 wounds Partial thickness burns not healed within 14 days 8.3 ± 5.2 % TBSA	24/40	27/40	% Epithelialization: E: 78.3% Control: 84.7% Days to epithelialization: E: 8.5 days Control: 10.1 days	Surgery: E: 6/40 Control: 18/40 Hypertrophy: E: 30% Control: 52.5%	10 weeks
Waymack 2000 (49)	Meshed Apligraft on STSG (38)	Meshed autograft on STSG (38)	38 wounds Partial-Full thickness burns 26.3% TBSA	% autograft take >75%: 100%	% autograft take >75%: 100%	Time to 75% take: 7 days (both groups)	VSS at 24 mths: Apligraft 2.55 Control 4.89	24 mths
Wood 2012 (39)	Biobrane+ReCell (5)	Biobrane only (4) Intrasite/Acticoat/ Duoderm (4)	13 paired wounds >2% TBSA scald injuries not healed in 10 days	Biobrane+Recell 95% (D10) 100% (D21)	Biobrane only 83.2% (D10) 97.7% (D21) Control 71.2% (D10) 90.1% (D21)	Median time to healing: B+R 16 days B 16 days Control 36.5 days	VSS: B+R 3.5 B 4.25 Control 4.25 Need for surgery (D10): B+R 0/5 B 1/4 Control 3/4	6 months
Yi 2015 (50)	ADM + STSG (9)	STSG only (10)	19 wounds Full thickness skin defects of extremities Median defect size 19-25 cm^2	NR	NR	Partial necrosis: ADM: 1/9 Control: 0/10	VSS: ADM: 4.6 Control: 7.9	12 weeks

Table 2-1 Summary of outcomes from studies involving skin substitutes for burns.

SKIN SUBSTITUTES	ADVANTAGES	DISADVANTAGES
AMNIOTIC MEMBRANE	• Increased number of wounds healed • Reduced mean time to healing • Increased percentage graft take	• No difference in length of hospital stay • No difference in infection rate • No difference in hypertrophic scarring
INTEGRA	• Reduced mean time to healing • Reduced scarring	• No difference in number of wounds healed
BIOBRANE	• Reduced mean time to healing • Reduced length of hospital stay	• No difference in number of wounds healed • No difference in pain • No change in need for further surgery • No difference in infection rate
MATRIDERM		• No difference in percentage graft take • No difference in percentage area healed
TRANSCYTE	• Reduced mean time to healing • Reduced scarring • Reduced pain • Reduced need for further surgery	• No difference in infection rate
SUPRATHEL		• Reduced number of wounds healed
CADAVERIC ALLOGRAFTS	• Reduced need for further surgery	• No difference in number of wounds healed • No difference in scarring • No difference in hypertrophic scarring
XENODERM	• Reduced rate of infection	
AUTOLOGOUS CULTURED SKIN SUBSTITUTES		• Reduced percentage graft take • Reduced percentage area healed • Increased need for further surgery
AUTOLOGOUS KERATINOCYTE SUSPENSION	• Reduced pain	• No difference in need for further surgery

Table 2-2 Summary of outcomes from meta-analysis by type of skin substitute for burns.

Discussion

Limitations of this review

Pooling of results between studies was difficult due to differences in types of skin substitutes, standard care dressings, time points for assessing healing outcomes and types/depth of wounds. Some studies involve the use of acellular scaffolds, while others involved the use of cellular scaffolds, allografts or cell-based therapy. There was a lack of consistency in standard care dressings with some studies using split thickness skin grafts alone or ointments as control. Depth of burns were also not clearly reported as burns often involve varying degrees of burn depending on location of the injury. Other confounding factors include differences in patient care e.g. timing to tangential excision, total burn surface area, use of antibiotics, surgical technique in skin grafting and types of wounds.

Despite the large number of studies, most studies were rather small with less than 30 patients and were insufficiently powered to achieve statistical significance. The studies also cover a wide patient demographic without a clear distinction between paediatric and adult populations in some instances.

Outcome reporting were also highly variable across studies. Several studies reported number of wounds healed at different time-points rather than giving mean time to healing. The assessment of percentage graft-take and percentage wound area healed were also inconsistent between studies and subject to inter-observer variance. Several studies reported histological analysis rather than clinical outcomes, which limited comparison between studies. Where studies were similar enough, results were pooled and meta-analysis was performed using the random effects model due to significant heterogeneity.

Additionally, the assessment of quality of scarring is difficult to compare across all studies as it is a subjective measure. Different studies utilized different scarring scores e.g. Manchester Scarring Scale, Hamilton Scarring Scale, Vancouver Scarring Scale, Patient and Observer Scar Scale (POSAS) which

made comparison between studies difficult. As the Vancouver Scar Scale (VSS) was the most commonly used score, cumulative mean VSS scores were used as a comparison across all studies

Most studies reported degree of pain using the visual analogue scale. However, some studies reported pain as a binary outcome. There are limitations for the assessment of pain as it is subjective and dependent on patient experience. For example, pain at one location may be affected by distracting injuries e.g. burns in other areas.

Efficacy of skin substitutes

In terms of efficacy, although there was no difference in the number of wounds healed between skin substitutes and standard care, there is an improvement in mean healing time of wounds (WMD -3.79, CI -5.38, -2.20). This may be due to difference in time points for assessment of wound healing. An alternative explanation is that although skin substitutes facilitate wound healing, ultimately most wounds would heal as part of the inflammatory response.

There was also no difference in percentage graft take or percentage wound area healed/epithelialized. Scarring (as quantified by the Vancouver Scar Scale) was significantly better in patients treated with skin substitutes compared to standard care (WMD -1.52, CI -2.43, -0.61). Scarring is often dependent on how quickly wounds can heal. By accelerating the healing process, skin substitutes result in less scarring.

However, hypertrophic scarring was not significantly different in patients treated with skin substitutes compared to standard care. This may be because hypertrophic scarring is also dependent on patient factors and not just the nature of the wound itself. Patients who are genetically predisposed to

hypertrophic scarring, are likely to scar despite interventions to prevent that from happening which includes skin substitutes. (51)

Adverse Effects of skin substitutes

Pain was significantly reduced in the group treated with skin substitutes (WMD -2.19, CI -3.43, -0.94). This may be because most skin substitutes are applied and left on permanently while standard care involves regular dressing changes as the dressings get soaked through and become a potential reservoir for infection.

The need for further surgery and length of hospital stay was not significantly different between the groups treated with skin substitutes vs standard care. The rate of infection was also not significantly different between patients treated with skin substitutes and standard care.

Summary

In conclusion, skin substitutes in general promoted faster mean healing time, less pain and less scarring in patients with burn, although there was no difference in number of wounds healed compared to standard care. There was also no significant adverse effects resulting from use of skin substitutes such as need for further surgery, length of hospital stay and rates of infection.

2.1.2.Skin Substitutes for Diabetic Ulcers

Introduction

Chronic wounds can be broadly defined as wounds that have not healed within a period of 6 weeks. They represent a significant disease burden, which can be broadly categorized into the following: diabetic foot ulcers, arterio-venous foot ulcers and pressure ulcers. More than 6 million people suffer

from chronic non-healing ulcers, costing USD $ 25 billion annually in the United States. (52) These wounds have a severe impact on the quality of life of patients and impose a significant financial burden on the health care system due to the long duration of therapy required to manage chronic wounds.

Current treatment modalities for diabetic foot ulcers include debridement, pressure off-loading, infection control, blood glucose control, revascularization and meticulous care with wound dressings. (53) Venous leg ulcers require compression therapy, debridement, infection control and off-loading. Similarly, pressure ulcers are managed by pressure offloading, careful debridement and infection control. Nevertheless, up to 30% of these chronic wounds remain hard-to-heal despite the best wound care management. (54)

The area of tissue engineering and regenerative medicine has resulted in an exponential growth of various skin substitutes that assist with wound healing. Most of these skin substitutes are derived from xenografts and cadaveric allografts. However, collagen-based scaffolds and matrices have also been developed to help accelerate wound healing as well. Naturally available human amnion and cellular based products such as autologous keratinocytes are gaining favour as products which promote wound healing by secretion of trophic growth factors as well.

Numerous randomized controlled trials have been undertaken to investigate the efficacy of bioengineered skin substitutes in achieving complete re-epithelialization of chronic wounds. This systematic review and meta-analysis aims to consolidate the current evidence with regards to the role of skin substitutes in healing of diabetic foot ulcers.

Methods

Search strategy

A literature search was performed on several electronic databases as listed below to identify relevant randomized controlled trials:

- The Cochrane Wound Specialist Register
- The Cochrane Central Register of Controlled Trials (CENTRAL)
- Ovid MEDLINE (1946 to 22 December 2015)
- Ovid MEDLINE (In-process & Other Non-Indexed Citations) (1946 to 22 December 2016)
- Ovid EMBASE (1974 to 22 December 2015)
- EBSCO CINAHL (1982 to 22 December 2015)

The search strategy comprised of the following keywords: (bioengineered OR synthetic OR artificial OR biosynthetic or graft) AND (skin) AND (randomi?ed controlled trials OR RCT) AND (diabetic foot ulcer* OR DFU). Studies were limited to randomized clinical trials only but did not include any language or age limits. Further relevant randomized controlled trials were identified by bibliographic review and citation tracing of selected papers.

Selection criteria

The titles and abstracts of articles identified through the literature search were reviewed thoroughly. The shortlisted articles were each evaluated to see if they met the pre-defined inclusion criteria:

- Studies must be a randomized controlled trial involving at least one skin substitute (including intra-patient studies) compared to standard wound care.
- Comparative studies between two or more skin substitutes are also included.
- Studies must include diabetic foot ulcers.

- Studies must involve humans only.
- Studies must have a reproducible and objective method of reporting primary and secondary outcomes.

Studies were excluded if they were not randomized controlled trials (e.g. retrospective case studies), did not include any skin substitute (e.g. wound dressings only), do not involve chronic wounds (e.g. burns, acute traumatic wounds), were purely animal studies, only involved subjective outcome measures or did not have sufficient length of follow up. The primary outcomes were the incidence of complete ulcer closure/re-epithelialization and time to complete closure of the chronic wounds. Secondary outcomes include rate of ulcer recurrence, change in ulcer area, rate of wound healing and incidence of adverse effects such as infection, pain and duration of stay.

Data collection and analysis

The full text of potentially relevant abstracts and citations were retrieved. Irrelevant or duplicate publications were excluded and the remaining studies were assessed for eligibility. Data from shortlisted studies were extracted using a standardized data extraction sheet. Data extracted included: author and year of publication, type of ulcer, mean duration of ulcer, mean initial ulcer size, details of intervention and control, primary and secondary outcome data, duration of follow up, number of adverse outcomes (e.g. infection, cellulitis, osteomyelitis, amputation, causal mortality). For missing or incomplete data, study authors were contacted to complete dataset.

Assessment of methodological quality and reporting bias

Methodological quality of each study was assessed for risk of bias using the Cochrane tool for assessing risk of bias. Each study was evaluated for random sequence generation, allocation concealment, blinding of participants and personnel, blinding of outcome assessment, incomplete outcome data, selective reporting and other bias (e.g. sponsorship from companies).

Statistical analysis and data synthesis

Summary statistics including mean, standard deviations, medians and ranges of primary and secondary outcomes were extracted from each study. For continuous variables, pooled means and standard deviations of each reported outcome was compiled into Forest plots and weighted mean difference was calculated. For dichotomous data, pooled risk ratios were calculated using the Mantel-Haenszel method. Where possible, subgroup analysis for similar studies were done e.g. autologous vs allogenic skin substitutes, cellular vs acellular skin substitutes, biological vs synthetic skin substitutes etc. Statistical significance was set at $p<0.05$ and confidence intervals at 95% were determined. Each study was assessed for degree of heterogeneity using the I^2 data statistic. A value of I^2 of more than 80% is considered to have significant heterogeneity. All statistical analysis was done on RevMan 5.3 Review Manager (The Nordic Cochrane Centre, Copenhagen, Denmark).

Results

Search outcomes

Initially, 1524 articles were identified using the search strategy as mentioned above. A further 9 relevant randomized controlled trials were included through bibliographic search and citation tracing of articles found from our literature review as well. After title and abstract screening, 59 articles were selected for a more thorough full text review. A total of 29 articles were eligible for inclusion based on selection criteria of this review.

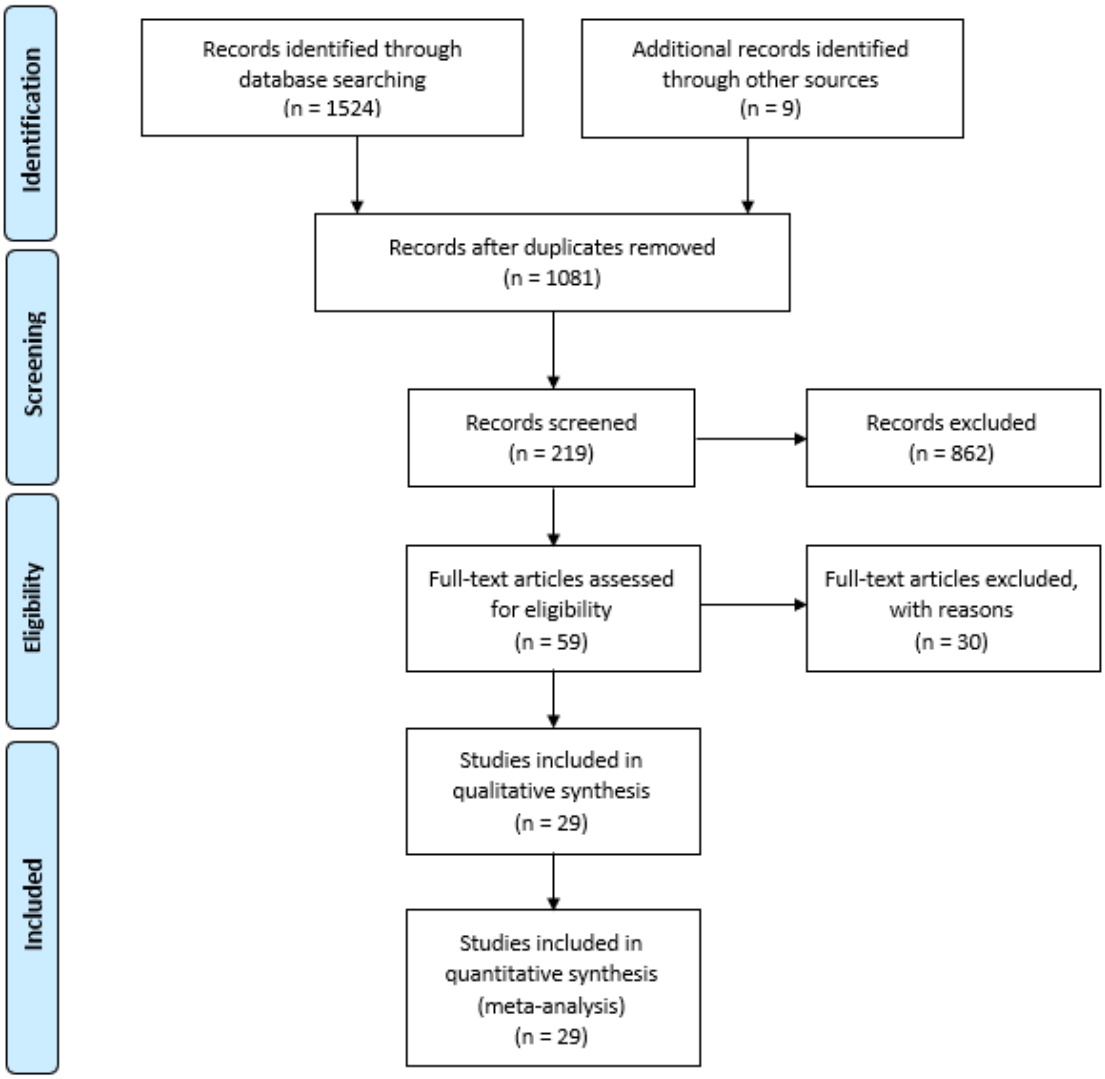


Figure 2-14 Flowchart for study selection for skin substitutes for diabetic foot ulcers.

Methodological quality of included studies

Nearly half of studies included did not clearly state method of random sequence generation while only a third of studies reported any evidence of allocation concealment. Due to the nature of wound care and skin substitutes, blinding of participants and investigators was not always done. Most studies reported results based on intention-to-treat analysis and patients who were lost to follow-up were included in the analysis. All studies reported primary and secondary outcomes as outlined in the study protocol. There was minimal reporting bias. Other sources of bias were also unclear in most studies.

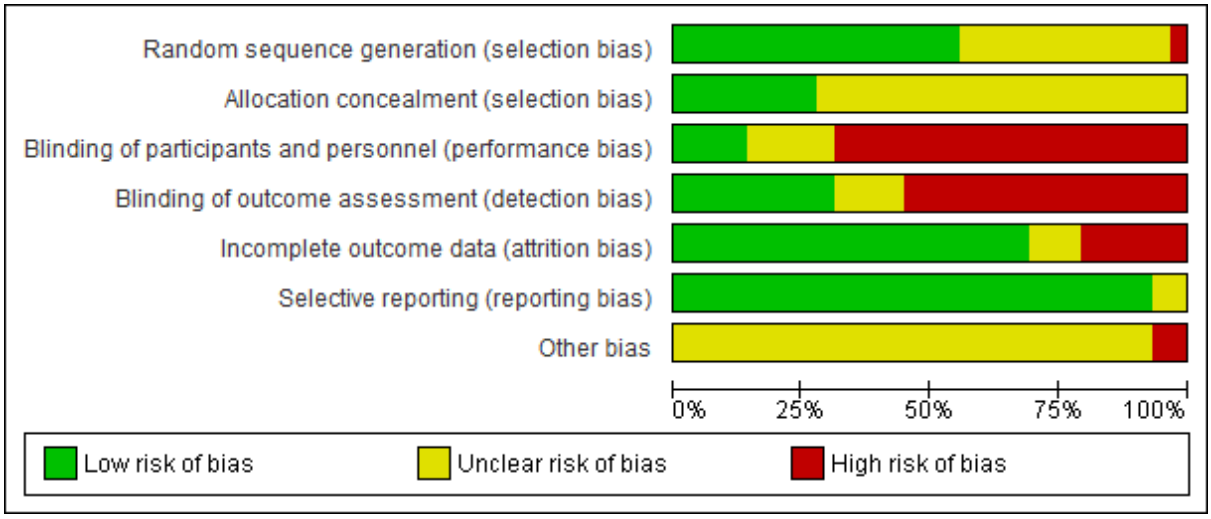


Figure 2-15 Risk of bias graph for studies on diabetic foot ulcers.

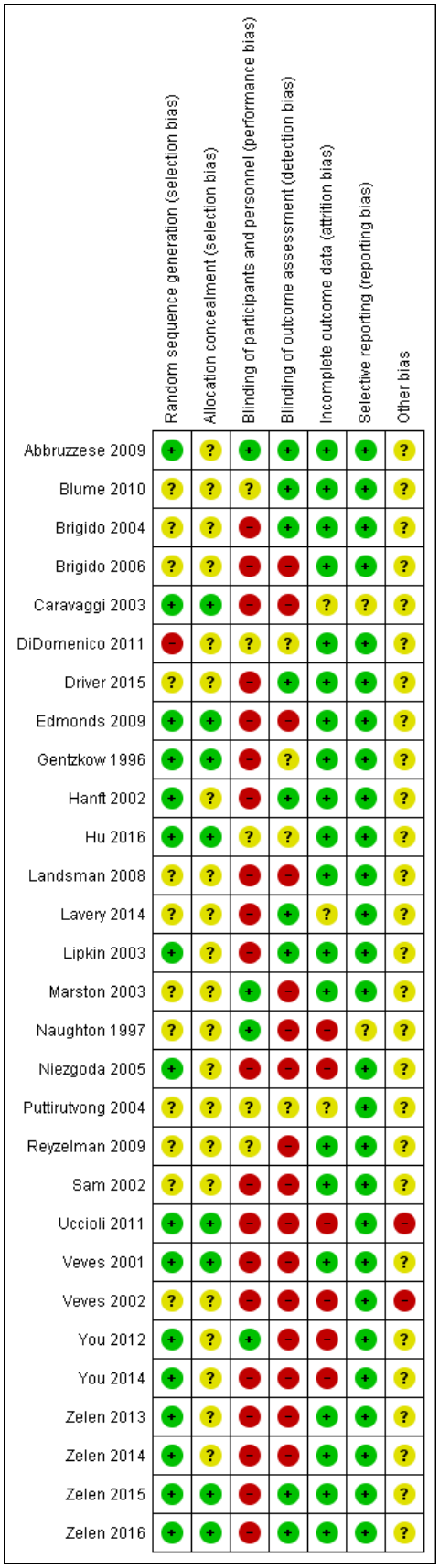


Figure 2-16 Risk of bias summary for studies on diabetic foot ulcers.

Primary and Secondary Outcomes for Diabetic Foot Ulcers

A total of 29 studies comprising of 18 types of skin substitutes were included in this systematic review. These include Vulnamin gel, formulated collagen gel (FCG), Graftjacket, HYAFF 11, Apligraf, Integra, Dermagraft, STSG+ADM, Grafix, Orcel, Oasis, meshed skin graft, Graftskin, HYAFF, Promogram, cultured allogenic keratinocyte, Hyalograft 3D and Epifix. A meta-analysis of the outcomes from the studies was performed by skin substitutes.

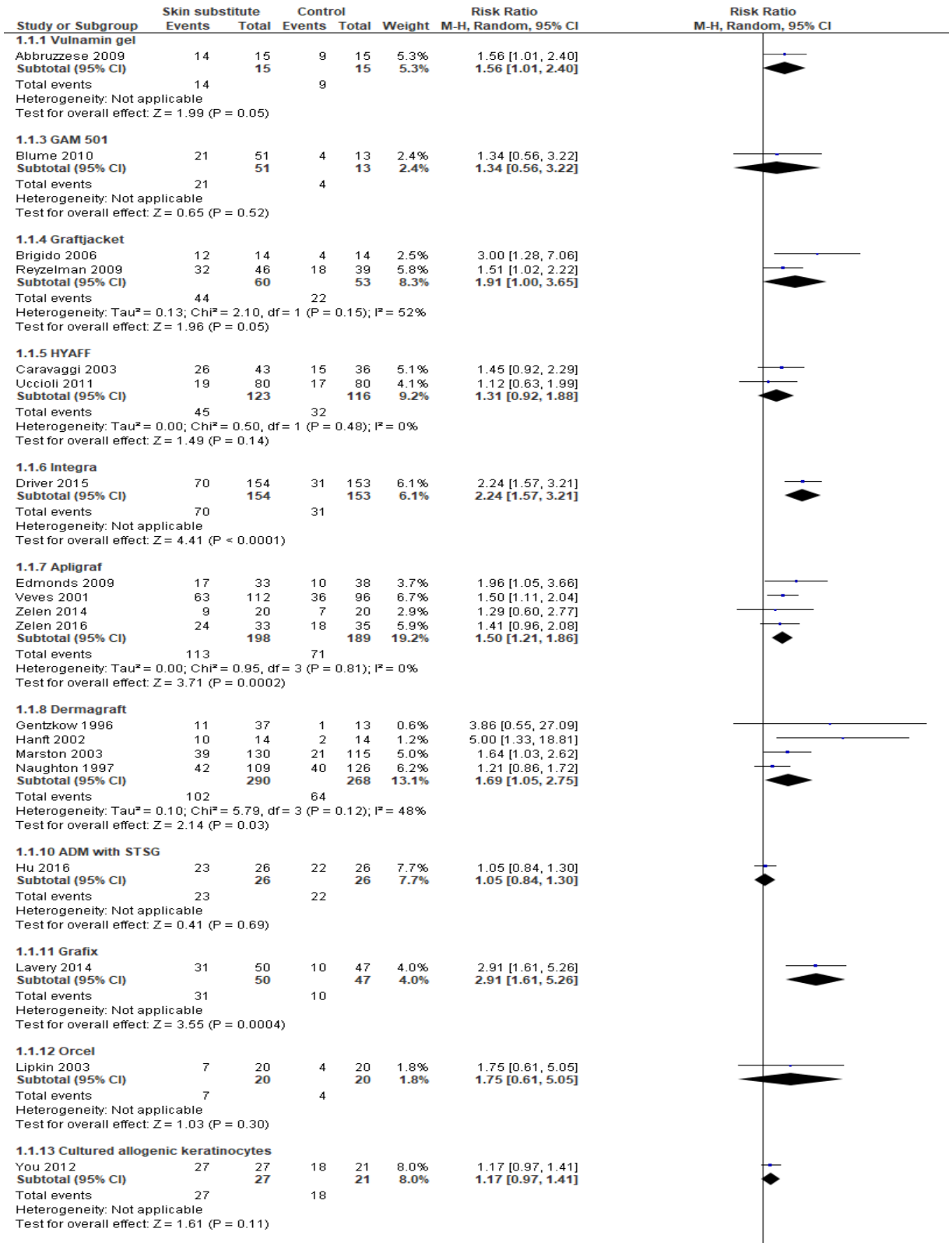
Incidence of complete ulcer closure

Number of ulcers healed after 12 weeks was significantly better in patients treated with skin substitutes compared to standard care (RR 1.63, CI 1.39, 1.91). GraftJacket, an acellular dermal matrix appears to promote diabetic foot ulcer healing significantly (RR 1.91, CI 1.00, 3.65). (55,56) Meanwhile, Integra, another acellular dermal matrix with a silicone backing was effective in promoting closure of diabetic foot ulcers as well (RR 2.24, CI 1.57.3.21). (57)

Apligraft, a cellular bilayer skin substitute also appears to effectively aid ulcer closure (RR 1.50, CI 1.21, 1.86). (58-60) Dermagraft, a cellular dermal replacement seeded with neonatal fibroblasts has also been shown to promote healing of diabetic foot ulcers (RR1.69, CI 1.05, 2.75). (61-64) While ReCell and split-thickness skin grafts marginally improved number of ulcers healed (RR 1.21, CI 1.01, 1.44). (65)

Grafix, a cryopreserved placental membrane results in significantly higher wound closure (RR 2.91, CI 1.61, 5.26). (66) Hyalograft3D, a hyaluronic acid based cellular dermal substitute, also results in significantly higher rate of wound closure (RR 2.44, CI 1.48, 4.03). (67) Epifix, a dehydrated human amnion/chorion membrane was shown to increase rate of ulcer healing significantly (RR 2.07, CI 1.50,

2.86). (60,68) However, collagen gel, GAM 501, HYAFF, ADM with STSG, Orcel and cultured allogenic keratinocytes did not appear to improve incidence of diabetic foot ulcer closure.



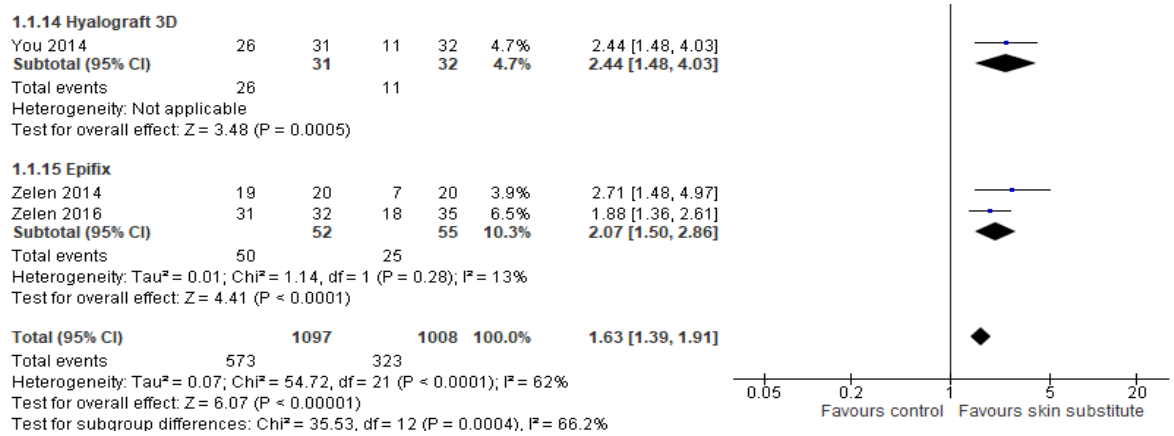


Figure 2-17 Forest plot of number of ulcers healed comparing skin substitutes vs standard care for diabetic foot ulcers.

Time to complete ulcer closure

Mean time to ulcer healing was significantly improved by three skin substitutes – Vulnamin gel, HYAFF and Hyalograft 3D (RR -19.5, CI -35.19, -3.81; RR -1.10, CI -2.15, -0.05 and RR-12, CI -19.68, -4.32 respectively). (69,70) However, GraftJacket and meshed skin grafting did not appear to improve mean healing time of ulcer significantly (RR -1.10, CI -2.54, 0.34 and RR -0.52, CI -3.72, 2.68 respectively). (56,71) The overall effect of skin substitute was therefore not significant in improving mean ulcer healing time (RR -2.01, CI -4.14, 0.12).

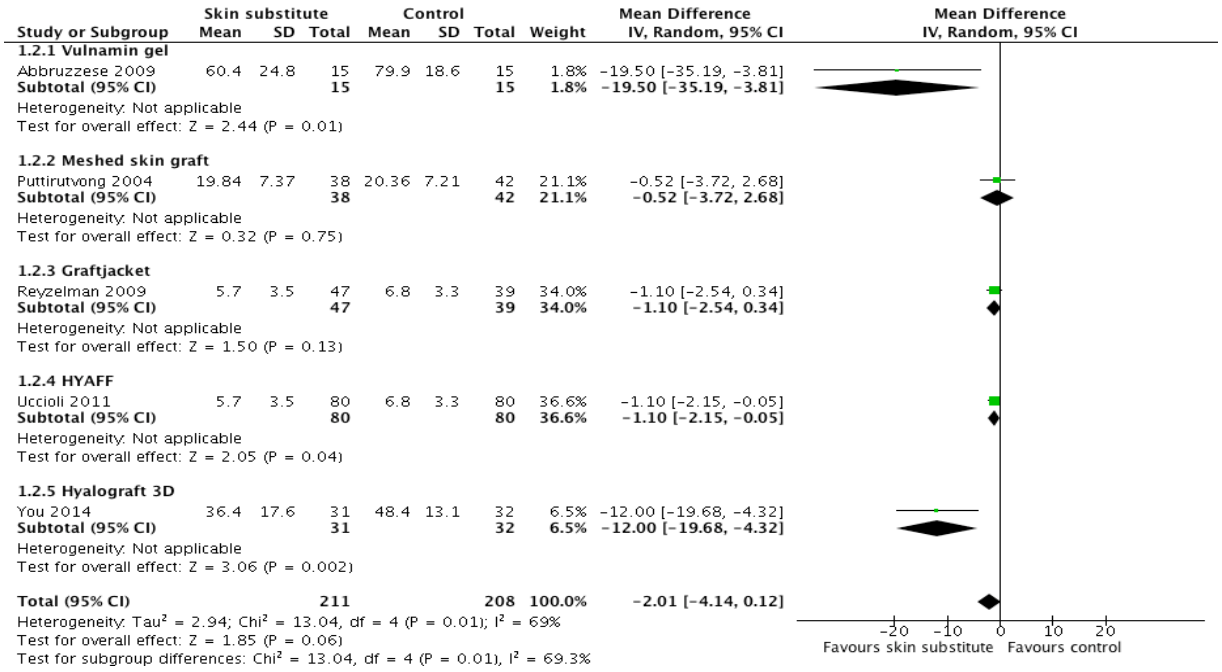


Figure 2-18 Forest plot of mean time to healing comparing skin substitutes and standard care for diabetic foot ulcers.

Percentage area healed/epithelialized

Percentage area healed/epithelialized was only reported by one study. Vulnamin gel appears to significantly increase mean area healed (WMD 34.5, CI 25.45, 43.55). (72)

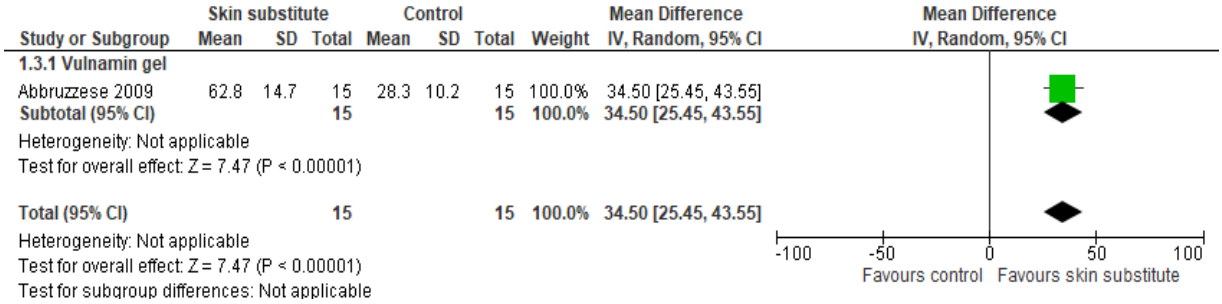


Figure 2-19 Forest plot of mean area healed/epithelialized comparing skin substitutes vs control for diabetic foot ulcers.

Wound infection

Pooled results show that rate of infection was significantly reduced in patients treated with skin substitutes compared to controls (RR 0.69, CI 0.52, 0.92). However, no individual skin substitute resulted in a significantly reduced rate of infection in each study due to small sample size. Dermagraft and Grafix appear to reduce rate on infection but this was not statistically significant (RR 0.64, CI 0.39, 1.06 and RR 0.50, CI 0.25, 1.01 respectively). (63,64,66)

Vulnamin gel did not reduce rate of infection (RR 0.80, CI 0.27, 2.41) (72) while GraftJacket showed no significant difference in rate of infection between skin substitutes and controls (RR 0.72, CR 0.23, 2.27). (55,56) HYAFF, is a hyaluronic acid-based scaffold which also did not show significant reduction in infection rate in diabetic foot ulcer patients treated with skin substitute vs controls (RR 0.87, CI 0.23, 3.30) (73,74) and neither did Hyalograft 3D (RR 0.36, CI 0.08, 1.68). (75)

Apligraf did not reduce rate of infection (RR 0.76, CI 0.39, 1.51) (58,59,76) and neither did ReCell with STSG (RR 0.33, CI 0.04, 3.08). (65) Kaloderm also did not reduce rate of infection (RR 0.79, CI 0.14, 4.39) (77) and neither did Epifix (RR 0.50, CI 0.05, 5.08). (76)

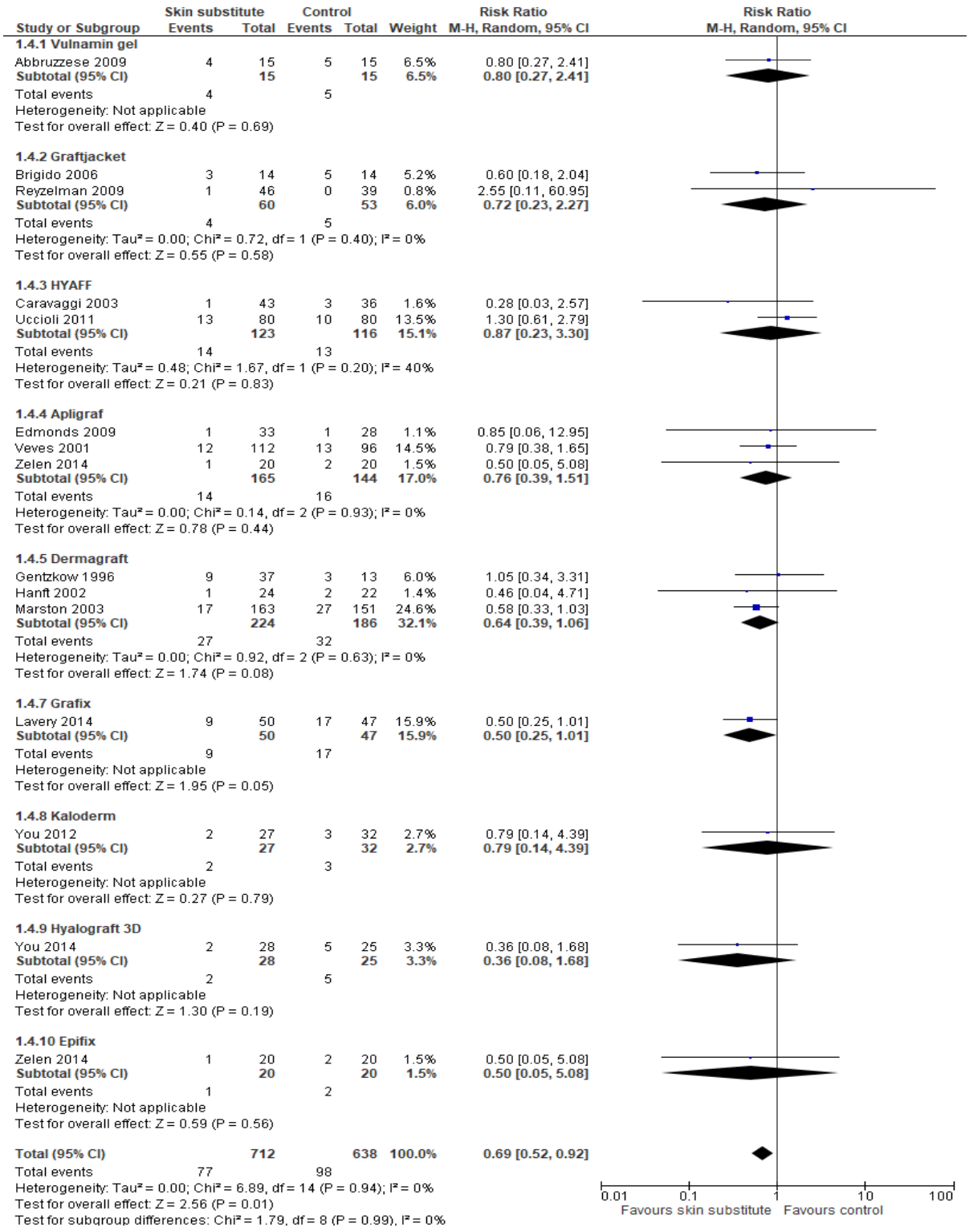


Figure 2-20 Forest plot of rate of infection comparing skin substitutes and control for diabetic foot ulcers.

Osteomyelitis

Skin substitutes did not appear to reduce rate of osteomyelitis overall (RR 0.54, CI 0.22, 1.32). HYAFF and Dermagraft did not reduce incidence of osteomyelitis in patients treated with skin substitutes compared to controls (RR 0.91, CI 0.09, 9.72 and RR 0.63, CI 0.14, 2.67 respectively). (63,64,73,74) However, Apligraf appears to reduce rate of osteomyelitis compared to controls (RR 0.24, CI 0.06, 0.89). (59)

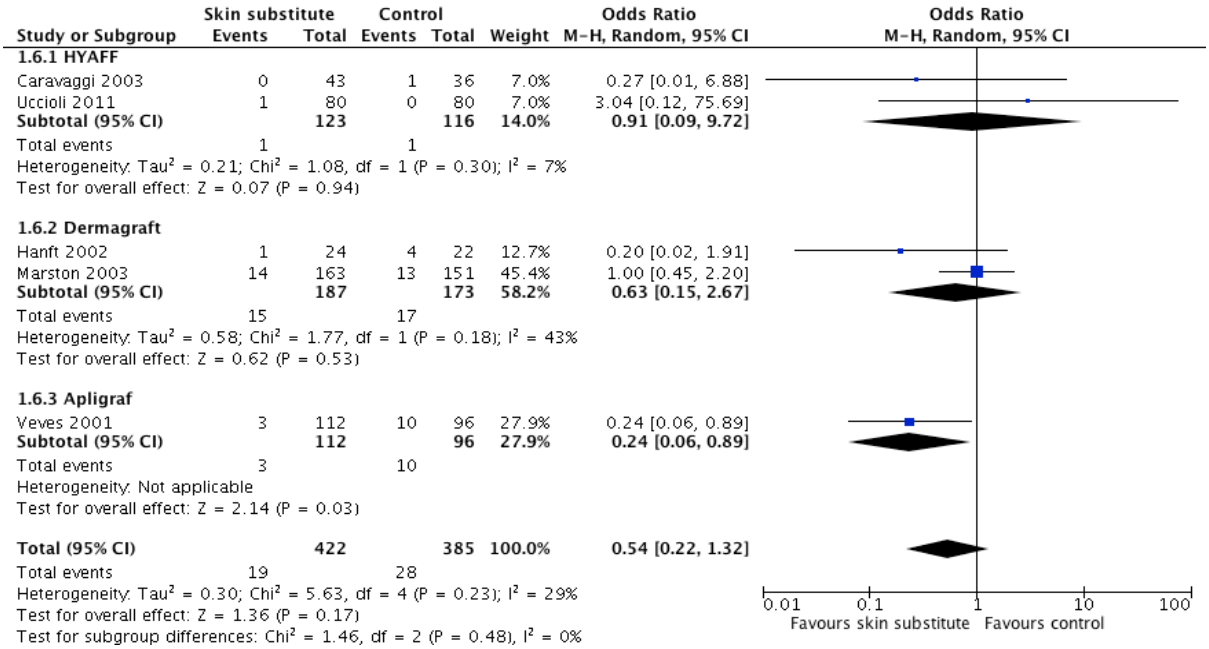


Figure 2-21 Forest plot of incidence of osteomyelitis comparing skin substitutes and controls in diabetic foot ulcers.

Cellulitis

Skin substitutes did not appear to reduce rate of cellulitis overall (RR 0.79, CI 0.42, 1.47). Dermagraft resulted in no significant reduction in rate of cellulitis (RR 0.53, CI 0.14, 1.94) (63,64) and neither did Apligraft (RR 1.07, CI 0.44, 2.61). (59)

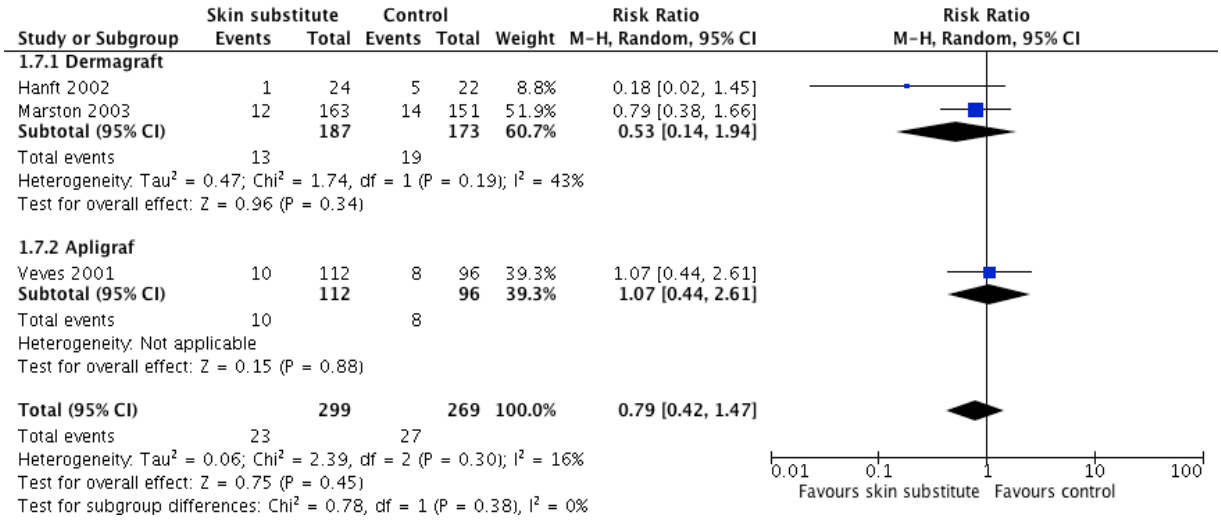


Figure 2-22 Forest plot of incidence of cellulitis comparing skin substitutes vs control in diabetic foot ulcers.

Rate of recurrence

Skin substitutes did not significantly reduce rate of ulcer recurrence (RR 0.57, CI 0.25, 1.33). Apligraf resulted in no significant reduction in rate of ulcer recurrence (RR 0.50, CI 0.14, 1.75). (58,59) Grafix and Kaloderm resulted in no change of ulcer recurrence (RR 0.60, CI 0.17, 2.05 and RR 0.94, CI 0.06, 13.68 respectively). (66,77)

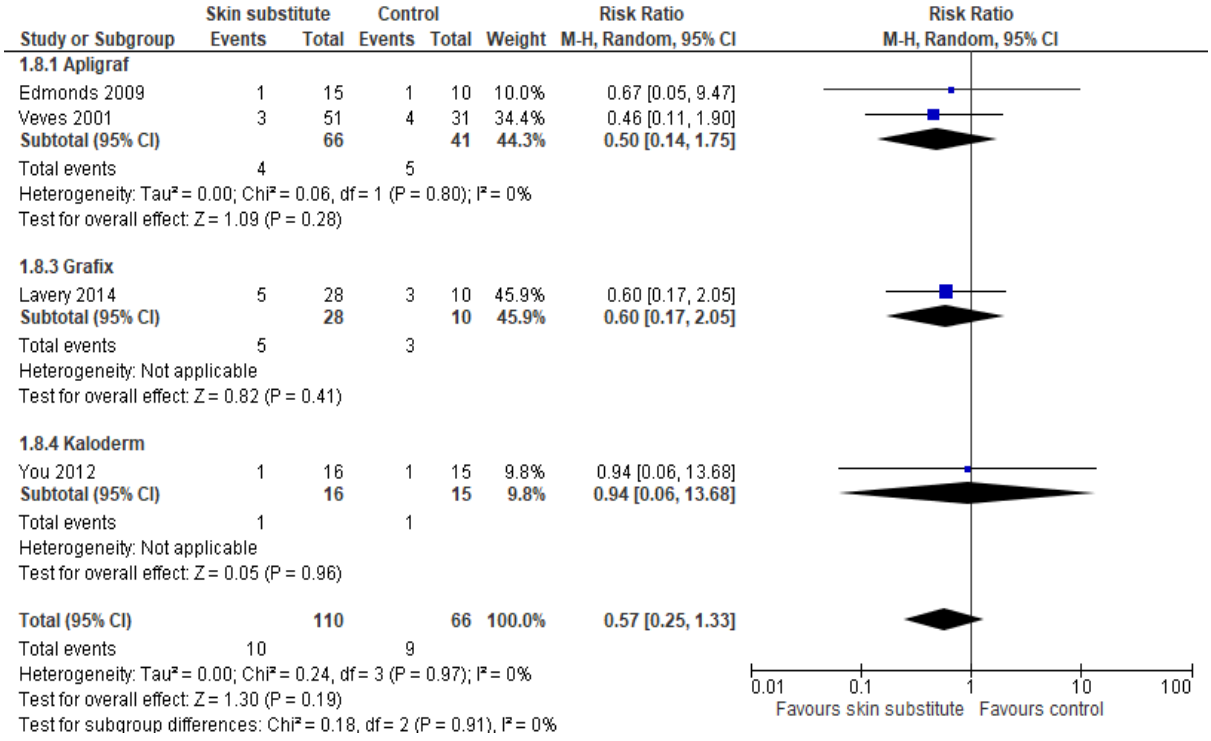


Figure 2-23 Forest plot of rate of ulcer recurrence comparing skin substitutes and standard care for diabetic foot ulcers.

Amputation

One of the more serious complications of diabetic foot ulcers is risk of amputation. Overall, there was a slight reduction of rate of amputation in patients treated with skin substitutes, however this did not reach statistical significance (RR 0.48, CI 0.23, 1.02). Apligraf was the only skin substitute which showed a reduction in amputation rate (RR 0.40, CI 0.17, 0.91) compared to other skin substitutes. (58,59) GraftJacket did not reduce rate of amputations (RR 0.85, CI 0.05, 13.11) (56) and neither did HYAFF (RR 5.00, CI 0.24, 102.53). (74) Kaloderm also did not reduce rate of amputation (RR 0.31, CI 0.01, 7.15). (77)

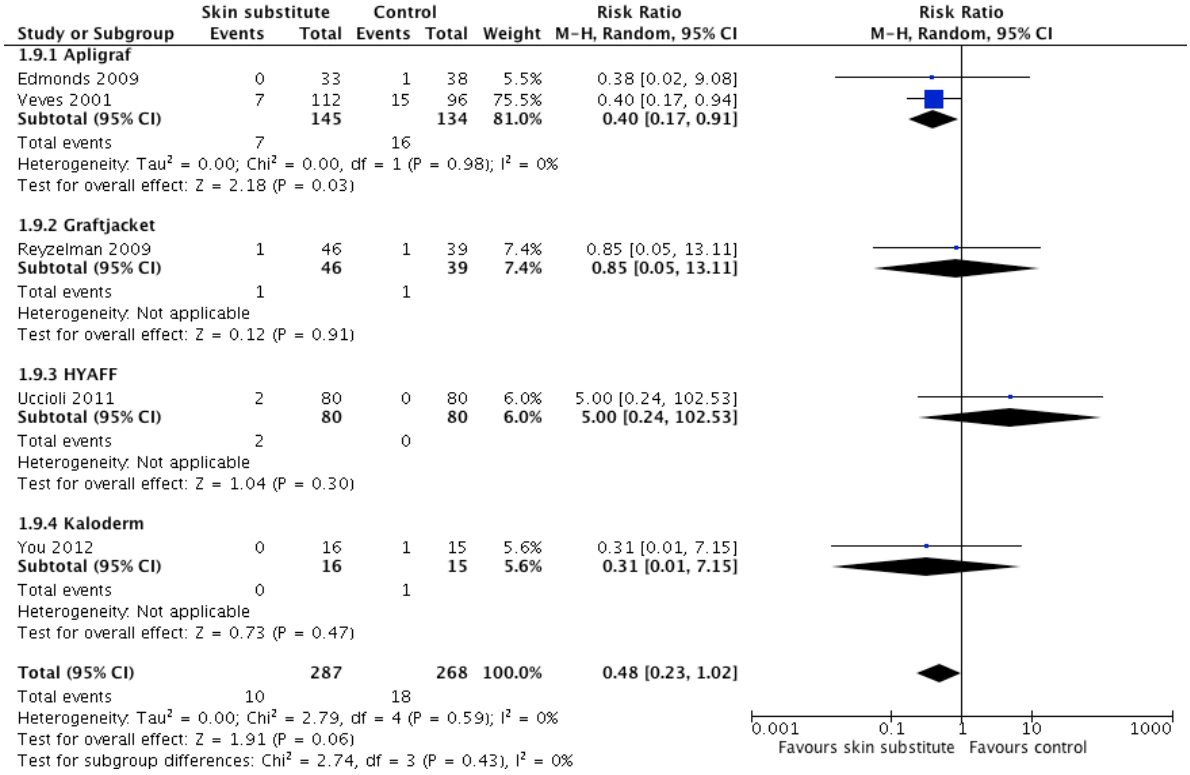


Figure 2-24 Forest plot of amputation comparing skin substitutes vs control for diabetic foot ulcers.

Hospitalization

Skin substitutes did not significantly reduce rate of hospital admission compared to controls overall (RR 0.56, CI 0.30, 1.05). Dermagraft resulted in slight reduction of hospitalization but this was not statistically significant (RR 0.55, CI 0.29, 1.05) and neither did GraftJacket (RR 0.85, CI 0.05, 13.11). (56,64)

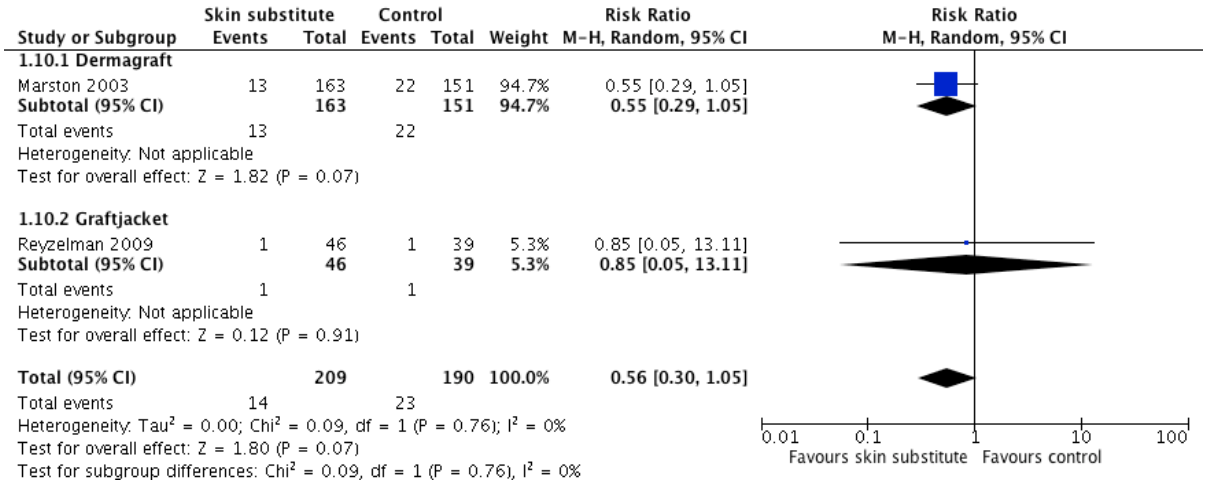


Figure 2-25 Forest plot of rate of hospitalization comparing skin substitutes vs control in diabetic foot ulcers.

Pain

Only one study reported outcomes for pain. Vulnamin gel did not significantly reduce number of patients who experienced pain (RR 1.50, CI 0.29, 7.73). (72)

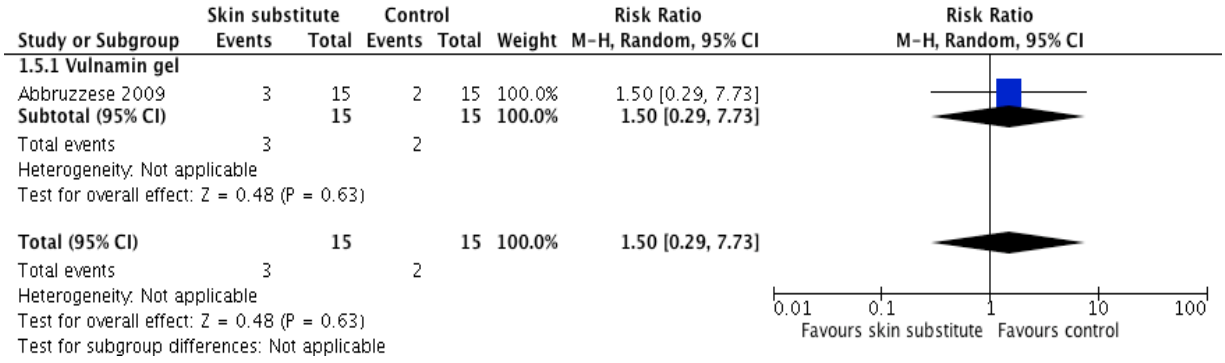


Figure 2-26 Forest plot of presence of pain comparing skin substitutes vs control in diabetic foot ulcers.

Comparison between skin substitutes

Number of ulcers healed

DiDomenico et al (78) compared number of ulcers healed between Apligraf and Theraskin. There was no significant difference between the two skin substitutes (RR 0.62, CI 0.31, 1.24). Landsman et al (79) compared number of ulcers healed between Dermagraft and OASIS. There was no significant difference

between the two skin substitutes (RR 0.91, CI 0.62, 1.33). Niezgoda et al (80) compared number of ulcers healed between OASIS vs Regranex. There was no significant difference between the two skin substitutes (RR 1.75, CI 0.94, 3.26). Sanders et al (81) compared number of ulcers healed between Dermagraft vs Theraskin. There was no significant difference between the two skin substitutes (RR 0.52, CI 0.21, 1.31). Zelen et al (76,82) compared number of ulcers healed between Epifix and Apligraf. There was a slight improvement in groups treated with Epifix but this did not reach statistical significance (RR 1.60, CI 0.99, 2.59). They also compared weekly vs biweekly application of Epifix and found that there was higher number of ulcers healed in the group that was treated weekly only (RR 1.32, CI 1.02, 1.72). (60)

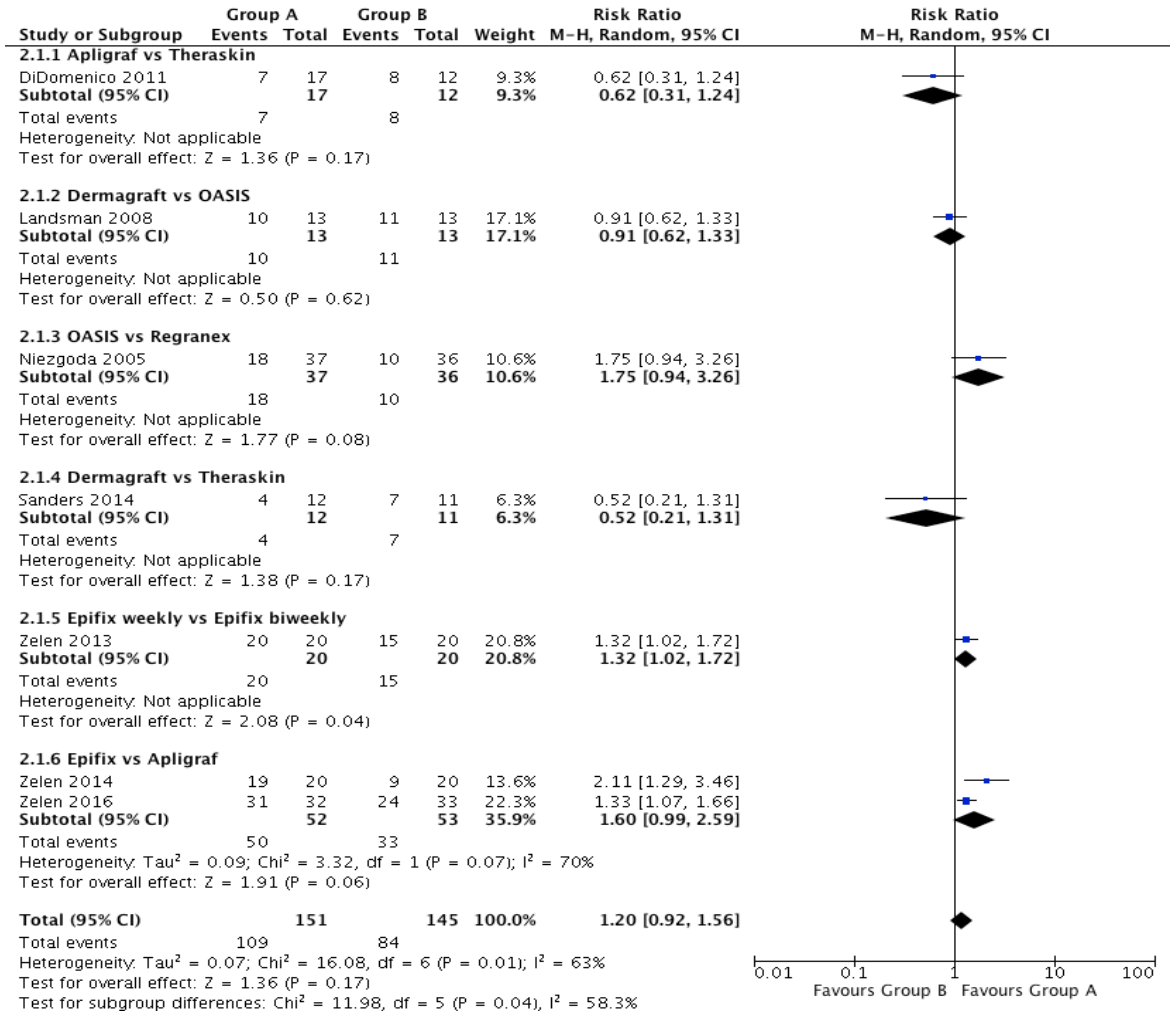


Figure 2-27 Forest plot of number of ulcers healed comparing different skin substitutes for diabetic foot ulcers.

Mean time to closure

DiDomenico et al (78) compared mean time to complete ulcer healing between Apligraf and Theraskin. There was no significant difference between the two skin substitutes (WMD 1.86, CI -0.90, 4.62). Landsman et al (79) compared mean time to wound closure between Dermagraft and OASIS. There was no significant difference between the two skin substitutes (WMD -5.23, -33.81, 23.35).

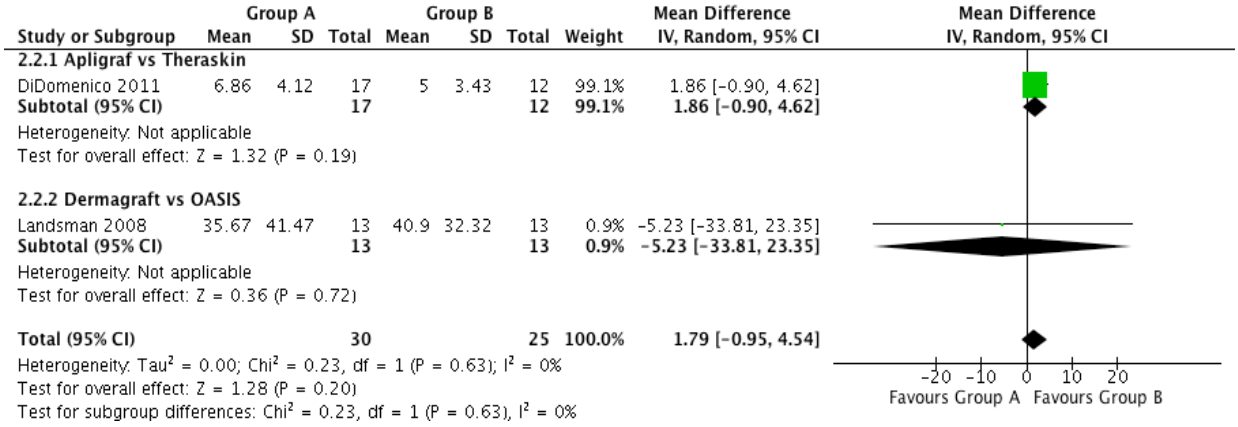


Figure 2-28 Forest plot of mean time to closure comparing different skin substitutes for diabetic foot ulcer.

Infection

DiDomenico et al (78) compared rate of infection between Apligraf and Theraskin. There was no significant difference between the two skin substitutes (RR 1.18, CI 0.35, 4.01). Meanwhile, Zelen et al (76) compared rate of infection between Epifix and Apligraf. There was no significant difference between the two either (RR 0.50, CI 0.05, 5.08).

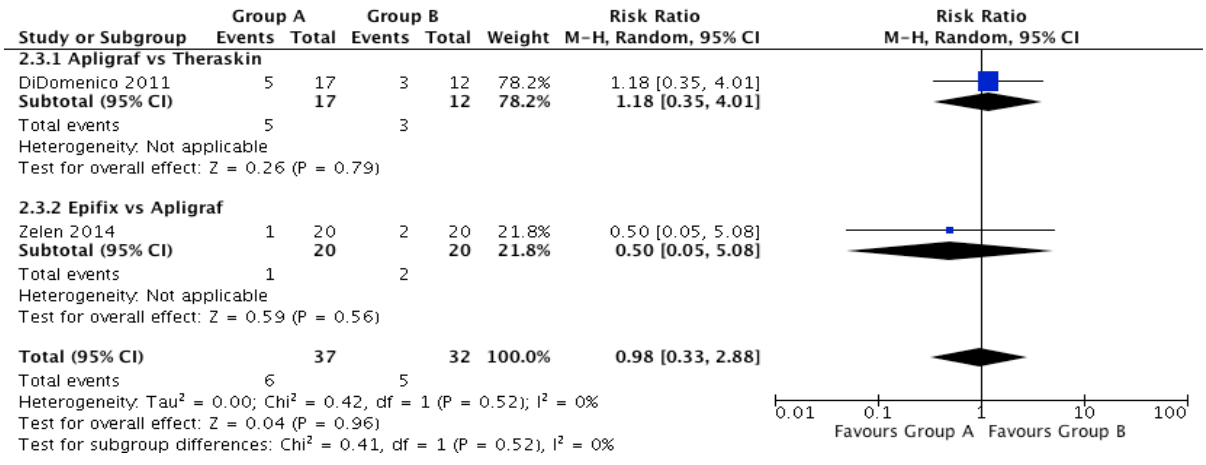


Figure 2-29 Forest plot of rate of infection comparing different skin substitutes for diabetic foot ulcers.

Rate of recurrence

Only one study reported rate of recurrence between skin substitutes tested – Apligraf and Theraskin. There was no significant difference in ulcer recurrence between those two groups (RR 0.24, CI 0.01, 5.45). (78)

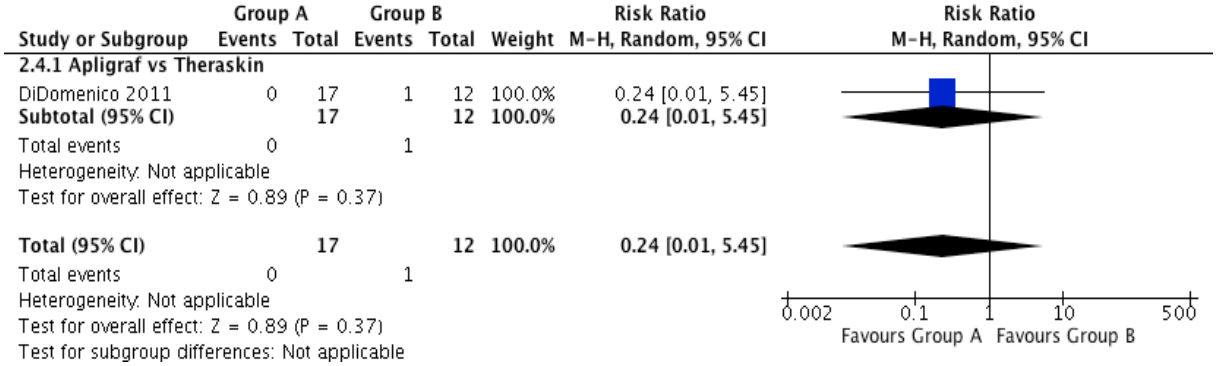


Figure 2-30 Forest plot of ulcer recurrence comparing different skin substitutes for diabetic foot ulcers.

Author (Year)	Treatment	Control	Number of ulcers; Duration of ulcers (months); Mean ulcer size (cm^2)	Primary outcome (percentage ulcer healed)		Secondary outcomes	Adverse Outcomes	Duration of follow up
				Treatment n/N (%)	Control n/N (%)			
Diabetic Ulcers								
Abbruzzese 2009 (72)	Vulnamin gel + compression (15)	Inert gel vehicle + compression (15)	30 diabetic foot ulcers Mean ulcer area 25 – 27 cm^2 Mean ulcer duration 22 – 30 cm^2	14/15 (93.3%)	9/15 (60%)	Mean time to closure: V: 60.4 ± 24.8 days Control: 79.9 ± 18.6 days Mean area healed: V: 62.8 ± 14.7% Control: 28.3 ± 10.2%	Infection: V: 4/15 Control: 5/15 Pain: V: 3/15 Control: 2/15	3 months
Blume 2010 (83)	Collagen gel (D1 vs D1+D29) (31) GAM 501 (D1 vs D1+D29) (66)	Control (16)	124 diabetic foot ulcers Mean ulcer size 2.8 – 3.1 cm^2 Mean ulcer duration 11-18 months	CG: 6/17 (35.3%) GAM: 21/51 (43.1%)	4/13 (30.8%)	Ulcer closure (Week 4): CG: 14/31 GAM: 27/66 Control: 5/16	NR	12 weeks
Brigido 2004 (84)	Graftjacket (20)	Control (20)	40 diabetic foot ulcers (full thickness lower extremity wound) Mean ulcer duration 25 - 27 weeks Mean ulcer size 5.4-9.7 cm^2	NR	NR	Decrease in wound area: G: 73.1% Control: 34.2%	Seroma: G: 1/20 Control: 0/20	4 weeks
Brigido 2006 (55)	Graftjacket (14)	Control (14)	28 diabetic foot ulcers	12/14 (85.7%)	4/14 (28.6%)	Mean time to closure: G: 11.92 ± 2.87 weeks Control: 13.5 ± 3.42 weeks	Infection: G: 3/14 Control: 5/14 Seroma: G: 1/14 Control: 0/14	16 weeks
Caravaggi 2003 (73)	HYAFF 11 (Hyalograft 3D + Laserskin) (43)	Paraffin gauze (36)	79 diabetic foot ulcers Mean ulcer size 5.3-6.2 cm^2 Mean duration ulcer 4 months	26/43 (65.3%)	15/36 (46.9%)	Median time to wound closure: H: 57 days Control: 77 days	Osteomyelitis: H: 0/43 Control: 1/36 Infection: H: 1/43 Control: 3/36	11 weeks
DiDomenico 2011 (78)	Apligraft (17)	TheraSkin (12)	28 diabetic foot ulcers Mean wound size 1.8 cm^2	7/17 (41.3%)	8/12 (66.7%)	Mean time to closure: A: 6.86 (4.12) T: 5 (3.43) % wounds closed at 20 weeks: A: 41.7% T: 66.7%	Infection: A: 5/17 T: 3/12 Recurrence: A: 0/17 T: 1/12	12 weeks 20 weeks
Driver 2015 (57)	Integra (154)	Saline gel (153)	307 diabetic foot ulcers Mean ulcer size 3.53 – 3.65 cm^2 Mean ulcer duration 303-308 days	70/154 (45.4%)	31/153 (20.3%)	Complete closure 16 wk: I: 79/154 Control: 49/153 Median time to closure: I: 43 days Control: 78 days Wound size reduction: I: 7.2%/wk Control: 4.8%/wk	Recurrence: I: 29/152 (19%) Control: 40/153 (26%)	12 weeks 16 weeks
Edmonds 2009 (58)	Apligraft (33)	Standard care (39)	72 diabetic foot ulcers Mean ulcer size 3 cm^2 Mean duration ulcer 1.7-2 years	17/33 (51.5%)	10/38 (26.3%)	Median time to closure: A: 84 days Control: NA	Infection: A: 1/33 Control: 1/38 Recurrence: A: 1/15	12 weeks

							Control: 1/10 Amputation: A: 0/33 Control: 1/38	
Gentzkow 1996 (62)	Dermagraft Group: A (12) B (14) C (11)	Group D (13)	50 diabetic foot ulcers Mean ulcer size 1.9-3.3 cm^2 Mean ulcer duration 40.7-87 weeks	A: 6/12 (50%) B: 3/14 (21.4%) C: 2/11 (18.2%)	D: 1/13 (7.7%)	Median time to closure: A: 12 weeks B, C, D: >12 weeks	Infection: A: 2/12 (17%) B: 4/14 (29%) C: 3/11 (27%) D: 3/13 (23%)	12 weeks
Hanft 2002 (63)	Dermagraft (14)	Saline gauze (14)	28 diabetic foot ulcers Mean ulcer duration 21-80 weeks Mean ulcer size 1.5 cm^2	15/24 (62.5%)	6/22 (27.3%)	For ulcers > 6 weeks, number of wounds healed: D: 10/14 (71.4%) Control: 2/14 (14.3%)	Cellulitis: D: 1/24 Control: 5/22 Infection: D: 1/24 Control: 2/22 Osteomyelitis: D: 1/24 Control: 4/22	12 weeks
Hu 2016 (85)	STSG + ADM (26)	STSG (26)	52 diabetic foot ulcers Mean ulcer size 28-32 cm^2 Mean ulcer duration 25-29 weeks	23/26 (88.5%)	22/26 (84.6%)	Scarring (MSS): ADM: 9 Control: 11 Re-grafting: ADM: 3/26 Control: 2/26	Amputation: ADM: 0/25 Control: 1/26 Recurrence: ADM: 1/23 Control: 5/22 Infection: ADM: 2/26 Control: 3/26	12 weeks
Lavery 2014 (66)	Grafix (50)	Standard therapy (47)	97 diabetic foot ulcer Mean ulcer size 3.41 – 3.93 cm^2 Mean ulcer duration 115-123 days	31/50 (62%)	10/47 (21.3%)	Median time to healing: G: 42 days Control: 69.5 days 50% reduction wound area: G: 31/50 Control: 19/47	Recurrence: G: 5/28 Control: 3/10 Infection: G: 9/50 Control: 17/47	12 weeks
Landsman 2008 (79)	Dermagraft (13)	OASIS (13)	26 diabetic foot ulcers Mean ulcer size 1.85 – 1.88 cm^2 Mean ulcer duration: not stated	10/13 (76.9%)	11/13 (84.6%)	Mean time to closure: A: 35.67 ± 41.47 days Control: 40.90 ± 32.32 days	NR	12 weeks
Lipkin 2003 (86)	Orcel (20)	Saline gauze (20)	40 neuropathic diabetic foot ulcers Mean ulcer size 5.5-6 cm^2 Mean ulcer duration 11.9 to 12.2 months	7/20 (35%)	4/20 (20%)	Healing for ulcers <6cm^2: O: 7/15 Control: 3/13 Healing for ulcers >6cm^2: O: 0/5 Control: 1/7 Rate of closure: O: 1.8 ± 2.5%/day Control: 1.1 ± 1.9%/day	NR	12 weeks
Marston 2003 (64)	Dermagraft (163)	Control (151)	314 diabetic foot ulcers Mean ulcer size 2.31 – 2.52 cm^2 Mean ulcer duration 41-67 weeks	39/163 (23.9%)	21/151 (13.9%)	NR	Infection: D: 17/163 Control: 27/151 Osteomyelitis: D: 14/163 Control: 13/151 Cellulitis: D: 12/163 Control: 14/151	12 weeks

							Hospitalization: D: 13/163 Control: 22/151 Amputation: D: 9/163 Control: 19/151	
Naughton 1997 (61)	Dermagraft (109)	Control (126)	235 diabetic foot ulcers Ulcer size of >1cm^2 Ulcer duration > 2 weeks	42/109 (38.5%)	40/126 (31.7%)	Median time to closure: D: 13 weeks Control: 28 weeks Median time to recurrence: D: 12 weeks Control: 7 weeks	NR	12 weeks
Niezgoda 2005 (80)	Oasis (37)	Regranex (36)	73 diabetic foot ulcers Mean ulcer size 3.2 – 5 cm^2 Mean ulcer duration: not reported	18/37 (48.6%)	10/36 (27.8%)	Mean time to wound closure: O: 67 days R: 73 days	Infection: O: 9/17 R: 3/10 Recurrence: O: 2/8 R: 2/6 Pain: O: 2/17 R: 1/10	12 weeks
Puttirutvong 2004 (71)	Meshed skin graft (38)	Non-meshed skin graft (42)	80 diabetic foot ulcers Mean ulcer size 82-104 cm^2 Mean ulcer duration: not stated	NR	NR	Mean time to healing: Meshed: 19.84 ± 7.37 days Non-meshed: 20.36 ± 7.21 days	NR	6 months
Reyzelman 2009 (56)	Graftjacket (46)	Control (39)	85 diabetic foot ulcers Mean ulcer size 3.6 – 5.1 cm^2 Mean ulcer duration 22.9 – 23.3 weeks	32/46 (69.6%)	18/39 (46.2%)	Mean time to wound closure: G: 5.7 ± 3.5 weeks Control: 6.8 ± 3.3 weeks Decreased in ulcer size: G: 85% Control: 71.4% 90% healed at 12 weeks: G: 3/14 Control: 6/21	Infection: G: 1/46 Control: 0/39 Amputation: G: 1/46 Control: 1/39 Hospitalization: G: 1/46 Control: 1/39	12 weeks
Sanders 2014 (81)	Dermagraft (12)	Theraskin (11)	23 diabetic foot ulcers Mean ulcer duration 11.7 to 43.6 weeks Mean ulcer size 4.78 – 5.45 cm^2	4/12 (33.3%)	7/11 (63.6%)	Healing at 20 weeks: D: 8/12 (66.67%) T: 10/11 (90.91%) Mean time to healing: D: 12.5wks (7-20 weeks) T: 8.9 weeks (5-20 weeks)	NR	20 weeks
Sams 2002 (87)	Graftskin (9)	Compression (8)	17 diabetic foot ulcers Mean ulcer size 260cm^2	5/9 (55.6%)	3/8 (37.5%)	NR	Osteomyelitis: G: 0/9 Control: 0/8 Cellulitis: G: 2/9 Control: 0/8	12 weeks
Uccioli 2011 (74)	HYAFF (80)	Paraffin gauze (80)	160 diabetic foot ulcers Mean area 6.7-8.8 cm^2 Mean duration 7.3-7.4 months	19/80 (24%)	17/80 (21%)	Healing at 20 weeks: H: 40/80 (50%) Control: 34/80 (43%) Mean time to closure: H: 5.7 ± 3.5 days Control: 6.8 ± 3.3 days	Infection: H: 13/80 Control: 10/80 Amputation: H: 2/80 Control: 0/80	20 weeks

						Mean time to 50% ulcer reduction: H: 40 days Control: 50 days Weekly percentage reduction: H: 29% Control: 14%	Osteomyelitis: H: 1/80 Control: 0/80	
Veves 2001 (59)	Graftskin (112)	Saline gauze (96)	208 diabetic foot ulcers Mean wound area 2.8-2.9 cm^2 Mean wound duration 11 weeks	63/112 (56%)	36/96 (38%)	Median time to healing: G: 65 days Control: 90 days	Infection: G: 12/112 Control: 13/96 Cellulitis: G: 10/112 Control: 8/96 Osteomyelitis: G: 3/112 Control: 10/96 Amputation: G: 7/112 Control: 15/96 Recurrence: G: 3/51 Control: 4/31	12 weeks
Veves 2002 (88)	Promogram (138)	Gauze (138)	276 diabetic foot ulcer Mean wound area 2.5-3.1 cm^2 Mean wound duration 3 months	51/138	39/138	Mean time to healing: P: 6.9 ± 0.4 weeks Control: 6.3 ± 0.4 weeks Time to heal for ulcers < 6 months: P: 43/95 Control: 29/89 Time to heal for ulcers > 6 months: P: 10/49 Control: 8/43	Infection: P: 17/138 Control: 26/138 No epithelialization: P: 17/138 Control: 25/138	12 weeks
You 2012 (77)	Cultured allogenic keratinocytes (27)	Vaseline gauze (32)	59 diabetic foot ulcers Mean ulcer size 4-5.2 cm^2 Mean duration 0.33-0.4 years Wagner Grade I or II	27/27 (100%)	18/21 (69%)	Median time to closure: CEA: 35 days Control: 57 days % area reduction: CEA: 100% Control: 85 ± 65%	Infection: CEA: 2/27 Control: 3/32 Recurrence: CEA: 1/16 Control: 1/15 Amputation: CEA: 0/16 Control: 1/15	12 weeks
You 2014 (67)	Hyalograft 3D (33)	Non-adherent foam dressing (32)	63 diabetic foot ulcers Mean ulcer size 2.9-3.5 cm^2 Mean ulcer duration 6.1 – 6.2 months	26/33 (78.8%)	11/32 (34.4%)	Mean time to healing: Hyalograft 36.4 ± 17.6 Control 48.4 ± 13.1 Wound area reduction: Hyalograft 3 ± 2.6 cm^2 Control 2.1 ± 1.5 cm^2	Infection: Hyalograft 2/28 Control 5/25	12 weeks
Zelen 2013 (68)	Epifix (13)	Standard Care (12)	25 diabetic foot ulcers Mean ulcer size 2.6 – 3.4 cm^2 Mean ulcer duration 14.1- 16.4 weeks	12/13 (92.3%)	1/13 (8.3%)	Mean time to healing: Epifix 2.5 ± 1.9 weeks Control 5 ± 0 weeks	Cellulitis: Epifix 0/13 Control 2/12	6 weeks
Zelen 2014 (76)	Epifix weekly (20)	Epifix biweekly (20)	40 diabetic foot ulcers Mean ulcer size 2 – 2.4 cm^2	20/20 (100%)	15/20 (75%)	Mean time to healing: 1x/week: 2.4 ± 1.8 weeks	NR	8 weeks

			Mean ulcer duration 16.9 – 17.5 weeks			1x/2week: 4.1 ± 2.9 weeks Wound size reduction (2 weeks): 1x/week: 0.09 ± 0.18 1x/2week: 0.9 ± 1.4 Wounds healed (4 weeks): 1x/week: 18/20 1x/2week: 10/20		
Zelen 2016 (82)	Epifix (32) Apligraf (33)	Standard care (35)	100 diabetic foot ulcer Mean ulcer size 2.6 – 3.1 cm^2 Mean ulcer duration 14-19.1 weeks	31/32 (97%) 24/33 (73%)	18/35 (51%)	Mean time to healing: Epifix: 23.6 days Apligraft: 47.9 days Control: 57.4 days	Infection: Epifix: 0/32 Apligraf: 0/33 Control: 2/35 Osteomyelitis: Epifix: 0/32 Apligraf: 0/33 Control: 1/35	12 weeks

Table 2-3 Summary of studies included in this systematic review for diabetic foot ulcers.

Skin substitutes	Advantages	Disadvantages
Vulnamin gel	• Reduced mean time to ulcers healed • Increased percentage area healed	• No change in number of ulcers healed • No change in infection rate • No change in pain
GAM 501		• No change in number of ulcers healed
Graftjacket	• Increased number of ulcers healed	• No change in mean time to ulcers healed • No change in infection rate • No change in amputation rate • No change in hospitalization rate
HYAFF	• Reduced mean time to ulcers healed	• No change in number of ulcers healed • No change in infection rate • No change in osteomyelitis rate • No change in amputation rate
Integra	• Increased number of ulcers healed	•
Apligraft	• Increased number of ulcers healed • Reduced rate of osteomyelitis • Reduced rate of amputation	• No change in infection rate • No change in cellulitis rate • No change in recurrence rate
Dermagraft	• Increased number of ulcers healed	• No change in infection rate • No change in osteomyelitis rate • No change in cellulitis rate • No change in hospitalization rate
ADM + STSG		• No change in number of ulcers healed
Grafix	• Increased number of ulcers healed	• No change in infection rate • No change in recurrence rate
Orcel		• No change in number of ulcers healed

Cultured allogenic keratinocytes		• No change in number of ulcers healed
Hyalograft 3D	• Reduced mean time to ulcers healed • Increaed number of ulcers healed	• No change in infection rate
Epifix	• Increased number of ulcers healed	• No change in infection rate
Meshed skin graft		• No change in mean time to ulcers healed
Kaloderm		• No change in infection rate • No change in recurrence rate • No change in amputation rate

Table 2-4 Summary of meta-analysis outcomes by skin substitutes for diabetic foot ulcers.

Discussion

Limitations of this study

There was significant heterogeneity in the meta-analysis due to significant differences in type of skin substitutes, type of standard care/control and study protocol/methodology. Most studies reported primary outcome as number of ulcers healed after 12 weeks. However, some studies reported other outcomes instead e.g. mean ulcers healed after 12 weeks or 6 weeks or time to ulcer healing. Standard care differs between institutions based on type of dressings used and how regularly they are changed. These differences between studies may affect rate of wound closure in patients treated with skin substitutes vs controls significantly.

Several studies also did not report mean area healed as this can be difficult to assess and subject to inter-observer variation. There may be a need for a third-party observer to objectively assess percentage area healed based on wound photographs. Rate of wound healing was also difficult to analyse as some studies reported rate of wound healing in terms of percentage/day and some reported rate of wound closure in mm^2/day or cm^2/day.

Not all studies reported all adverse outcomes. Most studies reported incidence of wound infection, however not all studies reported rates of cellulitis/osteomyelitis, amputation or pain. Only five studies reported rate of ulcer recurrence and even then, duration of follow up differs between studies. Pain is a subjective experience and only one study reported whether patients were in pain. However, this was not recorded as per visual analogue scale (VAS) which is a more accurate way of quantifying pain.

Comparison between skin substitutes are limited and there is significant heterogeneity due to various types of skin substitutes compared. There is no single gold standard for treatment of diabetic foot ulcers and therefore, it is unclear which skin substitute should be used as baseline comparator although

Apligraf and OASIS are commonly used as controls to compare against novel skin substitutes e.g. Theraskin, Epifix.

Most studies also have small sample size which may result in Type II bias where results that are statistically significant, are not considered to be so. Pooling of results from different studies may help eliminate such bias. However, this was limited due to differences in study protocol and reporting of outcomes. There is a need for a more standardized study protocol so that results from each individual study so that results can be pooled and meta-analysis performed appropriately.

Efficacy of skin substitutes

Use of skin substitutes appears to increase incidence of ulcer closure, especially for Vulnamin gel, GraftJacket, Integra, Apligraf, Dermagraft, Grafix, Hyalograft 3D and Epifix. Mean time to ulcer healing was also significantly better in patients treated with skin substitutes (RR -2.01, CI -4.14, 0.12). Although percentage area healed was significantly higher in patients treated with skin substitutes, only one study reported this outcome. Several other studies reported area healed in metric dimensions, rate of healing per week or number of ulcers healed by >50% by a certain time point. This makes comparisons between studies difficult. Overall, there is a beneficial effect of skin substitutes on diabetic foot ulcer healing and closure.

Adverse effects of skin substitutes

Rate of infection was also significantly lower overall in patients treated with skin substitutes compared to controls (RR 0.69, CI 0.52, 0.92). However, no particular skin substitute was shown to reduce rate of infection, due to low number of events in each category and small sample sizes. Rate of osteomyelitis or cellulitis was not significantly reduced in patients treated with skin substitutes. This may be due to

the fact that these ulcers are at the severe end of the spectrum and skin substitutes exert their effect at an earlier stage of wound healing.

Rate of ulcer recurrence was also not significantly reduced by any skin substitutes. This could be because recurrence is affected by host factors such as nursing care, patient compliance with pressure off-loading and progression of atherosclerosis affecting vascular supply to the feet of diabetic patients. One of the most dreaded complications of diabetic foot ulcers is risk of amputation. Apligraf was the only skin substitute which appears to reduce incidence of amputations in patients with diabetic foot ulcers. Rate of hospitalization was not significantly reduced by skin substitutes which may be due to the fact that these diabetic patients often have poor glycaemic control and multiple co-morbidities such as diabetic retinopathy, nephropathy and neuropathy which may affect decisions to admit these patients.

Summary

Skin substitutes result in significantly higher number of ulcers healed but did not significantly reduce mean time to ulcer healing or increase mean area epithelialized. Skin substitutes also significantly reduce rates of infection in diabetic foot ulcers, but not rate of cellulitis or osteomyelitis. Rate of recurrence and rate of amputation was marginally reduced but this was not statistically significant. Number of patients hospitalized for diabetic foot ulcers were slightly reduced but not statistically significant while pain was not significantly reduced by skin substitutes.

2.2. Rheological and Interfacial Chemistry of Emulsions: Key Concepts

2.2.1. Emulsions

As described in Chapter 1, this thesis aims to explore how emulsion templating can be used to create scaffolds for tissue engineering and wound healing purposes. To achieve this objective, we first must explore the surface rheological properties and interfacial chemistry of emulsions.

An emulsion is an immiscible dispersion of one liquid in another liquid which is the continuous phase. (89) It is essentially a colloid where both phases are liquids. Emulsions are inherently unstable and tend to phase separate into distinct oil and water phases without any added surfactant or emulsifier molecules. The mechanisms of destabilization include creaming, sedimentation, flocculation, phase inversion, coalescence and Ostwald ripening. (89)

Emulsions can exist in the form of oil-in-water (O-W) or water-in-oil (W-O) or mixed emulsions (O-W-O or W-O-W). The size of emulsion droplets can vary widely depending on the components of the emulsion and method of mixing. Nanoemulsions are emulsions with droplets of <1nm, microemulsions are emulsions with droplets of >1 nm and macroemulsions are emulsion with droplets of >1μm. (90)

Surfactants are surface active molecules which play an integral role in stabilizing the emulsion system at the interface. (91) Surfactants traditionally have a hydrophilic head and a hydrophobic tail which interacts with the separate aqueous and oil phases respectively. They act by lowering the surface tension at interfaces, thus creating a more stable emulsion.

They can be broadly categorized into non-ionic (e.g. Tween 20), cationic surfactants (e.g. DTAB), anionic surfactants (e.g. SDS) and zwitterionic surfactants (e.g. phospholipids). (91) Non-ionic and ionic surfactants can also be mixed to achieve better stabilization of the emulsion system. Other types of surfactants include polymers and proteins which can adsorb onto the interfacial regions. In particular, emulsions with solid particles adsorbed at the interface are called Pickering emulsions.

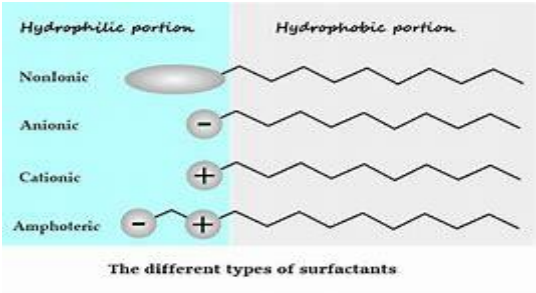


Figure 2-31 Types of surfactants as categorized by type of head group.

The properties of emulsions such as interfacial chemistry, surface rheology and stability can be characterized to define a particular emulsion system. This is explored in detail in the following sections.

2.2.2.Interfacial Chemistry of Emulsions

The interface between two phases of an emulsion is a unique region with interesting characteristics. The interface between two bulk phases can be defined by a dividing line (Gibbs dividing line) which delineates a region with markedly different properties compared to the bulk phase. (89)

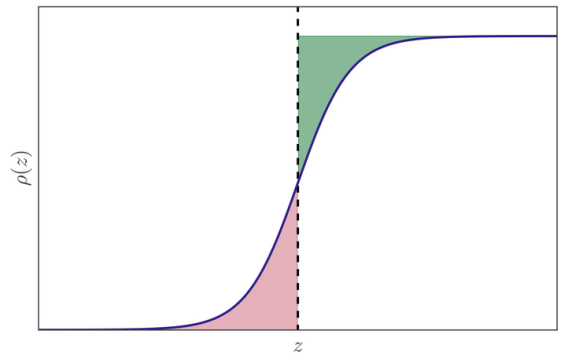


Figure 2-32 Diagrammatic representation of Gibbs dividing line. Bulk concentration of molecules in the aqueous and oil phase remain fairly constant but gradually tapers towards the Gibbs dividing plane.

Using Gibbs model, the surface energy at the interface can be represented by the Gibbs-Deuham equation below:

$$dG = -SdT + Ad\gamma + \sum ndu \qquad (2.1)$$

Where G is the surface free energy, S is the entropy, T is temperature, A is total surface area, γ is surface tension, n is number moles of a component with chemical potential of μ. This equation can be simplified to determine the minimum amount of surfactant required to create a metastable emulsion system in equilibrium (as shown below).

Assuming equilibrium conditions and constant temperature, the equation can be simplified to

$$dG = Ad\gamma + \sum nd\mu = 0 \tag{2.2}$$

$$Ad\gamma = -\sum nd\mu \tag{2.3}$$

$$d\gamma = -\sum \frac{n}{A} d\mu = -\sum \Gamma d\mu \tag{2.4}$$

Where Γ represents the concentration of surfactants adsorbed (also known as surface excess).

The chemical potential of surfactant μ is as below:

$$\mu = \mu + RT \ln a \tag{2.5}$$

Differentiating this equation gives

$$d\mu = RTd \ln a \tag{2.6}$$

Thus,

$$-d\gamma = \Gamma RTd \ln a \tag{2.7}$$

Substituting a for C where C is the concentration in moles of surfactant:

$$\frac{d\gamma}{d \ln C} = -\Gamma RT \tag{2.8}$$

Surface tension can then be calculated by solving for C and Γ assuming RT is constant.

2.2.3.Surface Rheology of Emulsion

Interfacial rheology describes the response of interfacial films to deformation either by shear or compressional forces. (92) Dilatational rheology measures variation in surface area while maintaining the same shape while shear rheology measures variation in shape over a constant area. (92) Various techniques can be used to measure these properties including pendant/sessile drop technique, Wilhelmy technique and du Nouy ring method.

Surface rheology in protein-surfactant mixtures depends on the nature of the protein of interest and type of surfactant which may be altered by factors such as concentration or proteins/surfactants, viscosity of oil/aqueous phase, temperature, pH, and shear forces. (92) It also gives an indication as to the stability of the emulsion system over time. Change in interfacial rheology may also depend on whether the protein and surfactants were added sequentially or simultaneously. (93)

In cases where protein and non-ionic emulsion systems are used, proteins and surfactants competitively adsorb onto interfacial regions. (94,95) There may be weak hydrophobic interactions between protein and surfactant molecules affecting rate of adsorption and protein conformation as well. Concentration and degree of surface activity of surfactant molecules and protein molecules may also affect rate of adsorption as proteins may preferentially displace surfactant molecules and vice versa. (95)

For emulsion systems with proteins and ionic surfactants, the protein and ionic surfactant molecules may form complexes until electrical neutrality is achieved. (96) With higher surfactant concentrations, there is preferential adsorption of the surfactant molecules at the interface compared to the less surface-active protein-surfactant complexes. Thus, surfactants molecules eventually displace any protein-surfactant complexes at the interface.

2.2.4.The Role of Surfactants for Emulsion Stability

As described above, surfactants increase the stability of emulsion systems by lowering interfacial tension. Surfactants may be characterized based on their hydrophile-lipophile balance (HLB) values. (97,98) The HLB values also provide a rough indication of potential applications for each type of emulsion as shown below:

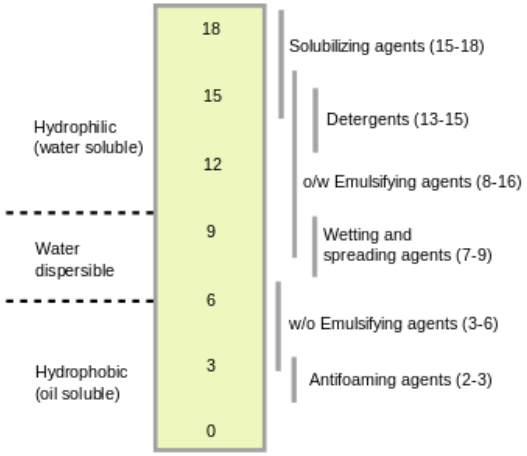


Figure 2-33 HLB values of surfactants and their uses. Surfactants with lower HLB values are much more oil soluble and form water in oil emulsions while surfactants with higher HLB values are much more water soluble and form oil in water emulsions. Reprinted with permission © Churchill Livingston. (99)

In general, surfactants with higher HLB values are more hydrophilic and surfactants with lower HLB values are more lipophilic. They hydrophobic surfactant tails are often made up of hydrocarbon chains which may be branches, linear or aromatic. They may also be made up of fluorocarbon chains and siloxane chains. For most surfactants, the classification is by the nature of the hydrophilic head group – non-ionic, cationic, anionic or amphotheric.

Non-ionic surfactants are often fatty acid or fatty alcohol esters and ethoxylates. Other members of this family of surfactants include: Alkylphenol ethoxylates (e.g. Triton X-100), amide/fatty acid amide ethoxylates, terminally blocked ethoxylates, amide oxides and sulfoxides etc.

Anionic surfactants have negatively charged functional groups at their heads such as sulfate, sulfonate, phosphate and carboxylates. Examples of anionic surfactants include ammonium lauryl sulfate, sodium dodecyl sulfate, sodium laureth sulfate and docusate etc.

Cationic surfactants have positively charged head groups which are mostly primary, secondary, tertiary or quarternary amines. Examples include methyl triethanolammonium, benzalkonium chloride, dimethyldioctadecylammonium chloride and more.

Zwitterionic surfactants have both cationic and anionic groups attached to the surfactant. Biological amphoteric surfactants such as phospholipid phosphatidylserine, phosphatidylethanolamine, phosphatidylcholine and sphingomyelins also fall into this group of surfactants.

Surfactants reduce the surface tension up to the critical micelle concentration, whereby any increase in surfactants does not change the value of surface tension. (100) This is because excess surfactant molecules form micelles with a hydrophobic core and do not adsorb at the interfacial regions. They may also interact with other molecules such as proteins and polymers which may alter their surface-active properties. (101)

2.2.5.Protein Surfactant Interaction – The Adsorption Problem

Proteins have surface active properties due to their amphiphilic structure which provides the thermodynamic drive for folding into their secondary and tertiary structures. Thus, they typically behave as surfactants by adsorbing onto interfacial areas. There is an active balance between the surfactant, protein and surfactant-protein complexes. Proteins which are adsorbed undergo conformational changes due to unfolding of their hydrophobic core at interfaces and the adsorption-desorption process. (102) This change in structure often results in denaturation of the protein and thus,

loss of functional activity. Theoretically, such denaturation will be associated with an enthalpy and entropy change but require an activation energy to overcome the native structure conformation.

Irreversible adsorption can occur when surfactants are unable to displace the protein layer due to permanent changes in conformation. For example, β-lactoglobulin tend to remain adsorbed despite the presence of surfactants. This may be because proteins form immobile viscoelastic films at the interface while surfactants form interfacial layers with low interfacial viscoelasticity. (92) There is a need to prevent this protein adsorption phenomenon in order to create a biocompatible emulsion system.

Biocompatible emulsions can be defined as emulsion systems which preserve the native structure and functionality of protein-containing emulsion systems. Hypothetically, this can be achieved by using surfactant molecules which are capable of displacing protein molecules from the interface by preferential binding (i.e. more surface active than the protein of interest) or saturating the interface with surfactants prior to addition of protein solution. Such competitive adsorption effect may result in proteins molecules being sequestered in the aqueous phase and retaining their conformation. (95)

Protein-surfactant complexes can also form when both are mixed together. They may result in increase or decrease in surface activity, depending on the hydrophilicity and hydrophobicity of the resulting complex. The formation of protein-surfactant complexes may also result in subtle or gross changes in conformation of protein structure which may result in reversible denaturation. For instance, ionic surfactant interaction can result in complete loss of secondary structures as exploited by SDS-PAGE. These protein-surfactant complexes are also bulkier than their own individual protein or surfactant molecule, which may affect their behaviour at interfaces. (102)

2.2.6.Forces of Interaction between Emulsion Droplets

Emulsion droplets are inherently unstable and tend to phase separate with time. The interaction between emulsion droplets may be broadly categorized into 3 types: van der Waals forces, electrostatic repulsion and steric repulsion. (89)

Van der Waals forces are made up of dipole-dipole, dipole-induced dipole and dispersion forces of interaction between two molecules. These forces depend on charge fluctuations and distance between two molecules. The van der Waals forces increase as two molecules approach each other (e.g. emulsion droplets) resulting in flocculation of emulsion droplets.

Electrostatic repulsions may result from adsorption of ionic surfactants at the interface of emulsion droplets. This occurrence forms an electrical double layer made up of the adherent Stern layer and the diffusely charged Gouy-Chapman layer. (89) The charge decreases as distance from the interface increases. This effect is dependent on valency of the charged particle and ionic concentration of the charge particles.

The Derjaguin, Landau, Verwey, and Overbeek (DLVO) theory describes the stability of colloidal systems and can be used to represent the effect of both van der Waals attraction and electrostatic repulsion (Figure 2-34). Initially, electrostatic repulsion outweighs van der Waals attraction, however this decreases to a primary minimum where attraction>repulsion forces, before increasing again as dispersion attraction increases at a slower rate compared to electrostatic repulsion up to a second peak where forces of repulsion outweigh attraction. This then gradually decreases as van der Waals forces increase while electrostatic repulsion decreases logarithmically, yielding a secondary minimum.

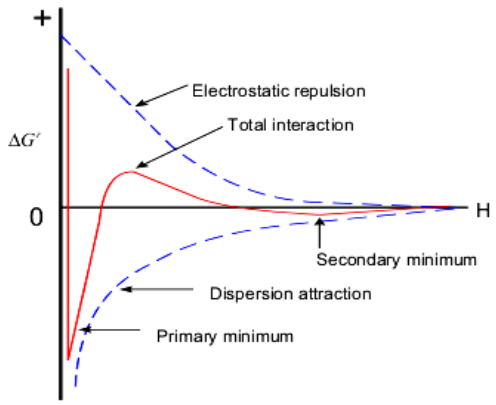


Figure 2-34 Diagram illustrating DLVO theory.

Steric repulsion may be another force of interaction between emulsion particles when non-ionic or polymeric surfactants are used. For example, soluble dispersed phase polymers such as polyvinylpyrrolidone (PVP) may be used as stabilizers in aqueous emulsions, as they prevent collision or aggregation of emulsion particles. Also, the long chains of block co-polymers e.g. Pluronic PEO-PPO-PEO block co-polymers act as a physical molecular barrier when adsorbed onto interfaces.

2.2.7. Emulsion-Templating and PolyHIPEs

Emulsion templating can be defined as a method of manufacturing scaffolds using emulsions as a template to create porous structures. This method of creating porous materials has traditionally been applied to polymers. High internal phase emulsions can be defined as emulsions with an internal phase of >74% of the total emulsion volume. (15) They can be used to create polyHIPEs which are polymeric high internal phase emulsions to create a highly porous and interconnected scaffold. Polymerisation of materials such as polystyrene, polyacrylamide, polymethacrylate, polysaccharides and denatured proteins have been found in literature. (103-105)

For most polyHIPES, polymerization is done by free radical initiation although photopolymerization is now increasingly used. (15) However, one of the main limitations of use of polymers is the poor

biodegradability of such materials. Although some polyHIPEs such as those made up of thiol-ene substrates are essentially degradable polyesters, native proteins such as collagen, fibrin, hyaluronic acid are more biocompatible as they have cell signalling motifs for cellular attachment and migration. Emulsion-templated proteins was first described by Barbetta et al. (106) However, the protein used was gelatin which is essentially denatured collagen. Although gelatin is biocompatible and biodegradable, there remains a challenge of using emulsion templating for native proteins due to adsorption denaturation at interfaces.

Some of the advantages of emulsion templating to produce scaffolds are control of porosity and biocompatibility of such scaffolds. This also gives the user flexibility to fine-tune the porosity and mechanical properties of bioengineered scaffolds, using different sized emulsion droplets, tailored to the needs of each application. For example, microporous scaffolds with pore sizes of about 20 microns allow growth of hepatocytes, while pore sizes of 20 to 150 microns are shown to promote fibroblast migration for skin regeneration. (107) Additionally, pore diameters of 100 to 400 microns are reported to promote osteogenesis and angiogenesis. (108,109)

There are several major limitations of emulsion templating of protein structures: protein denaturation, by adsorption at hydrophobic interfaces and by surfactant agents, emulsion instability, complexity of introducing stabilisation methods, and biocompatible oil-phase elution and surfactant removal. (110) Proteins typically adsorb to and denature at oil-water interfaces (16,111,112) so the creation of vary large surface area to volume ratio interface, and short diffusion distance necessarily presents a system that will favour any denaturation process. Moreover, the surfactants needed to form a stable emulsion are likely to adsorb onto and denature proteins. (113) Additionally, any process of emulsion ripening or maturation, will counteract the desired stability of the emulsion droplets as a template. Further issues of particular consideration for protein scaffolds concern post-formation stabilisation, for example by a compatible chemical cross-linking method, and elution of the emulsion phase without disruption of the

formed scaffold. For example, phase separation involves release of significant energy, which can disrupt the formed material as the oil phase separates. All these considerations determine the feasibility and resultant biocompatibility of the scaffold produced.

The underlying hypothesis is that a surfactant coated boundary layer prevents protein adsorption and denaturation at the emulsion interface. This enables protein-based three-dimensional hydrogels to be formed into porous scaffold structures with minimal denaturation. A biocompatible emulsion can be created using non-ionic surfactants to control emulsion droplet size, to prevent denaturation of proteins in the aqueous phase of emulsion, and to allow successful formation of protein scaffolds.

Almost all commercially available skin substitutes are made of collagen or collagen composites (2) and fibrin is also widely used as an extracellular matrix with pro-angiogenic effects. (114) Thus, these proteins were chosen as scaffold materials, to evaluate the influence of protein type on biocompatibility of emulsion-templated dermal scaffolds.

2.3. Principles of Lyophilization

Freeze-drying or lyophilization is a process where water is removed from a product through ice crystal sublimation under set temperature and vacuum conditions. The process is dependent on vapour pressure of the solvent removed. The aim is to create a dried product with extended shelf-life which is easier to store and transport. In the case of water, lyophilization is done under the triple point to prevent melting of ice-crystals. Thus, a key parameter during the process of freeze-drying is the vapour pressure of water to ensure the ice-crystals sublime, rather than melt-back.

Lyophilization is divided into three stages – freezing, primary drying and secondary drying. The rate of freezing determines the size of ice-crystals which can act as porogens to produce a porous product. A

fast rate of freezing would result in smaller ice-crystals which are less harmful to cells. Some biological samples can be snap frozen in liquid nitrogen before the drying phase as well. A slower rate of freezing can also be used to create larger ice-crystals which produce a more porous end-product which could be useful for tissue-engineered scaffolds e.g. Integra.

During primary drying, pressure is lowered and heat is introduced at a controlled rate to speed up the sublimation process. About 95% of water is removed in this phase and rate of heat applied can affect material structure significantly. Secondary drying is where tightly bound water on the material surface is removed. This is done at a higher temperature than that of primary drying.

For crystalline products, lyophilization should be done under the eutectic temperature where the product exists in solid state. For amorphous products, lyophilization should be done under the glass transition temperature. Failing to do so would result in collapse of the product due to loss of physical microstructure of the material during lyophilization. This is highly relevant in creating and preserving the structure of microporous scaffolds for tissue engineering purposes, which is explained later on.

2.4. Summary

In summary, the interaction of proteins and emulsions systems have yet to be characterized fully to explore the feasibility of emulsion templating. Emulsion templating is a cheap and highly scalable method of creating porous biocompatible scaffolds. Such scaffolds have applications for 3D culture, tissue engineering and reconstruction purposes. There is a need to further elucidate the mechanisms of interactions between protein and surfactant particles as well as behaviour of protein molecules at interfaces. Our hypothesis is that prevention of protein molecules from adsorption at interfaces will preserve the functionality and native conformation of proteins within emulsion systems, allowing formation of a microporous protein hydrogel scaffold.

Chapter 3 Formulation of an Emulsion-Templated Scaffold

3.1. Characterization of a Biocompatible Emulsion System

3.1.1. Introduction

Emulsions are commonly used in food processing, oil extraction, construction work, cosmetic and medical formulations as they are widely found in the natural environment and have versatile applications. For example, the use of emulsions greatly influences texture and consistency of food products such as yoghurt, milk and cream. They are useful delivery systems as the droplets within the emulsion systems greatly increase the available surface area for antigen binding and allow encapsulation of insoluble proteins as an injectable form of therapy.

Macroemulsions are metastable liquid-in-liquid dispersions with droplet sizes typically ranging between 1 – 100 microns. (115) These emulsions are inherently unstable and require surface-active molecules to improve their stability. (116) This can be understood through the second law of thermodynamics:

$$\Delta G = \Delta A\gamma - \Delta TS \tag{3.1}$$

where G is the energy of formation, A is the total surface area, γ is the surface tension, T is the temperature and S is entropy.

In most cases, $A\gamma >> -TS$, which means that G is positive, that is, the formation of emulsions requires energy input and the system is thermodynamically unstable. Surfactants help stabilize such emulsions systems by lowering the interfacial surface tension and creating a thermodynamically stable interfacial boundary layer. (117) Various factors affect the stability of emulsions systems including type of surfactant, hydrophile-lipophile balance (HLB) value of surfactants, presence of hydrophilic polymer excipients e.g. polyethylene glycol, polyvinylpyrrolidone, temperature and more. (118) The first part of

this study aims to characterize the effects of these factors on control of mean droplet size and stability of an oil-based emulsion system.

Protein-emulsion interactions have been investigated in the field of food processing industry, detergent industry, pharmaceutical industry, as well as oil extraction and purification industry. It is known that proteins tend to adsorb at oil-water interfaces due to their surface-active properties. (119) Unfortunately, the partitioning of hydrophopic oil phase and hydrophilic aqueous phase at interfacial boundaries tends to cause protein denaturation by unfolding of the secondary and tertiary structure of the protein. (112) Furthermore, the denaturation process that occurs at these interfacial boundaries is often irreversible. (112) This often results in loss of protein function e.g. enzymes in biodetergents.

One way of circumnavigating the problem of protein denaturation at oil-water emulsion interface is to use a non-denaturing surfactant molecule to displace proteins from the interfaces. Several studies have suggested that non-ionic surfactants such as Tween 20 may play a role in preventing protein denaturation in emulsions. (120) However, the mechanism by which this protection is conferred is unclear. Thus, for the second part of this study, bovine serum albumin (BSA) was used as a model plasma protein to study the role of non-ionic surfactants such as Tween 20 and Span 20 in preserving the native state of BSA in emulsions. The aim is to create an emulsion system where the bulk of the protein remains in the aqueous phase, rather than in the oil phase or interface, to prevent unfolding of the protein structure and thus, preventing denaturation.

Lastly, the possibility of using non-denaturing biocompatible emulsions to produce emulsion-templated scaffolds was explored in a separate study. (121) Factors controlling emulsion droplet size that indirectly affect porosity of such scaffolds and how proteins interact with emulsion systems to minimize denaturation of proteins used to create such scaffolds are investigated in this chapter.

3.1.2.Materials and Methods

Materials

Pharmaceutical grade mineral oil, Tween 20 and Span 20, 2-(N-morpholino) ethanesulfonic acid (MES), sodium chloride (NaCl), Oil Red O, bovine serum albumin (>95% purity), FITC-BSA and butanol were all purchased from Sigma. Polyvinylpyrrolidone (PVP) excipient (Kollidon 90, MW 300 kDa) was obtained from BASF Pharmaceutical Co. The lactate dehydrogenase (LDH) assay was purchased from ThermoFisher Scientific, UK.

Emulsion preparation

Effect of HLB ratio on emulsification

Tween 20 and Span 20 were mixed to obtain a range of HLB values of 9.5 to 14 as shown below (Table 3-1). The use of a mixture of two surfactants allows for control of emulsion droplet sizes and subsequent pore size of emulsion-templated scaffolds. 0.75% of surfactant was added to 5ml of mineral oil. 2% of PVP was added to 2.5ml of 25mM MES/150 mM NaCl buffer (pH 7.4). The solution was vortexed for 15 seconds to emulsify the mixture.

HLB value	**10**	**10.5**	**11**	**11.5**	**12**	**12.5**	**13**	**13.5**	14
Tween 20 (µl)	180	220	300	360	420	480	540	600	660
Span 20 (µl)	820	790	700	640	580	520	460	400	340

Table 3-1 Tween 20 and Span 20 mixing volume ratio.

Effect of excipient concentration on emulsification

0.5% of Tween 20/Span 20 surfactant mix with HLB ratio of 13 was added to 5ml of mineral oil. 0%, 0.5%, 2% and 4% of polyvinylpyrrolidone (PVP) was added to 2.5ml of 25mM MES/150 mM NaCl buffer (pH 7.4). The solution was vortexed for 15 seconds. PVP (Kollidon) is an emulsifying agent

which helps further stabilize the emulsion system by nature of their long molecular chain, which results in steric stability by preventing droplet collision and increased viscosity, allowing for better control of the emulsion droplet size and stability.

Effect of surfactant concentration on emulsification

0.25%, 0.5%, 0.75%, 1% and 1.5% of Tween 20/Span 20 surfactant mix with HLB value of 13 was added to 5ml of mineral oil. 2% PVP was added to 2.5ml of 25mM MES/150 mM NaCl buffer (pH 7.4). The solution was vortexed for 15 seconds.

Effect of temperature on emulsification

0.75% surfactant concentration of Tween 20/Span 20 surfactant mix with HLB ratio of 13 were added to 5ml of mineral oil and 2.5ml of 25mM MES/150 mM NaCl buffer (pH 7.4). The mixture was stored at 4, 22 and 37 degree Celsius for an hour and vortexed for 15 seconds.

Effect of varying surfactant concentration at different shear rates

0.25%, 0.5%, 1% and 1.5% of Tween 20/Span 20 surfactant mix with HLB ratio of 13 were added to 5ml of mineral oil and 2.5ml of 25mM MES/150 mM NaCl buffer (pH 7.4). The mixture was homogenized with a high-speed mixer (Caframo, Canada) at 500 rpm, 1000 rpm, 1500 rpm, 2000 rpm, 2500 rpm and 3000 rpm.

Emulsion droplet size analysis

10µl of Oil Red O was added to 100µl of all emulsion mixes and placed on a glass slide with a cover slip. Droplet diameter was characterized using simple light microscopy and Image J (NIH, USA).

Emulsion stability analysis

Stability analysis was peformed by measurement of turbidity (Turbiscan emulsion stability analyzer, Formulaction, France). Change in light transmission and backscatter throughout the sample was used to characterize effect of HLB ratio, surfactant concentration and PVP concentration on the stability of each emulsion mix. 2ml of each emulsion mix was pipetted into glass cells and 21 scans were done over a period of 10 minutes (1 scan every 30 seconds). Change in light transmission and backscatter throughout the length of the glass cell was plotted over time to obtain time point measurements of emulsion destabilization.

Emulsion viscoelasticity analysis

The viscoelastic properties of emulsions were measured using a rheometer (Anton Paar, Germany) to evaluate effect of changes in HLB values, surfactant and PVP concentration on the viscoelastic properties of each emulsion system. A rotating concentric cylinder system was used to maximize surface area for measurement of viscosity of the emulsions. An amplitude sweep was done to determine the point at which the internal properties of the emulsions were most stable and a frequency sweep was performed to investigate the storage moduli and loss moduli of each emulsion system. A series of emulsions with HLB 10 to 13, surfactant concentration of 0.25% to 1.5% and PVP concentration of 0% to 4% were prepared as described above. 7 ml of each emulsion system was then transferred into the concentric cylinder for measurement.

Characterization of protein-emulsion interaction

Localization of proteins in emulsion mix

10µl of 1mg/ml FITC-BSA was added to each emulsion mix and vortexed for 15 seconds. The mixtures were incubated at 37 °C for 30 minutes before imaging under confocal microscopy. Distribution of

FITC-BSA for each emulsion mix was recorded and confocal green fluorescence images were taken at 10x magnification.

Quantification of protein in oil and aqueous phase

10µl of 1mg/ml FITC-BSA was added to each emulsion mix and vortexed for 15 seconds. The mixtures were incubated at 37 °C for 30 minutes before centrifuging at 10 000 g for 10 minutes to induce creaming. 200µl of the aqueous subnatant was carefully removed and transferred into a 96 well plate in triplicates (50µl per well). 100µl of the creamed supernatant was removed and mixed with 100µl of butanol to break the emulsion before transferring onto a 96 well plate in triplicates (50µl per well). Relative fluorescence was measured against a control solution containing 10µg/ml of FITC-BSA in MES/NaCl buffer. Plates were read using the Spectramax i3x Multi-Mode Detection Platform (Molecular Devices, CA, USA) at an excitation wavelength of 495nm and an emission wavelength of 530nm. A standard curve using a range of FITC-BSA concentration was used to quantify amount of proteins in the aqueous and cream phase.

Assessing adsorption of BSA in oil phase

Attenuated total reflection - Fourier transform infrared spectroscopy (ATR-FTIR) was used to assess denaturation of adsorbed BSA in the cream phase. Each emulsion mix was prepared as described above, however 3% BSA in MES/NaCl buffer was added to the aqueous phase prior to vortexing and centrifugation at 10 000 g. This concentration would ensure that even if 0.1% of total BSA was adsorbed, it would be above the threshold of detection limit (3mg/ml). Spectra of pure native BSA and denatured BSA (heated to 80 °C for 2 hours) were also measured.

Around 20µl of cream phase was loaded onto the crystal of a TENSOR 37 spectrometer (Bruker) with a MIRacle single-reflection ATR unit (Pike Technologies, Wisconsin, USA). The sample detector was

purged with nitrogen and an absorption spectrum was recorded in the range of 800–4000 cm^{-1}, Background measurements were based on 64 scans, and sample measurements were based on 64 scans. The data obtained by FTIR were processed using the options of OPUS version 6.5. Each emulsion spectra was subtracted from the protein-emulsion spectra to obtain only protein signals, if present. The spectra were then deconvolved using secondary derivative and linear baseline correction of the amide I band was performed to discern if any protein peaks from BSA was present.

Assessing conformation of BSA in aqueous phase of emulsion

Near-UV circular dichroism (Jasco J-815 Spectropolarimeter, Japan) was used to assess for changes in conformation of BSA in the aqueous phase of the emulsion. An HLB 13 emulsion mix with 0.25% surfactant concentration was prepared using a phosphate buffer. BSA solution was prepared at a concentration of 4 mg/ml in a 10mM phosphate buffer (pH 7.4). As controls, native and denatured BSA samples, as well as pure emulsion samples (no proteins) were prepared as well. The emulsion mix was incubated with BSA (at 1:1 volume ratio) for 30 minutes and then centrifuged at 10 000 g and filtered three times, using a 0.02µm filter to remove all emulsion particles. The filtrate was analyzed using near-UV circular dichroism. The near-UV spectra was collected between 260 nm to 310 nm using a 1cm path length quartz cell in 0.1nm steps with 4 scans per sample. All measurements were done at 25 °C and baseline corrected using the 10mM phosphate buffer. To ensure reliable results were obtained, only spectra below 1 kV high tension (HT) dynode voltage were included. Far-UV spectra was not included in this study as the HT voltage exceeded 1kV.

Assessing intrinsic tryptophan fluorescence of fibrinogen in aqueous phase of emulsion

Intrinsic fluorescence of protein due to aromatic amino acids such as tryptophan provides another way of assessing tertiary structure of proteins in the aqueous phase of emulsions which may be altered by the presence of surfactants and hydrophobic emulsion droplets. Tryptophan excites at around 275 nm

and has an emission of 350 nm in aqueous environment. Denaturation of proteins result in exposure of tryptophan residues which leads to shifts in the emission peak.

A series of emulsion mixes with different surfactant (0.25% SA, 0.5% SA, 0.75% SA) and PVP (1% PVP, 2% PVP, 4% PVP) concentration was prepared with a final concentration of 1% fibrinogen. As controls, native and denatured (in 1% SDS) fibrinogen samples without emulsions were prepared as well. Each emulsion mix was incubated with fibrinogen for 30 minutes and centrifuged at 10 000 g to separate the aqueous phase of the emulsion. 50µl of each sample was pipetted into a 96 well plate in triplicates and plates were read using the Spectramax i3x Multi-Mode Detector (Molecular Devices, CA, USA) at an excitation of 275 nm and emission spectra was collected from 300 nm to 400 nm.

Assessing function of lactate dehydrogenase in aqueous phase of emulsion

In addition to examining structural changes of proteins exposed to emulsions, the functional changes of proteins exposed to emulsions were also investigated. A colorimetric assay using lactate dehydrogenase (ThermoFisher, UK) was utilized to investigate the effect of exposure of the enzyme to surfactants and hydrophobic emulsion droplets. A series of emulsion mixes with different surfactant (0.25% SA, 0.5% SA, 0.75% SA) and PVP (1% PVP, 2% PVP, 4% PVP) concentration was prepared.

2µl of LDH Positive Control was added to 1ml of each emulsion mix and incubated for 30 minutes. The emulsions were then centrifuged at 10 000 g to separate the aqueous phase of the emulsion. 50µl of each sample was pipetted into a 96 well plate in triplicates together with 50µl of Reaction Mix per sample, according to the assay protocol. Plates were read using the Spectramax i3x Multi-Mode Detector (Molecular Devices, CA, USA) at OD 450 nm in kinetic mode, every 3 minutes for 30 minutes at 37 °C.

Statistical Analysis

All statistical analysis was done using GraphPad Prism Version 4.0 (GraphPad Software Inc.). All measurements are expressed as mean ± standard deviation. One-way ANOVA and Tukey's post-hoc correction was used to analyze the data. A value of $p<0.05$ is statistically significant. Where applicable, * denotes a p–value of <0.05, ** denotes a p–value of <0.01 and *** denotes a p-value of <0.001.

3.1.3.Results

Emulsion droplet size characterization

Effect of HLB ratio on droplet size

At HLB of 9.5 no emulsions were obtained and only colloidal aggregates were formed. At HLB values of 10 and 10.5, small unstable oil-in-water and water-in-oil droplets forming biphasic emulsions were obtained. At HLB of 11, complex emulsions of water-in-oil-in-water (W-O-W) emulsions were formed. From HLB of 11.5 to 15, metastable oil-in-water emulsions were obtained. Therefore, increasing the HLB ratio stabilizes the oil-in-water emulsion phase with a trend towards smaller mean droplet sizes. However, mixtures of HLB >15 were again unstable.

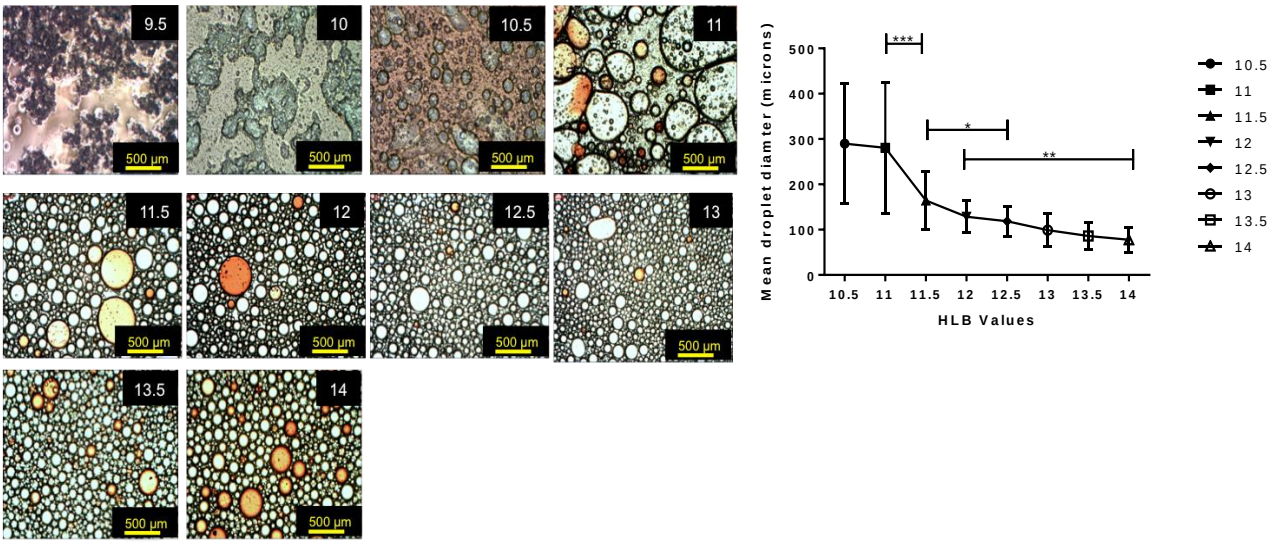


*Figure 3-1 Light microscopy of Oil Red O stained emulsions showing phase transition of the emulsions as HLB value increases (Magnification 10x). Mean droplet diameter decreased significantly as HLB values increased. * denotes a p–value of <0.05, ** denotes a p–value of <0.01 and *** denotes a p-value of <0.001. (mean ± SD, n=20)*

Effect of surfactant concentration on droplet size

When no surfactant was added to the mineral oil, 25mM MES/150 mM NaCl buffer (pH 7.4) with 2% PVP, no emulsions were obtained. At concentrations of 0.25% to 1.5% of HLB 13 surfactant mix, increase in surfactant concentration tended to decrease droplet diameter.

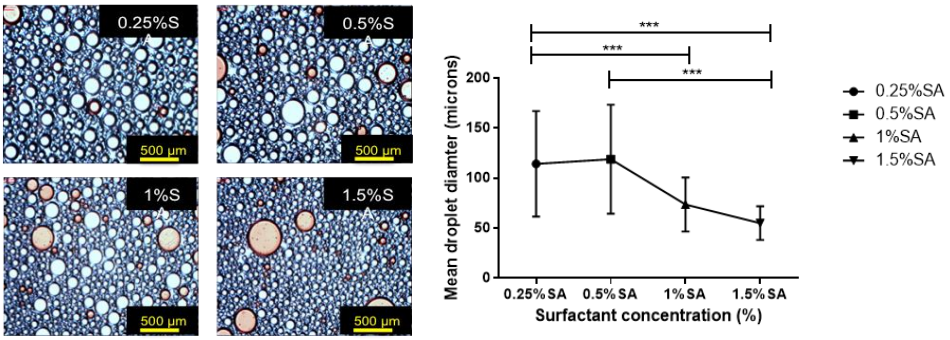


*Figure 3-2 Light microscopy of Oil Red O stained emulsions showing decrease in mean droplet diameter as surfactant concentration increased ($p<0.05$). *** denotes a p-value of <0.001. (mean ± SD, n=20)*

Effect of PVP concentration on droplet size

In the HLB 13 emulsion mixture with 0.5% surfactant mix concentration without PVP, large droplet diameters of about 200 microns were obtained. Increasing the PVP concentration makes droplets smaller and more uniform. This suggests that PVP may have surface-active properties or interacts with surfactant molecules at the interfacial regions that further stabilizes the emulsion. This range was selected to establish a minimum effective concentration for stabilizing the emulsion system. Higher concentrations of PVP result in a very viscous emulsion system which is difficult to mix.

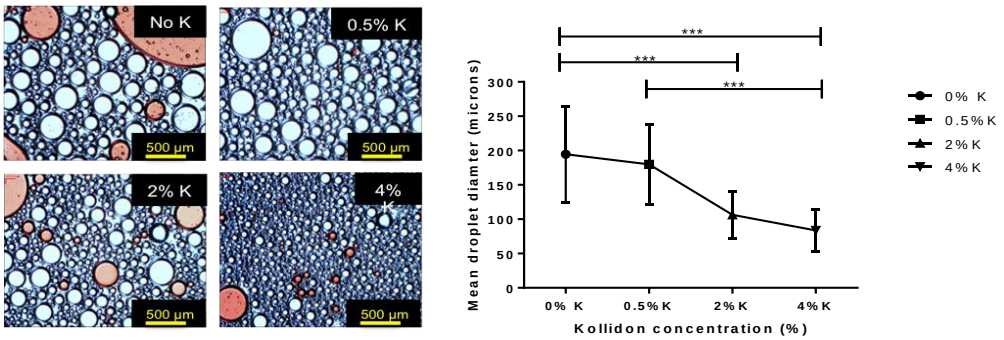


*Figure 3-3 Light microscopy of Oil Red O stained emulsions showing decrease in mean droplet diameter as PVP (Kollidon) concentration increased ($p<0.05$). *** denotes a p-value of <0.001. (mean ± SD, n=20)*

Effect of temperature on droplet size

Between 4 °C and 37 °C, temperature change had negligible effect on droplet size. There was a slight increase in mean droplet size when temperature was changed from 22 °C to 37 °C to about 105 microns. However, this was not a significant effect. Temperatures above 37 °C were not tested as proteins are denatured beyond physiological temperatures. No phase inversion was observed in temperatures between 4 °C and 37 °C.

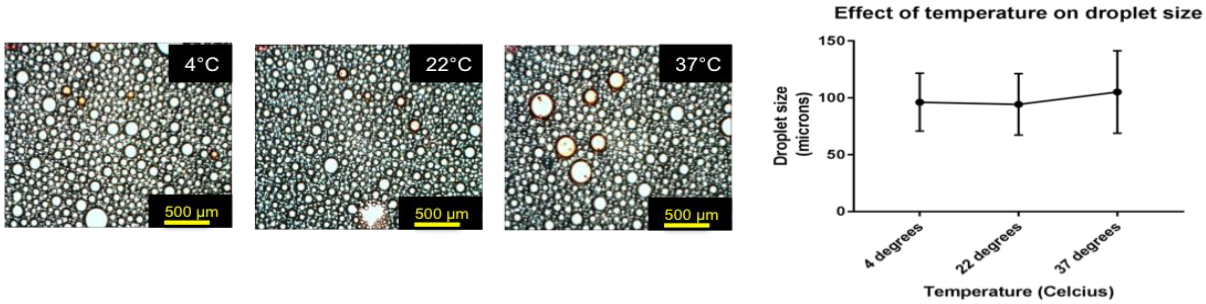


Figure 3-4 Light microscopy of Oil Red O stained emulsions showing no change in mean droplet diameter as temperature is increased ($p>0.05$). (mean ± SD, n=20)

Effect of varying surfactant concentration at different shear rate

Increasing the shear rates for each of the surfactant concentration resulted in a gradual decrease of mean droplet sizes. No emulsions were obtained for shear rates of 500 rpm and 1000 rpm for all ranges of surfactant concentration indicating that there is a threshold of shear rate to be reached for emulsion formation (i.e. non-spontaneous emulsification process). Increasing surfactant concentration at 1500 rpm did not significantly change the mean droplet sizes as the emulsions formed were unstable and flocculating/coalescing. This resulted in very large standard deviations of mean droplet diameter.

However, from 2000 rpm increasing surfactant concentration results in a trend towards smaller mean droplet sizes. Increasing shear rate at all surfactant concentrations appear to reduce droplet size. However, increasing the shear rate at surfactant concentration of 0.25% appears to decrease the mean

droplet size of the oil-in-water emulsion up to a threshold of 2500 rpm (mean droplet size 85 ± 37 microns) as the fragmentation limit (*f*) is reached.

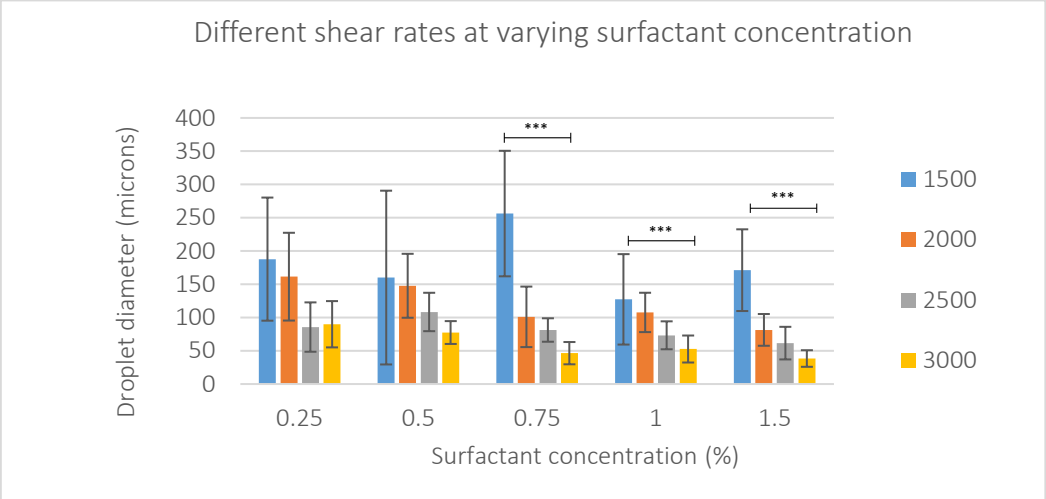


*Figure 3-5 Effect of increasing shear rate and surfactant concentration on mean droplet diameter of emulsions. Mean droplet size decreased as shear rate increased from 1500 rpm to 3000 rpm and as surfactant concentration increased from 0.25% to 1.5%. *** denotes a p-valus of <0.001. (mean ± SD, n=20)*

Emulsion stability characterization

Effect of HLB value on emulsion stability

At HLB 9.5 and 10, the emulsion stability was poor with large increases in backscatter at the bottom of the cells, indicating sedimentation. At HLB 10.5, sedimentation was less pronounced. However, at HLB 11, changes in light transmission and backscatter indicated formation of 3 distinct layers indicating phase transition from water-in-oil to oil-in-water emulsions. From HLB 11.5 to HLB 13, changes in light transmission and backscatter due to creaming decreased as HLB values increased, indicating greater stability of the emulsion system (Figure 3-6).

Effect of surfactant concentration on emulsion stability

Emulsions without surfactants phase separated instantaneously into immiscible oil and water phases. As surfactant concentration increased, changes in light transmission and backscatter due to creaming decreased indicating increase in stability of the emulsions (Figure 3-6).

Effect of PVP concentration on emulsion stability

Emulsions without PVP creamed rapidly but did not phase separate completely. As concentration of PVP increased, the emulsions became much more stable with little changes in light transmission and backscatter (Figure 3-6).

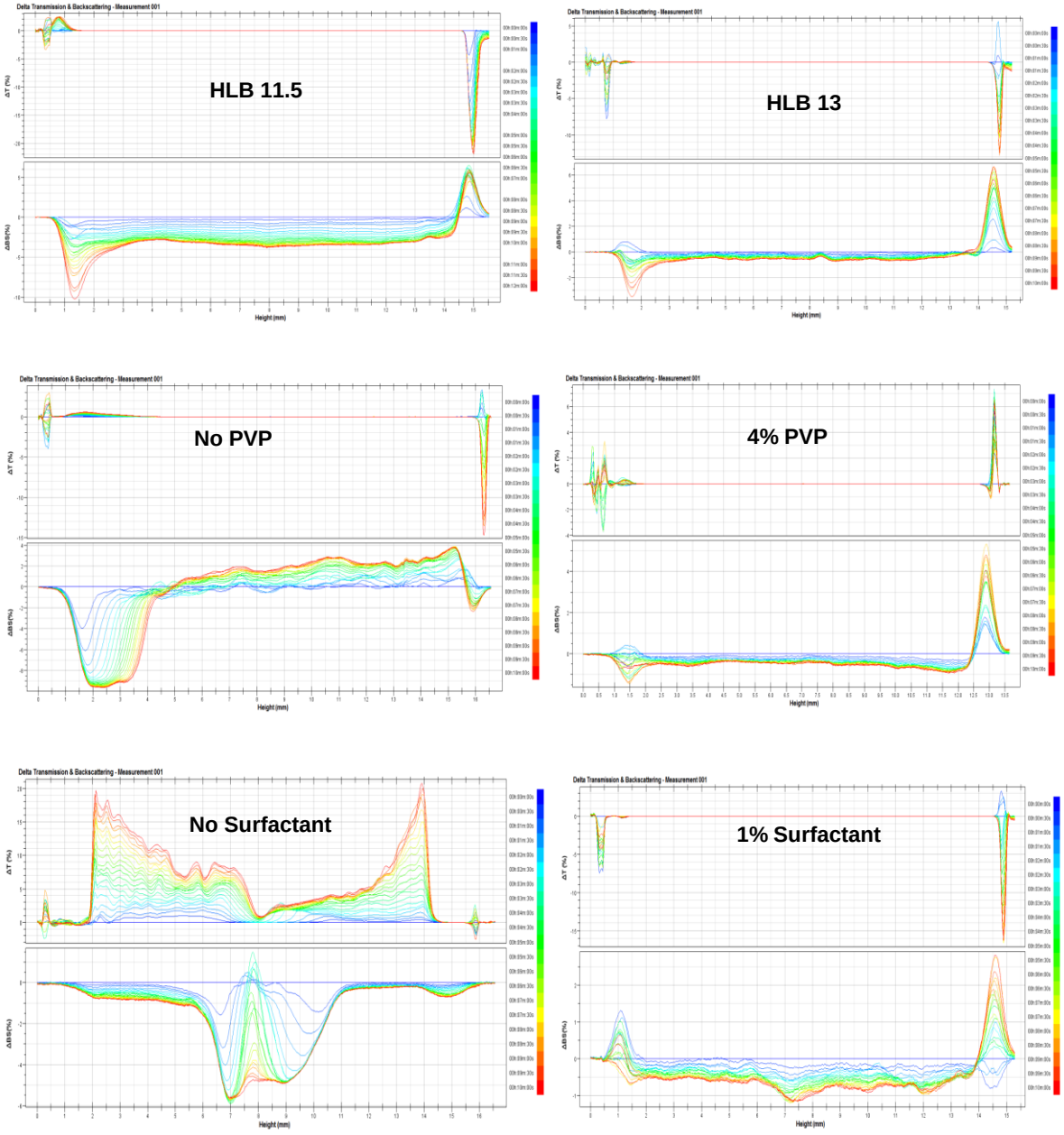
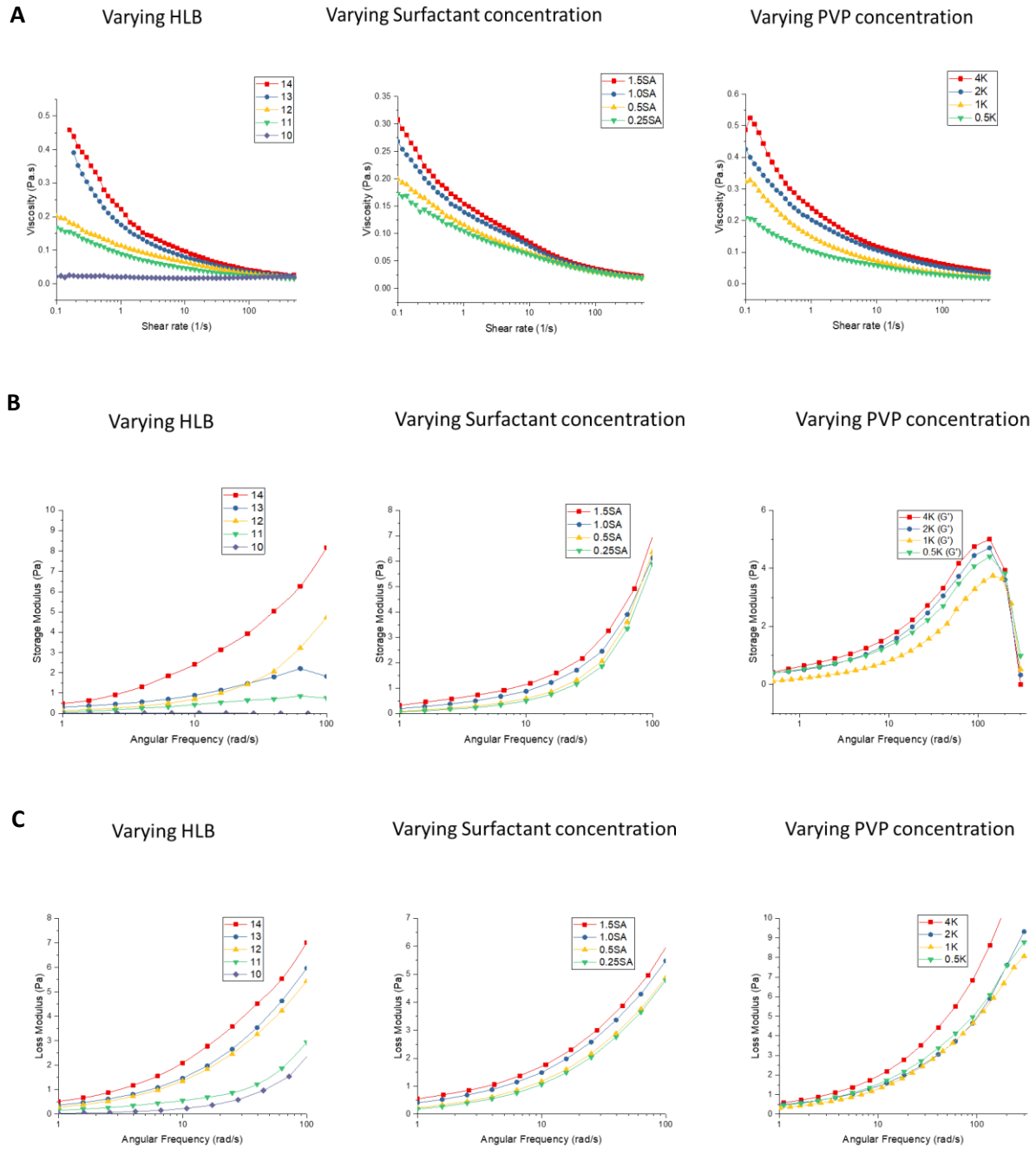


Figure 3-6 Turbiscan emulsion stability profile over time for emulsions at different HLB values, PVP concentration and surfactant concentration. As HLB, PVP and surfactant concentration increased, change in light transmission and backscatter decreased. Coloured bar on the right represents timepoints of measurement indicating stability over time. (n=3)

Emulsion viscoelasticity characterization

The viscosity of the emulsions increased as HLB values, surfactant concentration and PVP concentration increased. This correlates with our findings that increase in HLB values, PVP and surfactant concentration results in increased emulsion stability. Storage moduli and loss moduli also increased as HLB, surfactant concentration and PVP concentration increased. Interestingly, for unstable emulsions e.g. HLB 10 emulsion system, the storage moduli values became erratic as angular frequency increased. This may be due to instability and phase separation of the emulsion (Figure 3-7).



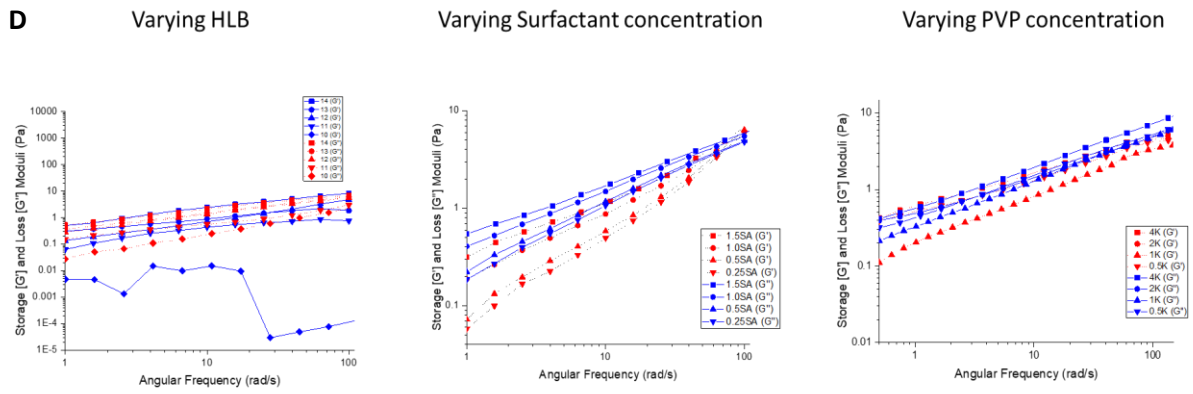


Figure 3-7 Viscoelastic properties of each emulsions system as represented by: (A) viscosity, (B) storage moduli and (C) loss moduli of each emulsion as angular frequency increases. (D) Storage and loss moduli are graphed together in logarithmic scale showing that storage moduli of the HLB 10 emulsion was highly variable indicating emulsion instability. (n=3)

Characterization of protein-emulsion interaction

Localization of proteins in emulsion mix

There was marked increase of fluorescence intensity around emulsion droplets compared to background levels throughout the dispersed phase of the emulsion. FITC-BSA was observed to preferentially localize around each emulsion droplet rather than becoming uniformly dispersed in the aqueous phase, suggesting that protein the proteins had either adsorbed onto the interface boundary, displacing the Tween 20/Span 20 surfactants or formed an outer shell surrounding the surfactant-lined emulsion droplets (Figure 3-8).

To distinguish between the two, the emulsions mix was centrifuged to induce creaming of the emulsions. If FITC-BSA was adsorbed at the interface, it is likely to remain in the creamed layer. However, if FITC-BSA had formed a loose outer shell surrounding each droplet, centrifugation would disrupt the protein-surfactant interaction, allowing the FITC-BSA to return into the aqueous phase. The protein concentrations in each phase was quantified to measure proportion of FITC-BSA in the oil and aqueous phase.

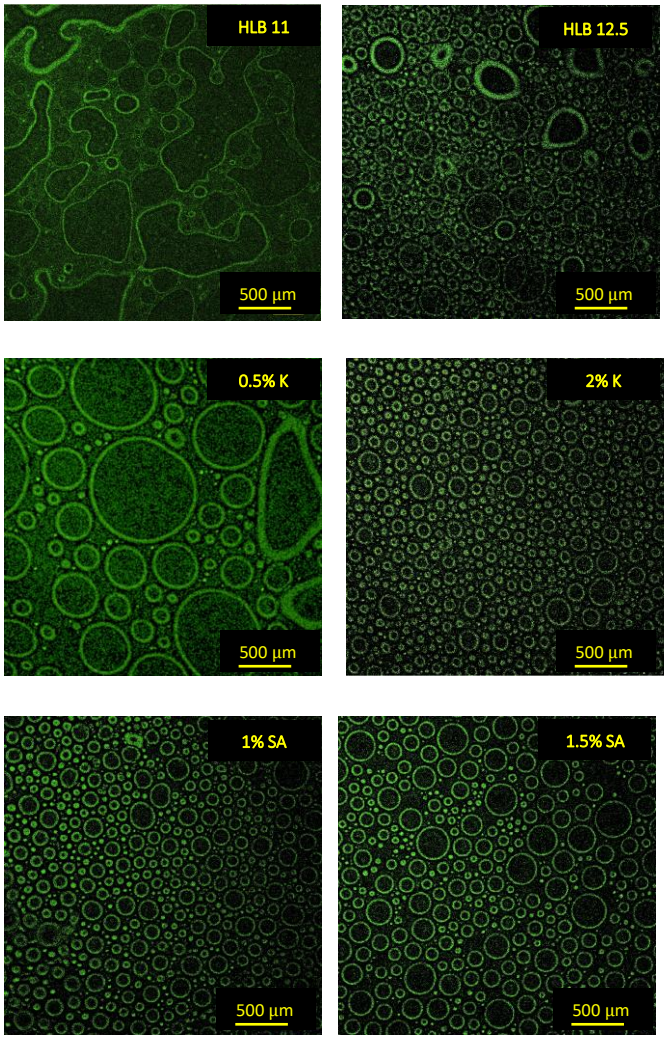
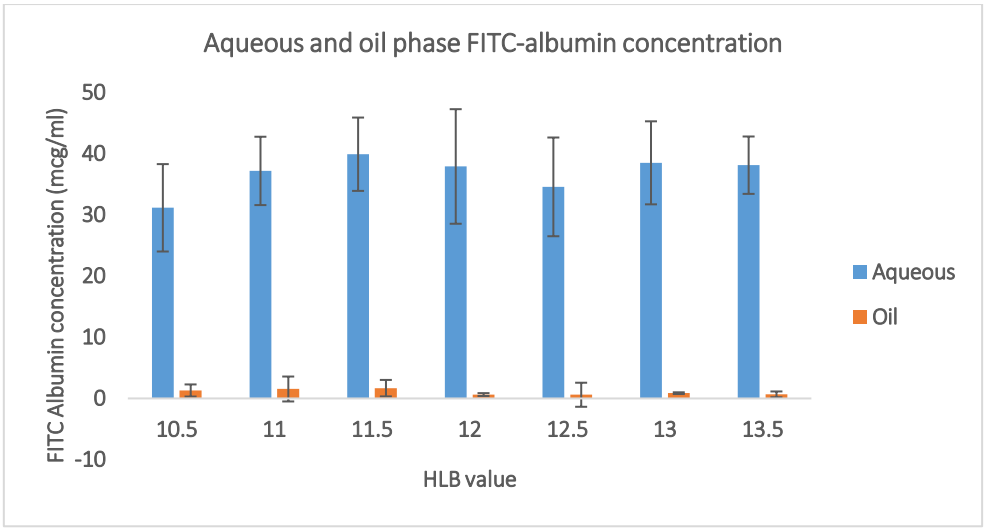
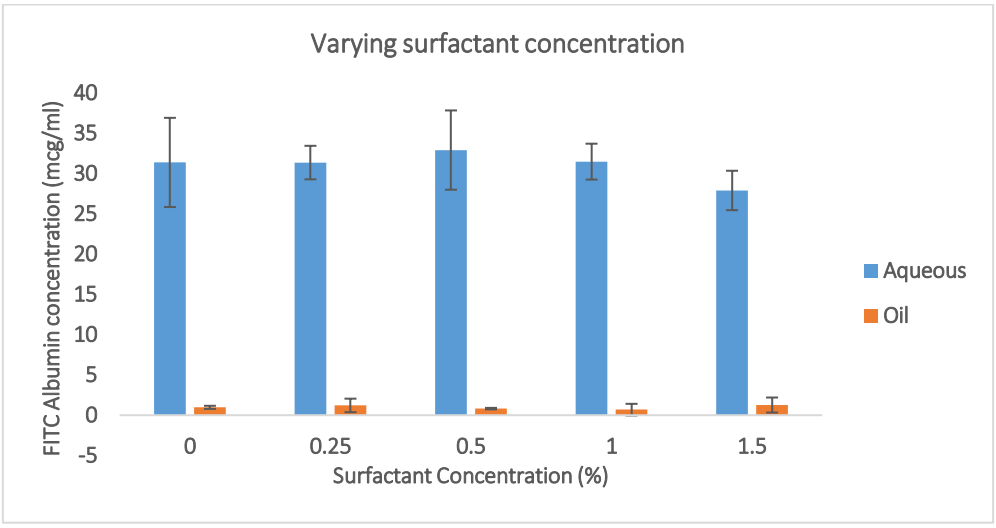


Figure 3-8 Confocal microscopy images showing 'coating-effect' as FITC-BSA and surfactant interact close to interfacial oil-aqeuous regions using emulsions with differing HLB values, PVP concentration and surfactant concentration at 10x magnification. (scale bar= 500µm, n=3)

Quantification of protein in oil and aqueous phase

Relative fluorescence in the aqueous and oil phase shows that >90% of the FITC-BSA is concentrated in the aqueous phase rather than oil phase, regardless of HLB value, surfactant concentration, PVP concentration or temperature (Figure 3-9). Minimal FITC-BSA is detectable in the oil phase (<1%), suggesting that the FITC-BSA shells were only loosely bound to the emulsion droplets rather than being primarily adsorbed at the interface. This suggests that Tween 20 protects protein denaturation at interfaces by its preferential adsorption at the interface, blocking that of the protein.





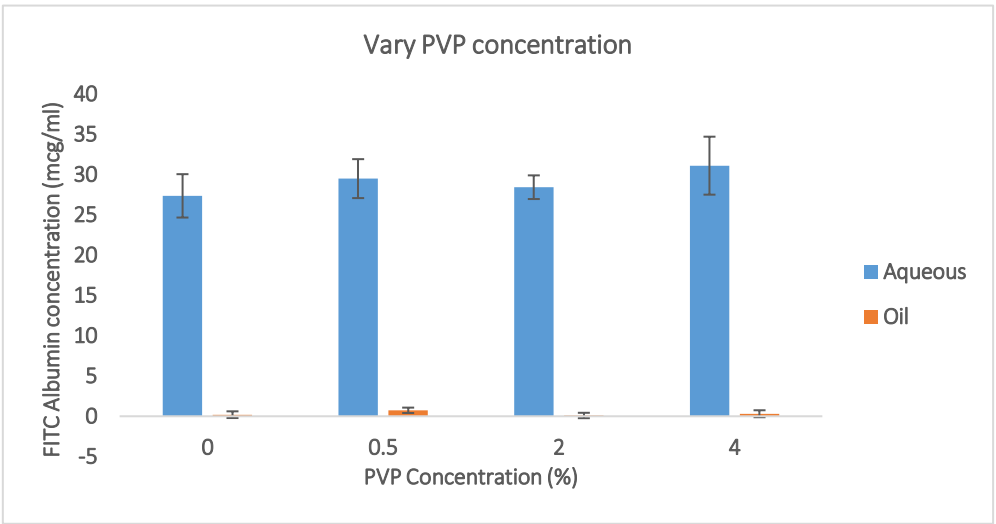


Figure 3-9 Quantification of relative fluorescence intensity of FITC-BSA in aqueous phase vs oil phase demonstrating that most of the protein remains in concentrated in the aqueous phase while the amount of protein in the oil phase is too low to be reliably quantified. (mean ± SD, n=3)

Assessing conformation of adsorbed BSA in oil phase

To further confirm our findings, FTIR spectra of the cream phase of emulsions with and without BSA were obtained. The spectra of both emulsions with and without BSA were similar with no demonstrable changes in the Amide I region (1600-1700 cm^{-1}). As there were no detectable protein signals, this suggests that almost all the BSA is desorbed from the surface of emulsion droplets on centrifugation. This is consistent with the fluorescence quantification results. This result was further validated by deconvolving the FTIR spectra obtained by second derivative to reveal any hidden peaks. Four separate peaks were seen in the solution containing pure BSA. In contrast, only one peak was seen in all emulsion spectra with and without BSA (Figure 3-10). This is likely to be due to the water peak observed in the 1650 cm^{-1} region, owing to differences in amount of water in the dispersed phase of the emulsion cream.

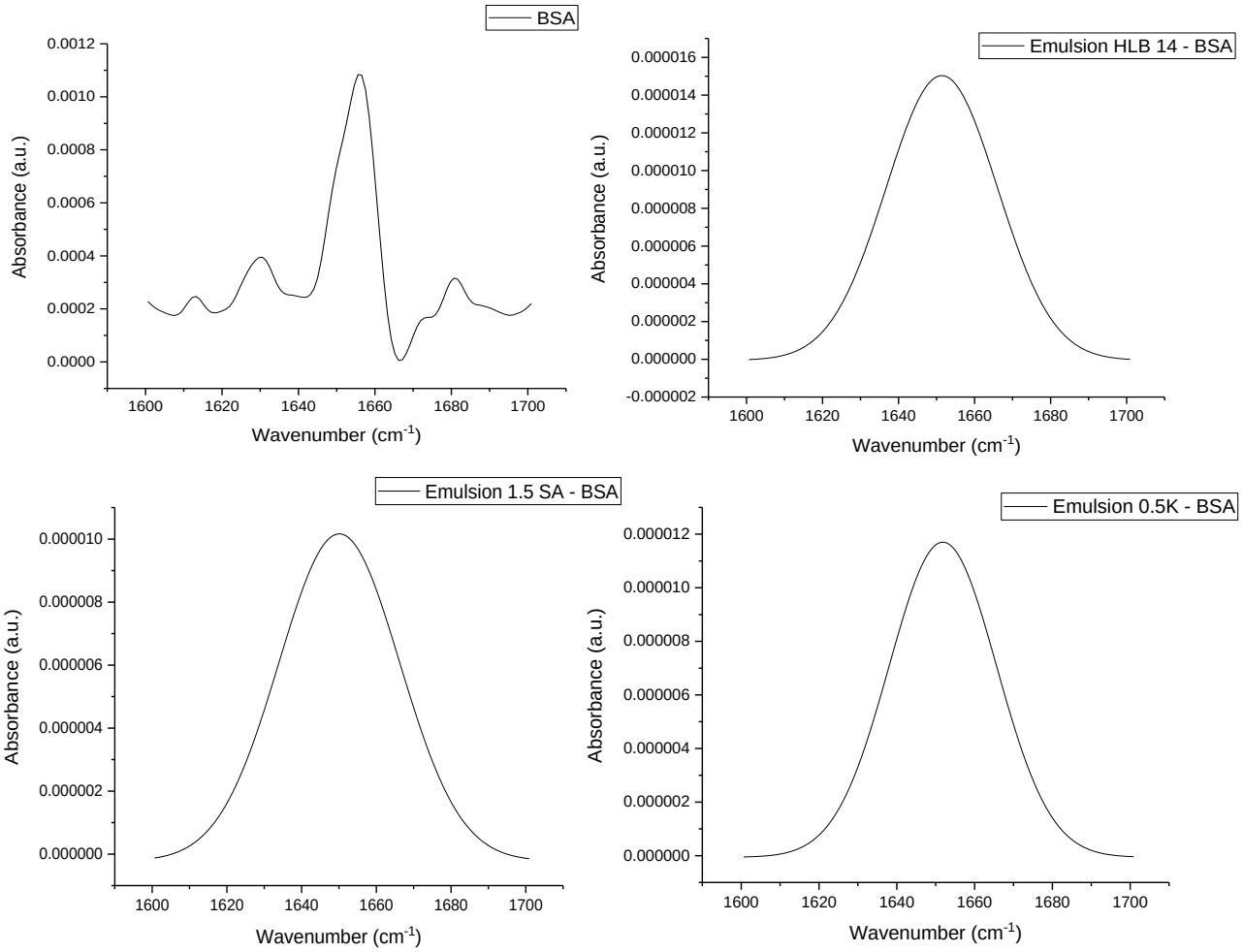


Figure 3-10 Second derivative of subtracted FTIR spectra of cream phase of the emulsions with BSA at different HLB, surfactant and PVP concentrations, showing only water peaks with no protein signals, compared with the four peaks in BSA. (n=3)

Assessing conformation of BSA in aqueous phase of emulsion

Near-UV spectra of native BSA in phosphate buffer and BSA recovered after emulsification and incubation with the HLB 13 emulsion system demonstrated a change in θ from 260 nm to 290 nm, indicating that BSA in the aqueous phase of emulsions was still in a folded state. (Figure 3-11) By contrast, the spectra of denatured BSA was a horizontal line indicating loss of polarization of the aromatic residues (Tryptophan, Tyrosine, Phenylalanine) due to unfolding of the protein molecule. An additional control showed that samples with only filtered emulsions was a horizontal line and did not show any changes in θ from 260 nm to 290 nm, indicating that any residual emulsion particle not removed by the filtration process did not interfere with CD spectra readings.

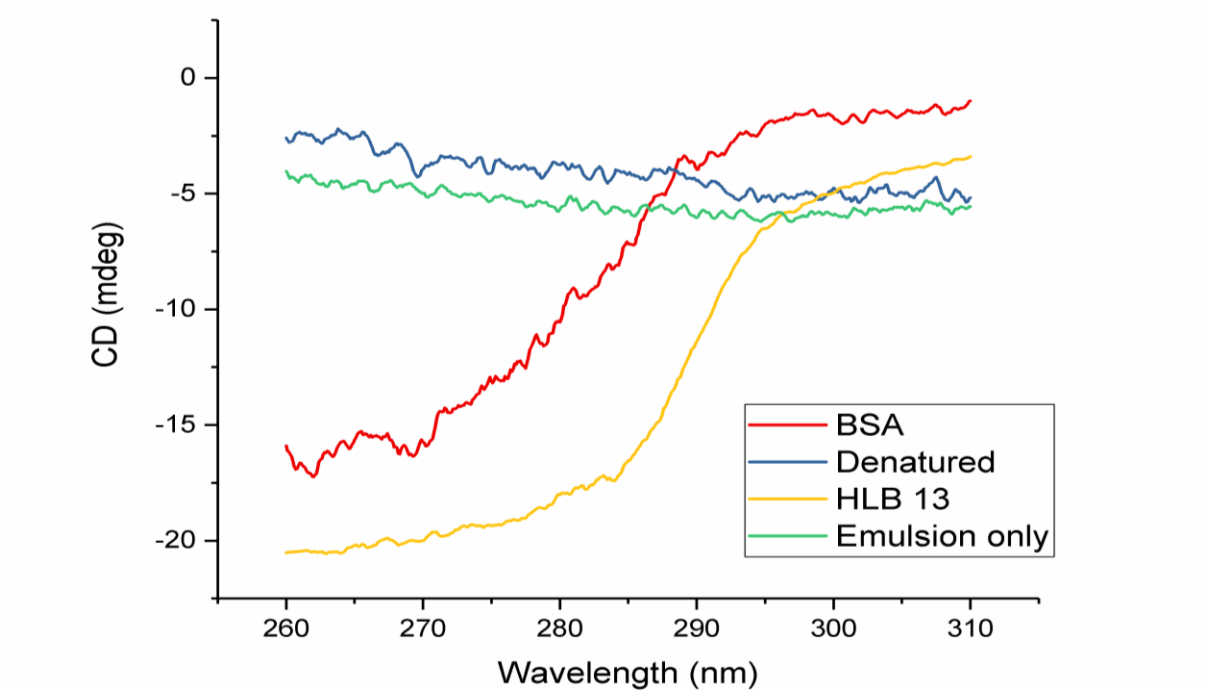


Figure 3-11 Near-UV circular dichroism to assess conformation of BSA. Both emulsion only and denatured BSA did not show significant changes in CD value while buffered BSA solution and BSA incubated in HLB 13 demonstrated changes in CD value, indicating that the BSA molecules retained their folded state. (n=3)

Assessing intrinsic tryptophan fluorescence of fibrinogen in aqueous phase of emulsion

Peak emission in fluorescence spectra of tryptophan was at approximately 350 nm, regardless of concentration of surfactant or PVP. This indicates that fibrinogen molecules in the aqueous phase of the emulsions are still in their native state. Upon denaturation with 1% SDS, there is a red-shift of the

maximum intensity of the peak to 340 nm. This suggests that the fibrinogen is no longer in native state and has unfolded, thus exposing the native tryptophan residues in fibrinogen to surfactants available.

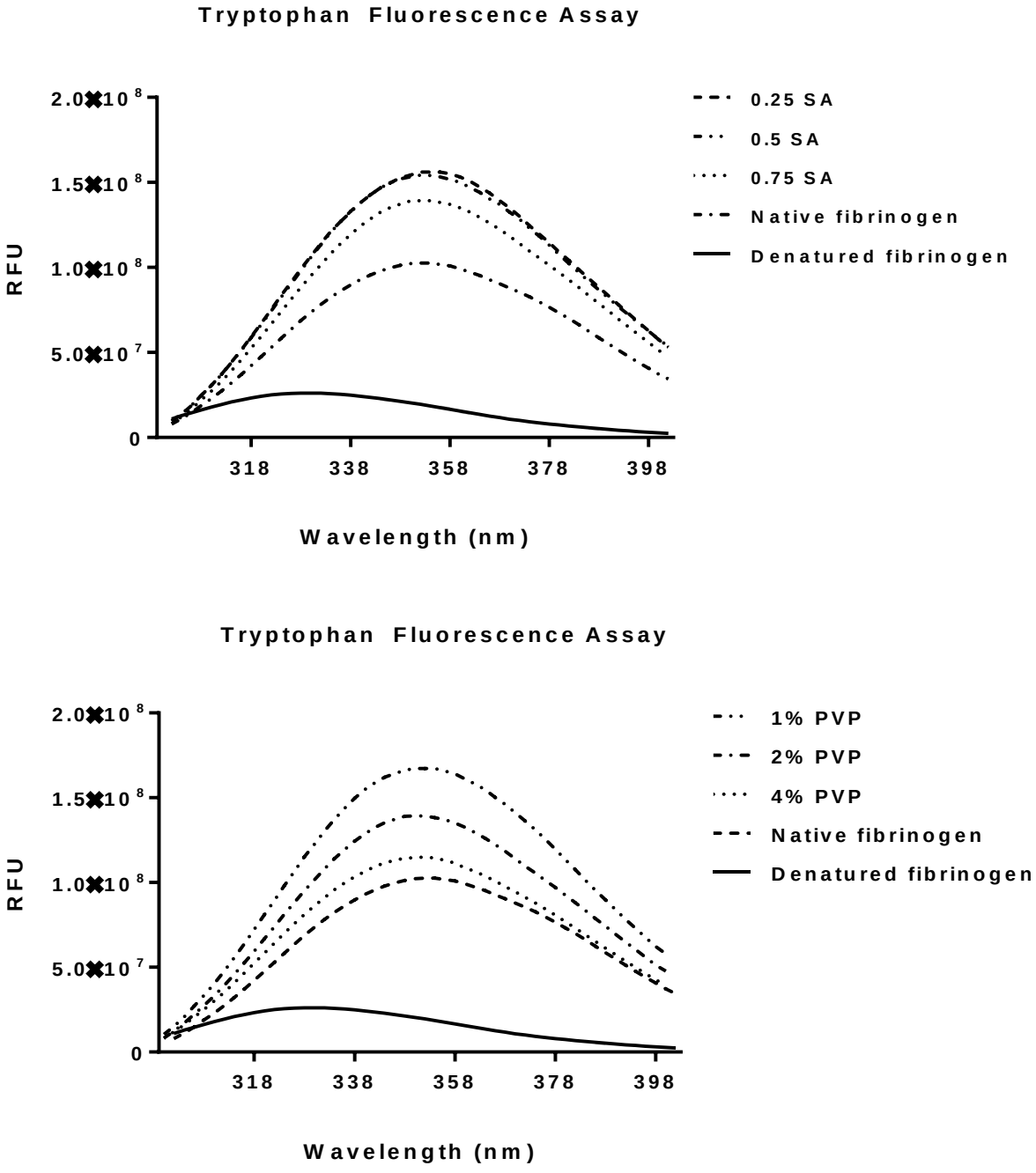


Figure 3-12 Tryptophan assay to assess conformation of fibrinogen. Denatured fibrinogen demonstrated left-shift whilst fibrinogen incubated in various surfactant and PVP concentrations retained their folded state. (n=3)

Assessing function of lactate dehydrogenase in aqueous phase of emulsion

Functional changes to proteins exposed to emulsions were also assessed using an enzyme, lactate dehydrogenase (LDH). It is well known that LDH reduces nicotinamide adenine dinucleotide (NAD^+) to NADH. The formation of NADH can be quantified by colorimetry. In Figure 3-13, addition of 0.25% surfactant did not significantly affect LDH enzyme activity. However, at 0.5% surfactant concentration and above, there is a slight decrease in enzyme activity compared to the positive control. Similarly, addition of PVP resulted in decrease in enzyme activity in a concentration dependent manner

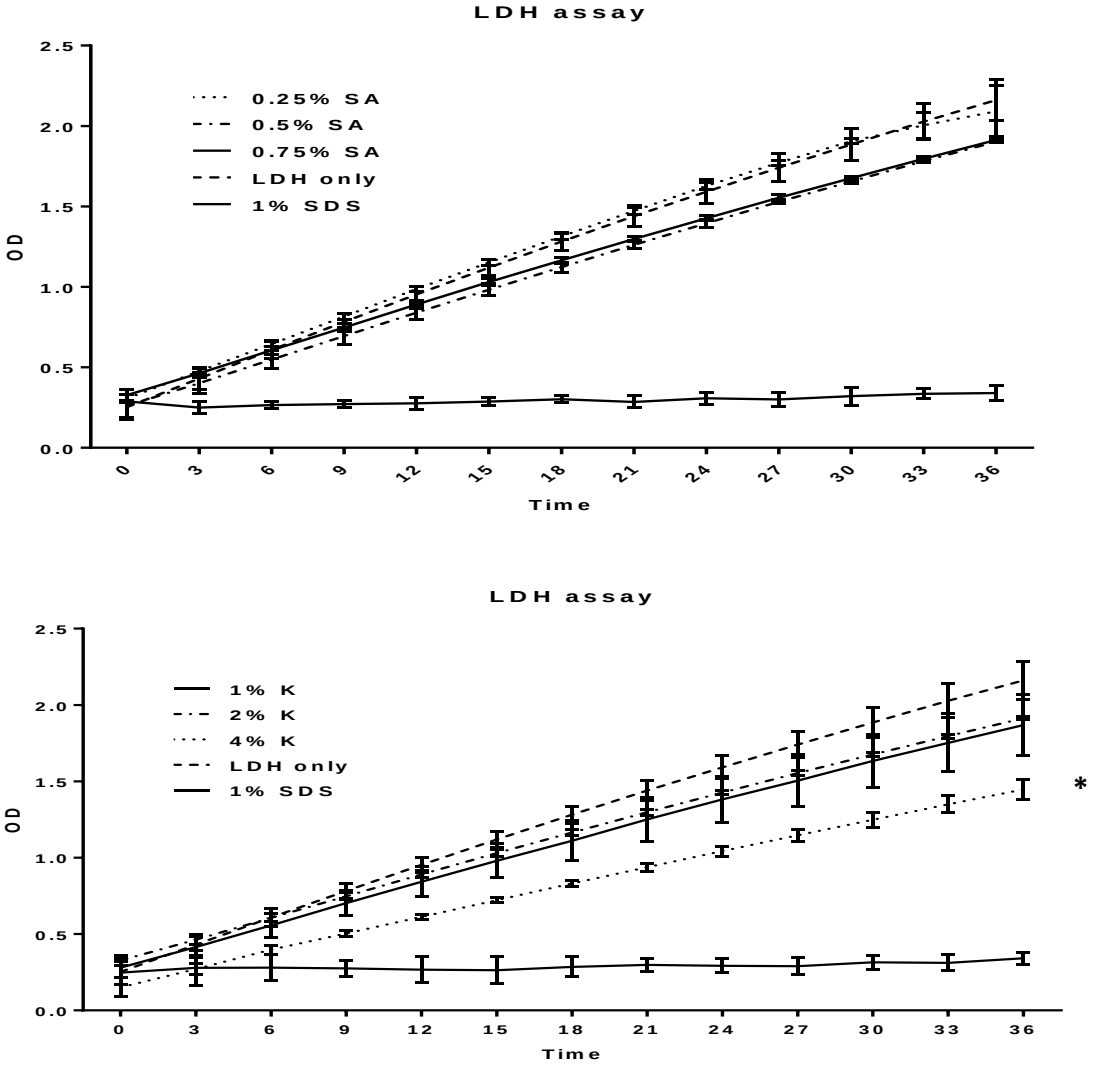


*Figure 3-13 LDH assay to assess enzyme function on exposure to emulsion mix. LDH enzyme activity is largely preserved regardless of surfactant concentration and is minimally affected by PVP (Kollidon) concentration (except at 4% K) * denotes a p-value of <0.05. (mean ± SD, n=3)*

3.1.4. Discussion

In this study the control of O/W emulsion stability and droplet size using various parameters in a mineral oil emulsion system was demonstrated. Mineral oil was chosen as it is widely used as a simple, inert, biocompatible phase and can be obtained at high purity (pharmaceutical grade). Macro-emulsions are by nature unstable due to large droplet sizes which tend to flocculate and coalesce. Meanwhile, proteins are surface-active molecules which tend to adsorb at interfaces and denature. The aim of this study was to explore the mechanism by which protein structure and function is preserved using an emulsion system with non-ionic surfactants. There is a need for developing biocompatible macro-emulsion systems for food, cosmetic, pharmaceutical, tissue engineering and medical purposes as these emulsions can act as carriers for drugs and growth factors, as well as act as a template for tissue engineered scaffolds.

The hydrophile-lipophile balance (HLB) system was initially described by Griffin et al (97) to aid selection of non-ionic surfactants for emulsification of oils. Required HLB values of various oils can also guide selection of surfactant blends to create stable emulsions, by matching HLB values of surfactants to rHLB values of oil types.

For this study, the Tween 20/Span 20 surfactant mixture was used as both are non-ionic surfactants which are expected to be non-denaturing when located at the oil-water interface. Increasing the HLB value of surfactant mixes appears to have a stabilizing effect on the mineral oil emulsions. Interestingly, although rHLB values of oils are often used to guide choice of emulsifiers (122,123) it was difficult to achieve a stable emulsion when a surfactant mix of HLB 10 was used, which corresponded with the reported rHLB of mineral oil. This may be due to differences in mineral oil composition from batch to batch, as mineral oil is a composite product made up of hydrocarbons of different chain lengths. (124)

Critical micelle concentrations (CMC) for Tween 20 and Span 20 at room temperatures are 8.04×10^{-5} mol/L and 2.3×10^{-5} mol/L. (125,126) Through preliminary experiments, the emulsion fragmentation

limit was found to be at 0.25% Tween 20/Span 20 surfactant mix, which prevented any further decrease in emulsion droplet size even at high mixing rates. At this surfactant concentration, increasing the mixing rate beyond 2500 rpm did not cause a decrease in mean droplet size, but instead caused a slight increase in droplet size. Calculation of surface area to volume ratio of using mean droplet size showed that there is a limit of total surface area for given droplet sizes of 0.04 m^2 at 0.25% surfactant concentration which implies that all usable surfactant molecules have been adsorbed onto the surface of each micelle droplet. Further increases in mixing rates simply cause greater collision and coalescence of emulsion droplets due to higher kinetic energy, resulting in a slight increase in mean droplet sizes.

Also, increased surfactant concentrations correlated with a decrease in the mean droplet size for the emulsion. This is consistent with results from other studies with different oil systems. (127) This may be due to the greater availability of surfactant molecules during mixing of the emulsions, which allowed surfactants to rapidly migrate areas, which are surfactant deficient from the bulk phase, as each droplet is disrupted to create smaller and smaller droplets. An alternative explanation is that increase in interfacial surface area is more thermodynamically stable at high surfactant concentrations due to lowering of interfacial surface tension. According to Gibb's adsorption isotherm equation as shown below, increasing the bulk concentration of the surfactants results in a higher chemical potential and therefore a lowering of the surface tension of the oil-water interface (128).

$$dG = -SdT + Ad\gamma + \sum nd\mu \tag{3.2}$$

Where G is the free energy of the system, S represents entropy and T represents temperature. A is the total surface area while γ represents interfacial energy.

At constant temperature,

$$d\gamma = -\sum \frac{n}{A} d\mu = -\sum \Gamma d\mu \tag{3.3}$$

Where n is the number of moles with chemical potential μ and Γ is surface excess.

Polymers such as PVP, P68, PVA and PEG are often used as excipients in manufacturing processes. However, the role of excipients in emulsification is not very well understood. In this study, increase in PVP concentration resulted in a decrease in mean emulsion droplet size and increase in stability. It may be possible to distinguish any potential rheological effect from a steric effect, by comparing effect of PVP addition on droplet size versus droplet stability. If the effect of PVP is mediated by increase in viscosity, this is likely to affect emulsion droplet sizes as the rheological effect would affect shear rate around emulsion droplets. However, if the stabilization is mediated through steric effects, then the stability of emulsions with PVP would be more marked over time as the PVP molecules prevent collision of emulsion droplets and prevents coalescence and flocculation.

No significant changes in emulsion droplet sizes was found when temperature was changed. These temperatures were chosen as they are common storage temperatures for biological compounds and may influence the characteristics of biologically compatible emulsions systems over time. Another parameter that were tested but not shown here are oil: aqueous phase ratio. The ratio is generally known to influence emulsion stability of a given surfactant system. Briefly, stable emulsions were formed with no significant difference in mean droplet size when a ratio of oil: aqueous phase below 7:3 was used. Therefore, the upper limit of 2:1 (oil: aqueous volume) was set for subsequent emulsion systems used.

In terms of stability, it was found that results from the turbidity analysis corresponded closely with the findings of mean droplet sizes. In general, emulsions with smaller droplet sizes were much more stable compared to emulsions with larger droplets (129). Emulsions with smaller droplet sizes were more closely packed and would require more droplets to coalesce for phase separation to occur, contributing to the stability of the emulsions. Thus, the stability of the emulsions increased along with increase in HLB value, surfactant concentration and PVP concentration.

To ensure emulsions are biocompatible, proteins added to emulsions systems must retain their native conformation. Numerous studies suggest that proteins, which adsorb onto interfaces are likely to unfold and denature (130). However, non-ionic surfactants have been shown to exert a protective effect on preserving the native structure of proteins in emulsions systems (120). This can be envisaged through preferential adsorption of such surfactants, and subsequent steric blockade of aqueous phase proteins to adsorb. Moreover, for a protein to adsorb, its conformation would need to change for hydrophobic groups to interact with the oil phase, and this may be relatively slow due to the activation energy required, in comparison to surfactant adsorption.

Using FITC-BSA as a model protein, it is shown that this effect may be mediated by surfactants that block BSA adsorption at the interface. Instead, BSA forms a protein coat around emulsion droplets, which are loosely bound. This could be due to a combination of steric effects, van der Waals forces, hydrogen bonding and hydrophobic interactions between proteins and surfactants. At low HLB values however, the surfactant and proteins form distinct aggregates rather than protein-coated oil-in-water emulsions. Changes in surfactant concentration or PVP concentration, and thus total interfacial area, did not affect distribution or conformation of proteins.

Choice of surfactant is another factor to take into consideration for formulation of biocompatible emulsions. The surfactant must lower surface tension more favourably than the protein used in the emulsion (otherwise the protein will preferentially adsorb). Anionic or cationic surfactants are not ideal as they may interact with protein charged groups causing denaturation itself (131). In addition, pH and ionic strength of buffers used to formulate the emulsion mix may affect degree of protein coating on the emulsion droplets due to change of net protein charge.

At pH above or below the isoelectric point (pI) of the protein, the protein molecule becomes charged and may adsorb to a greater or lesser degree onto charged surfactants emulsion droplets (depending on

net electrostatic forces). However, for non-ionic surfactants, proteins at the pI (non-charged) may form colloidal aggregates or bind to a greater degree on the surface of the emulsion droplets as hydrogen bonding, hydrophobic interactions and van der Waals forces predominate. Therefore, in this study a buffer with physiological pH (pH 7.4) was used, which is above the pI of BSA (pI 4.7). This is likely to minimize protein-surfactant interaction and protein adsorption at the interface since charged molecules preferentially stay in the hydrophilic aqueous phase.

The results from this study are consistent with the findings from Chen et al which reported that addition of non-ionic surfactants protected β-lactoglobulin from adsorbing at the oil-water interface. (111) They also reported a time dependence of the competitive adsorption between milk proteins and surfactants at oil-in-water emulsions. (132) No time-dependence was noted for competitive adsorption to occur in our emulsion system. This is likely due to the use of non-ionic surfactants for emulsification de novo, rather than using proteins as the initial emulsifier.

The preservation of protein tertiary structure and activity is further confirmed using the tryptophan fluorescence assay using fibrinogen as test protein. Protein function and native confirmation was largely preserved, as shown by presence of enzyme activity using lactate dehydrogenase (LDH) assay. The effect of emulsion on slight reduction of LDH activity may be due to partitioning of lactate from available enzymes due to presence of emulsion particles. The effect of PVP may be due to increased viscosity as the enzyme assay requires protein mobility to work. The complete ablation of LDH activity by SDS demonstrated the biocompatibility of this emulsion system compared to ionic surfactants.

These findings demonstrate the possibility of creating a biocompatible o/w emulsion system with relatively high oil phase (up to 70%) without protein denaturation, using a non-ionic surfactant molecule which preferentially adsorbs at the interface. This technology could potentially bear applications in the pharmaceutical industry as emulsions can be used to encapsulate biological drugs to prevent

immunogenic response, whilst delivering the protein of interest in its native state. Such biocompatible emulsions can also be used to develop emulsion templated protein scaffolds with tunable properties using several structural proteins e.g. collagen and fibrin, with preserved bioactive properties. (7)

3.1.5.Summary

In summary, a biocompatible, metastable and controllable macroemulsion system is introduced and tested using mineral oil, MES/NaCl buffer, Tween 20/Span 20 surfactant mix and several model proteins such as bovine serum albumin, fibrinogen and lactate dehydrogenase. The control of parameters, which can be manipulated to control mean droplet size and stability of the emulsion such as HLB values, surfactant concentration and excipient concentration is described. The mechanism by which non-ionic surfactants are used to prevent denaturation of proteins in an emulsion mixture is investigated. This is caused by a competitive adsorption process where there is preferential adsorption of surfactants at interfaces compared to proteins. This fascinating phenomenon may be useful in the field of biomedical applications (e.g. tissue engineering and drug delivery) in the future.

3.2. Optimization of EmDerm Fabrication: Key Parameters

3.2.1. Introduction

An emulsion is a stable dispersion of one liquid (dispersed phase) in another liquid (continuous phase). Emulsion templating was originally used to produce porous scaffolds using polymers dissolved in solvents. (133,134) This technique is commonly used to synthetize polymer filtration membranes (e.g. Alvetex®), microbeads for drug encapsulation (135) and tissue-engineered polymeric scaffolds or growth factor delivery systems (103,136). However, the use of macroemulsions to synthesize tissue-engineered scaffolds using protein hydrogels is a relatively new area of research, which has yet to be fully harnessed in tissue engineering. (137)

Control of porosity is a key factor in scaffold processing. (138) Traditional methods of freeze-drying, gas foaming and solvent casting/particulate leaching do not produce controllable pore sizes. (139) Emulsion templating, as a form of 'polymerisation of high internal phase emulsion systems (HIPEs)' is a well-established method of manufacturing nanoporous polymer membranes e.g. for water purification films, catalytic panels, controlled release storage and tissue regeneration. (133) Its potential benefits as a method of manufacturing porous scaffolds for tissue engineering are the ease of control of porosity by controlling emulsion droplets size, relatively rapid structure formation in bulk, and cost-effectiveness.

Meso-macroporous polymeric scaffolds have been synthesized using polymerised-high internal phase emulsions (polyHIPE) and Pickering polyHIPEs in previous studies (15,133). However, to our knowledge, no studies have been done to investigate the possibility of using emulsion templating as a method to create tissue scaffolds using natural extracellular matrix material such as collagen or fibrinogen. Its use with biological polymers has so far been limited to polysaccharides (137) and the denatured polypeptide, gelatin (106) and not with native proteins such as collagen and fibrin.

Using a decane-based biocompatible emulsion system developed for this project, our aim was to develop several porous emulsion-templated protein hydrogels using collagen, collagen-fibrin and fibrin for tissue engineering purposes. Collagen was chosen as it is a key component of the skin dermis while fibrin is known to have pro-angiogenic properties. Decane was selected as the oil phase because mineral oil from the earlier emulsion system was found to be too viscous for oil elution from the scaffold during the final manufacturing step of creating emulsion templated scaffolds.

The key parameters for manufacturing emulsion-templated scaffolds were characterized such as emulsion stability, rheological properties, gelation time, freeze-drying parameters and excipient effect.

The mechanical properties of the resulting emulsion-templated scaffolds were also quantified by tensile testing, as well as pore size and scaffold morphology.

3.2.2.Materials and Methods

Materials

Span 20, Tween 20 and decane were purchased from Sigma. 2-(N-morpholino) ethanesulfonic acid (MES), sodium chloride (NaCl), sodium hydroxide (NaOH) and sodium bicarbonate (Na_2CO_3) were purchased from Sigma as well. hTERT human dermal endothelial cells (CRL-4025), Vascular Basal Medium and Microvascular Endothelial Cell Growth Kit-VEGF was purchased from ATCC. CellTracker Green CMFDA Dye was purchased from Thermo Fisher Scientific. Rat-tail collagen I in 0.1M acetic acid (2mg/ml) was purchased from First Link. HEPES (4-(2-hydroxyethyl)-1-piperazineethanesulfonic acid)), 10X Dulbecco's Modified Eagle's Medium (DMEM), 1-Ethyl-3-(3-dimethylaminopropyl) carbodiimide (EDC), sulfa- N-hydroxysuccinimide (sulfa-NHS), Pluronic F68 and mannitol were purchased from Sigma. Polyethylene glycol (PEG 3000) and polyvinyl alcohol/polyethylene glycol graft copolymer (Kollicoat) were obtained from BASF Pharmaceutical Co.

Preparation of emulsions

5ml of decane and 5ml of 150mM MES/25mM NaCl buffer (pH 7.4) are added into a Falcon tube. 0.1% v/v of HLB 13 (Tween 20/Span 20) surfactant mix is added to the oil/buffer mixture. Vortex the mixture for 15 seconds until a homogenous white emulsion is obtained. Alternatively, mix the solution at 1000 rpm using a hand-held mixer.

Characterization of emulsions

Droplet size

Several emulsions were tested to obtain the ideal droplet size of about 100 µm. (139,140) HLB value, surfactant concentration and mixing rate (rpm) were varied for each emulsion. HLB values tested were

11 to 14, as the emulsion were unstable beyond this range. Surfactant concentrations ranged from 0.1% to 0.7% while mixing rate was varied from 1000 rpm to 3000 rpm. 30ul of each emulsion mix was then placed onto a microscope slide and imaged under light microscope at 10X magnification. Measurements of the droplet diameter of 20 random droplets per frame were taken and analysed, using ImageJ (NIH, USA).

Stability of emulsions

Stability analysis was done by measurement of turbidity (Turbiscan Stability Analyzer, Formulaction, France) for each emulsion as well. 2ml of the emulsion was pipetted into a glass cell and readings were taken every 30 seconds for 10 minutes. Changes in light transmission and backscatter readings were taken across the length of the glass cell and plotted over time to obtain time point measurements of emulsion destabilization.

Rheological properties of emulsions

7ml of each emulsion mixture was added to the concentric cylinder rheometer apparatus (Anton Paar, UK). Viscosity of the emulsions were measured between a shear rate of 1 to 500 (1/s). An amplitude sweep was done to identify the linear viscoelastic region. Subsequently, a frequency sweep was performed to measure storage moduli (G') and loss moduli (G'') of the emulsions between 0.5 and 500 rad/s at 1% strain. All measurements were done at 25 °C.

Preparation of emulsion-templated collagen scaffolds

10ml of the emulsion and 10ml of neutralized collagen solution was transferred into a 50ml syringe with an open end and mixed at 1000 rpm. 4ml of the mixture was then poured into five square casting trays and allowed to gel at 37 °C for 30 minutes. The emulsion-hydrogel scaffolds were then cross-

linked using EDC: NHS (5:2 molar ratio) at room temperature for 3 hours. After cross-linking, each scaffold was washed with deionized water twice to remove excess cross-linker.

Each scaffold was then washed with 80% isopropanol for 15 minutes on a shaker to elute the trapped oil droplets within the collagen gel. Following that, each scaffold was washed with deionized water three times to remove any excess solvent and oil. 5% excipient solution of choice (mannitol, PEG or P68) was added to the scaffolds and allowed to incubate for 10 minutes. Finally, the scaffolds were quickly rinsed with deionized water to remove any excess excipient solution before freeze-drying at -30°C for 15 hours.

Preparation of emulsion-templated fibrin scaffolds

10ml of the emulsion, 8ml of 2% fibrinogen solution and 2ml of thrombin (10 unit/ml) was transferred into a 50ml syringe with an open end and mixed at 1000 rpm. 4ml of the mixture was then poured into square casting trays and allowed to gel at 37°C for 30 minutes. The emulsion-hydrogel scaffolds were then cross-linked using EDC: NHS (5:2 molar ratio) at room temperature for 3 hours. After cross-linking, each scaffold was washed with deionized water twice to remove excess cross-linker. Each scaffold was then washed with 80% isopropanol for 15 minutes on a shaker to elute the trapped oil droplets within the collagen gel. Following that, each scaffold was washed with deionized water three times to remove any excess solvent and oil. 5% excipient solution of choice (mannitol, PVA, PEG or P68) was added to the scaffolds and allowed to incubate for 10 minutes. Finally, the scaffolds were quickly rinsed with deionized water to remove any excess excipient solution before freeze-drying at -30°C for 15 hours.

Preparation of emulsion-templated collagen-fibrin scaffolds

Composite emulsion-templated collagen-fibrin scaffolds were also developed using the decane emulsion system. 2ml of the emulsion was added to neutralized collagen solution and 2% w/v

fibrinogen-thrombin in a 2:1:1 volume ratio and mixed at 1000 rpm. Each emulsion-hydrogel scaffold was then poured into square casting trays and allowed to gel at 37°C for 30 minutes. The emulsion-hydrogel scaffolds were then cross-linked using EDC: NHS (5:2 molar ratio) at room temperature for 2 hours. After cross-linking, each scaffold was washed with deionized water twice to remove excess cross-linker. Each scaffold was then washed with 80% isopropanol solution for 15 minutes on a shaker to elute the trapped oil droplets within the scaffolds. Following that, each scaffold was washed with deionized water three times to remove any excess solvent and oil. 5% excipient solution of choice (mannitol, PVA, PEG or P68) was added to the scaffolds and allowed to incubate for 10 minutes. Finally, the scaffolds were quickly rinsed with deionized water to remove any excess excipient solution before freeze-drying at -30°C for 15 hours.

Characterization of scaffolds

Characterization of pore size

Scanning electron microscopy (SEM) images of the scaffolds were used for characterization of pore sizes of each scaffold. Briefly, scaffolds were sputter coated with gold for 60 seconds and imaged using the Zeiss SEM Machine (Zeiss, Germany) at 1000x magnification. Mean and standard deviation of pore sizes of 30 pores were obtained using the ImageJ software (NIH, USA).

Scaffold Degradation

A) Hydrolytic degradation

8mm punch biopsies of the scaffold were taken and weighed in dry state. The scaffolds were then placed into petri dishes containing phosphate buffered saline (PBS) and incubated for 30 days. At Day 5, 10, 15, 20, 25 and 30 the scaffolds were removed from PBS and washed twice with deionized water, then vacuum-dried. The dried scaffolds were then weighed and change in mass was recorded.

B) Enzymatic degradation

8mm punch biopsies of the scaffold were taken and weighed in dry state. The scaffolds were then placed into petri dishes containing 1X trypsin solution and incubated for 72 hours. At 6 hours, 12 hours, 18 hours, 24 hours, 48 hours and 72 hours the scaffolds were removed and washed twice with deionized water, then vacuum-dried. The dried scaffolds were then weighed and change in mass is recorded.

Mechanical testing of Scaffold

The mechanical properties of each scaffold were measured using a universal testing machine (Instron, USA). The samples were cut into rectangular strips measuring 40mm x 5mm x 2mm. A uniaxial force was applied at a rate of 10mm/min using a 100 g load cell. Stress-strain curves were plotted using force-displacement data obtained from the Bluehill software. From the stress-strain curves, ultimate tensile strength (UTS) and Young's modulus of each membrane was obtained. Three replicates were tested for each sample.

Gelation time

Gelation time of collagen emulsions, collagen-fibrin emulsions and fibrin emulsions were also measured using a coagulometer (Stago, Canada). Neutralized collagen gel, fibrinogen solution and thrombin were prepared as described previously. An HLB 13 emulsion mixture was also prepared separately and added to the measurement cuvettes with a moving ball bearing inside. The collagen gel or fibrinogen/thrombin solution or both was pipetted into the cuvette and mixed thoroughly at a 1:1 volume ratio. For collagen-fibrin gel, collagen, fibrinogen/thrombin and the emulsion were mixed at a 1:1:2 volume ratio respectively. The cuvette was inserted into the machine measurement system which records the time at which the ball bearing stops oscillating, indicating that the mixture has gelled. An average of three readings were done per emulsion gel (i.e. collagen, fibrin and collagen-fibrin gel).

Effect of excipients on pore size

The effect of excipients on pore size of scaffolds were also investigated using a variety of polymer excipients and sugar excipients. Sugar excipients tested included: dextran glucose, mannitol, sorbitol, sucrose and trehalose. Meanwhile, polymer excipients tested included Kollicoat, P68, PEG, PVA and PVP. These excipients were chosen as they have been previously shown to confer better stability for freeze-drying of materials.

Differential scanning calorimetry

10 mg of scaffold material was carefully measured out and placed in a hermetic aluminium pan. The pans were placed into a differential scanning calorimetry machine (DSC Q2000, TA Instruments, Hertfordshire, UK) and cooled to -60 °C. The sample was then heated at a rate of 1 °C/min up to -10 °C. The glass transition temperature (T_g) was determined by change in slope of the tangent of the heating curve, while heating rate remains constant.

Statistical Analysis

All data were expressed as mean ± standard deviation. Results were analysed using one-way analysis of variance (ANOVA) and a post-hoc Tukey test. Repeated measures ANOVA was used for the values which were measured repeatedly at different time points. A p-value of less than 0.05 is statistically significant. Where applicable, * denotes a p–value of <0.05, ** denotes a p–value of <0.01 and *** denotes a p-value of <0.01. All statistical analysis was performed using GraphPad Prism Version 4.0 for Windows.

3.2.3.Results

Emulsion Characterization

Droplet size

Increasing the HLB value of the surfactant mix in the emulsion from 11 to 12 was found to have a significant effect on increase in mean droplet diameter of the emulsion droplets. However, increasing the HLB value further from 12 to 14 was found to have no significant changes to droplet diameter.

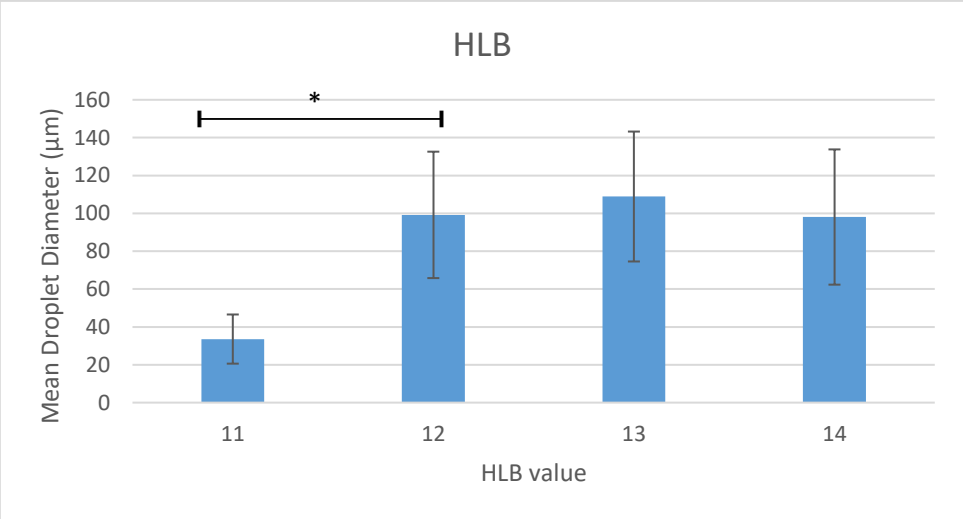


*Figure 3-14 Mean droplet diameter of decane emulsions did not change significantly between HLB values of 12 to 14. * denotes a p-value of <0.05. (mean ± SD, n=20)*

Increasing the mixing speed from 1000 rpm to 3000 rpm appears to result in a trend towards smaller droplet diameter at surfactant concentrations from 0.3% to 0.7%. However, no change in droplet diameter was observed when emulsion mixtures with 0.1% surfactant concentration was mixed at different rates. This may be due to limited availability of surfactants to lower interfacial surface tension as all available surfactant molecules are adsorbed at the oil-in-water droplet interfaces.

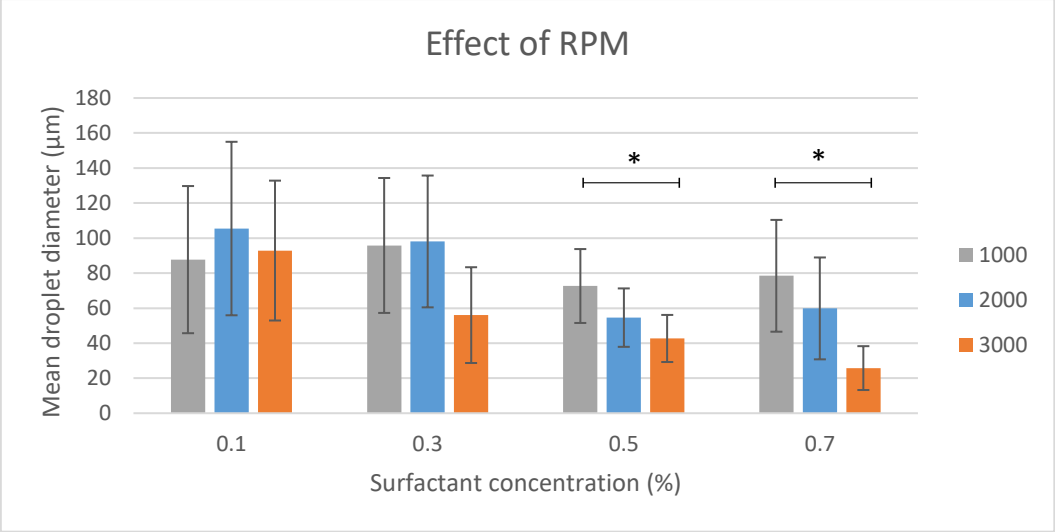


*Figure 3-15 Mean droplet diameter for decane emulsion according to shear rate and surfactant concentration. Mean droplet diameter decreased as shear rate increased from 1000 to 3000 rpm and as surfactant concentration increased from 0.3% to 0.7%. At 0.1% there is minimal change in mean droplet diameter due to the fragmentation limit. * denotes a p-value of <0.05. (mean ± SD, n=20)*

Stability

Increasing the HLB value of the surfactant mix resulted in improved stability of the emulsions. However, significant creaming was still noted. Increasing the surfactant concentration resulted in less fluctuations in light transmission and backscatter, indicating improved stability of the emulsions. Increasing the mixing rate also resulted in less variability in light transmission and backscatter, indicating a more homogenous emulsion mix.

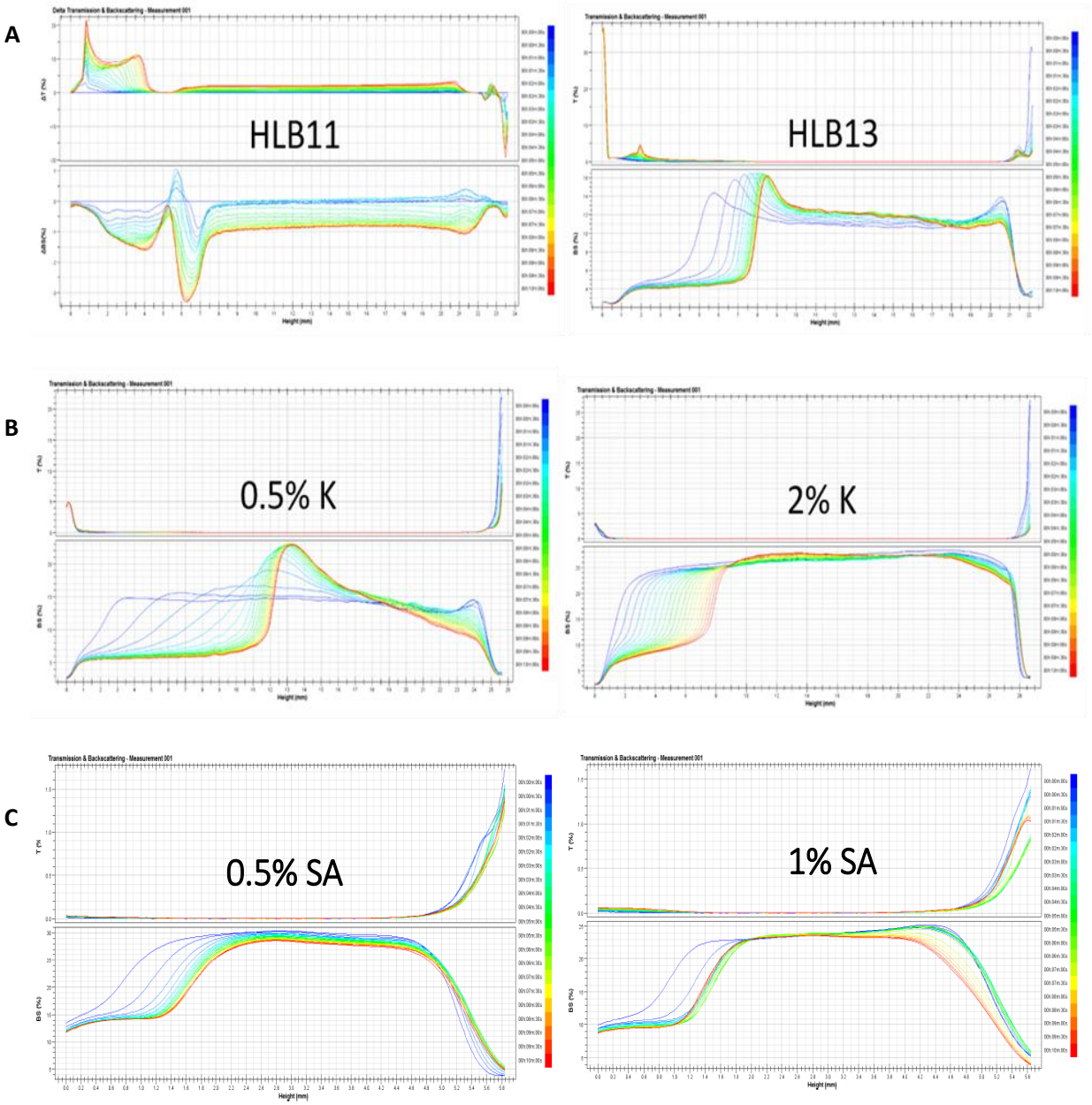


Figure 3-16 Turbiscan emulsion stability profile. Increase in (A) HLB value, (B) surfactant concentration and (C) PVP (Kollidon) concentration resulted in increasing stability of the resulting emulsion. Coloured bars on the right represent the different time points measurements were taken. (n=3)

Emulsion Rheology

The viscosity of the emulsions increased as concentration of surfactant concentration increased and as HLB values increased. Viscosity of the emulsions remained relatively stable at varying shear rates. Storage modulus decreased as surfactant concentration increased but increased as HLB values increased. Storage modulus for emulsions with HLB 10 and 11 decreased at higher frequencies.

However, storage modulus for emulsions with HLB 12 to 14 increased at higher frequencies. The loss modulus of emulsions increased with increasing HLB value but remained relatively stable at varying surfactant concentration. The loss moduli increased as frequency increased as well.

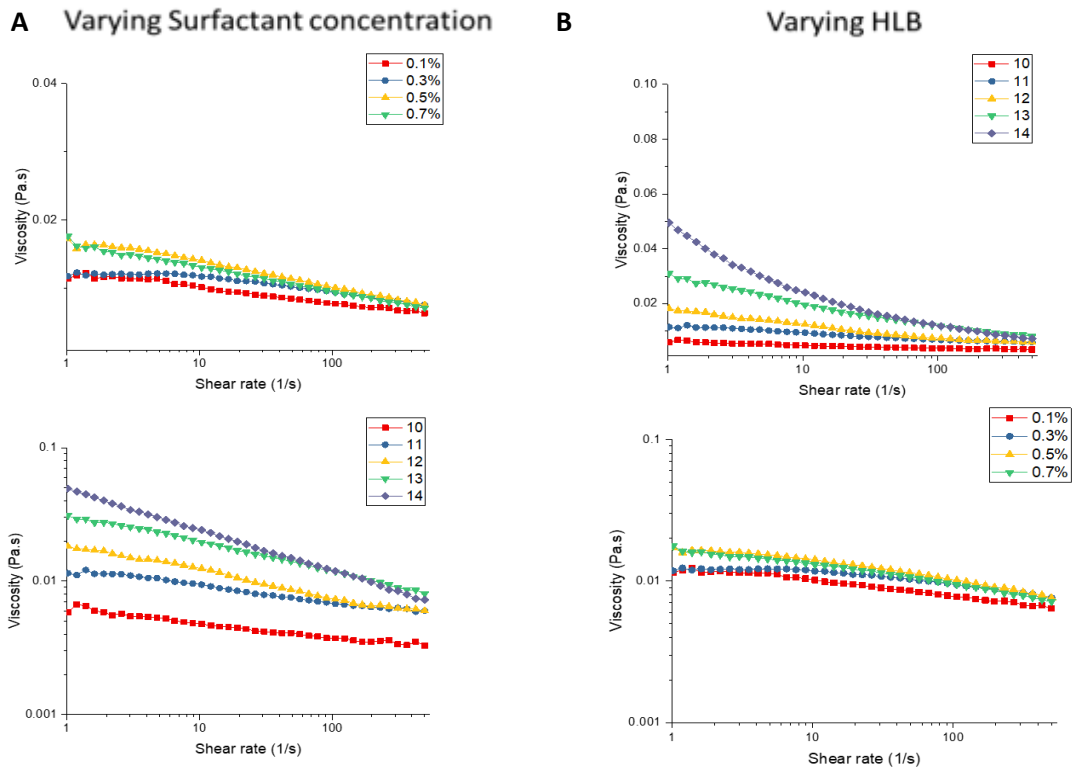
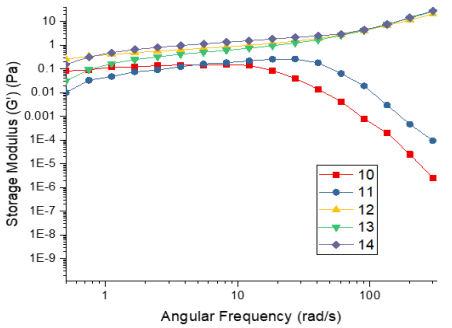
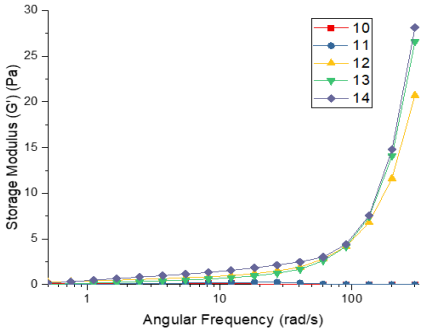


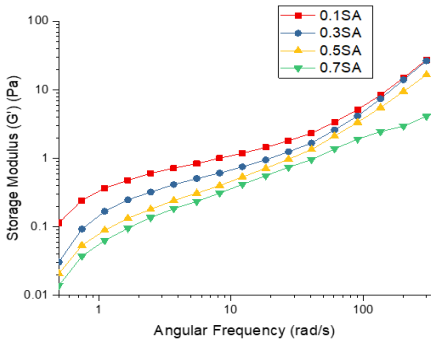
Figure 3-17 Viscosity of decane emulsions remains relatively stable regardless of (A) HLB value and (B) surfactant concentration. (n=3)

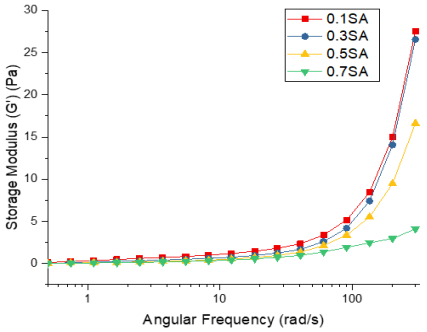
A Varying HLB



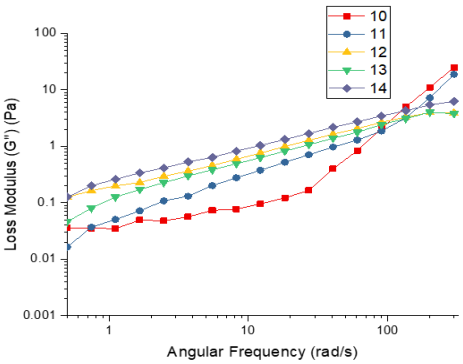


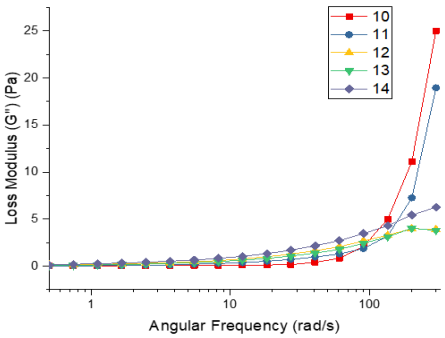
B Varying Surfactant concentration



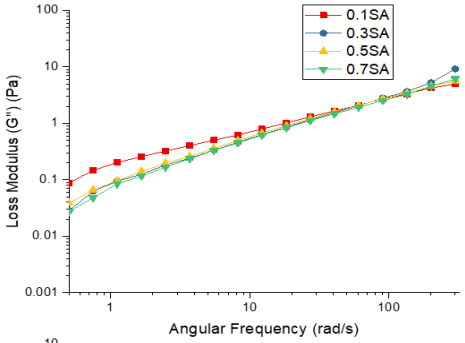


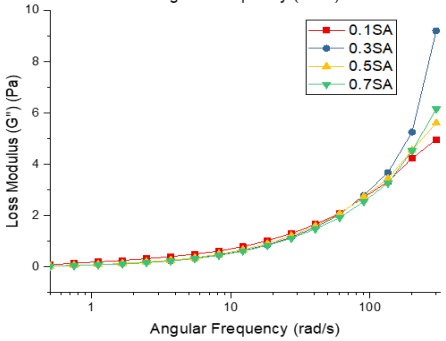
A Varying HLB





B Varying Surfactant concentration





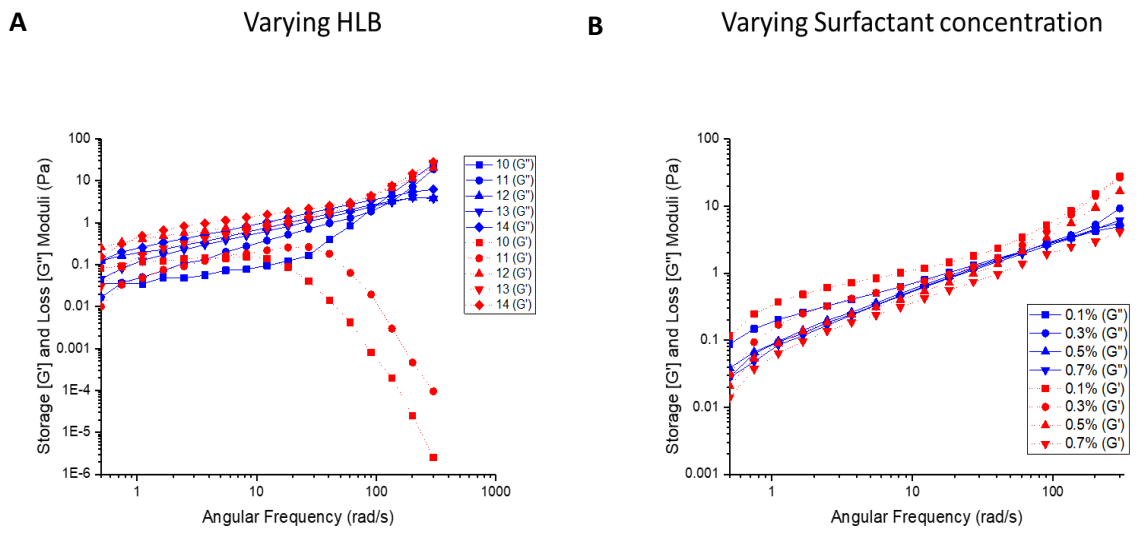


Figure 3-18 Storage and loss moduli values for decane emulsions by (A) HLB value and (B) surfactant concentration. The emulsions remain relatively stable across a range of HLB values and surfactant concentration. (n=3)

Scaffold Characterization

Pore Size

A) Collagen emulsion scaffolds

Addition of collagen to emulsions resulted in mean droplet sizes of approximately 100 to 150 microns, with the largest mean droplet diameter for the 0.1% surfactant concentration (mean 146 ± 51 µm) and smallest mean droplet diameter for the 0.7% surfactant concentration (mean 101 ± 43 µm). Pore size analysis of SEM images of scaffold cross-sections (Figure 3-22) demonstrated that mean pore sizes decreased to 50 to 100 µm, which is slightly smaller relative to emulsion droplet diameter sizes upon freeze-drying.

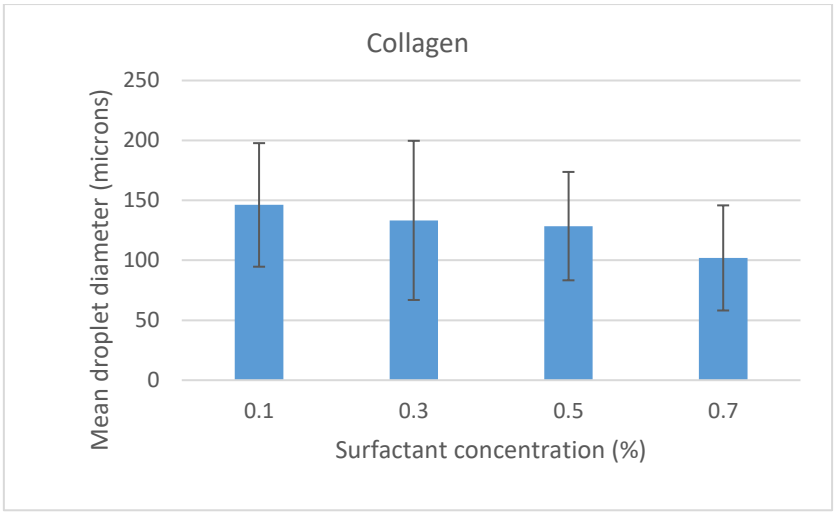


Figure 3-19 Mean droplet diameter for collagen protein-emulsion hydrogels gradually decrease with increasing surfactant concentration. (mean ± SD, n=20)

B) Fibrin emulsion scaffolds

Addition of fibrinogen/thrombin to emulsions resulted in mean droplet sizes of approximately 30 to 90 microns, with a trend towards smaller droplet sizes as concentration of surfactants within the emulsion mix is increased. Mean droplet size for 0.1% surfactant concentration was 94 ± 38 µm while mean droplet size for 0.7% surfactant concentration was 34 ± 10 µm. Pore size analysis of SEM images of scaffold cross-sections (Figure 3-22) demonstrated a mean pore sizes of about 40 to 60 µm, which is slightly smaller relative to emulsion droplet diameter sizes upon freeze-drying.

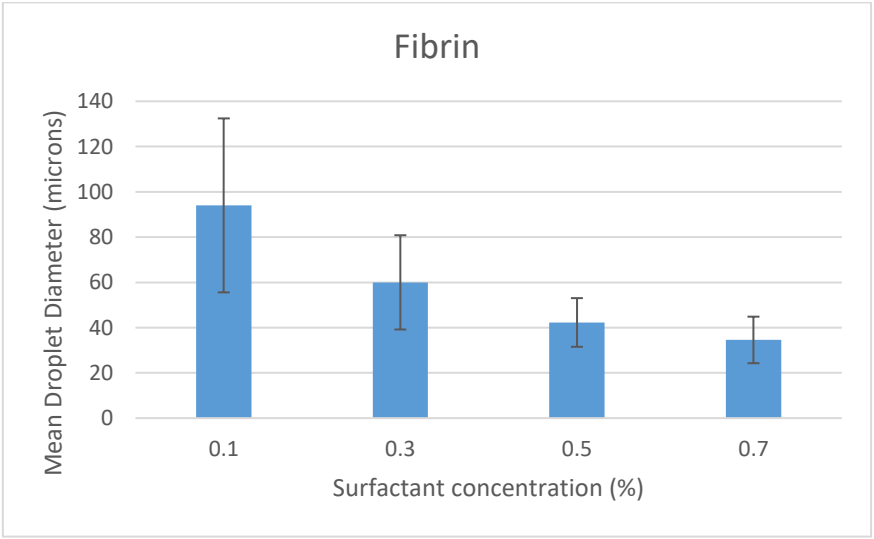


Figure 3-20 Mean droplet diameter for fibrin protein-emulsion hydrogels decrease with increasing surfactant concentration. (mean ± SD, n=20)

C) *Collagen-fibrin emulsion scaffolds*

The addition of collagen and fibrinogen/thrombin to emulsions resulted in mean droplet size of about 60 to 100 microns in the emulsion hydrogels. Mean droplet diameter was 101 ± 47 µm for 0.1% surfactant concentration but 62 ± 29 µm for 0.7% surfactant concentration. However, the pore sizes of the collagen-fibrin scaffolds showed a pore size of between 50 to 90 µm which is significantly smaller compared to the emulsion droplet diameters in a hydrogel state. This is consistent with the findings from the collagen and fibrin scaffolds as well.

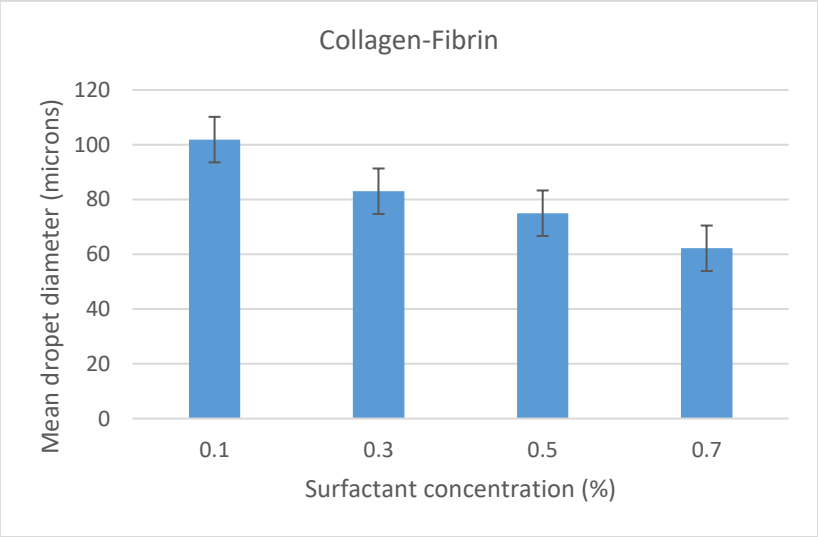


Figure 3-21 Mean droplet diameter for collagen-fibrin protein-emulsion hydrogels decrease with increasing surfactant concentration. (mean ± SD, n=20)

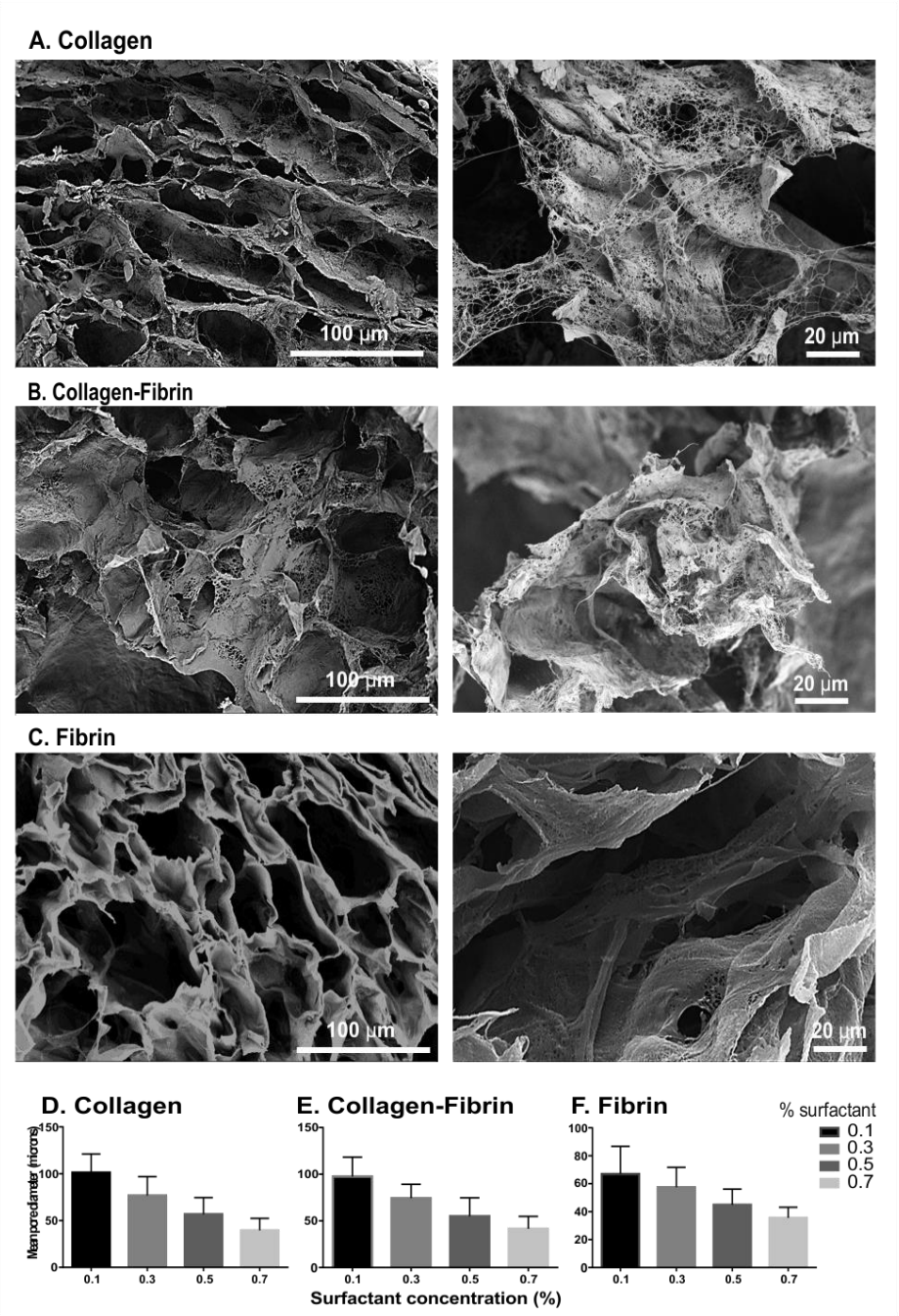


Figure 3-22 SEM images of emulsion-templated collagen, collagen-fibrin and fibrin scaffolds and mean pore size of each scaffold by percentage surfactant. (mean ± SD, n=20) Low magnification SEM images (x1000) on left panel showing microporous scaffold architecture while high magnification SEM images (x5000) on right panel demonstrates the nanofibrillar texture of the scaffold walls.

Degradation

A) Hydrolytic degradation

Scaffold degradation by hydrolysis was determined by measuring residual dry weight of scaffolds soaked in PBS for extended periods (Fig 3-23). Collagen scaffolds showed a large drop in dry mass of

40-50% over the first week. This is largely due to the dissolution of excipients during the initial hydration of the scaffold. At the end of 5 weeks, all scaffolds retained about 40 – 60% of their dry mass. Although EmDerm-C scaffold stability was achieved at the shortest cross-linking time, EmDerm-CF and EmDerm-F scaffolds which were cross-linked for a longer duration degraded slower compared to scaffolds which were cross-linked for 30 minutes (Figure 3-23) although this was not statistically significant in this experiment. Notably, fibrin scaffolds which were cross-linked for only 30 minutes degraded completely by 5 weeks.

B) Enzymatic degradation of scaffold

EmDerm-C and EmDerm-CF scaffolds remained incompletely degraded by Day 7 when incubated in trypsin solution (Figure 3-23). All EmDerm-F scaffolds which were cross-linked for less than 2 hours were completely degraded within 7 days. Those were cross-linked for 0.5 hours were completely degraded by 3 days, followed by those cross-linked for 1 hour on Day 5 and those cross-linked for 1.5 hours on Day 7 (Figure 3-23). As with the hydrolytic degradation, the mass of each scaffold decreased significantly over the first day. Dissolution of excipients was likely to contribute to the initial drop of scaffold dry mass.

Based on the results of the hydrolytic and enzymatic degradation of scaffolds, it was found that 1 hour of cross-linking worked the best as the scaffolds degraded at a slower rate and yet, retained its biocompatible properties when cultured with cells (shown later on). There was also better mechanical handling property when scaffolds were cross-linked for at least 1 hour. Other cross-linking reagents such as glutaraldehyde were also tested but was found to be cytotoxic and required a further reduction step to improve its biocompatibility while transglutaminase, a natural non-toxic cross-linker worked just as well as EDC/NHS but was significantly more costly compared to EDC/NHS.

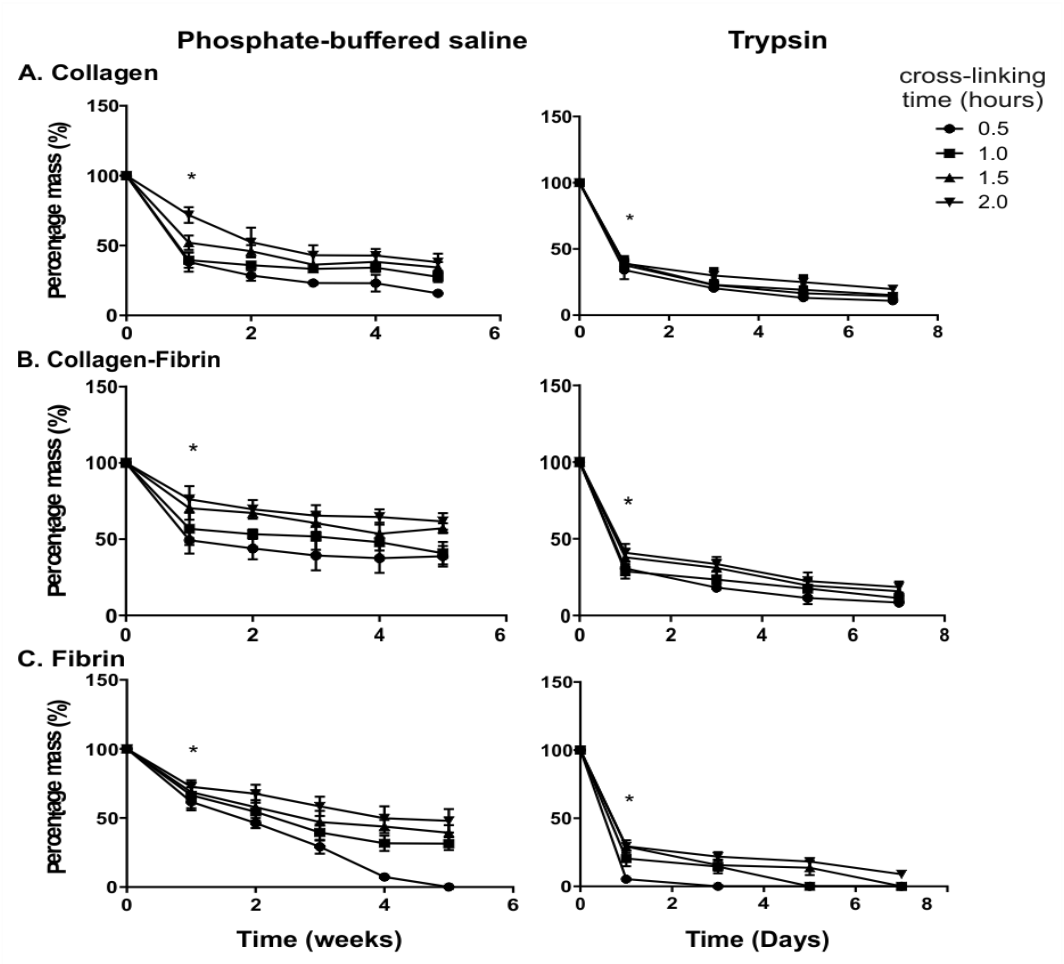


*Figure 3-23 Hydrolytic and enzymatic degradation of emulsion-templated collagen, collagen-fibrin and fibrin scaffolds. Fibrin scaffolds degraded much more rapidly compared to collagen and collagen-fibrin scaffolds. Percentage decrease in mass is significant after Day 1 due to initial dissolution of excipients. * denotes p-value of <0.05. (mean ± SD, n=3)*

Mechanical properties

The measurement of the tensile properties of each EmDerm scaffold type (Table 3-1) showed that the collagen-fibrin scaffolds had the highest Young's modulus and Ultimate Tensile Strength (UTS), approximately 1 to 2 MPa and 12 to 16 MPa respectively. This is followed by collagen scaffolds, which had a Young's modulus of about 1 to 2 MPa and UTS of about 7 to 9 MPa. Fibrin scaffolds had a Young's modulus of about 1 to 2 MPa and UTS of about 4 to 5 MPa. Change in porosity of the scaffolds and excipients used did not have a significant impact on mechanical properties of the scaffolds, as compared to type of material the scaffolds are made of.

Scaffold	Young's modulus (MPa)	Ultimate Tensile Strength (MPa)
CF scaffolds		
0.1CF	2.03 ± 0.81	12.82 ± 3.45
0.3CF	2.43 ± 0.45	14.07 ± 2.67
0.5CF	2.55 ± 0.98	15.15 ± 3.92
0.7CF	2.89 ± 0.72	16.47 ± 5.39
CF-M	1.89 ± 0.58	12.55 ± 3.89
CF-P68	1.46 ± 0.33	13.25 ± 2.66
CF-PEG	1.74 ± 0.76	11.53 ± 1.96
Collagen scaffolds		
0.1C	1.95 ± 0.49	8.28 ± 1.62
0.3C	1.45 ± 0.76	7.87 ± 1.45
0.5C	1.71 ± 0.21	7.99 ± 1.02
0.7C	2.14 ± 0.34	8.85 ± 0.97
C-M	1.27 ± 0.48	9.65 ± 2.81
C-P68	1.25 ± 0.74	8.26 ± 1.78
C-PEG	1.70 ± 0.51	8.87 ± 1.24
Fibrin scaffolds		
0.1F	1.52 ± 0.38	4.98 ± 0.96
0.3F	1.16 ± 0.29	4.81 ± 0.72
0.5F	1.18 ± 0.41	4.77 ± 0.42
0.7F	1.12 ± 0.29	4.62 ± 0.58
F-M	1.26 ± 0.35	4.25 ± 0.63
F-P68	1.48 ± 0.32	4.59 ± 0.22
F-PEG	1.37 ± 0.21	5.13 ± 0.51
F-PVA	2.01 ± 0.11	4.43 ± 0.49

Table 3-2 A summary of mechanical properties of each scaffold. (mean ± SD, n=3)

Gelation time

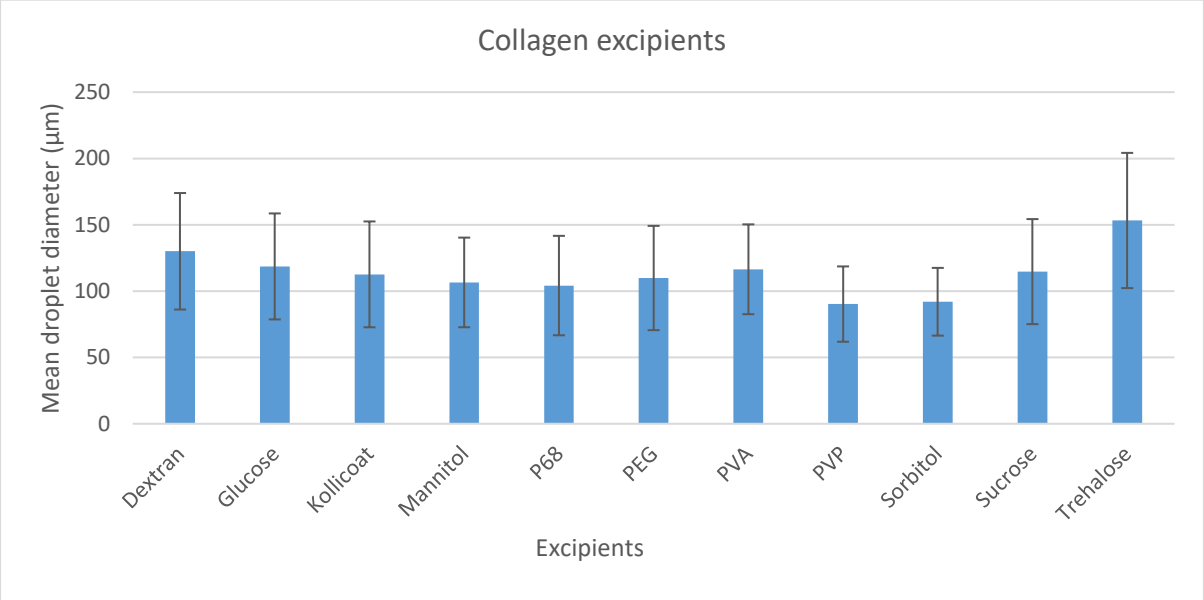
Mean gelation time of collagen scaffolds was the fastest with a mean of 62 ± 5 seconds. Mean gelation time for collagen-fibrin scaffolds were 93 ± 7 seconds and mean gelation time for fibrin scaffolds was 125 ± 4 seconds.

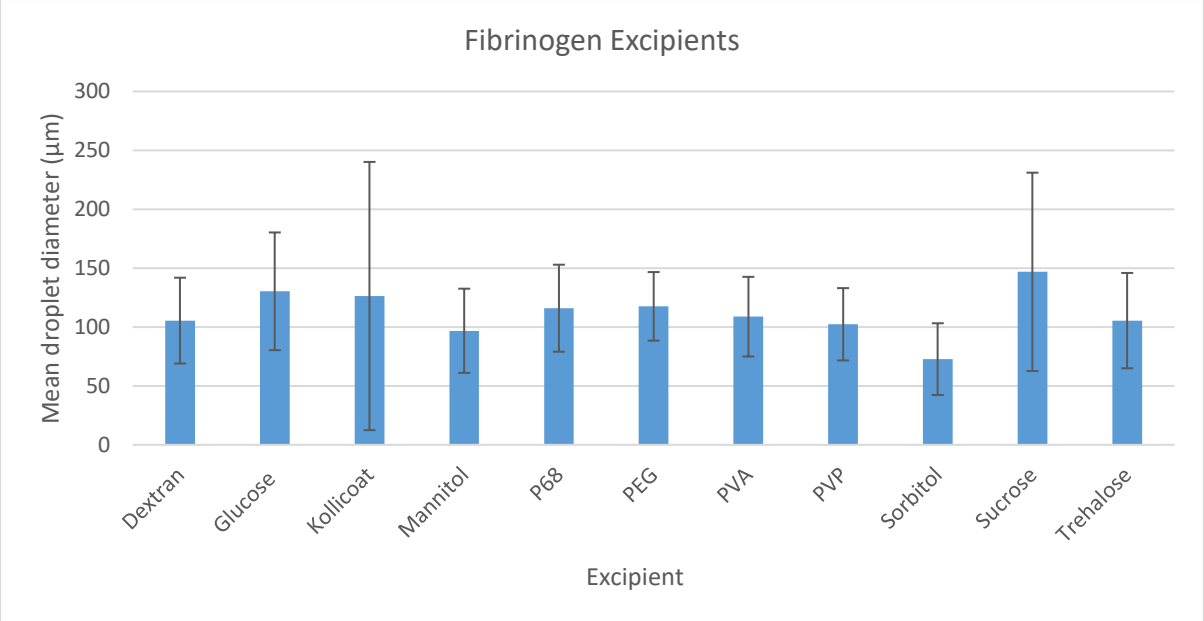
Scaffold	Mean gelation time
EmDerm-C	62 ± 5 seconds
EmDerm-CF	93 ± 7 seconds
EmDerm-F	125 ± 4 seconds

Table 3-3 Mean gelation time for each protein hydrogel. (mean ± SD, n=3)

Effect of excipients on scaffolds structure

Addition of a range of excipients did not cause a significant change to pore size of collagen scaffolds, fibrin scaffolds or collagen-fibrin scaffolds, although there is a trend towards smaller droplet sizes in protein emulsions with sorbitol as an excipient.





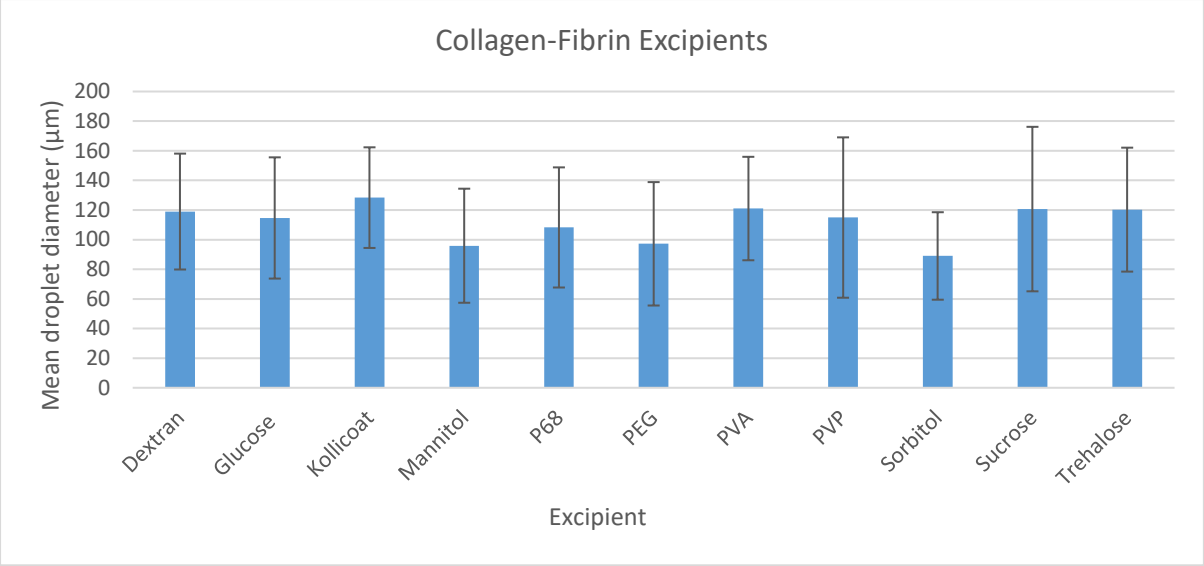
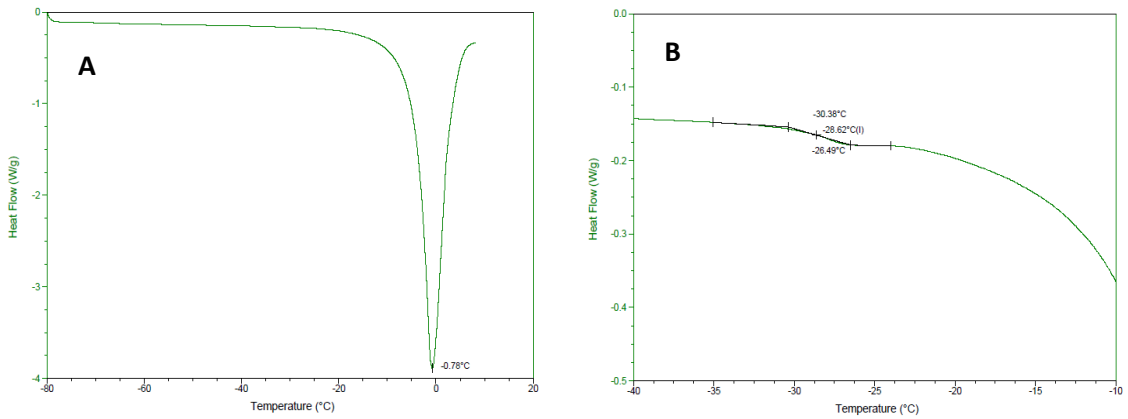


Figure 3-24 Addition of excipients into protein-hydrogels did not significantly affect mean droplet diameter.(mean ± SD, n=20)

Differential scanning calorimetry (DSC)

No glass transition temperature was found for collagen or collagen-fibrin scaffolds at the temperature ranges tested. However, for fibrin scaffolds, the glass transition temperature appears to be around – 28 °C. Therefore, freeze drying of scaffolds were all done at -30 to -40 °C.



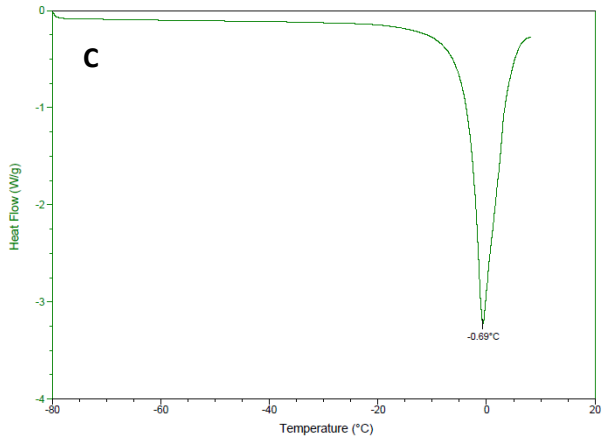


Figure 3-25 DSC profile of collagen (A), fibrin (B) and collagen-fibrin (C) scaffolds. Note glass transition temperature (Tg) of fibrin scaffolds was around -28°C. (n=3)

3.2.4. Discussion

In the previous section, a biocompatible emulsion system using mineral oil as the oil phase was characterized. However, the use mineral oil emulsion to manufacture emulsion-templated scaffolds was problematic. It was simply too viscous to remove from the scaffolds during the washing and lyophilization stage. The resulting scaffold did not retain the nanofibrillar architecture and was covered in a thick coat of mineral oil despite multiple washing and drying steps, when imaged under SEM. Therefore, a less viscous oil phase (decane) was chosen instead as it is biologically inert, has low viscosity (920 µPA at 20°C) and a low vapor pressure (195 Pa), thus freeze drying under vacuum will remove any remaining decane residues from the scaffold itself.

The characterisation and basic properties of these o/w emulsions have been described earlier. Structurally, there was no evidence of protein denaturation. When used with acidic extracted type I collagen, which exhibits spontaneous gelation in warming after pH neutralisation, the emulsion does not prevent gelation, and the nanostructure fibrils as seen on SEM imaging, indicate preservation of the intrinsic structure of the hydrogel. Furthermore, the successful use of emulsion system for fibrin, demonstrates that fibrinogen/thrombin enzymatic coagulation can proceed in the mixed phased system,

and the resultant fibrin fibril formation is indicative of the native structural self-assembly behaviour of fibrinogen after thrombin cleavage of the fibrinopeptides.

The stability of the decane emulsions is reflected in the rheological properties of the emulsion. The more viscous the emulsion, the more stable the emulsion droplets are. As HLB values and surfactant concentration increased, the viscosity of the emulsion system increased as well. This may be due to a slower rate of collision between emulsion particles and thus, less coalescence and flocculation. (89)

Scaffold porosity is a principle physical determinant of functionality of scaffolds. (141-143) Control of pore size was achieved through varying the emulsion size though surfactant concentration in the primary manufacture step, at a constant ratio of the aqueous protein phase to the templating oil phase. A direct relationship was found between the surfactant concentration in the primary manufacture step, which determines the mix phase template droplet diameter, and resultant lyophilised scaffold pore diameter by SEM. This applied over the range of mean pore diameters from around 40 to 100 μm. This suggests that the porosity EmDerm scaffolds can be readily tuned according to needs. A mean pore size between 80 to 100 microns as a suitable target is consistent with optimal migration through scaffolds with this pore size range. (144)

There is a trend towards smaller mean emulsion droplet sizes which correlates with smaller scaffold pore sizes as surfactant concentration increases. However, due to scaffold shrinkage during freeze-drying the final mean pore size of scaffolds are smaller than the mean droplet sizes in the protein-emulsion hydrogel state. The addition of excipients did not result in significant changes to the mean droplet size of the protein-emulsions.

Rate of degradation can also be controlled by changing the duration of cross-linking with EDC-NHS as well. This effect is particularly marked in EmDerm-F scaffold which disintegrates after three days when cross-linked for only half an hour. Enzymatic degradation was noted to be much more rapid than hydrolysis as the EmDerm scaffolds are made up of protein. This may be a significant factor if the scaffolds were to be used in chronic wounds as there would be higher secretion of degradative enzymes resulting in imbalance of ECM synthesis vs breakdown in such environment. Other ways to reduce rate of degradation of these scaffolds would be to use other methods of cross-linking e.g. UV or dehydrothermal cross-linking or incorporating polymers with predictable biodegradation rates.

Post-implantation stability of scaffolds is an important aspect of their function, and resorption of tissue regeneration scaffolds allows for new extracellular matrix deposition. (144) Here, an assay of accelerated proteolytic degradation is introduced in order to compare the kinetic profiles of degradation over a relatively short assay period. The cross-linking duration had a direct effect on scaffold stability, demonstrating that this can be readily controlled. Based on our findings, an incubation time of 1 hour for cross-linking should be sufficient to maintain integrity of the scaffolds post-implantation. A shorter duration significantly decreased hydrolytic and proteolytic stability of fibrin-based scaffolds, although the greater stabilisation achieved for collagen scaffolds indicates greater reactivity to the EDC/NHS.

The mechanical properties of EmDerm scaffolds suggest that they can be strong enough to be handled physically and do not tear easily. This is imperative as it allows the scaffolds to be positioned and sutured during surgery. With collagen scaffolds there was an inverse relationship between the mechanical strength (Young's modulus and UTS) and porosity which suggests that some differences in fibril organisation. With fibrin and collagen-fibrin scaffolds, the pore size did not have a marked effect on these parameters.

The mechanical properties of the scaffolds can also be tuned, depending on type of material used. Collagen-fibrin scaffolds had highest tensile strength compared to collagen and fibrin emulsion-templated scaffolds. Changes in type of excipient and pore size did not significantly result in changes ultimate tensile strength and Young's modulus of scaffolds. However, the mechanical properties may be further tuned based on type of cross-linking reagent (e.g. glutaraldehyde) and concentration of the cross-linker. However, for the purposes of this study, EDC-NHS was chosen which is a zero-length cross-linker as they have been shown to be much more biocompatible that other cross-linking reagents.

The gelation time of collagen scaffolds were shortest as it is pH and temperature dependent which occur rapidly. Fibrin formation depends on the enzymatic reaction between fibrinogen and thrombin which takes time to occur. Therefore, it is rather unsurprising that fibrin emulsion scaffolds take the longest to form a gel and collagen-fibrin emulsion scaffolds require slightly less time than that. However, even at 120 seconds, this process is relatively quick and the viscosity of the protein gel/solution results in greater stability of the emulsions when added. Hence, consistency is scaffold pore size can be achieved using this meta-stable protein-emulsion templated hydrogel system.

Lyophilization is a process of removing solvent (usually water) from a product by sublimation. It is widely used to preserve biological products. In addition, lyophilization can be used to create scaffolds whereby ice crystals act as porogens to create a porous scaffold and sublimed under a specified vacuum condition. The rate of growth of ice crystals is dependent on rate of cooling during freeze-drying. However, in this study the glass transition temperature (T_g) is the primary determinant of whether scaffolds formed were collapsed or not. Freeze drying above the T_g results in a smooth flattened featureless scaffold, while freeze-drying under the T_g with vacuum conditions below the vapour pressure of water and decane preserves the microporous nanostructure of the resulting emulsion-templated scaffolds. No T_g was noted for collagen and collagen-fibrin scaffolds, however the T_g of fibrin scaffolds was found to be -28 °C. Thus, primary freeze-drying step was done below -30 °C.

The addition of excipients such as P68, mannitol and PVA to scaffolds prior to lyophilization also appears to have a role in preserving the nanostructure of scaffolds. By contrast, scaffolds without excipients did not have nano-fibrous walls, rather they were smooth and featureless when imaged under SEM. These findings suggest firstly that collagen is able to undergo structural reorganisation under freeze-drying involving fusion of the fibrillar hydrogel structure into microscale lamellae; secondly that excipient interaction with the protein matrix is a stabilising factor which prevents nanostructure fusion. One of the aims of this method of manufacture is to create scaffolds with nano-structured architecture, which current commercial scaffolds lack. The nano-fibrous architecture can provide cells with oriented cell adhesion signals and promote migration of cells, as there is an aligned fibre matrix for cells to move along (145). In this regard, the effect on excipients on preserving the collagen nanostructure of EmDerm scaffolds is notable.

3.2.5.Summary

In conclusion, a manufacturing method (emulsion templating) was developed where the pore size of scaffolds can be controlled by manipulating emulsion mean droplet sizes. The rate of degradation can be controlled by duration of cross-linking, while mechanical properties of the scaffold is dependent on type of protein hydrogel used. The gelation process occurs within around 120 seconds and the emulsion stability is reflected by the minimal change in viscosity over different shear rates. Freeze-drying of the scaffolds under -30°C with added excipients preserves the nanostructured porous architecture of the resulting emulsion-templated scaffolds.

Chapter 4 Biocompatibility of Emulsion-templated Bio-intelligent Scaffolds

4.1. Introduction

In the previous chapter, a biocompatible emulsion system was used for manufacture of EmDerm scaffolds. These scaffolds were noted to have hierarchical interconnected porosity and nanostructured architecture which have promising potential for better cellular migration and proliferation due to greater surface area for cell attachment and greater diffusion of nutrients and oxygen for cell growth. These attributes are fundamental requirements of three-dimensional protein-based bio-intelligent scaffolds and are essential for the functions of cell conductivity, nutrient perfusion, angiogenesis and vasculogenic differentiation. (139,146,147)

In this chapter, the suitability of EmDerm scaffolds as a dermal skin substitute is explored using cell proliferation assays of various cell types including human epidermal keratinocytes, human dermal fibroblasts, human dermal microvascular endothelial cells and bone-marrow mesenchymal stem cells. These cell types were chosen as they are relevant for the reconstruction of a bilayer skin substitute. Cell proliferation was quantified and compared to commercial scaffolds Matriderm and Integra.

To create a bilayer skin scaffold, there is a need to develop a vascularized dermal layer and stratified epidermal layer. Thus, co-culture of fibroblasts and keratinocytes on EmDerm scaffolds was performed and matured at air-liquid interface to create a stratified epithelium. Meanwhile, co-culture of fibroblasts/mesenchymal stem cells and endothelial cells was also performed to create a vascularized dermal construct. The suitability of EmDerm scaffolds for delivery of stem cells to modulate the wound healing process was also investigated by seeding mesenchymal stem cells onto EmDerm scaffolds.

Co-culture of human epidermal keratinocytes and fibroblasts (HEK/HDF), human dermal endothelial cells and fibroblasts (HDE/HDF) and mesenchymal stem cells and human dermal fibroblasts

(MSC/HDF) was also performed on EmDerm scaffolds to investigate the interaction between the different cell types. Widefield imaging as well as analysis of the proteome and secretome from cells seeded on EmDerm scaffolds was also performed. The effect of scaffold architecture has been shown to have a pronounced effect on gene expression, protein production and growth factor secretion such as cytokines and growth factors which acts as a chemoattractant for cellular ingress as well as remodelling of scaffold structure. These effects could be mediated by changes in cell protein synthesis profile and secretion of various factors which affect cell behaviour within the scaffold itself.

Here, several candidate proteins were selected – including enzymes and growth factors to investigate the mechanism by which EmDerm scaffolds encourage cell proliferation and migration into the scaffolds, matrix remodelling and promote vasculogenesis. Using a multiplex magnetic ELISA assay, the concentration of various factors within the cell lysate and cell supernatant were quantified. Monoculture and co-cultures were compared to investigate change in cell secretome and proteome due to interaction between two cell types.

For scaffold remodelling, quantification of several key structural proteins and degradative enzymes such as Type I collagen and Type IV collagen, as well as levels of tissue inhibitor of matrix metalloproteinase 1 (TIMP1), matrix metalloproteinase 1 and 2 (MMP1 and MMP2) were selected. MMP1 initiates cleavage of fibrillar collagen, especially Type I collagen while MMP2 is known to breakdown Type IV collagen. TIMP1 is a key inhibitory molecule that regulates activity of matrix metalloproteinases. Thus, these proteins were included in the assay for quantification.

In terms of vasculogenesis, there were a myriad of growth factors to select. However, based on a review of current literature, seven growth factors/cytokines were chosen as they have been shown to exhibit significant effect on angiogenesis and vascularization. Vascular endothelial growth factor A (VEGF-A) is a key factor which promotes proliferation and migration of endothelial cells, angiogenesis and vessel

permeability. (148,149) It is often upregulated in hypoxic conditions e.g. necrotic tumours. Basic fibroblast growth factor (FGF-B) is a growth factor which is often bound to heparin. It has broad mitogenic and angiogenic properties and has been shown to be more potent than VEGF-A itself. (150) Hepatocyte growth factor (HGF) is another growth factor which has a broad range of actions in angiogenesis and tissue regeneration. (151) Angiopoeitin-1 (ang-1) plays an important role in vascular development and angiogenesis. It also contributes to blood vessel maturation and stability. (152,153)

Fibronectin is a high molecular weight glycoprotein which binds to extracellular matrix such as collagen and fibrin. It plays a role in cellular adhesion, migration, proliferation and differentiation. (154,155) Von Willibrand factor (VWF) is another large multimeric glycoprotein which plays a role in platelet aggregation and wound healing (156) while IL-8 is a chemokine stored by endothelial cells which is another crucial growth factor for promoting angiogenesis. (157)

4.2. Materials and Methods

Materials

Unless otherwise stated, all reagents were purchased from Sigma. Type 1 rat tail collagen (5mg/ml) was obtained from FirstLink (Wolverhampton, UK). Bovine fibrin and thrombin were obtained from Sigma. 2-(N-morpholino) ethanesulfonic acid (MES) biochemical grade (Fisher Scientific, Loughborough, UK) and sodium chloride were used for the buffer. Decane, Tween 20 and Span 20 were used for emulsions. 1-ethyl-3-(-3-dimethylaminopropyl) carbodiimide hydrochloride (EDC) and sulfo-*N*-hydroxysuccinimide (NHS), pure ethanol and isopropanol were used for cross-linking and oil elution. The excipients used were polyvinyl alcohol (PVA) (99% hydrolysed, MW 89,000 to 98,000), polyethylene glycol (PEG) (MW 6000), Pluronic F-68 (P68) and mannitol (M). 0.25% Trypsin-EDTA solution for cell culture was used for stability testing and the Cell Counting Kit (CCK-8) assay was used to measure cell proliferation.

Manufacture of scaffolds

Macro-emulsion mixtures comprising of decane, Span 20/Tween 20 at a calculated HLB of 13 and an aqueous buffer (25 mM MES, 150 mM NaCl pH 7.4) were mixed in a 60 ml syringe with the tip removed, for 15 seconds at 1000 rpm using a high-speed mixer (Caframo BDC6015, Ontario, Canada). Emulsions with 0.1, 0.3, 0.5 and 0.7% surfactant concentration were prepared.

To manufacture scaffolds from each protein type, each of the emulsions was added to each protein solution designated as follows: collagen (Col), fibrinogen plus thrombin (Fbn) or a mixture of collagen and fibrin solution at a 1:1 volume ratio (ColFbn). The gelling solution of type-I collagen was used at 4.5 mg/ml, fibrinogen was prepared at 20 mg/ml and thrombin at 10 units/ml in in 25 mM MES/150 mM NaCl (pH 7.4) buffer. Each emulsion-scaffold was left to gel at 37 °C for 30 min and then cross-linked with EDC: NHS (5:2 molar ratio) in 80% ethanol. (158) The scaffolds were then washed in 80% isopropanol, then deionized water three times for 15 minutes. At this point scaffolds were further incubated with a 5% w/v excipient solution (e.g. P68, PVA, PEG or M). The scaffolds were freeze-dried at −30 °C.

The possible effects of the different excipients used, on functional parameters and scaffold morphology, were compared using scaffolds made at large pore size with 0.1% surfactant concentration. The effect of surfactant concentration was compared between scaffolds made using F68 as the excipient.

Scaffold preparation

Scaffolds were cut into 6mm discs using punch biopsies. Each scaffold was washed in phosphate buffered solution (PBS) three times and UV-irradiated for 15 minutes. Each scaffold was incubated in the respective media overnight for 24 hours before used for cell seeding experiments.

Cell culture

HEK cells were sub-cultured using Epilife media with added HKGS. Human dermal fibroblasts derived from neonatal foreskin (HDF) were obtained from Invitrogen, UK. They were cultured in standard Dulbecco's Modified Eagle Medium (DMEM) media (Gibco, ThermoFisher Scientific, UK) with 20% foetal bovine serum (FBS) and 1% penicillin/streptomycin. Only cells from Passage 2 to 9 were used in the experiment. Human dermal microvascular endothelial cells derived from neonatal foreskin that have been hTERT immortalized (HDE), were obtained from ATCC, UK. They were cultured using Vascular Cell Basal Medium with Microvascular Endothelial Cell Growth Kit-VEGF supplement containing: rhVEGF (5 ng/ml), rhEGF (5 ng/ml), rhFGF basic (5 ng/ml), rhIGF-1 (15 ng/ml), L-glutamine (10 mM), heparin sulfate (0.75 Units/ml), hydrocortisone (1 µg/ml), ascorbic acid (50 µg/ml) and foetal bovine serum (5%). Immortalized human bone marrow mesenchymal stem cells transfected with GFP (MSC) were obtained courtesy of Dr James Li (Hong Kong University) and cultured in low glucose (1g/L) DMEM media.

Cell Proliferation Assay

Scaffolds were seeded with three different cell types (HDE, HDF, MSC) to determine the cytocompatibility of each scaffold. Scaffolds were prepared as described above. Each scaffold was seeded with 5000 cells/well and left overnight for cells to attach onto the scaffold material. On the next day, the seeded scaffolds were transferred into a new well plate and allowed to incubate up to 14 days. Media was changed on alternate days.

On Day 3, 7 and 14, a cell proliferation assay using CCK-8 (Sigma, UK) was done to determine cell growth in each scaffold. CCK-8 is a highly sensitive colorimetric cell counting assay based on a highly water-soluble tetrazolium salt (WST-8), which is reduced by dehydrogenase in cells to give a yellow-coloured formazan dye. The amount of the formazan dye generated by cellular metabolism is directly proportional to the number of living cells. Briefly, 10µl of CCK-8 solution (neat) was pipetted into each

well of 100µl cell media. Each plate was incubated for 4 hours in the incubator at 37 °C and 5% CO_2. Subsequently, 50µl of each well's contents were pipetted into a fresh plate and absorbance was measured at 450 nm using the Spectramax i3 Multi-Mode Plate Reader (Molecular Devices, CA, USA). 10µl of CCK-8 was also added to a dilution series of known concentrations of cells to obtain a calibration curve in a 96 well plate. Cell-free media with CCK-8 solution was used as negative controls. Three replicates were tested for each sample. Lastly, the scaffolds were fixed in neutral buffered formalin (NBF) on Day 14 for further imaging.

Comparison with Commercial Scaffolds

0.1C, 0.1CF and 0.1F scaffolds were compared with commercial scaffolds Matriderm and Integra. Matriderm and Integra were chosen as both are gold standard dermal skin substitutes currently used for burns and chronic wounds. Each scaffold was cut using a 6mm punch biopsy and placed into a 96 well plate. All scaffolds were rinsed with PBS three times and then incubated in cell media overnight. On the next day, each scaffold was seeded with 1000 cells/well and left overnight for cell attachment. A lower cell count was chosen so that the difference in cell proliferation between each scaffold can be easily detected. The seeded scaffolds were moved to a new well plate the following day and allowed to incubate for 14 days. Media was changed on alternate days. On Day 3, 7 and 14, a cell proliferation assay using CCK-8 (Sigma, UK) was done to determine cell growth in each scaffold (as described earlier). Finally, the scaffolds were fixed in NBF on Day 14 for further imaging.

Wide-field imaging of seeded scaffolds (monoculture)

Each of the seeded scaffolds was stained using fluorescent antibodies for downstream imaging. Scaffolds seeded with human dermal fibroblasts were stained with 1:6 phalloidin (Alexa Fluor 488, Thermo Fisher) and scaffolds seeded with human dermal endothelial cells were stained with 1:250 mouse anti-human CD31 (Dako) and 1:1000 rabbit anti-human vWF (Dako). Secondary staining was

done using goat anti-mouse (Alexa Fluor 488, Thermo Fisher) and goat anti-rabbit (Alexa Fluor 568, Thermo Fischer).

Scaffolds seeded with mesenchymal stem cells were not stained as they were GFP expressing cells. All scaffolds were counterstained using Hoescht 33342 staining (Thermo Fisher). Z-stacks were taken to visualize cell migration through the scaffold by wide-field imaging at 20X magnification. Images were deconvoluted using AutoQuant X3 (Media Cybernetics) and visualised using Bitplane (Imaris software, Version 9.1).

Co-culture of scaffolds

Each cell type was passaged using 1x Trypsin-EDTA and suspended in their respective medium. 10µl of the cell suspension was added to 10µl of tryphan blue and counted using the Countess Cell Counter. The cell suspensions were then serially diluted to achieve a concentration of 5 x 10^4 cells/ml. 200µl of each cell suspension mixture (HEK/HDF, HDF/HDE, MSC/HDE) was then added in a dropwise manner onto each respective scaffold (EmDerm-C, EmDerm-CF, EmDerm-F) to achieve an evenly seeded scaffold and left to incubate at 37 °C at 5% CO_2 for 4 hours in a 96 well plate. Cells were fed every 2-3 days for up to 14 days. Two sets of co-culture experiments were performed – one for cell lysis and one for fixation and imaging.

Air-Liquid Interface (ALI) Co-Culture of Human Keratinocytes and Dermal Fibroblasts

5000 cells/well of HDFs were seeded onto each scaffold (EmDerm-C, EmDerm-CF, EmDerm-F, Matriderm and Integra) and cultured for a week in DMEM (4.5g/L glucose) + 10% FBS + 1% penicillin/streptomycin. After a week, 5000 cells/well of HEK were seeded onto the other side of each scaffold and cultured for a week in a transwell plate, fully immersed in media. Media used was Epilife + HKGS and DMEM (4.5g/L glucose) + 10% FBS + 1% penicillin/streptomycin (at a 2:1 volume ratio).

After 7 days, the scaffolds were lifted to air-liquid interface to allow for differentiation and stratification of the keratinocytes. Media was changed every other day. On Day 21 of culture, the scaffolds were fixed in neutral buffered formalin for scanning electron microscopy (SEM) imaging and histological assessment.

Immunofluorescence staining of co-cultured scaffolds

Each seeded scaffold was fixed in neutral buffered formalin for at least 24 hours. The scaffolds were washed 3 times with PBS. The fixed cellularized scaffolds were then permeabilized using 0.1% Triton X-100 in PBS for 30 minutes and washed 3 times with PBS. The scaffolds were then blocked with 1% bovine serum albumin (BSA) in PBST (PBS + 0.1% Tween 20) for an hour and washed. Primary antibodies were then added and left overnight on an orbital shaker. On the following day, the primary antibody solution was aspirated, and scaffolds were washed with PBS 3 times. Secondary antibodies were then added and left overnight on an orbital shaker. Cells were then counter-stained with 0.1µg/ml of Hoescht for 5 minutes and then rinsed with PBS three times.

For the HEK/HDF co-cultured scaffolds, 1:100 mouse anti-human pancytokeratin (Abcam) was used to stain for HEK. Phalloidin 488 (ThermoFisher) is an F-actin binding agent which was used to stain HDF and HEK as well. 1:500 goat anti-mouse antibody (AlexaFluor 568, ThermoFIsher) was used as a secondary antibody. For the HDF/HDE co-cultured scaffolds, 1:4 mouse anti-human CD31 (Dako) and 1:1000 rabbit anti-human vWF (Dako) were used as primary antibodies. Goat anti-mouse (AlexaFluor 488, ThermoFisher) and goat anti-rabbit (AlexaFluor 568, ThermoFisher) were used as secondary antibodies. Phalloidin 647 was also used to stain actin filaments. For MSC/HDE co-cultured scaffolds, 1:4 mouse anti-human CD31 (Dako) and 1:1000 rabbit anti-human vWF (Dako) were used as primary antibodies. Goat anti-mouse (AlexaFluor 647, ThermoFisher) and goat anti-rabbit (AlexaFluor 568, ThermoFisher) were used as secondary antibodies.

SEM Imaging Scaffold Preparation

HEK/HDF scaffolds which were cultured at air-liquid interface were imaged under scanning electron microscopy to observe for stratification of keratinocytes when lifted to air-liquid interface. Fixed scaffolds were dehydrated in an ethanol gradient as follows: 25% ethanol, 50% ethanol, 75% ethanol, 80% ethanol, 90% ethanol and 100% ethanol. Finally, the scaffolds were transferred into wells containing hexamethyldisilazane (HMDS) and left to dry in the fume hood overnight. This is to ensure that the samples are completely dried prior to imaging. Each scaffold was then sputter coated with gold for 120 seconds and imaged using a scanning electron microscope (Zeiss, Germany).

Cell Culture Supernatant Preparation

Cells seeded onto scaffolds were maintained in culture for up 13 days. On Day 13, media was aspirated and each well was washed with PBS. Serum free media was then added and left for 24 hours. On the following day, cell culture supernatant was aspirated and centrifuged at 1500 rpm for 10 minutes. The supernatant was then immediately stored at -80 °C and thawed to room temperature just before use for the multiplex assay.

Cell Lysate Preparation

After the media was removed, the seeded scaffolds were washed with chilled PBS. The scaffolds were transferred into a microcentrifuge tube in an ice box. 100 µl of extraction buffer with Halt Protease Inhibitor was added to each scaffold and vortexed for 1 minute each. The cell lysate extract was then centrifuged at 13 000 rpm to pellet any insoluble materials. The supernatant was then immediately stored at -80 °C and thawed to room temperature just before use for the multiplex assay.

Magnetic Multiplex Assay

Reagents were brought to room temperature and reconstituted as per manufacturers instruction. Serial dilutions of the standards were prepared as per protocol and Certificate of Analysis. Cell culture supernatant and cell lysates were thawed and diluted at 1:2 ratio using the manufacturer's diluent. 50µl of each standard and sample were pipetted into the 96 well plate. Serum free media was used as negative control. Microparticle Cocktail was added to each well and incubated for 2 hours at room temperature on a shaker. Each well was then washed with a wash buffer, using a magnetic plate to hold the beads to the bottom of the plate. Biotin-Antibody cocktail was then added to each well and incubated for an hour at room temperature on a shaker. The wells were washed, then Strepavidin-PE was added to each well and incubated for 30 minutes at room temperature on a shaker. The wells were then washed and the magnetic microparticles were resuspended in 100µl of wash buffer in each well. The mean fluorescence intensity of beads in each well was then was read using the Luminex 100 analyzer. The experiment was done in duplicates.

Statistical analysis

All data were analysed using one-way analysis of variance (ANOVA) to evaluate statistical significance between comparisons and a post-hoc Tukey test. Two-way ANOVA was used where there were two independent variables. Repeated measures ANOVA was used for the values which were measured repeatedly at different time points. A p-value of less than 0.05 is statistically significant. Where applicable, * denotes a p–value of <0.05, ** denotes a p–value of <0.01 and *** denotes a p-value of <0.001. All statistical analysis was performed using GraphPad Prism Version 4.0 for Windows.

4.3. Results and Discussion

4.3.1. Cell Proliferation on EmDerm Scaffolds

The assessment of the biocompatibility of EmDerm scaffolds was investigated by measuring the proliferation three cell types central to skin reconstruction, HDF, HDE and MSC. Net proliferation of

each cell type occurred over 7 days in each scaffold material (Figure 4-1). Importantly, there was no significant effect of varying the excipient used, compared to the Pluronic excipient (Figure 4-1). However, it is notable that HDE and MSC proliferation in collagen scaffold made without an excipient (C-GEL) was significantly lower than EmDerm collagen scaffolds with excipient (C-P68 and C-M). Also, HDF showed lower proliferation on CF-PEG and F-M scaffolds.

While proliferation was marked in scaffolds with high porosity, there was a general trend for proliferation to be progressively lower with decreased porosity (Figure 4-2). This effect was most pronounced for HDF in collagen scaffolds at the lowest porosity, corresponding to 0.5% and 0.7% surfactant mix in the emulsion template (Figure 4-2), and in collagen-fibrin scaffolds at the lowest porosity (Figure 4-2). This suggests that there may by an effect of surfactant residues remaining on the scaffolds which were not completely removed during the washing phase. It may also be that scaffolds with smaller pore sizes were less ideal for cellular conductivity and proliferation.

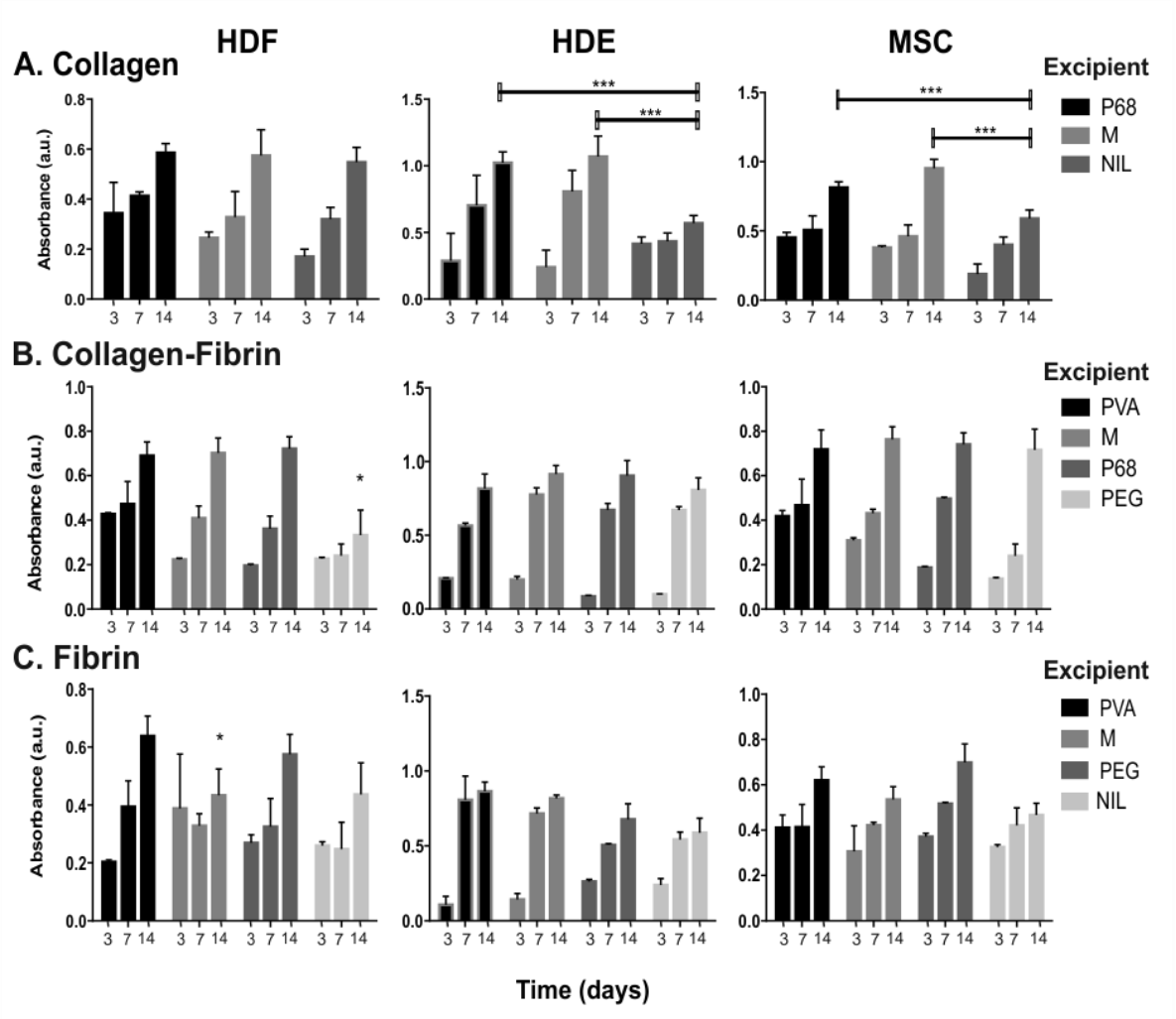


Figure 4-1 Cell proliferation results by cell type and type of excipient. HDE and MSC had significantly higher proliferation rate in collagen scaffolds with P68 and mannitol as excipients compared to collagen scaffolds without excipients ($p<0.001$). HDF had significantly lower proliferation rate in collagen-fibrin scaffolds with PEG as excipient compared to collagen-fibrin scaffolds with other excipients ($p<0.05$) and fibrin scaffolds with mannitol as excipient had lower HDF proliferation rate compared to fibrin scaffolds with other excipients ($p<0.05$). Data expressed as mean ± SD, ($n=3$).

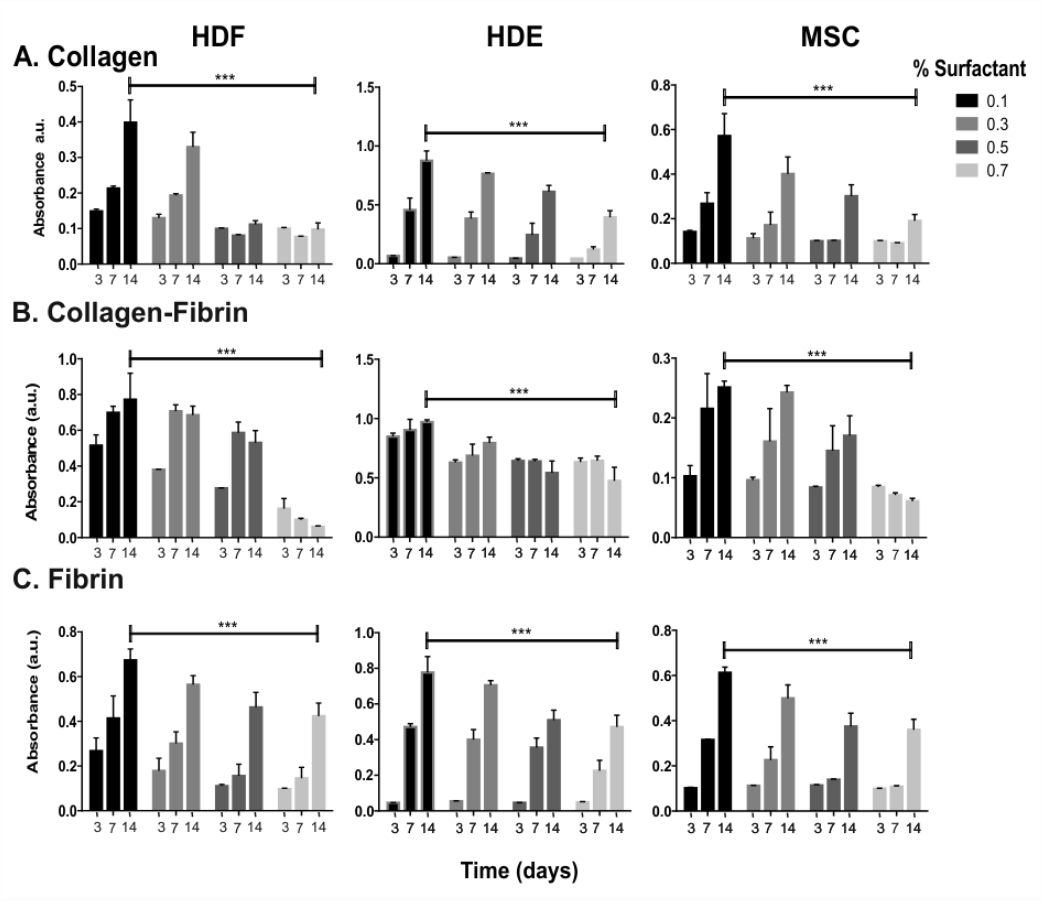


*Figure 4-2 Cell proliferation outcome by concentration of surfactant. All three cell lines (HDF, HDE, MSC) had significantly higher proliferation rate in scaffolds made with 0.1% surfactant concentration indicating a surfactant concentration effect. *** denotes p-value of <0.001. (mean ± SD, n=3)*

Comparison with commercial scaffolds

There was greater proliferation of each cell type in the EmDerm scaffolds with 0.1% surfactant concentration and P68 as excipient compared to commercial scaffolds, Matriderm and Integra (Figure 4-3). It is notable that 0.1F-P68 supported greatest HDE proliferation, while 0.1C-P68 promoted the better mesenchymal cell proliferation, both effects being statistically significant (Figure 4-3). Matriderm and Integra were used as controls as they are existing gold standard dermal skin substitutes for single-stage and two-stage reconstruction for burns and chronic wounds respectively.

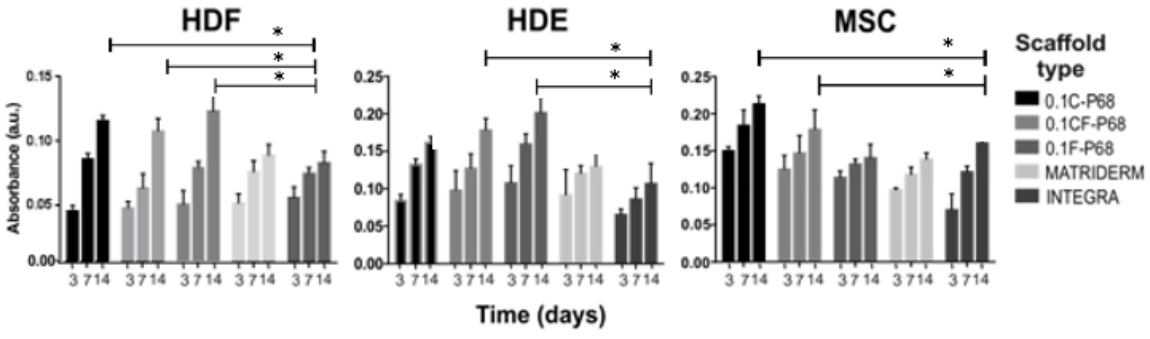


*Figure 4-3 Cell proliferation outcome comparing EmDerms and controls (Matriderm and Integra). HDFs in EmDerms proliferated at a higher rate compared to Matriderm and Integra. HDEs proliferated significantly better in EmDerm-CF and EmDerm-F. Meanwhile, MSCs in EmDerm-C and EmDerm-CF had higher proliferation rates compared to the other scaffolds. * denotes p-value of <0.05. (mean ± SD, n=3)*

Wide-field microscope imaging of seeded scaffolds

Based on the Z-stacks obtained, each cell type was found to infiltrate into the scaffold uniformly over the XY plane and Z plane (Figure 4-4). Due to limitations in light penetration, cells were only imaged up to a depth of about 100 microns. In particular, cell infiltration into collagen scaffolds was observed to a similar extent as for fibrin-containing scaffolds, suggestive of effect of the preserved fibre nanostructure in these scaffolds. Interestingly, the endothelial cells seemed to form ring-like structures when seeded onto EmDerm scaffolds, most notably with EmDerm-CF and EmDerm-F (arrows in Figure 4-4, HDE panels). It is also notable that HDE ingress into the EmDerm C scaffolds, and although show less cytoskeletal spreading, demonstrate some association into annular structures. By contrast, the stromal cell types adopt an elongated spindle-like morphology when seeded on to EmDerm scaffolds, more pronounced with fibroblasts than mesenchymal stem cells (Figure 4-4).

Overall, EmDerm scaffolds demonstrate excellent cell penetrance, or conductivity, for different cell types (Figure 4-4). The present results contrast with previous studies which have shown that collagen as a scaffold material does not support complete cell conductivity, despite a high degree of interconnected porosity. (159,160) Thus, creating a nanostructured form of collagen may significantly

increase the cell migratory behaviour to penetrate the scaffold. This could translate to accelerated integration of collagen scaffolds in wound healing settings. The generally greater cell proliferation and migration in the nanostructured EmDerm scaffold may be due to increase in surface area available for cells to attach and move on, as well as greater permeability to nutrients and oxygen throughout the scaffold. (144)

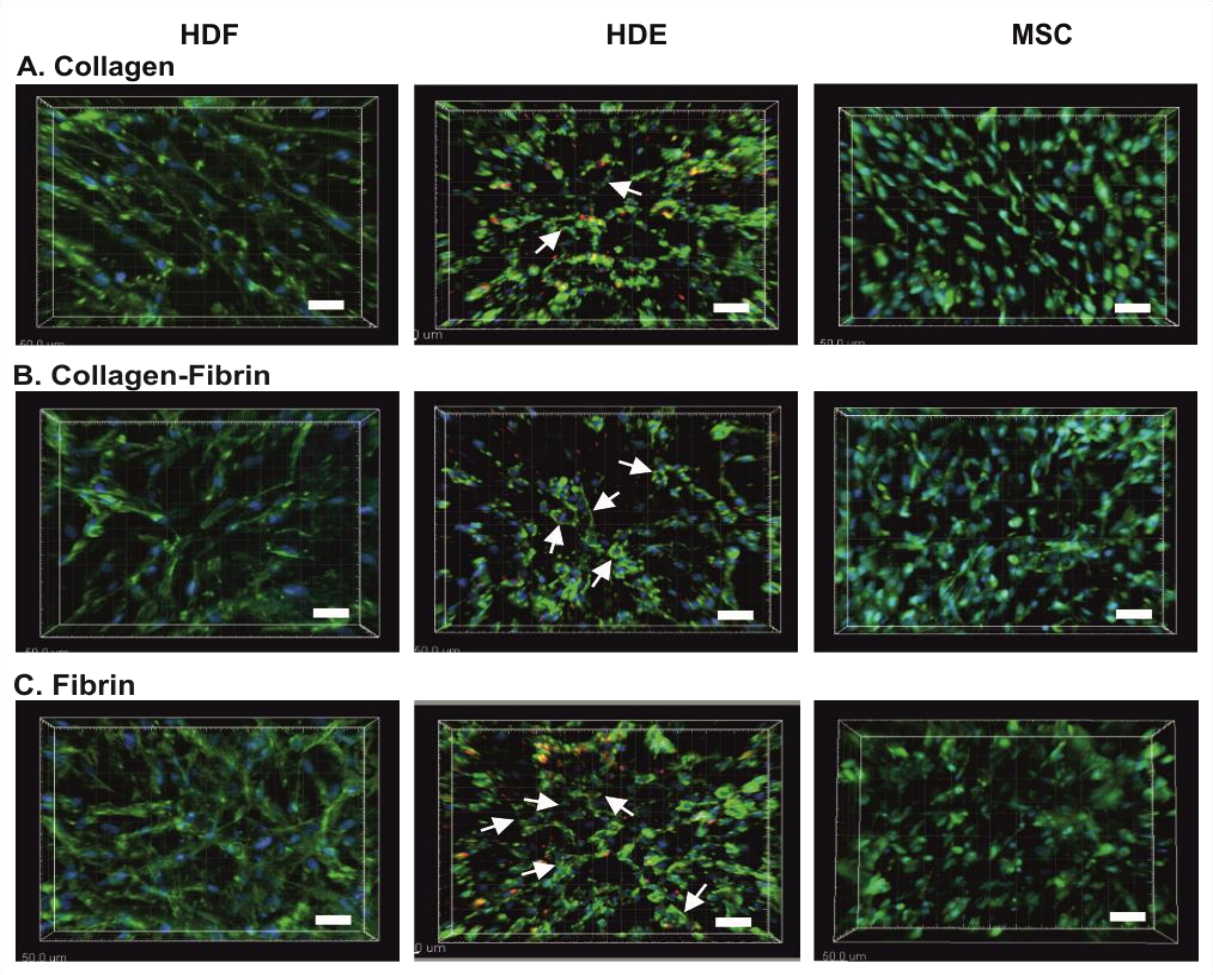


Figure 4-4 Widefield microscopy of HDF, HDE and MSC seeded on EmDerm scaffolds at 20x magnification. Arrows showing annular structures in EmDerm scaffolds cultures with HDEs. (scale bar = 50 µm, n=3)

In summary, the feasibility of using emulsion templating as a novel method of creating microporous nanofibrous protein scaffolds which are unique and easily tuned according to wound healing and tissue regeneration need was demonstrated. This is a versatile method of templating various protein polymers, including collagen and fibrin. These EmDerm scaffolds also have excellent biocompatibility and is able to support various types of cell growth and have excellent potential as dermal or soft tissue substitutes.

Overall, nanostructured EmDerm scaffolds show differential morphological responses of different cell types which form connective tissues. The differential effects of each scaffold material on proliferation and cell morphology suggests that composition may have some cell type specific benefit. In particular, the greater proliferation of endothelial cells in collagen-fibrin and fibrin scaffolds than collagen scaffolds is associated with the formation of annular nascent vascular structures. This behaviour, associated with the endothelial interaction with organised fibrin structures, is consistent with other angiogenic properties of fibrin. (159,161-163) However, the migratory and morphological response of endothelial cells to the nano-structured collagen scaffolds suggests that the nano-structure increases its angiogenic potential. Further examination of the cellular morphological and cell-communication responses will extend our understanding of the role of scaffold nanostructure in influencing cellular behaviour (164) and particularly angiogenesis and vasculogenesis.

4.3.2. Co-culture of Cells on EmDerm Scaffolds

Cell Proliferation Assay

Cell Proliferation of co-cultures (HEK/HDF, HDF/HDE and MSC/HDE) were measured using the CCK-8 assay. In the HEK/HDF co-culture, EmDerm-C had similar rates of cell proliferation to Integra and Matriderm. This is rather unsurprising as all three are made up of collagen scaffolds. EmDerm-F was partially degraded by Day 3 and completely degraded by Day 7. EmDerm-CF had significantly lower cell proliferation compared to the controls - Matriderm and Integra on Day 3. In the HDF/HDE and MSC/HDE co-culture, all the EmDerm scaffolds had comparable rates of cell proliferation compared to both Integra and Matriderm controls. This was consistent from Day 3 to Day 14 of the co-culture experiment.

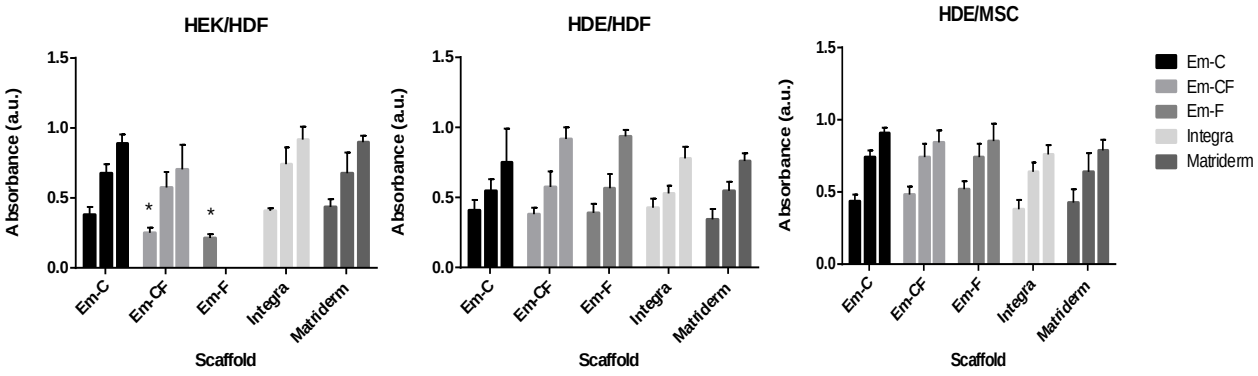


Figure 4-5 Cell proliferation outcome of co-cultures comparing EmDerm and controls. HEK/HDF in EmDerm-CF and EmDerm-F had significantly lower cell proliferation rate compared to other scaffolds on Day 3 ($p<0.05$). (mean ± SD, n=3)

Fluorescence Imaging

A) *EmDerm-C*

Co-culture of HDF and HDE

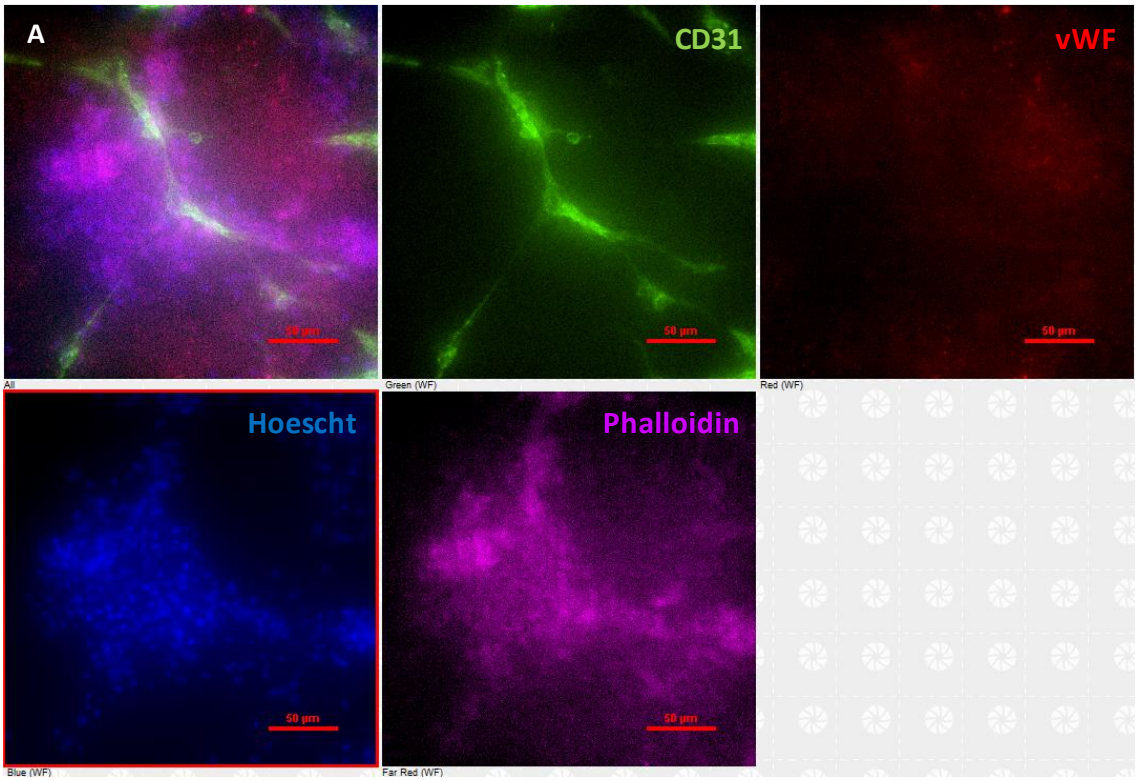
There was good cell growth of both cell types. There were more fibroblasts present compared to endothelial cells due to the faster rate of growth of fibroblasts. The fibroblasts and endothelial cells also appear to grow in clusters with the endothelial cells forming pseudo-tubular structures and networks while the fibroblasts appear to grow around the endothelial cells. (Figure 4-6)

Co-culture of MSC and HDE

Both cell types proliferated well on the scaffolds. However, there were more MSCs compared to endothelial cells as they tend to grow faster and are less fastidious. The endothelial cells did not appear to express or secrete vWF significantly and were proliferating in a disorganized manner. There was no clear formation of nascent vascular structures noted, as seen in the HDF/HDE co-culture. (Figure 4-6)

Co-culture of HEK and HDF

There is good proliferation of HDF and HEK. HEK cells had flattened, stretched out morphology and mostly grew on the surface of the scaffold, while HDF cells migrated into the scaffold and had a more elongated morphology. (Figure 4-6)



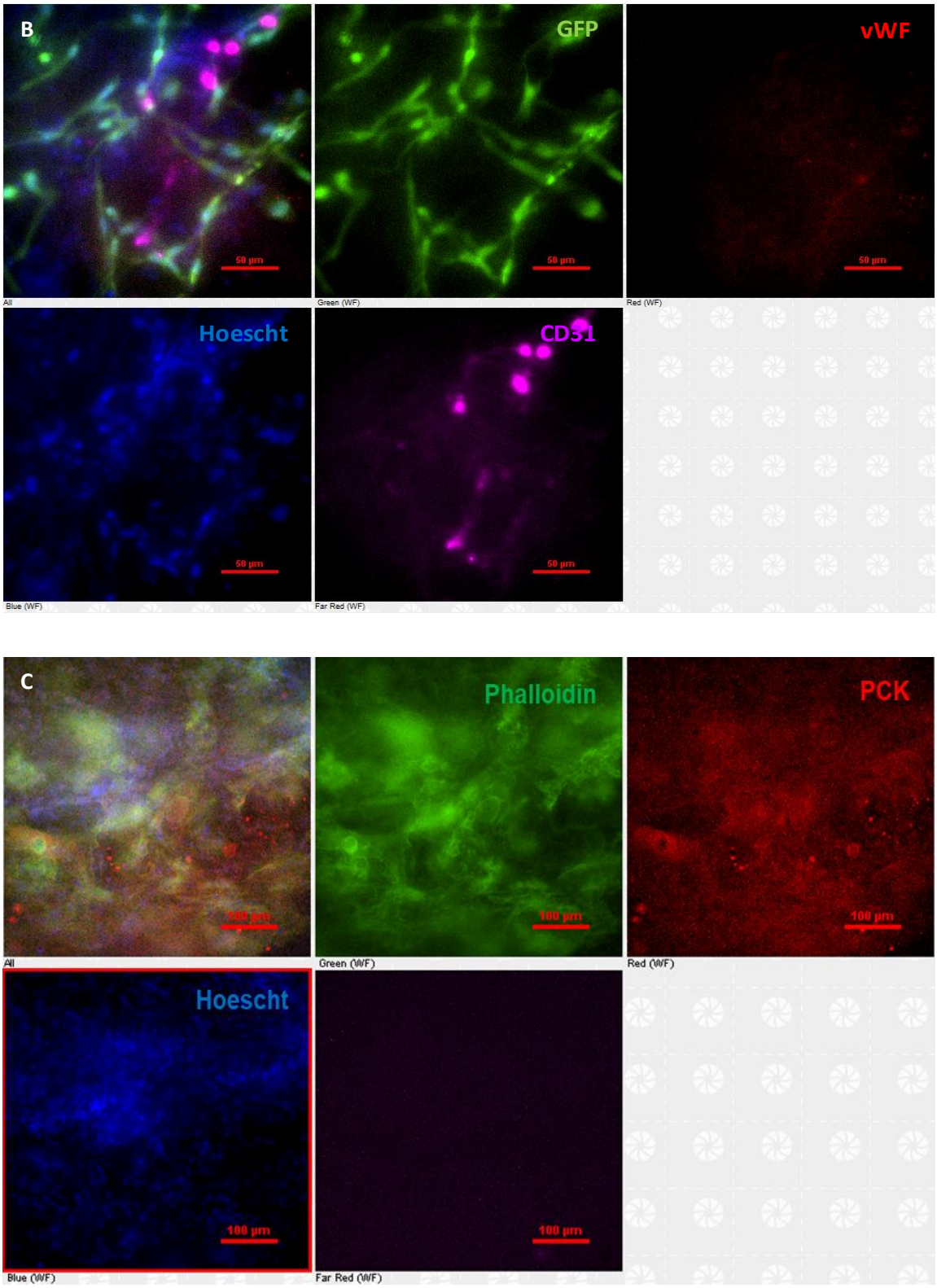


Figure 4-6 Co-culture of cells on EmDerm-C scaffolds. (A) HDF/HDE – HDEs appear to form vascular networks with HDFs growing around these vessel-like structures. (B) MSC/HDE – MSCs retained their elongated morphology while the HDEs are interspersed between MSCs. (C) HEK/HDF - HEK grew in a sheet-like manner with HDFs scattered in between. (n=3)

B) EmDerm-CF

Co-culture of HDF and HDE

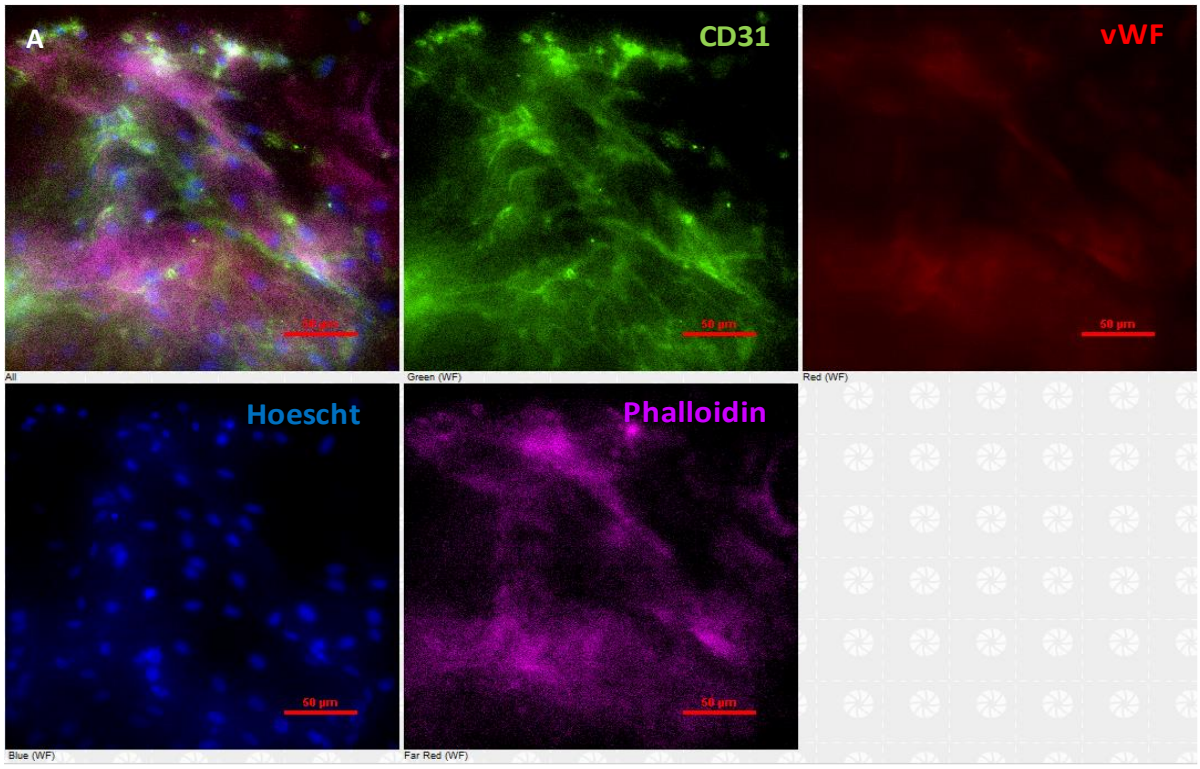
The fibroblasts and endothelial cells grew in clusters with both the fibroblasts growing around the networks formed by the endothelial cells. They also appear to grow around pore structures of the scaffold. (Figure 4-7)

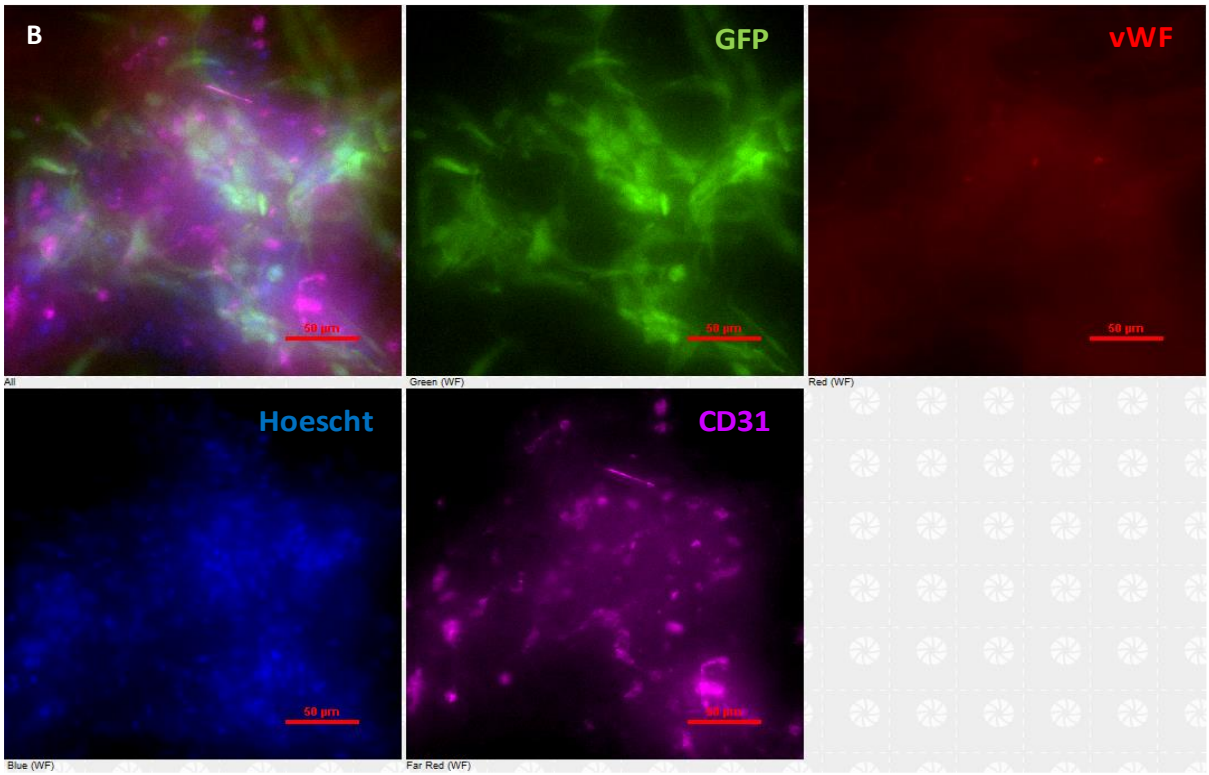
Co-culture of MSC and HDE

The MSC and endothelial cells grew around each other and adhered to the walls of the pores of the scaffolds. The MSCs retained their spindle like morphology. There was minimal production of vWF intracellularly and extracellularly. (Figure 4-7)

Co-culture of HEK and HDF

There was good proliferation of both cell types. HEK cells grew in sheet-like layer while HDF cells grew in clusters. (Figure 4-7)


A
CD31
vWF
All
Green (WF)
Red (WF)
Hoescht
Phalloidin
Blue (WF)
Far Red (WF)


B
GFP
vWF
All
Green (WF)
Red (WF)
Hoescht
CD31
Blue (WF)
Far Red (WF)

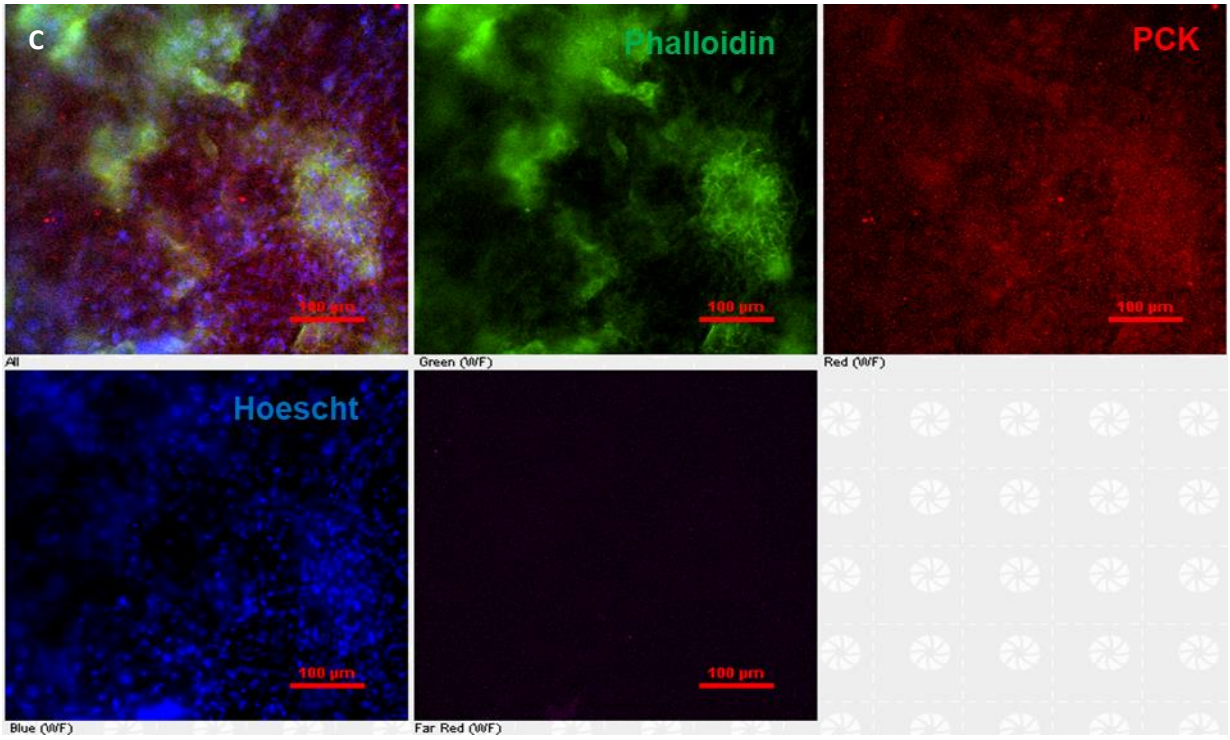


Figure 4-7 Co-culture of cells on EmDerm-CF scaffolds. (A) HDF/HDE - HDEs.and HDFs appear to grow in an inter-dispersed manner around each other. (B) MSC/HDE – MSCs retain their elongated morphology and HDEs were scattered around the scaffold. (C) HEK/HDF – HEKs grew in sheets while HDFs grew in clusters. (n=3)

C) EmDerm-F

Co-culture of HDF and HDE

There was formation of vascular networks of endothelial cells with fibroblasts clustering around the endothelial cells. The cells also appear to grow around the pores of the scaffold. There was minimal expression of vWF. Also, vWF does not appear to coincide with CD31 which may be due to secretion of vWF from the endothelial cells, rather than being retained in Weibel-Palade bodies intracellularly. (Figure 4-8)

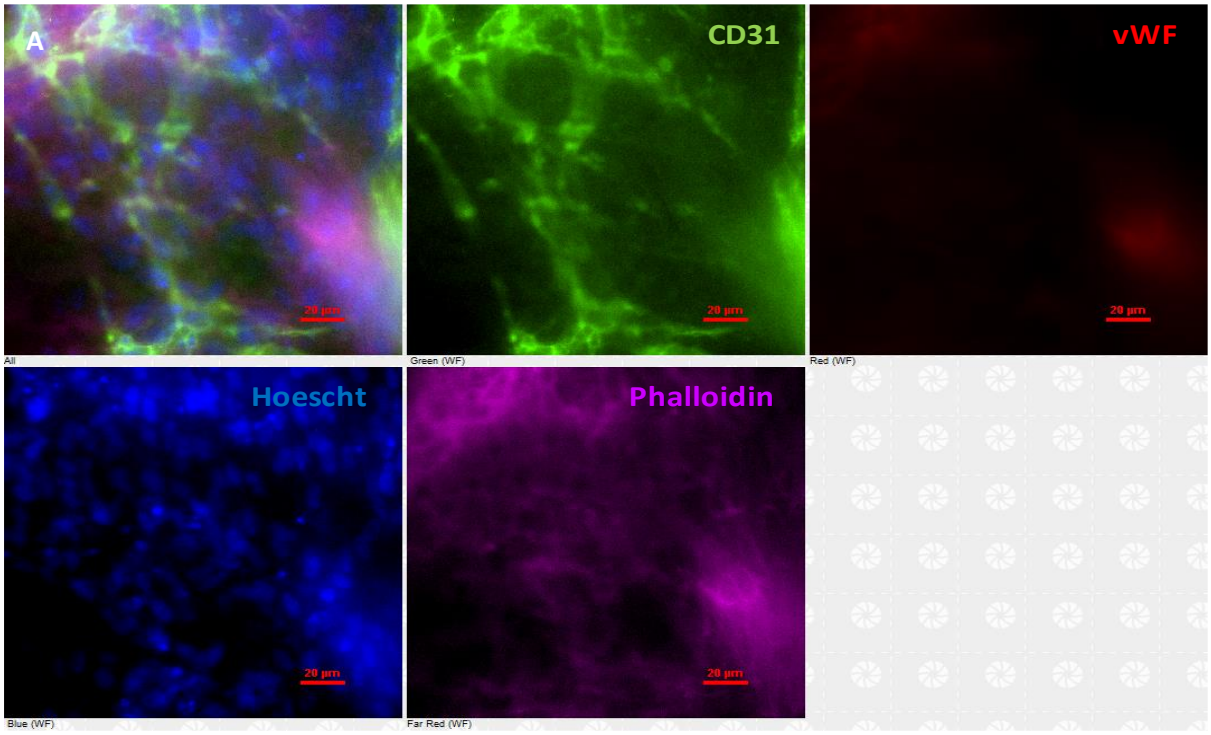
Co-culture of MSC and HDE

There was good cell growth of both cells. However, the MSCs were much more abundant and grew around scaffold surfaces, while the endothelial were interdispersed between MSCs. There was minimal

expression of vWF. Again, vWF does not appear to co-localize with CD31 despite both being endothelial cell markers, as it is likely to have been secreted. (Figure 4-8)

Co-culture of HEK and HDF

EmDerm-F scaffolds seeded with HEK and HDF were completely degraded after Day 3. Therefore, no images were obtained. (Figure 4-8)



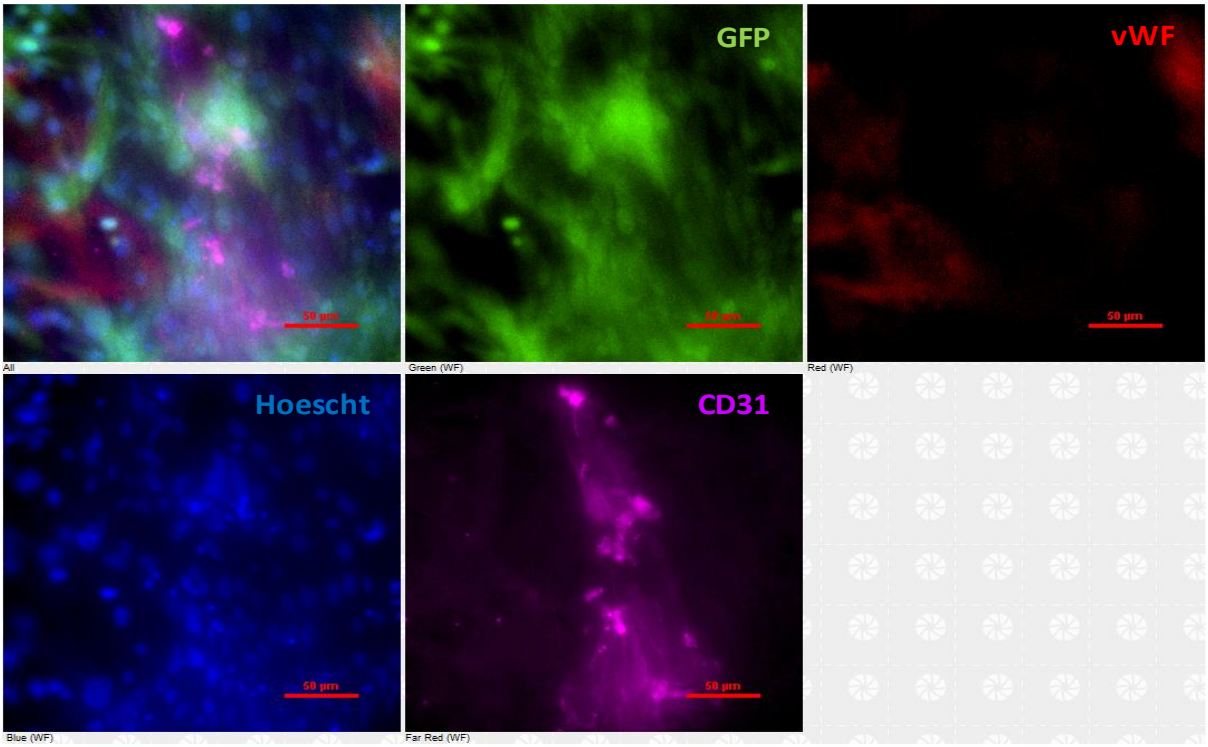


Figure 4-8 Co-culture of cells on EmDerm-F scaffolds. (A) HDF/HDE – HDEs grew in a network-like manner with HDFs growing in between. (B) MSC/HDE – MSCs retained their elongated morphology with HDEs scattered amongst the MSCs. (n=3)

D) Integra

Co-culture of HDF and HDE

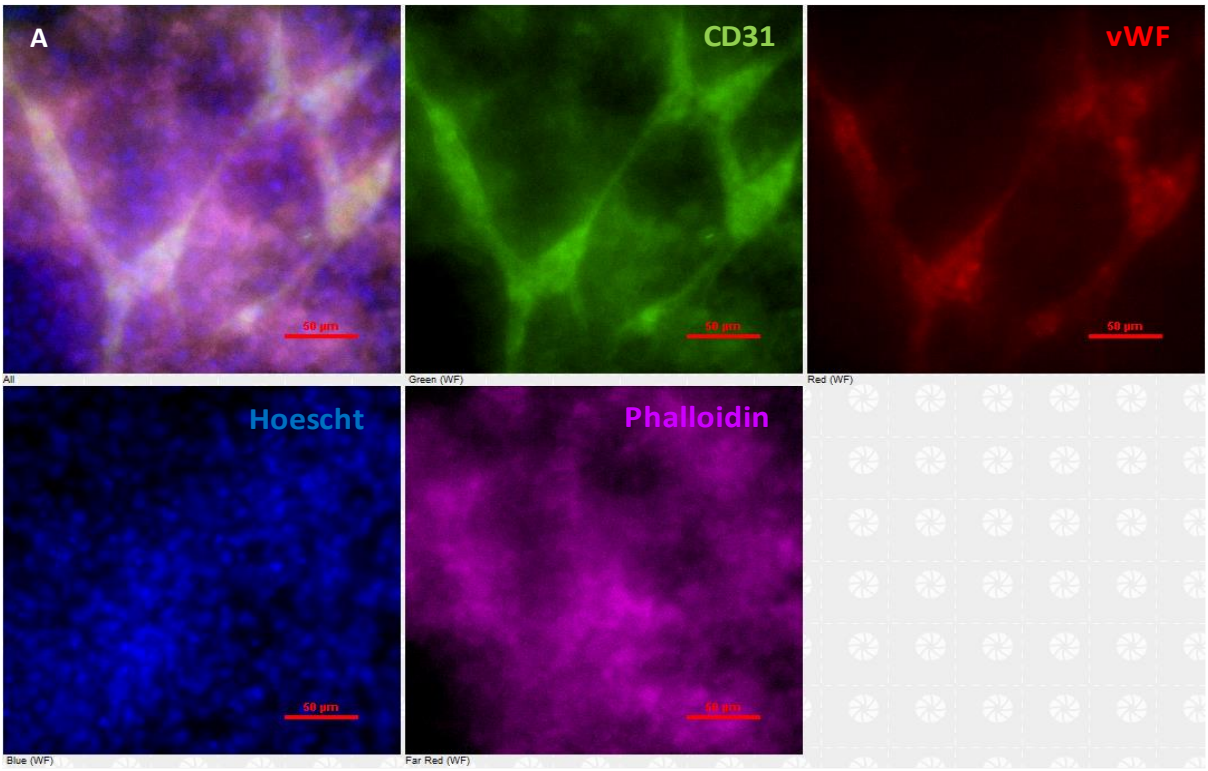
The fibroblasts grew in sheets with the endothelial cells forming network-like structures in between. There was a much higher cell proliferation of fibroblasts as compared to endothelial cells. There was significant production of intracellular vWF as seen in the red channel within the endothelial cells as well. (Figure 4-9)

Co-culture of MSC and HDE

There was a very high proliferation of MSCs with minimal organization. MSCs appeared to grow in clumps, with loss of their spindle-like morphology. The endothelial cells appear to also grow interspersed amongst the MSCs with no formation of vascular networks. There is also minimal expression of vWF intracellularly or extracellularly. (Figure 4-9)

Co-culture of HEK and HDF

There is extensive growth of both HEK and HDF in a sheet-like manner. Due to the high rate of proliferation of cells, there was overcrowding of cells and it is difficult to distinguish HEK from HDFs as HEK cells do not adopt the polygonal spread out morphology as in EmDerm-C and EmDerm-CF scaffolds. (Figure 4-9)



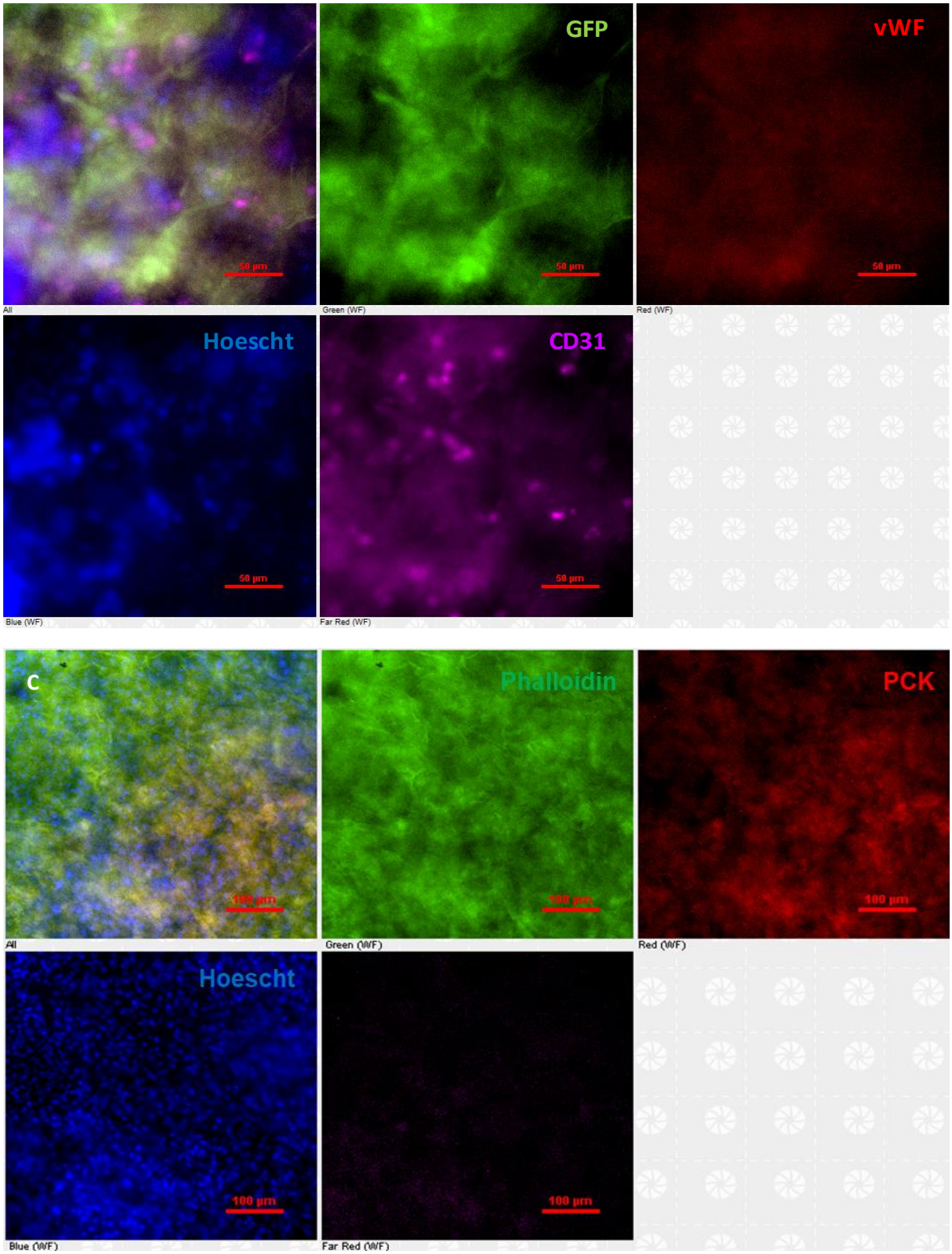


Figure 4-9 Co-culture of cells on Integra scaffolds. (A) HDF/HDE co-culture – HDFs grew in sheets with HDEs forming network-like structures. (B) MSC/HDE – MSCs grew in clusters with HDEs interspersed in between. (C) HEK/HDF - HEK and HDFs grew in a sheet-like manner. (n=3)

E) Matriderm

Co-culture of HDF and HDE

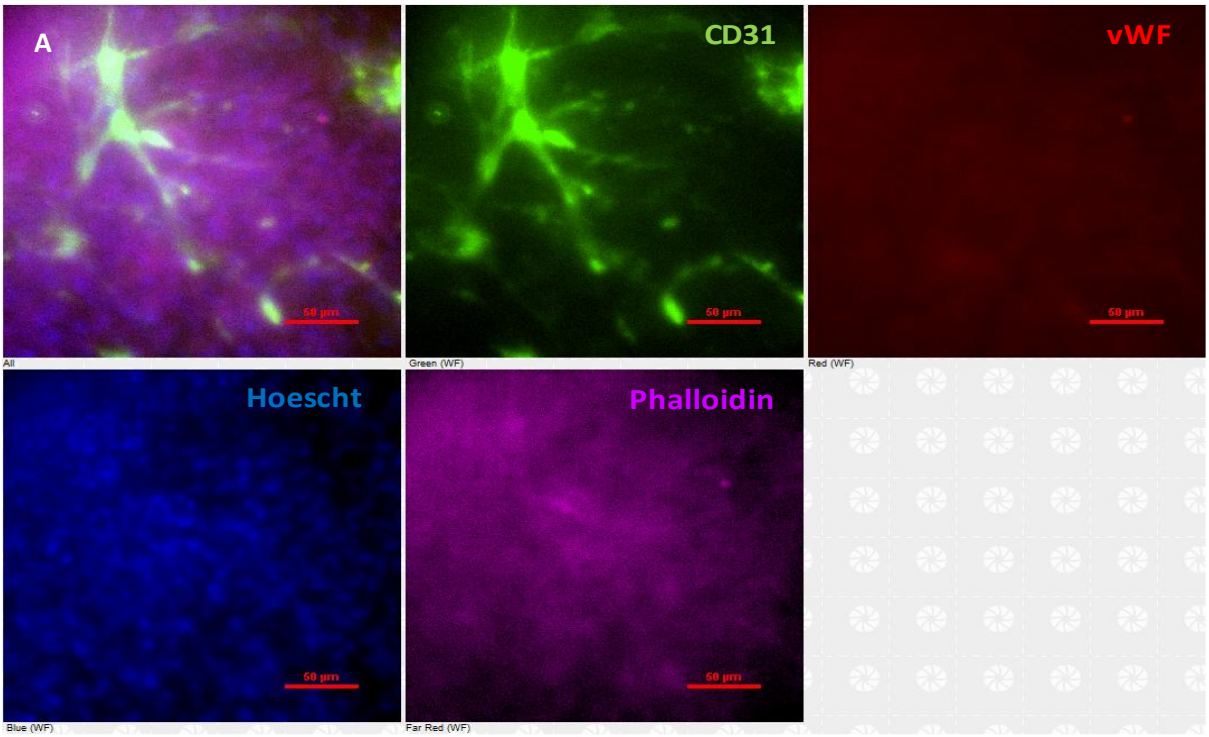
There was significant growth of fibroblasts throughout the scaffold, with endothelial cells forming network like structures within the scaffold itself. There was minimal expression of vWF as well, intracellularly and extracellularly. (Figure 4-10)

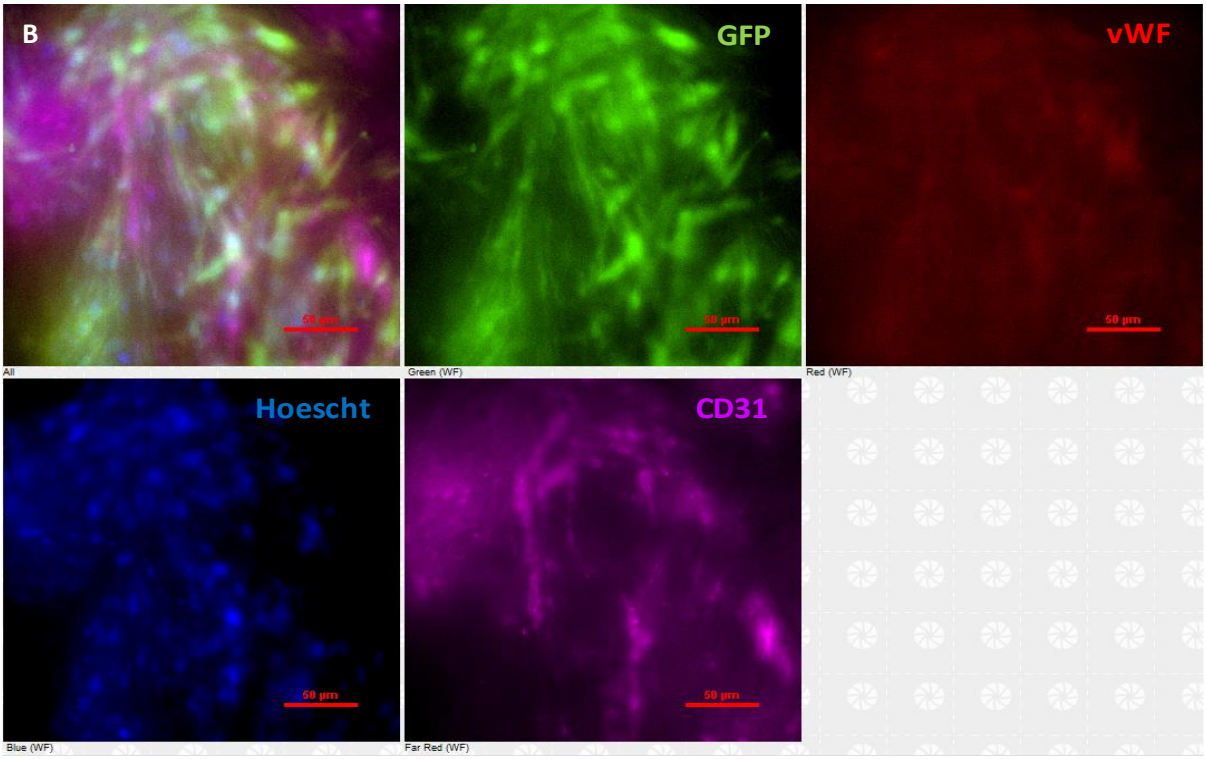
Co-culture of MSC and HDE

There was good cell growth of both MSC and endothelial cells. However, they tend to grow in clusters around each other. There was minimal production of vWF as well. There was no clear vascular network pattern of endothelial cell growth. (Figure 4-10)

Co-culture of HEK and HDF

There is extensive growth of both HEK and HDF in a sheet-like manner. However, it is difficult to distinguish HEK from HDFs as HEK cells do not adopt the characteristic flattened-out morphology typical of differentiated keratinocytes. (Figure 4-10)


A
CD31
vWF
50 µm
All
Green (WF)
Red (WF)
Hoescht
Phalloidin
Blue (WF)
Far Red (WF)


B
GFP
vWF
50 µm
All
Green (WF)
Red (WF)
Hoescht
CD31
Blue (WF)
Far Red (WF)

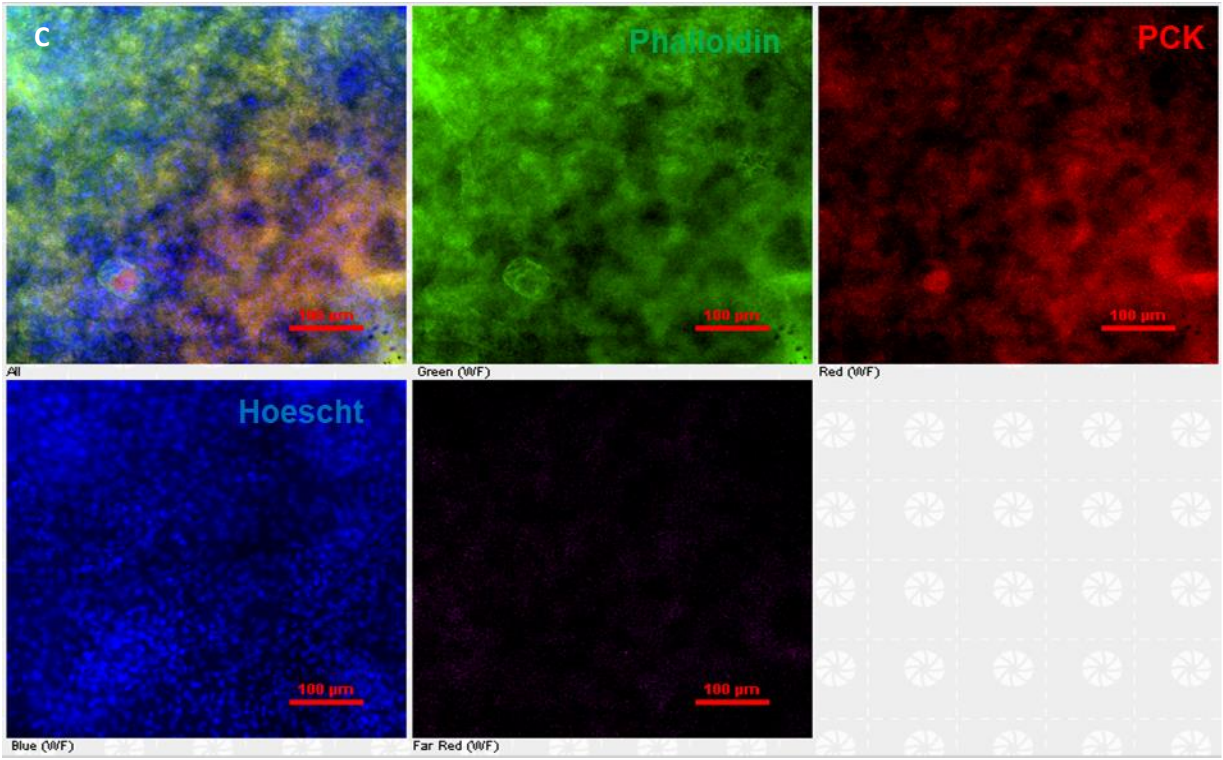


Figure 4-10 Co-culture of cells on Matriderm. (A) HDF/HDE – HDFs grew in a sheet-like manner while HDEs formed vessel-like structures. (B) MSC/HDE – MSCs grew in a haphazard manner with HDEs scattered in between. (C) HEK/HDF – HEKs and HDFs grew in a sheet-like manner. (n=3)

Scanning Electron Microscopy Imaging

The HEK cells adopted a very flattened, spread-out morphology when seeded onto scaffolds which is a key characteristic of keratinocytes, indicating good cellular attachment. The cells were also found to grow over each other in a stratified manner. (Figure 4-11)

Interestingly, the keratinocytes appear to degrade the EmDerm-F scaffolds completely by Day 7, which suggests that fibrin-based EmDerm scaffolds were less suitable to create a bilayer skin construct as compared to collagen-based scaffolds.

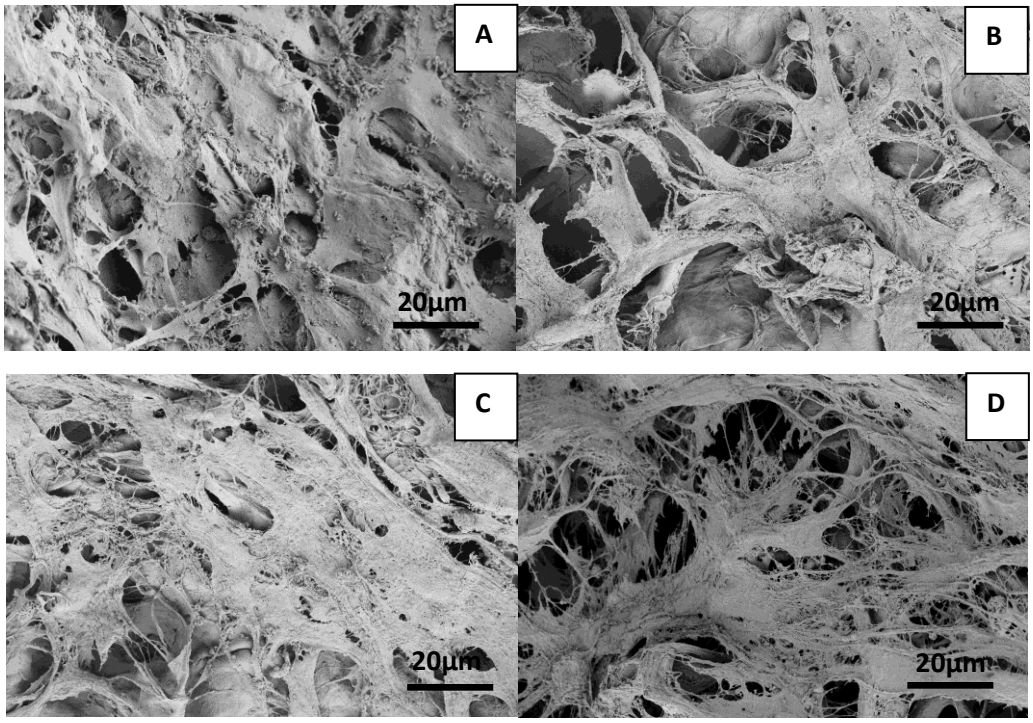


Figure 4-11 Keratinocytes seeded on EmDerm-C in Transwell plates lifted at air-liquid interface after 14 days of culture (A), EmDerm-CF (B), Integra (C) and Matriderm (D) showing a flattened, stretched out morphology and partial stratification. (scale bar = 20µm, n=3)

The aim of this study was to evaluate the possibility of using EmDerm scaffolds as a co-culture platform for creating a skin bilayer made up of an upper layer of keratinocytes and a lower layer of fibroblasts. The second objective of this study was to evaluate the behaviour of endothelial cells when co-cultured with either mesenchymal stem cells or human dermal fibroblasts to evaluate the potential for using EmDerm scaffolds as a pro-angiogenic dermal substitute.

In this study, cell proliferation of co-cultured HEK and HDF in EmDerm-C is shown to be comparable to Integra and Matriderm. This may be due to the fact that these scaffolds are all made up of collagen material which is favourable for growth of keratinocytes and fibroblasts. HEK/HDF growth was slower in EmDerm-CF scaffolds compared to commercial scaffolds – Integra and Matriderm on Day 3 but improved between Day 7 to Day 14. Meanwhile, EmDerm-F scaffolds were noted to be partially degraded by Day 3 of HEK/HDF co-culture. This is likely due to release of fibrinolytic degradative enzymes by keratinocytes. (165)

All EmDerm scaffolds co-cultured with HDF/HDE and MSC/HDE had similar rates of cell proliferation with Integra and Matriderm. This result is rather surprising as EmDerm-CF and EmDerm-F had better cell proliferation compared to controls when seeded with only HDEs and EmDerm-C had greater cell proliferation compared to controls when seeded with only MSCs. This may be due to unequal rates of growth of both cell types in a co-culture environment which results in compensation of slower growth of one cell type by faster growth of another cell type e.g. HDF growing faster than HDE.

Interestingly, EmDerm-C scaffolds seeded with HDE and HDF appear to form nascent networks of vascular structures with HDFs growing around these tubular networks. This was also seen in EmDerm-CF and EmDerm-F but in a less organized fashion. It is unclear why this occurs. More generally, cells seeded onto each scaffold had different morphological patterns when co-cultured. This may be due changes in the proteome and secretome of cells seeded onto emulsion templated scaffolds, resulting in changes in expression of various growth factors. This is investigated in further detail in the next section.

The penetration of cells appear to be better on EmDerm scaffolds compared to Integra and Matriderm. Although there is excellent cell proliferation in both Integra and Matriderm, cells seeded appear to proliferate and spread on the surface of the scaffolds. Meanwhile, cells on EmDerm scaffolds appear to migrate better into the scaffolds, rather than growing along the scaffold surface. The improvement in depth of cell penetration may be due to micro- and nano-structure of EmDerm scaffolds which allows better diffusion of oxygen and nutrients into the scaffold.

Stratification of keratinocytes when cultured at air-liquid interface is also observed in EmDerm-C and EmDerm-CF scaffolds. There is good cellular attachment and proliferation of keratinocytes. Based on previous research, co-culture of HEKs with HDFs provides biochemical cues to induce keratinocyte proliferation, migration and stratification of keratinocytes, as well as scaffold remodelling. (166)

In summary, EmDerm scaffolds have been shown to be effective as dermal skin substitutes, supporting growth of fibroblasts, keratinocytes and endothelial cells. They also promote the vascularization process by stimulating organization of endothelial cells into nascent vascular networks. The scaffolds also can be used as an epidermal-dermal bilayer skin substitute as they support growth of keratinocytes and fibroblasts, as well as stratification of keratinocytes when grown at air-liquid interface. This may be useful for single stage reconstruction of burns and chronic wounds as both the dermal and epidermal layers can be applied simultaneously.

4.3.3. Analysis of Proteome and Secretome of Cellularized EmDerm Scaffolds

In the earlier section, the EmDerm scaffolds were shown to be highly biocompatible with excellent cell growth and ingress. Co-culture of fibroblasts and endothelial cells were also shown to induce formation of vascular-like tubules in EmDerm scaffolds. This effect is less pronounced in conventional Integra or Matriderm scaffolds. Cell morphology and behaviour were also notably different between scaffold types. This may be due to the interaction of cells with scaffold material and structure. Therefore, the secretion and production of a panel of growth factors and degradative enzymes were quantified using a magnetic multiplex assay (Luminex) to investigate these findings. The results from the assay are broadly categorized into monoculture and co-culture analysis and further subdivided by cell type.

Monoculture analysis

HEK Supernatant

Degradation of scaffolds are affected by activity of matrix metalloproteinase and tissue inhibitor of metalloproteinase such as MMP1, MMP2 and TIMP1. In scaffolds seeded with HEK, secretion of MMP1 and TIMP1 was highest for Integra scaffolds compared to EmDerm scaffolds. (Figure 4-12) This was followed by EmDerm-C scaffolds. However, there was no net change in amount of collagen type I and collagen type IV produced, indicating a higher rate of remodelling of Integra scaffolds compared to EmDerm scaffolds. (Figure 4-12)

Vasculogenesis is a key process which determines rate of integration of scaffolds in wounds. This is dependent on secretion of several growth factors such as VEGF, FGF, HGF, ang-1, fibronectin and IL-8. In Figure 4-12, there is no difference in production of VEGF-A, ang-1 and HGF between the different scaffolds indicating that other growth factors influence this process to a greater extent. In particular, concentration of IL-8 a known chemokine affecting vascularization is highest for Integra scaffolds followed by EmDerm-C, EmDerm-CF and EmDerm-F respectively. FGF-B secretion is highest in both Integra and EmDerm-C, compared to EmDerm-CF and EmDerm-F. Interestingly, fibronectin secretion is detected in EmDerm-CF but not in other scaffolds. (Figure 4-12)

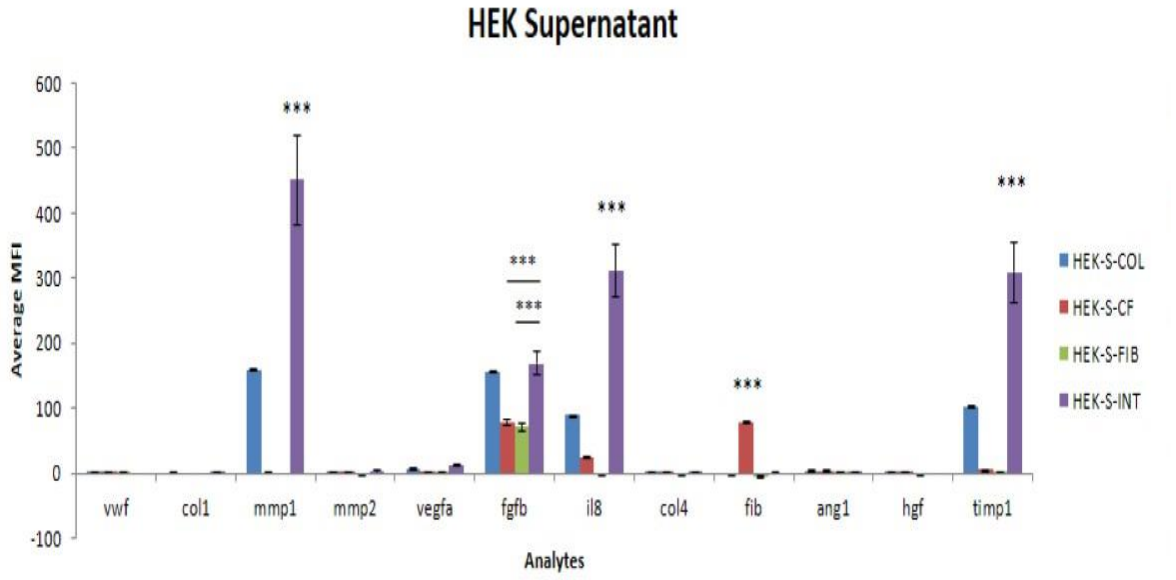


*Figure 4-12 Secretome profile of HEK monoculture on scaffolds. Keratinocytes seeded on Integra secreted higher amounts ECM remodelling proteins and vascular growth factors e.g. MMP1, FGF-B, IL-8 and TIMP-1. * denotes a p–value of <0.05, ** denotes a p–value of <0.01 and *** denotes a p-value of <0.001 (mean ± SD, n=2)*

HEK Lysate

MMP1 and TIMP1 synthesis was highest in Integra compared to EmDerm scaffolds. However, there was no change in production of collagen type I, collagen type IV and MMP2 between the different types of scaffolds. These findings are largely similar to the results from the cell supernatant as shown above, indicating a correlation between the protein production and secretion of HEK cells seeded on scaffolds. (Figure 4-13)

In terms of vasculogenic growth factors, VEGF-A, FGF-B and IL-8 synthesis was highest in Integra compared to EmDerm scaffolds. There was no significant difference in production of fibronectin, HGF and ang-1 between the different scaffolds. These results are again similar to the secretome profile of keratinocytes seeded on these scaffolds. (Figure 4-13)

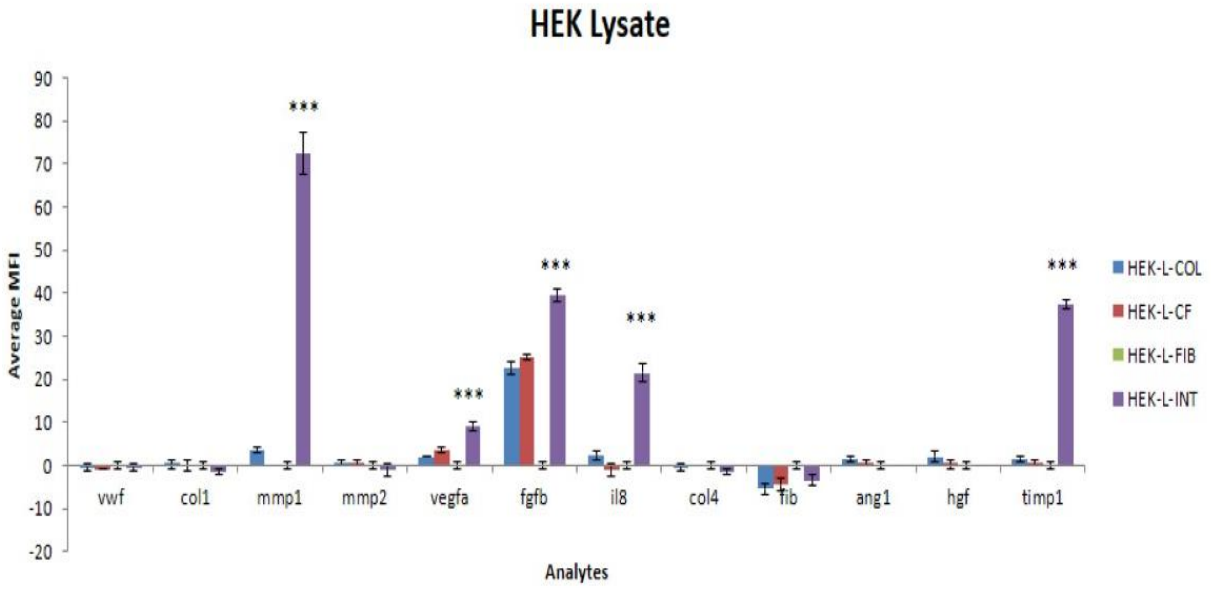


*Figure 4-13 Proteome profile of HEK monoculture on scaffolds. Keratinocytes seeded on Integra scaffolds produced higher amounts of ECM remodelling proteins and vasculogenic factors e.g. MMP1, FGF-B, IL-8 and TIMP-1. * denotes a p–value of <0.05, ** denotes a p–value of <0.01 and *** denotes a p-value of <0.001 (mean ± SD, n=2)*

HDF Supernatant

The secretion of collagen type I was significantly higher for HDFs seeded on Integra compared to other scaffolds. MMP1 and MMP2 secretion were lowest in EmDerm-CF. MMP1 secretion was not significantly different between EmDerm-C, EmDerm-F and Integra while MMP2 secretion was highest in EmDerm-F and Integra. TIMP1 secretion were also similar across the different scaffolds. Meanwhile, there is no difference in the secretion of collagen 4 between the different scaffolds. (Figure 4-14)

IL-8, fibronectin and HGF secretion was highest in Integra scaffolds. There were no significant differences in VEGF-A, FGF-B and ang-1 secretion across the different scaffolds. This indicates that different growth factors, in particular IL-8, fibronectin and HGF affect growth of HDFs in scaffolds such as Integra. (Figure 4-14)

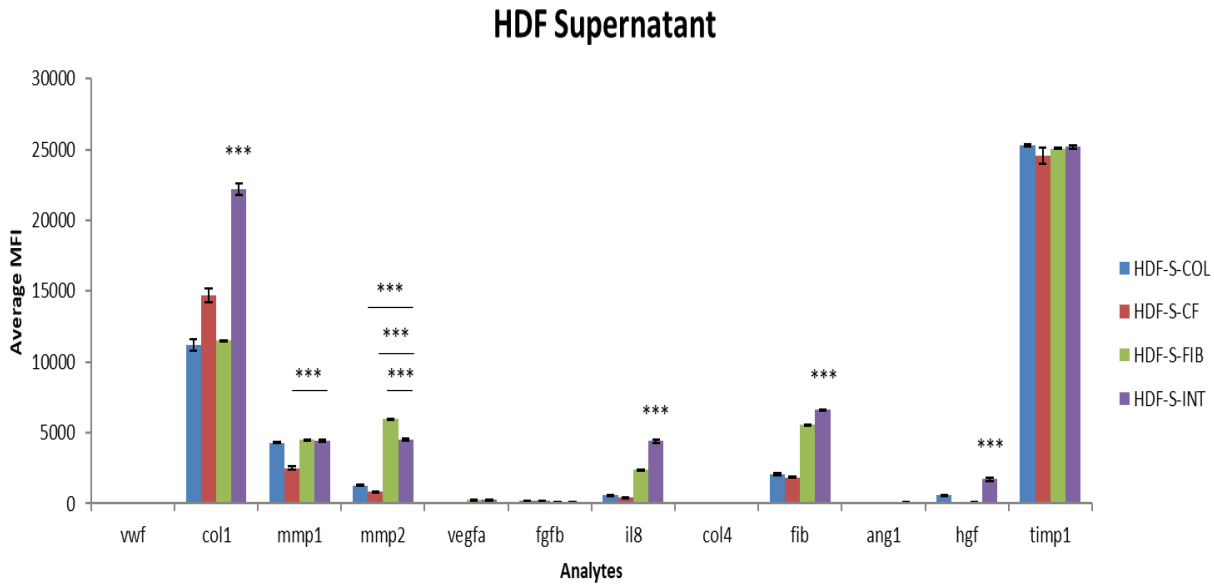


*Figure 4-14 Secretome profile of HDF monoculture on scaffolds. Fibroblasts seeded on Integra scaffolds secreted higher amounts of collagen and vasculogenic factors e.g. IL-8 and fibronectin compared to EmDerm scaffolds. * denotes a p–value of <0.05, ** denotes a p–value of <0.01 and *** denotes a p-value of <0.001 (mean ± SD, n=2)*

HDF Lysate

Collagen type I production was highest in EmDerm-F, followed by Integra. MMP1, MMP2 and TIMP1 synthesis was also highest in the fibrin scaffold, compared to other scaffolds. There was no difference in collagen type IV synthesis across the different types of scaffolds. (Figure 4-15)

FGF-B and HGF protein synthesis was highest in Integra compared to other scaffolds while IL-8 and fibronectin production was highest in EmDerm-F scaffolds. There was no significant difference in VEGF-A or ang-1 production across the different scaffolds. (Figure 4-15)

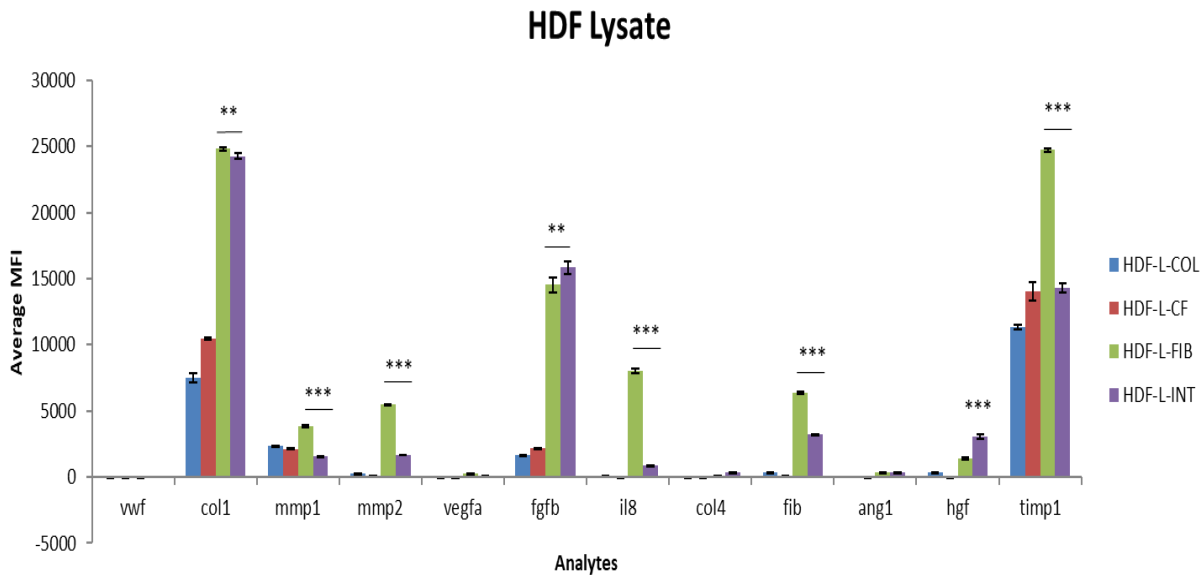


*Figure 4-15 Proteome profile of HDF monoculture on scaffolds. HDF seeded on EmDerm-F scaffolds produced higher amounds of collagen and ECM remodelling proteins e.g. MMP1, MMP2 and TIMP-1 as well as vasculogenic proteins e.g. IL-8 and fibronectin. * denotes a p–value of <0.05, ** denotes a p–value of <0.01 and *** denotes a p-value of <0.001 (mean ± SD, n=2)*

HDE Supernatant

Collagen type I and TIMP1 secretion was highest in Integra compared to other scaffolds, suggesting that breakdown of collagen for Integra scaffolds was reduced. MMP2 secretion was highest in EmDerm-F compared to other scaffolds. MMP1 secretion was unchanged across all scaffolds. There was no significant difference in collagen type IV secretion across all scaffolds. (Figure 4-16)

VEGF-A secretion was highest in EmDerm-CF scaffolds while FGF-B secretion was highest in EmDerm-C scaffolds. IL-8 secretion was highest in Integra while fibronectin secretion was highest in EmDerm-F. These results suggest that there is an effect of scaffold environment on the secretion of growth factors of HDE cells, as each scaffold resulted in greater secretion of a different type of vasculogenic factor. (Figure 4-16)

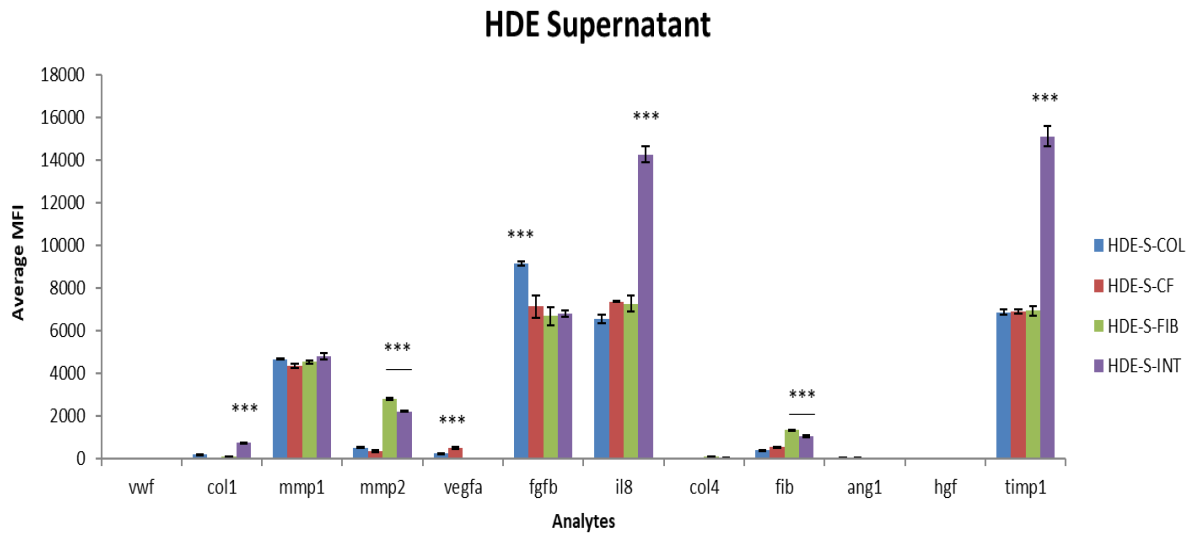


*Figure 4-16 Secretome profile of HDE monoculture on scaffolds. Endothelial cells seeded on Integra secreted the highest amount of collagen, IL-8 and TIMP-1. Endothelial cells seeded on EmDerm-C secreted the highest amount of FGF-B, while endothelial cells seeded on EmDerm-F secreted highest amount of fibronectin and endothelial cells on EmDerm-CF secreted highest amount of VEGF. * denotes a p–value of <0.05, ** denotes a p–value of <0.01 and *** denotes a p-value of <0.001 (mean ± SD, n=2)*

HDE Lysate

Collagen type I, collagen type IV, MMP1, MMP2 and TIMP1 secretion was highest in EmDerm-C scaffolds. This indicates that collagen production and remodelling is greatest in EmDerm-C scaffolds compared to other scaffolds. (Figure 4-17)

FGF-B, IL-8 and fibronectin protein synthesis were also highest in EmDerm-C scaffolds compared to other scaffolds. There was no significant difference in production of VEGF-A, ang-1 and HGF across the various scaffolds. These results suggest that the increased amount of growth factors resulted in greater cell proliferation and thus remodelling of the scaffold. (Figure 4-17)

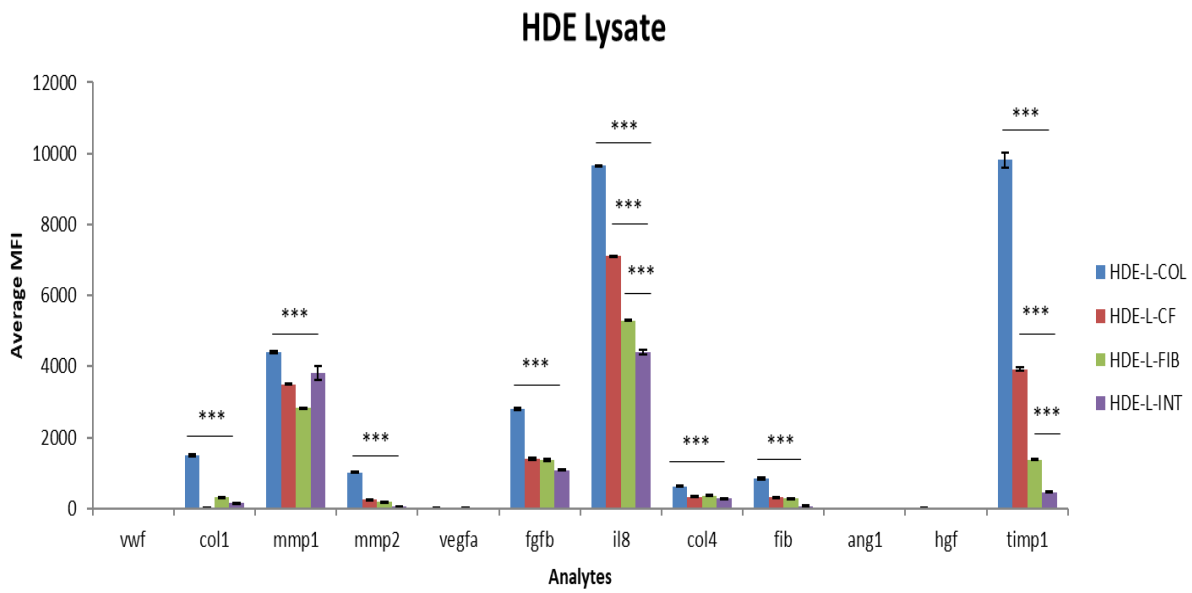


*Figure 4-17 Proteome profile of HDE monoculture on scaffolds. Endothelial cells seeded on EmDerm-C produce the highest levels of collagen 1, collagen 4, MMP1, MMP2, TIMP1 and vasculogenic factors e.g.FGF-B, IL-8, fibronectin. * denotes a p–value of <0.05, ** denotes a p–value of <0.01 and *** denotes a p-value of <0.001 (mean ± SD, n=2)*

MSC Supernatant

Collagen type I, MMP1, MMP2, TIMP1 secretion was highest in Integra, which suggests that collagen production and turnover is highest in Integra scaffolds. There was no significant difference in concentration of collagen type IV between the different scaffolds. (Figure 4-18)

VEGF-A, IL-8, fibronectin, ang-1 and HGF secretion were highest in Integra as well, while there was no difference in FGF-A secretion across the scaffolds. These results suggest that the increased amount of growth factors resulted in greater cell proliferation and thus remodelling of the scaffold. (Figure 4-18)

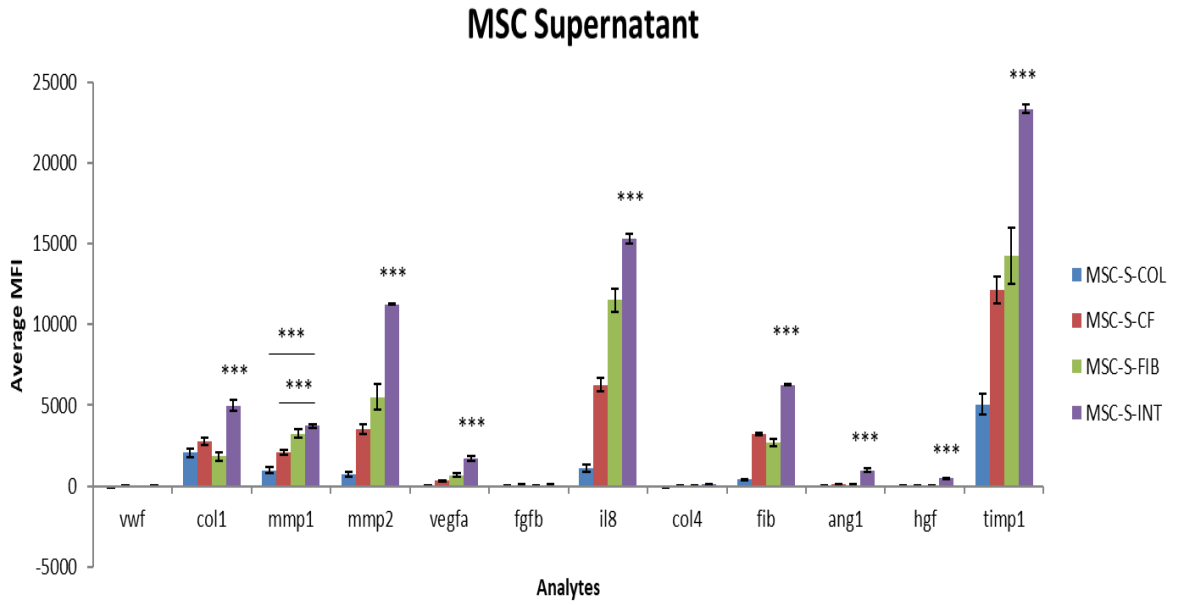


*Figure 4-18 Secretome profile of MSC monoculture on scaffolds. MSCs seeded on Integra secreted highest amount of collagen, MMP1, MMP2, TIMP1 and vasculogenic factors e.g. VEGF-A, IL-8, fibronectin, ang-1 and HGF. * denotes a p–value of <0.05, ** denotes a p–value of <0.01 and *** denotes a p-value of <0.001 (mean ± SD, n=2)*

MSC Lysate

Collagen type I and MMP1 synthesis was higher in EmDerm-F while MMP2 synthesis was higher in EmDerm-CF compared to other scaffolds while TIMP1 synthesis is greatest in Integra scaffolds. There was no significant difference in production of collagen type IV across the various scaffolds. (Figure 4-19)

FGF-B production is highest in Integra while IL-8 synthesis is higher in EmDerm-CF scaffolds. Fibronectin synthesis is highest in EmDerm-F scaffolds compared to Integra. However, there was no significant difference in production of VEGF-A, ang-1 and HGF across the scaffold types. These results suggest that production different angiogenic factors is affected by type of scaffold. (Figure 4-19)

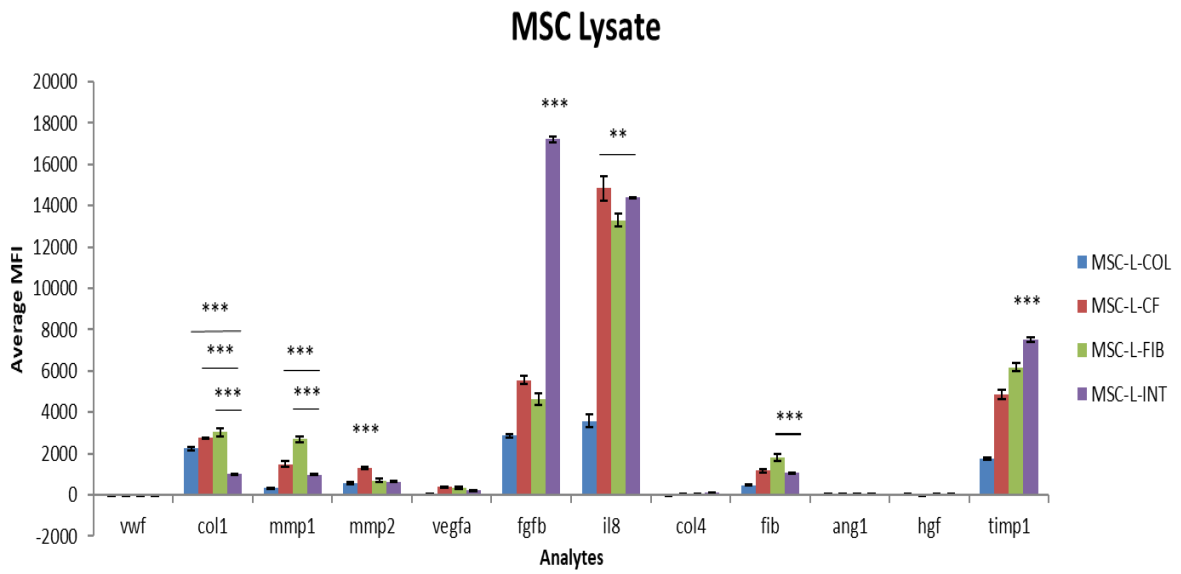


*Figure 4-19 Proteome profile of MSC monoculture on scaffolds. MSC seeded on EmDerm-F produced the highest levels of collagen, MMP1, and fibronectin while MSC seeded on EmDerm-CF produced highest levels of MMP2 and IL-8. FGF-B and TIMP1 levels were highest in Integra scaffolds seeded with MSC. * denotes a p–value of <0.05, ** denotes a p–value of <0.01 and *** denotes a p-value of <0.001 (mean ± SD, n=2)*

Co-culture analysis

HEK/HDF Supernatant

Collagen type I secretion is highest in EmDerm-CF compared to other scaffolds. MMP1 and MMP2 secretion is higher in EmDerm-C compared to Integra. TIMP1 secretion is significantly lower in EmDerm-CF compared to other scaffolds. (Figure 4-20)

VEGF-A secretion is highest in EmDerm-C while FGF-B, HGF and IL-8 secretion is highest in EmDerm-CF. Fibronectin secretion is greatest in Integra compared to other scaffolds. There was no significant difference in ang-1 secretion between the different scaffolds. These results suggest that EmDerm-CF has greatest effect on angiogenic factor secretion and collagen secretion when seeded with HEK/HDF. (Figure 4-20)

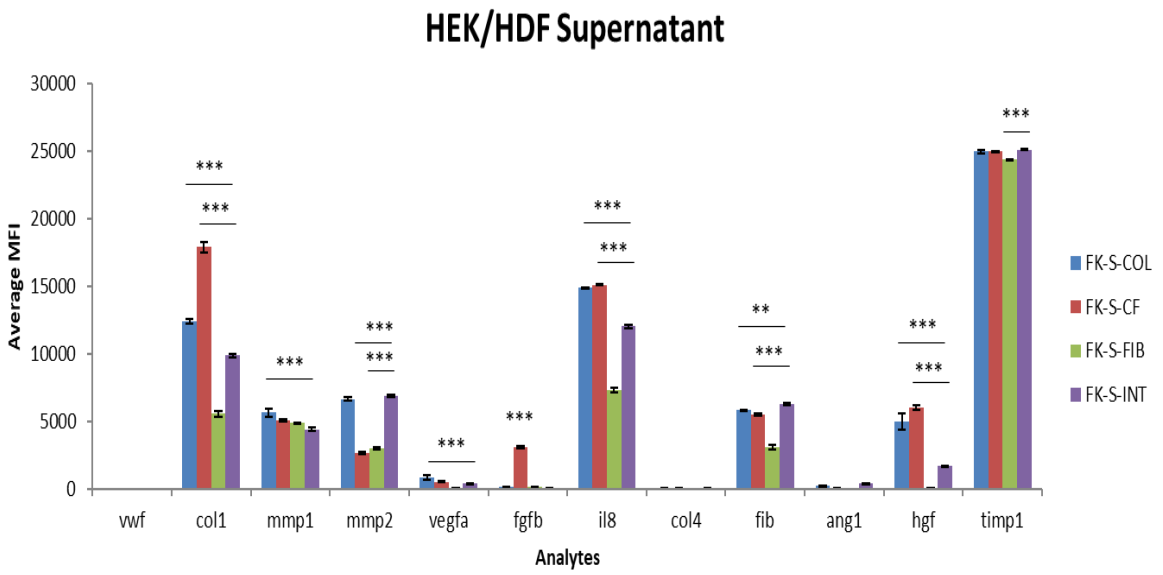


*Figure 4-20 Secretome profile of HEK/HDF co-culture on scaffolds (not at air-liquid interface). HEK/HDF seeded on EmDerm-C secreted highest levels of MMP1, MMP2 and vasculogenic factors e.g. VEGF-A, fibronectin while HEK/HDF seeded on EmDerm-CF secreted highest amounts of collagen, IL-8 and HGF. * denotes a p–value of <0.05, ** denotes a p–value of <0.01 and *** denotes a p-value of <0.001 (mean ± SD, n=2)*

HEK/HDF Lysate

Collagen type I, MMP2 and TIMP1 synthesis is higher in EmDerm-C scaffolds compared to Integra. MMP1 concentration was higher in EmDerm scaffolds compared to Integra. There was no significant difference in collagen type IV production. (Figure 4-21)

FGF-B synthesis was highest in EmDerm-C and Integra; however, IL-8 production was highest in EmDerm-CF and EmDerm-F. Fibronectin production was highest in EmDerm scaffolds compared to Integra. HGF production was higher in EmDerm-C and EmDerm-CF scaffolds compared to other scaffolds as well. There was no significant difference in concentration of VEGF-A and ang-1 across the different scaffolds. (Figure 4-21)

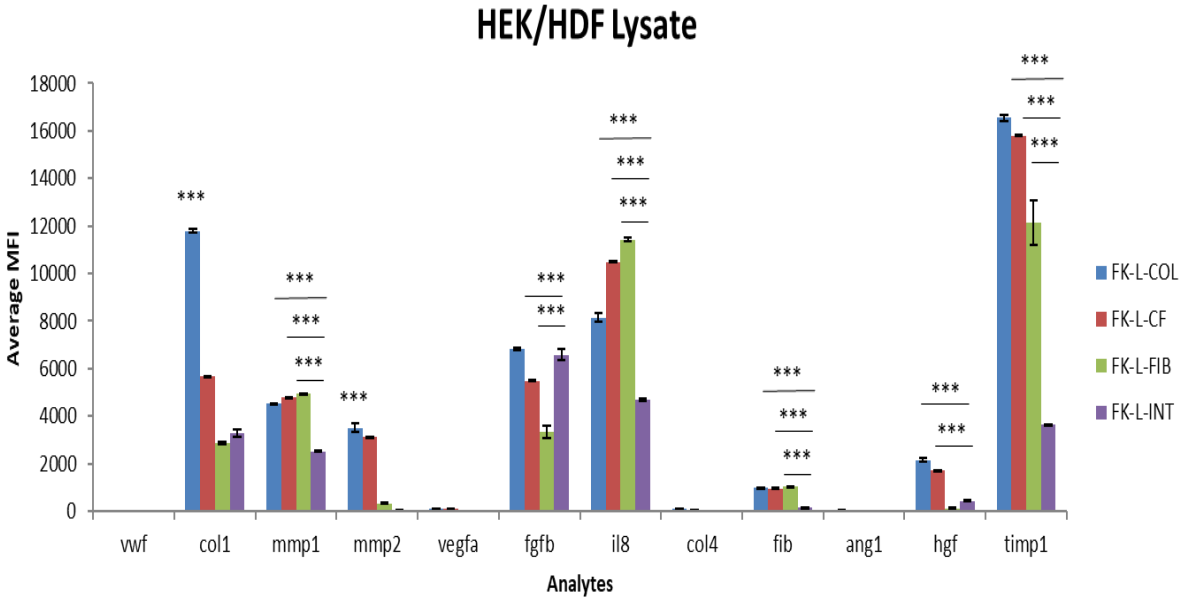


*Figure 4-21 Proteome profile of HEK/HDF co-culture on scaffolds (not at air-liquid interface).HEK/HDF seeded on EmDerm-C produced the highest amount of collagen, MMP2, TIMP1 and vasculogenic factors FGF-B, HGF. HEK/HDF seeded on EmDerm-F produced highest amount of MMP1 and IL-8. * denotes a p–value of <0.05, ** denotes a p–value of <0.01 and *** denotes a p-value of <0.001 (mean ± SD, n=2)*

HDF/HDE Supernatant

Collagen type I secretion is higher in EmDerm scaffolds comparted to Integra. MMP1 secretion is least in EmDerm-CF compared to other scaffolds. MMP2 secretion is highest in Integra. TIMP1 secretion is highest in EmDerm-CF. Collagen type IV secretion is highest in Integra compared to other scaffolds. (Figure 4-22)

VEGF-A, IL-8 and HGF secretion is highest in EmDerm-C while FGF-B secretion is highest in Integra. Fibronectin secretion is lowest in EmDerm-CF. There was no significant difference in secretion of ang-1 between the different scaffolds. (Figure 4-22)

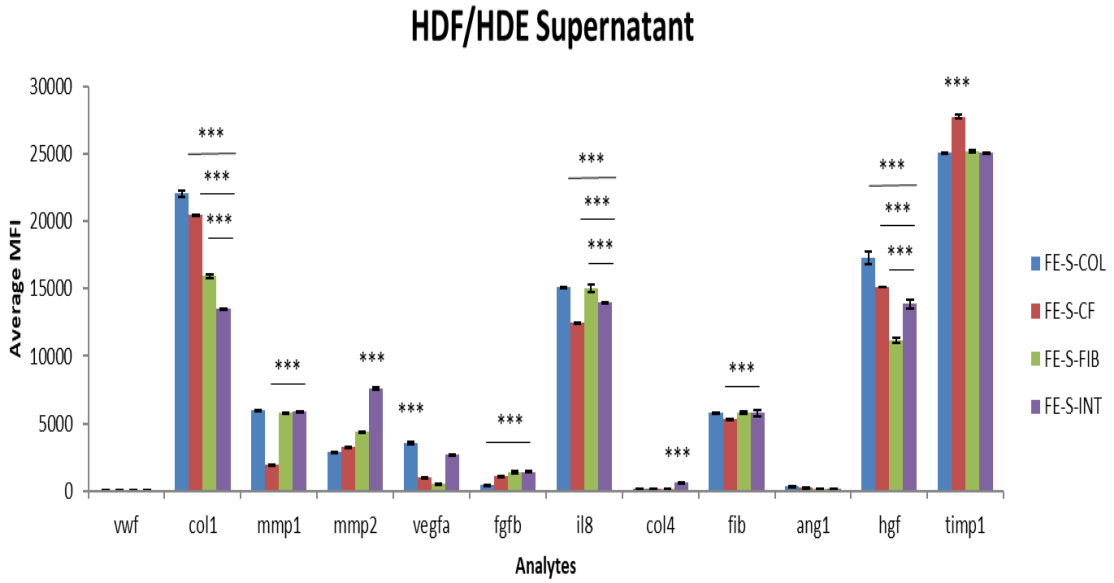


*Figure 4-22 Secretome profile of HDF/HDE co-culture on scaffolds. HDF/HDE seeded on EmDerm-C secreted highest amounts of collagen and vasculogenic factors VEGF-A, Il-8, fibronectin and HGF. * denotes a p–value of <0.05, ** denotes a p–value of <0.01 and *** denotes a p-value of <0.001 (mean ± SD, n=2)*

HDF/HDE Lysate

Collagen type I synthesis was highest in EmDerm-F while MMP1 and MMP2 production was highest in EmDerm-C scaffolds. TIMP1 production was higher in EmDerm scaffolds comparted to Integra. Collagen type IV production was also highest in EmDerm-C scaffolds. (Figure 4-23)

VEGF-A synthesis was highest in EmDerm-C and IL-8. Fibronectin was produced more in EmDerm scaffolds compared to Integra. However, FGF-B and HGF synthesis was higher in Integra compared to other scaffolds. (Figure 4-23)

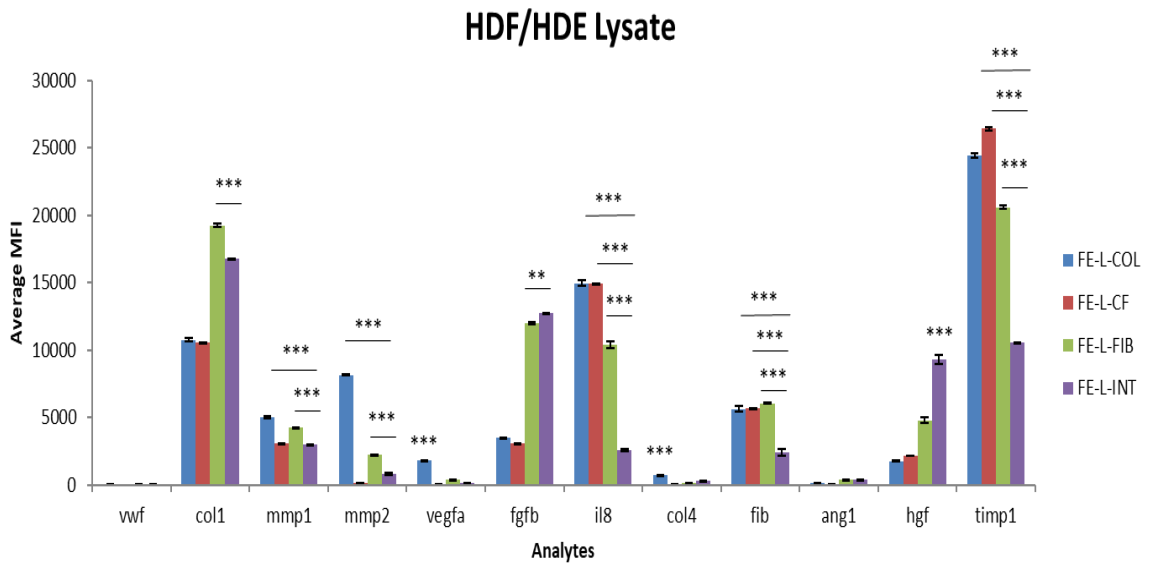


*Figure 4-23 Proteome profile of HDF/HDE co-culture on scaffolds. HDF/HDE seeded on EmDerm-C scaffolds produced highest amounts of collagen 4, MMP1, MMP2 and VEGF-A. HDF/HDE seeded on Integra produced highest amounts of FGF-B and HGF. * denotes a p–value of <0.05, ** denotes a p–value of <0.01 and *** denotes a p-value of <0.001 (mean ± SD, n=2)*

MSC/HDE Supernatant

Collagen type I secretion is highest in EmDerm-C while collagen type IV secretion was lowest in EmDerm-CF. There was no difference in MMP1 and TIMP1 secretion between the different scaffolds while MMP2 secretions was highest in EmDerm-CF and Integra scaffolds. (Figure 4-24)

VEGF-A secretion was highest in EmDerm-CF scaffolds while FGF-B secretion was least in EmDerm-CF scaffolds. HGF secretion was highest in EmDerm-C scaffolds. There was no significant difference in IL-8, fibronectin or ang-1 secretion between the various scaffolds. (Figure 4-24)

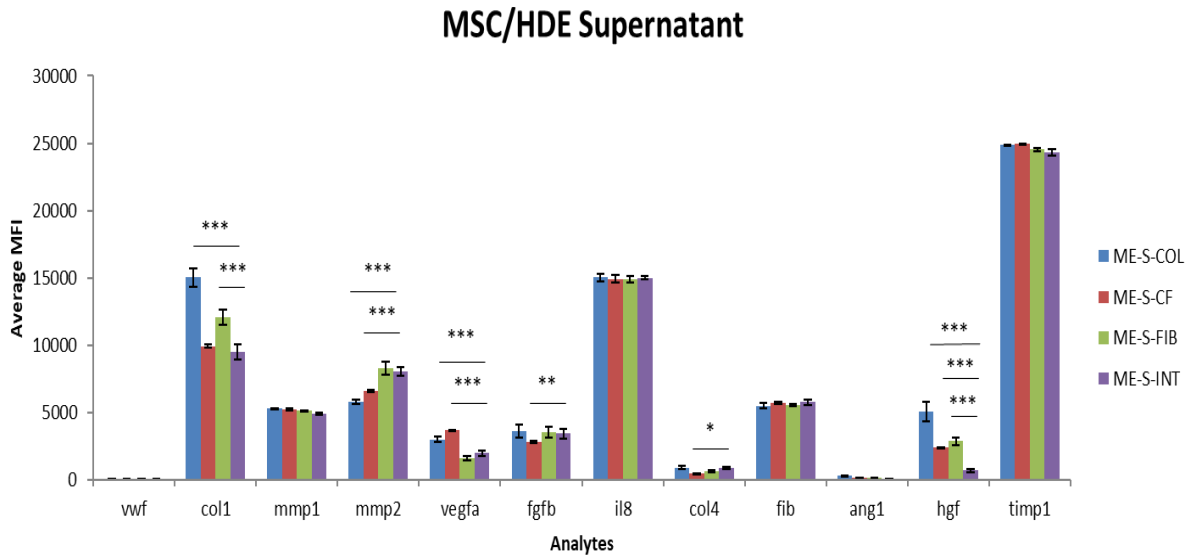


*Figure 4-24 Secretome profile of MSC/HDE co-culture on scaffolds. MSC/HDE seeded on EmDerm-C secreted highest amounts of collagen, FGF-B and HGF. * denotes a p–value of <0.05, ** denotes a p–value of <0.01 and *** denotes a p-value of <0.001 (mean ± SD, n=2)*

MSC/HDE Lysate

Collagen type I production was highest in EmDerm-C scaffolds while MMP1 and MMP2 secretion was greatest in EmDerm-CF scaffolds. TIMP1 secretion was higher in EmDerm scaffolds compared to Integra. Collagen type IV synthesis did not differ significantly between the different scaffolds. (Figure 4-25)

VEGF-A, FGF-B, IL-8 and fibronectin production was highest in EmDerm-CF while HGF synthesis was highest in EmDerm-C scaffold. There was no significant difference in ang-1 secretion between the various scaffolds. (Figure 4-25)

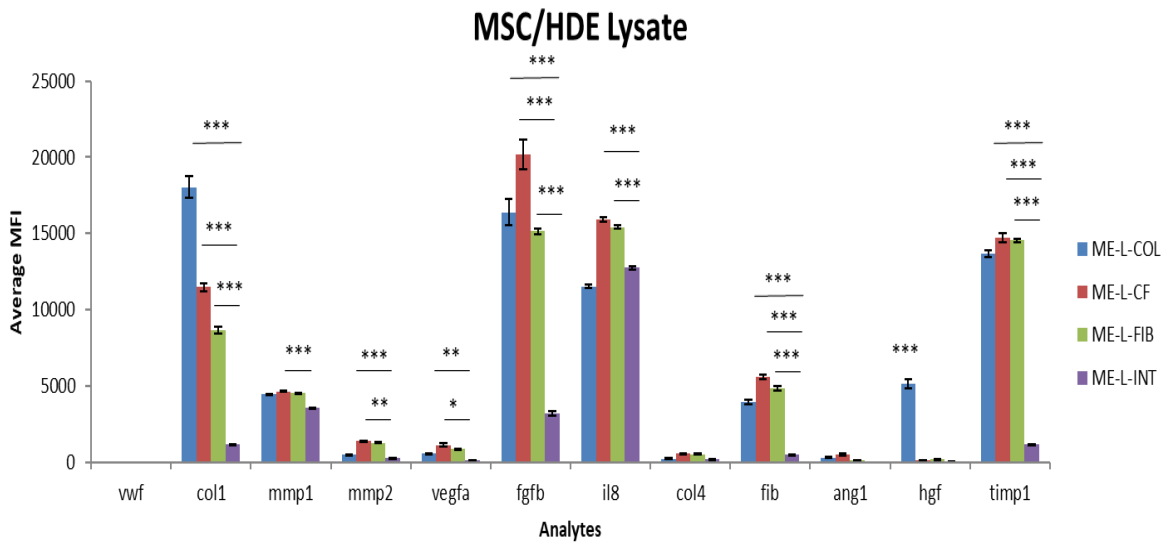


*Figure 4-25 Proteome profile of MSC/HDE co-culture on scaffolds. MSC/HDE seeded on EmDerm-C produced highest amounts of collagen and HGF. MSC/HDE seeded on EmDerm-CF scaffolds produced highest amounds of FGF-B, IL-8 and fibronectin. * denotes a p–value of <0.05, ** denotes a p–value of <0.01 and *** denotes a p-value of <0.001 (mean ± SD, n=2)*

In this section, a panel of growth factors and degradative enzymes/inhibitors were assayed to measure the concentration of various secreted and intracellular growth factors across four different scaffolds: EmDerm-C, EmDerm-CF, EmDerm-F and Integra as control. From an over-arching perspective, it appears that the proteome and secretome of cells seeded onto scaffolds differ significantly in a cell-specific and scaffold-specific manner. In addition, the behaviour of cells in co-culture, differ significantly when compared to the proteome and secretome profile of cells in monoculture. However, there are distinct patterns to these behaviours as explained further below.

Keratinocytes appear to be much more metabolically active in Integra scaffolds and EmDerm-C scaffolds. Integra scaffolds seeded with HEK cells appear to undergo most remodelling due to greater secretion of MMP1 and TIMP1. The key angiogenic growth factors secreted by keratinocytes appears to be FGF-B, IL-8 and fibronectin. These growth factors are known to be expressed by keratinocytes and influences the behaviour of other types of cells present in the skin e.g. fibroblasts, melanocytes and Langerhan's cells. (167-169) Interestingly, collagen type I and type IV were not expressed by

keratinocytes although both are key components of the dermis and basement membrane. This could be because keratinocytes induce the production of collagen by fibroblasts rather than producing it de novo. (170,171)

In general, fibroblasts appear to produce much more collagen type I, MMP1 and MMP2 in Integra and EmDerm-F, whilst secreting high levels of TIMP1. This suggest that there is high levels of extracellular matrix synthesis and remodelling. Meanwhile, key angiogenic factors secreted by the fibroblasts are IL-8, fibronectin and HGF. This is in contrast to key angiogenic factors released by fibroblasts when cultured on hyaluronic acid/collagen sponge (predominantly VEGF, FGF-B and HGF) or Dermagraft (predominantly VEGF, HGF, TGF-β, IL-8, IL-6 but not FGF-B). (172,173) This suggests that cell-scaffold interaction may play a significant role in modifying paracrine factors secreted by cells in a wound environment. Interestingly, although FGF-B is produced in high quantities when the fibroblasts are seeded onto EmDerm-F and Integra, very little of it is secreted. This may not be all that surprising given that the secretory pathway of FGF-B is not well-known. (174)

Scaffold seeded with HDE had high secretion of angiogenic growth factors such as FGF-B, IL-8, fibronectin and VEGF-A, but not angiopoietin-1 or HGF. There is also a high secretion of MMP1, MMP2 and TIMP1, especially for Integra scaffolds. All of these factors are key regulators for angiogenesis. (175,176) Interestingly, collagen type IV production was noted in HDE cell lysates indicating the induction of angiogenesis as endothelial cells begin to lay down type IV collagen to form a basement membrane for formation vascular walls. (177) It also plays a vital role for the angiogenic cascade, endothelial cell adhesion and migration. (178,179) Intracellularly, production of angiogenic growth factors and remodelling proteins were highest for EmDerm-C scaffolds. This disparity may be due to slower secretion of these factors or rapid uptake of these factors by adjacent cells.

MSCs seeded on Integra appear to have the highest secretion of growth factors and remodelling proteins. This is unsurprising as mesenchymal stem cells are known to secrete various growth factors during wound healing. (180,181) Interestingly, there was almost no secretion of FGF-B, although they were expressed intracellularly which is similar to findings by Leuning et al. (182) They also demonstrate that topographical cues from surface structure of the microenvironment significantly affect the cytokine secretion profile of MSCs. In contrast, intracellularly, apart from FGF-B and TIMP-1, the production of other factors were higher in EmDerm scaffolds. This may be due to slower release of the enzymes and growth factors into the culture media.

Co-culture of HEK and HDF appear to result in higher production and secretion of angiogenic growth factors and remodelling proteins (collagen type I, MMP1, MMP2, TIMP1) across all scaffolds, but more so in EmDerm-C and EmDerm-CF scaffolds. Key angiogenic factors are similar to HDF monoculture secretory profile in that IL-8, fibronectin and HGF are expressed and secreted, but at much higher levels indicating some synergistic effect when fibroblasts are co-cultured with keratinocytes. Again, FGF-B was highly expressed intracellularly but only secreted by cells seeded on EmDerm-CF. In addition, trace levels of VEGF-A was detected in the secretome of HEK/HDF co-cultures. There was almost no production or secretion of collagen type IV indicating no formation of a basement membrane in the HEK/HDF co-culture as well.

Co-culture of HDF and HDE result in higher levels of secretion of angiogenic factors (HGF, fibronectin, IL-8, VEGF-A except for FGF-B and ang-1) and remodelling proteins across all scaffolds compared to individual monocultures of HDF or HDE. There was trace secretion and expression of collagen type IV in Integra and EmDerm-C scaffolds respectively as well. It is unclear why FGF-B expression was downregulated in EmDerm-C and EmDerm-CF scaffolds especially. Also, there is no clear pattern as to which scaffold is superior as each scaffold stimulated expression and secretion of different types

proteins. For example, VEGF-A expression was highest in EmDerm-C, FGF-B expression was highest in EmDerm-F and Integra while IL-8 production was highest in EmDerm-C and EmDerm-CF.

Co-culture of MSC and HDE also resulted in higher levels of secretion of angiogenic factors and remodelling proteins across all scaffolds compared to monocultures. While monoculture of MSCs on Integra resulted in higher production and secretion of growth factors and degradative enzymes, the effect is less pronounced in MSC/HDE co-cultures. Secretory profile of MSC/HDE co-culture appear rather uniform, regardless of type of scaffolds the cells were cultured on. However, EmDerm scaffolds appear to result in higher intracellular synthesis of collagen 1, FGF-B, fibronectin and TIMP-1. According to literature, there may be an upregulation of IL-6 when MSC and HDEs are co-cultured but this was not measured in our panel of cytokines. (183)

In general, production of most growth factors and degradative enzyme/structural protein were increased in co-cultures compared to monocultures suggesting a synergistic effect and cellular cross-talk between the different cell types. For example, HDF/HDE co-cultures resulted in significant increase in HGF secretion and production as compared to HDF monoculture - which is more than an additive effect, due to stimulation of its production by paracrine factors secreted by HDE. This is consistent with the earlier findings where endothelial cells and fibroblasts appear to organize around each other in clusters, indicating that there is interaction between the two cell types in vitro. Meanwhile, collagen I production was significantly increased in MSC/HDE co-cultures compared to MSC or HDE monocultures, which could be due to stimulation of collagen production of MSCs by growth factors secreted by HDE.

Limitations of the study

The aim of this study was to evaluate the secretion profile of various types of cells seeded on EmDerm scaffolds to explore the potential of using seeded EmDerm scaffolds as a potential cellular scaffold for

wound healing and regeneration. The second aim was to assess the extent of remodelling of the scaffold material by quantifying amount of collagen produced, as well as degradative enzymes and inhibitory enzymes which affect collagen turnover.

The overall results from this study suggest that EmDerm scaffolds are highly biocompatible and promote the production and secretion of various growth factors for cell growth and enzymes/inhibitors for remodelling of scaffold.

One of the limitations of this study is that these growth factors and enzymes are measured over a 24-hour collection period on Day 14. Therefore, the measurements reflect the secretory profile of the cells at a steady state after 14 days of culture rather than during the proliferative phase. It also does not represent the changes in protein expression and secretion profile of time. This in vitro model also does not include the complete repertoire of cells present in wounds e.g. inflammatory cells and does not fully recapitulate in vivo conditions. It is simply a monoculture and co-culture model with no perfusion flow to simulate variations in protein concentration gradients vital for chemotaxis of cells and changes in cell behaviour.

Moreover, although some of the growth factors are expressed intracellularly, the concentration in the supernatant may be low due as they do not get secreted. Conversely, the growth factors may have already been absorbed by cells from cell culture media. Therefore, quantification of protein levels intracellularly and extracellularly may not give a clear picture about the interaction between cells and their environment.

Additionally, it was found from previous experiments that cell concentration differed between cell types and type of scaffold. Changes in concentration of proteins secreted or synthesized may be due to

differences in number of cells present in scaffolds. For the co-culture experiments, it is also difficult to quantify the proportion of each cell type in relation to total number of cells as the cells grow at different rates. Therefore, the secretion of growth factors and enzymes may be affected by the ratio of one cell type to another.

Moreover, the concentration of proteins from cell lysates and supernatant is dependent on the half-life of the protein itself and is a balance between protein synthesis and breakdown. There may be growth factors and enzymes trapped within the scaffolds which were not completely extracted into the cell lysis buffer which may affect the readings on the multiplex assay. Also, not all proteins synthesized are secreted.

Nevertheless, the overall aim of this study was to assess the effect of cellularized scaffolds on the cell milieu and suggests that the key growth factors and enzymes expressed by the cells may be beneficial in promoting vasculogenesis and integration of the scaffolds into wounds when implanted. They are also highly biocompatible and have been shown to promote excellent cell proliferation within the scaffold itself as well.

In summary, EmDerm scaffolds promote the secretion of various growth factors and remodelling of extracellular matrix by secretion of various degradation enzymes and inhibitors. This is dependent on type of scaffold and cell types seeded onto scaffolds as there are differences in expression of proteins within these cellularized scaffolds. Although in vitro results are promising, there is a need to test the scaffolds in vivo to monitor how the scaffolds (acellular and cellular) interact with the wound environment and modulate the wound healing response.

4.4. Summary

In summary, EmDerm scaffolds are biocompatible and support the cell proliferation of HEK, HDF, HDE and MSCs. EmDerm-F scaffolds were rapidly degraded when seeded with keratinocytes which suggest that the fibrin scaffold is less suitable for creating a bilayer skin substitute, compared to EmDerm-C and EmDerm-CF. For monocultures, cell proliferation was highest in EmDerm scaffolds with the lowest surfactant concentration (0.1%) and EmDerm scaffolds with P68 as an excipient across the different cell types. Therefore, those scaffolds were used for downstream experiments. The EmDerm scaffolds were also shown to have comparable biocompatibility to commercial scaffolds – Integra and Matriderm in vitro. For co-cultures, cell proliferation of EmDerm-C was shown to be comparable to commercial scaffolds when seeded with HEK/HDF, HDF/HDE and MSC/HDE. On widefield imaging, formation of nascent vascular networks were noted in EmDerm-C scaffolds as well. In terms of proteome and secretome analysis, there was greater production of growth factors and degradative enzymes in co-cultures compared to mono-cultures likely due to synergistic interaction between cell types. In particular, HDF/HDE co-cultures produced high levels of various angiogenic growth factors (VEGF-A, IL-8, fibronectin and HGF) when seeded on EmDerm-C scaffolds which could explain the formation of vascular networks in vitro. However, there was no clear pattern of which particular growth factor or enzyme was greater for the various cell types seeded onto the EmDerm scaffolds, as the secretion profile varied by cell type and scaffold material.

Chapter 5 In Vivo Assessment of Emulsion Templated Scaffolds

5.1. Introduction

In the earlier chapter, the cell proliferation, protein expression and secretory profiles of various cell types and co-culture of several cell types within emulsion templated scaffolds were characterized. There were cross-talk effects between the two cell types in the co-culture experiments which indicate that integration and remodelling of the scaffolds are co-dependent. However, there is still a need to assess the scaffold properties and behaviour in vivo, as the next step towards clinical trials and use of such scaffolds in patients.

Various wound healing models which have been proposed to test for biocompatibility of skin substitutes including burns wound models, chronic wound models, acute wound models and implantation studies. According to Medicines and Healthcare Regulatory Agency (MHRA) guidelines, there is a need to show that these scaffolds are biocompatible in vivo for skin substitutes to be approved for clinical use.

In this chapter, two concurrent experiments were performed – one to assess the biocompatibility of emulsion-templated scaffolds in a rat model and one to assess the efficacy of such scaffolds in a rat wound healing model. The aim of the biocompatibility experiment was to assess if the surfactants, excipients or residual cross-linker used during the templating process were physiologically toxic or inflammatory.

Meanwhile, the aim of the second experiment was to evaluate the efficacy of emulsion templated scaffolds in terms of the vascularization process, degradation process and scaffold integration. Histological assessments and blood tests were performed to monitor for signs of local and systemic inflammatory response.

5.2. Materials and Methods

Materials

Type I collagen from rat tail was commercially obtained from FirstLink (Wolverhampton, UK). Bovine fibrin and thrombin were obtained from Sigma UK. Unless otherwise stated, all reagents were obtained from Sigma UK. In order to measure the amount of lipopolysaccharide endotoxin, the Limulus amebocyte lysate (LAL) assay was used (Hycult Biotech, PA, USA). Rats were obtained from a licensed animal provider in the UK.

Scaffold Preparation

EmDerm-C, EmDerm-CF and EmDerm-F scaffolds were manufactured as described in Chapter 4. All scaffolds were made using 0.1% surfactant mix and cross-linked for an hour using EDC-NHS with 5% P68 as excipient prior to freeze-drying. Scaffolds were cut into 8mm discs using punch biopsies. Each scaffold was washed in phosphate buffered solution (PBS) three times and UV irradiated for 15 minutes. The scaffolds were then left overnight in 5% penicillin/streptomycin solution. The scaffolds were then given one final rinse with normal saline before used for implantation.

Endotoxin assay

The reagents were brought to room temperature and prepared as per manufacturer protocol. Each scaffold was weighed and cut into 1g portions and incubated in 200µl endotoxin free water to dissolve any endotoxin present in the scaffold (neat sample solution). Standards were prepared as per manufacturer instructions. Serial dilutions of each sample solution were prepared in duplicates. 50µl of each sample solution was added to the endotoxin free 96-well plate. Endotoxin free water was used as a negative control. 50µl of LAL reagent was then added to each sample solution. The plate was incubated at room temperature for 20 minutes. Absorbance values were determined using a UV-Vis plate reader (Spectramax i300, Molecular Devices, CA, USA) at 405nm.

Animals

Three healthy Sprague-Dawley rats (2-month old, males, body weight between 500 – 600 grams) were individually housed. All animals had free access to standard nutritionally balanced food and drinking water and were maintained on a 12-hour light/dark cycle. Environmental enrichment was provided to keep the rats active and healthy. The study was carried out at Northwick Park Institute of Medical Research (NPIMR). This study was conducted with ethical approval from the Animal Welfare and Ethical Review Bodies (AWERB) at NPIMR under a project license granted by the Home Office. All surgical procedure was done under isofluorane inhalational anaesthesia and analgesia was provided pre- and post- procedure to minimize animal suffering. All animals were acclimatized for two weeks prior to study and monitored closely for signs of complications post-operatively.

Scaffold implantation

Four scaffolds were implanted on the dorsum of each rat. Scaffolds tested were EmDerm-C, EmDerm-CF and EmDerm-F. A total of three rats were used in this study (one scaffold per rat). A diagrammatic representation of the scaffold implantation in each rat is shown in Figure 5-1. Two wounds were subcutaneous pockets with scaffold implanted subdermally, while the other two wounds were abraded to remove part of the dermis and panniculli carnosus, leaving only the epidermis and part of the dermis overlying the scaffold to simulate and split-thickness skin graft wound model.

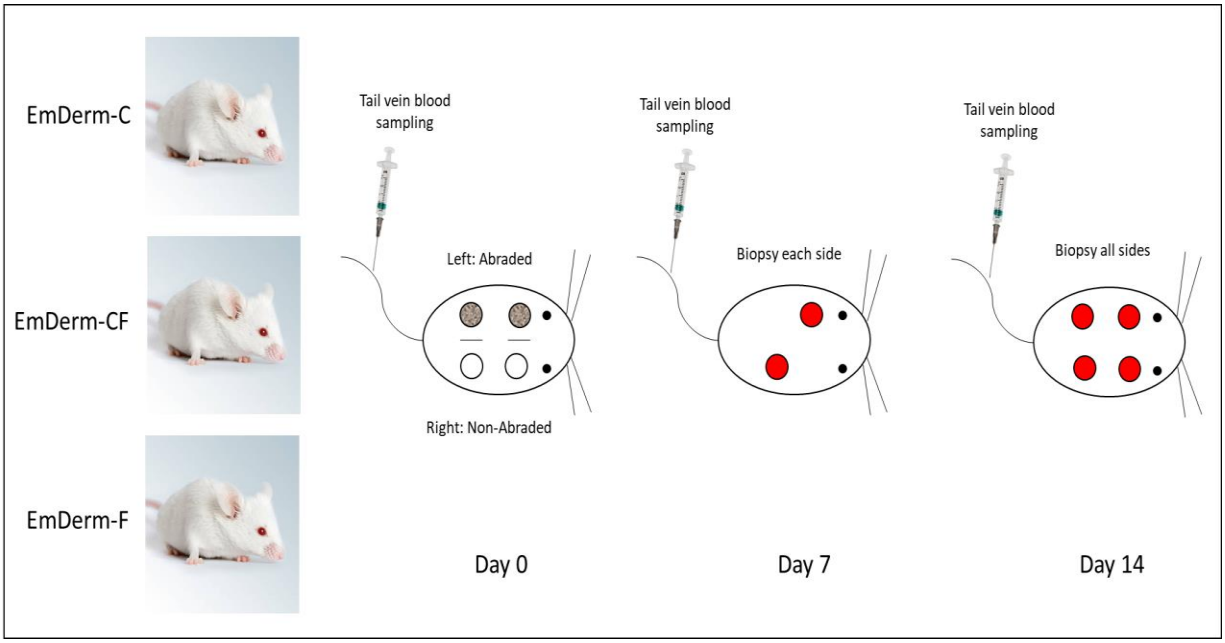


Figure 5-1 Schematic representation of in vivo experimental plan. 3 rats were used for the study and each rat was implanted with 4 scaffold discs. Wounds on one side were abraded to remove part of dermis while the other side was not. Biopsies were taken on Day 7 and Day 14. Blood sampling was done on Day 0, Day 7 and Day 14.

Surgical procedure

All surgical procedures were aseptically performed using sterile equipment in the animal facility operating rooms. The dorsum of each animal was shaved and cleaned using chlorhexidine. Two vertical incisions measuring 15mm were made and blunt dissection was done to create subcutaneous pockets in either side of the incision. For the abraded wounds, a scalpel was used to remove part of the dermis and paniculli from the incision edge (approximately 225 mm^2). Scaffolds were carefully inserted into each subcutaneous pocket. A tunnelling stitch was used to close the subcutaneous pockets, to prevent scaffold migration. The wounds were sutured close using Vicryl sutures and clips were applied to protect the wound and prevent the animals from biting the suture ends.



Figure 5-2 4 subcutaneous pockets containing scaffolds on either side of the rat's flank were created. At Day 7, wound biopsies were taken from the abraded and non-abraded sides. Finally, on Day 14, full-thickness excision of the wounds was performed on termination.

Wound biopsies

At Day 7, wound biopsies were performed on each rat for the non-abraded and abraded wound. 5mm punch biopsies were used. As far as possible, biopsies were done in a manner which included the part of the scaffold and part of the surrounding tissues around the scaffold to determine if there was any inflammatory reaction within the scaffold and in the tissue around the scaffold. Biopsy specimens were immediately fixed in neutral buffered formalin for 24 hours before embedding in paraffin blocks. Photographs of the biopsies and biopsy wounds were also taken. Wounds were then sutured close with Vicryl and clips applied. At Day 14, all animals were euthanized and all four wounds were biopsied/excised.

Blood sampling

At Day -7 (baseline), Day 7 and Day 14 tail vein blood sampling was done to assess if there was any systemic inflammatory response. Briefly, each rat was immobilized using a tunnel and a 24G needle was used to aspirate 1.5mL of blood volume from the superficial caudal vein at each time point for downstream haematological and biochemical assessment. 500µl of blood was collected into an EDTA

tube and the remaining blood was kept in a heparinised tube for C-reactive protein (CRP) ELISA analysis.

Haematological and biochemical assessment

For the haematological assessment, the blood samples were transferred from the EDTA tubes into an automated veterinary haematology analyser (Procyte Dx Analyser) which gave the following readings: erythrocyte count (RBC), total leucocyte count (WBC), differential white cell count (Diff), haemoglobin (Hb), haematocrit (Hct), mean cell volume (MCV), mean cell haemoglobin (MCH), mean cell haemoglobin concentration (MCHC), platelets (PLT), mean platelet volume (MPV). In particular, the WBC and PLT values were compared at each time point to determine if there was any change in these inflammatory markers in each rat.

C-reactive protein (CRP) ELISA analysis was performed using the Abcam Rat CRP ELISA kit, according to the manufacturer's protocol. Serum samples were centrifuged at 3000 g for 10 minutes then diluted at 1: 60 000. Briefly, reagents were brought to room temperature. Serial dilutions of standards and samples were prepared in duplicates. 50µl of each standard/sample was added to the 96-well plate and incubated for 2 hours. The content of each well was then aspirated and washed five times with the 1x wash buffer. Subsequently, 50µl of biotinylated CRP antibody was added and incubated for an hour. The wells were then washed again and 1x SP Conjugate was added to each well and incubated for 30 minutes. Then, the wells were washed again and 50µl of chromogen substrate were added to each well and incubated in the dark for 10 minutes. Finally, 50µl of stop solution was added to each well and absorbance was read at 450 nm immediately (wavelength correction done at 570 nm). OD readings from each sample was compared at different time points to determine if there was any change in CRP levels in each rat.

Histological assessment of inflammatory response

Each tissue sample was fixed for 24 hours in neutral buffered formalin (NBF), processed and embedded into paraffin blocks. A microtome was used to section the samples into 10 um thickness, mounted on glass slides, deparaffinized then stained using conventional Haematoxylin-Eosin (H&E) protocol. Briefly, each slide was deparaffinized in Citroclear for 3 minutes (x2), then transferred into 100% ethanol for 3 minutes (x2), 70% ethanol for 3 minutes, 50% ethanol for 3 minutes, and tap water for 3 minutes. The slides were then transferred into filtered Harris' Haematoxylin for 4 minutes then back into running tap water for 3 minutes. Then, slides were dipped ten times in 1% acid alcohol, Scott's tap water and 0.5% lithium carbonate (with tap water washes between each solution). The slides were then dipped in 50% ethanol and 70% ethanol ten times before incubating in Eosin Y for 1 minute. The slides were then washed in 90% ethanol for 1 minute (x4), 100% ethanol for 1 minute (x2) and xylene for 1 minute (x2) before mounting with a coverslip. Each slide was imaged using a Leica Scanscope at 40x magnification for downstream analysis.

Quantification of scaffold vascularization

Degree of vascularization of each scaffold were quantified at Day 14. Ten frames per slide for each tissue specimen were taken at 40x magnification using a light microscope. Each frame was taken at random. The number of vascular structures found within the scaffolds were manually counted for quantification. Mean ± SD for each scaffold were calculated and analysed for statistical significance.

Quantification of local inflammation

Degree of inflammation surrounding each scaffold was quantified at Day 7. Ten frames per slide for each tissue specimen were taken at 40x magnification using a light microscope. Each frame was taken at random. The degree of inflammatory response found within the scaffolds were manually graded as: 1 - minimal, 2 - mild, 3 - moderate and 4 - severe. This was done using reference frames for neutrophil

density. Mean ± SD of total inflammatory grade for each scaffold were calculated and analysed for statistical significance.

Statistical analysis

All values are expressed as mean ± SD for each experiment. One-way ANOVA was used to determine significance with post-hoc Tukey test. Repeated measures ANOVA was used for the values which were measured repeatedly at different time points. All statistical analysis was done using GrapPad Prism 4 (Graph Pad, La Jolla, CA) and a p-value of <0.05 was considered statistically significant.

5.3. Results

Endotoxin Assay

The endotoxin assay (LAL assay) is one of the recognized assays for quantifying amount of endotoxin in materials under the Food and Drug Administration (FDA) Regulations. The accepted endotoxin limit is 10 EU/g. (184) In all our scaffolds tested, the endotoxin levels were below this detection limit. The mean endotoxin level for EmDerm-C was 0.08 EU/g, while EmDerm-CF was 0.10 EU/g and EmDerm-F was 0.12 EU/g respectively.

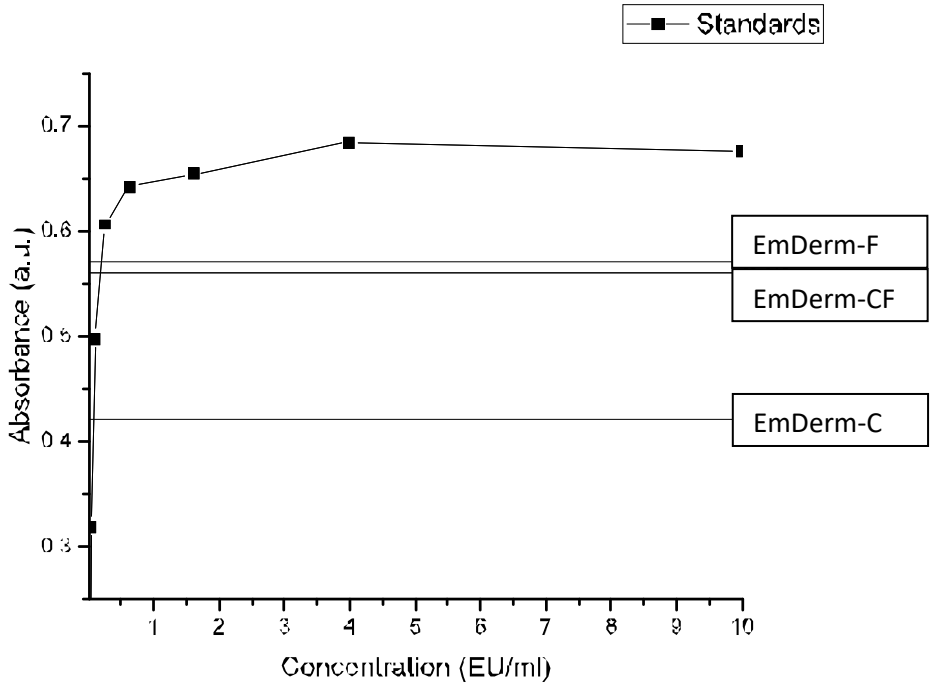
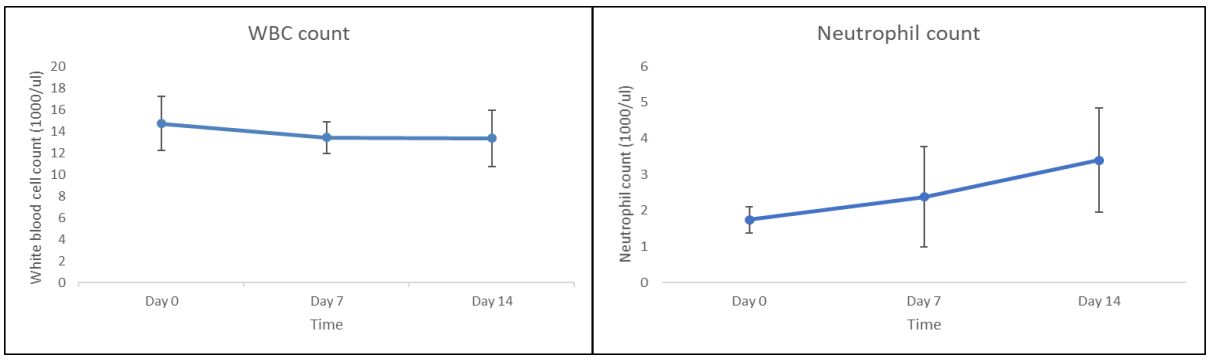


Figure 5-3 Endotoxin assay with lines representing levels of endotoxin concentrations in each of the scaffold (n=3).

Haematological analysis of systemic inflammatory response

There was no significant change in total white blood cell count (WBC), neutrophil count or lymphocyte count in all three animals during the entire period of the study (14 days). There was also no significant change in platelet count, which is a known marker of systemic inflammation. There was also no gross evidence of localized inflammation such as erythema, swelling, or increased warmth in the area of scaffold implantation which is consistent with the blood results.



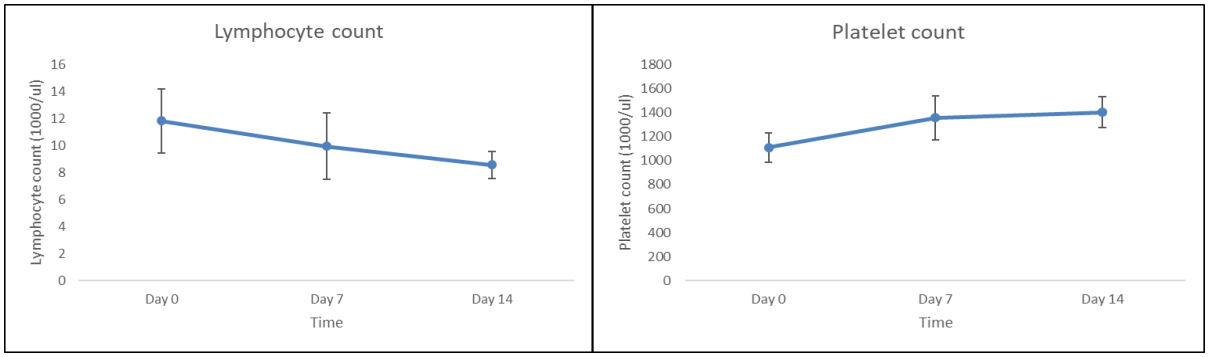


Figure 5-4 Haematological analysis of inflammatory markers. There was no significant change from baseline of any of the white cell, neutrophil, lymphocyte or platelet counts. (mean ± SD, n=3)

Biochemical analysis of acute phase reactant

There was no significant change in concentration of C-reactive protein (CRP) as measured using the ELISA assay. This is consistent with the haematological analysis as above, indicating that the EmDerm scaffolds were not pro-inflammatory at a systemic level.

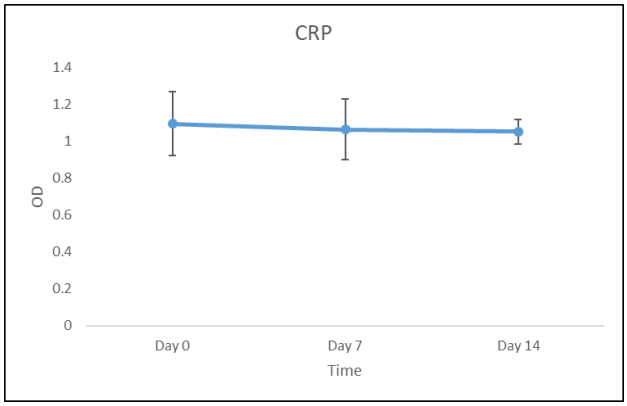


Figure 5-5 Biochemical analysis (C-reactive protein ELISA) of inflammation. There was no significant change from baseline of CRP levels. (mean ± SD, n=3)

Histological assessment of inflammatory response

Week 1

A) EmDerm-C

There was no evidence of significant localized inflammation within and around the collagen scaffold. Scaffolds were partially degraded and were loosely attached to the connective tissue surrounding the scaffold. There was no evidence of revascularisation at Day 7.

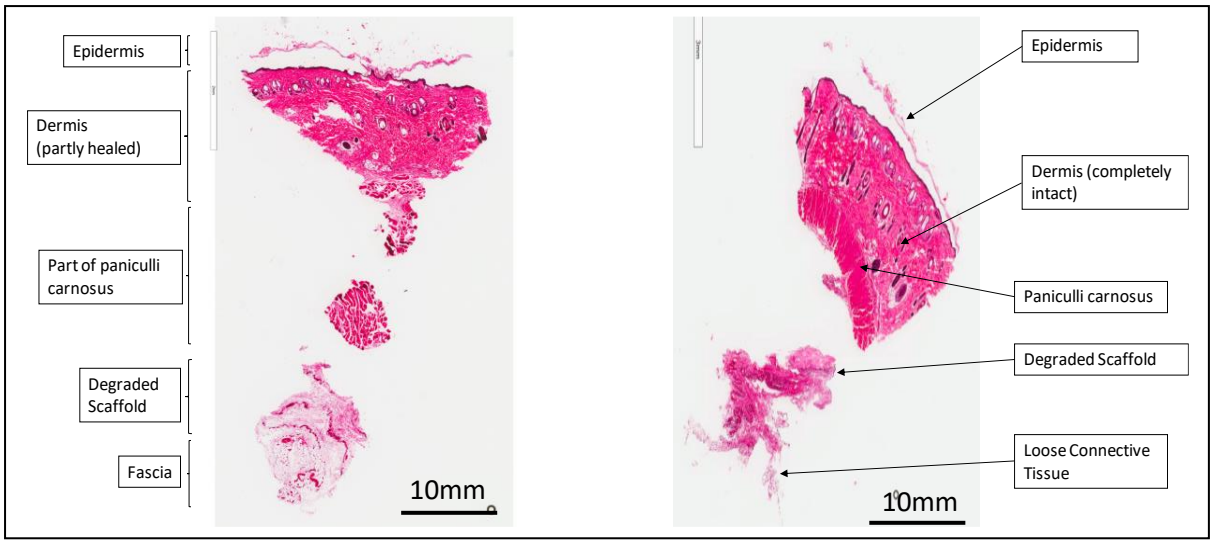


Figure 5-6 Day 7 biopsy of EmDerm-C. Left (abraded) and right (non-abraded). Both show minimal local inflammatory changes and partly degraded scaffolds.

B) EmDerm-CF

A moderate degree of inflammation was present within the scaffold and around the EmDerm-CF scaffolds. There was a lesser degree of scaffold degradation despite the influx of inflammatory lymphocytes around the scaffold. There was also no nascent vascular structures present at this stage.

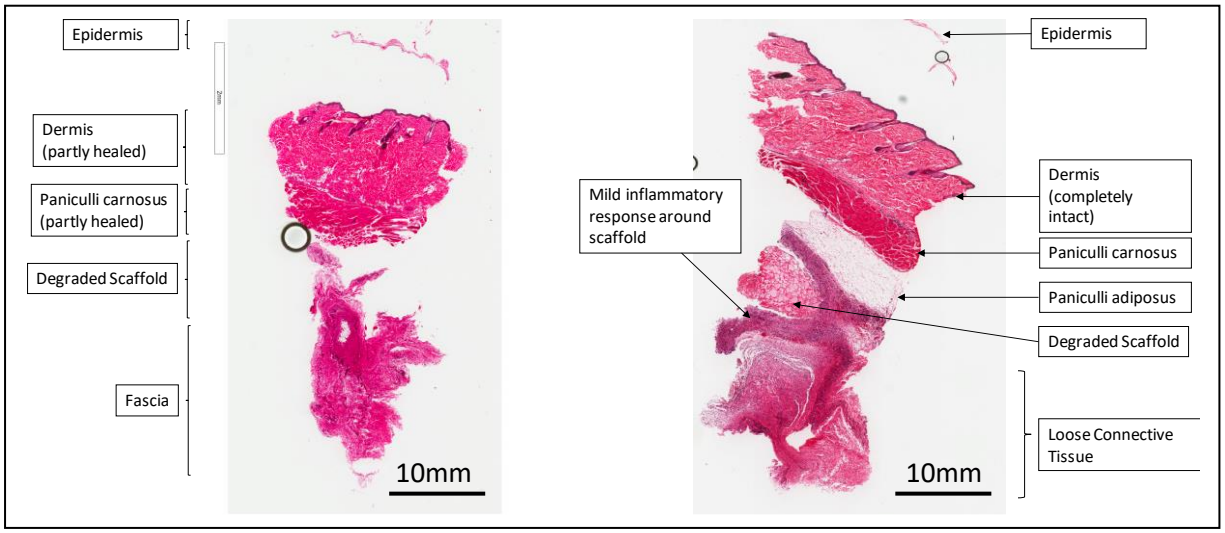


Figure 5-7 Day 7 biopsy of EmDerm-CF. Left (abraded) and right (non-abraded). The abraded wound showed minimal inflammatory reaction compared to the non-abraded wound where there is a mild to moderate inflammatory reaction around the scaffold. In both cases, scaffolds were partly degraded.

C) EmDerm-F

A moderate degree of inflammation was present within or around the EmDerm-F scaffolds, which is similar to the EmDerm-CF scaffolds. However, there was minimal scaffold degradation despite the inflammatory response around the scaffold. There was also no vascularization of the scaffold present at this stage.

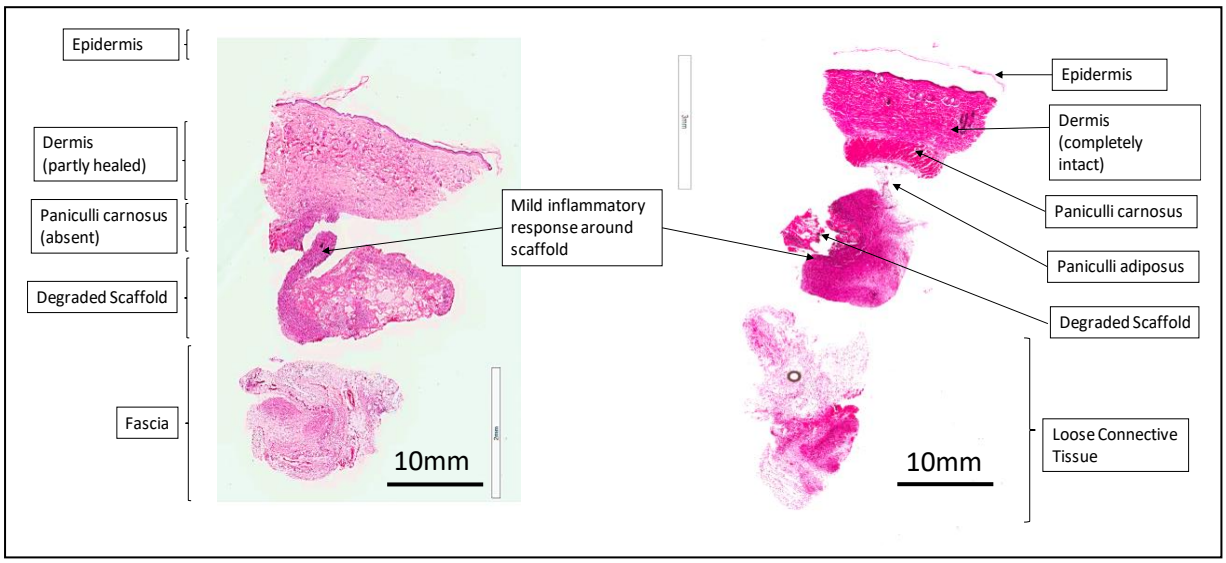


Figure 5-8 Day 7 biopsy of EmDerm-F. Left (abraded) and right (non-abraded). In both scaffolds, there is mild to moderate inflammatory reaction within and around the partially degraded scaffolds.

Week 2

Abraded Wounds

EmDerm-C

There was no evidence of inflammation within the scaffold or around the scaffold. The were many vascular structures present containing red blood cells within the lumen, suggesting active blood flow within the scaffold and integration with surrounding tissue. There was also significant regeneration of the dermal layer with deposition of collagen and part regeneration of the paniculli carnosus.

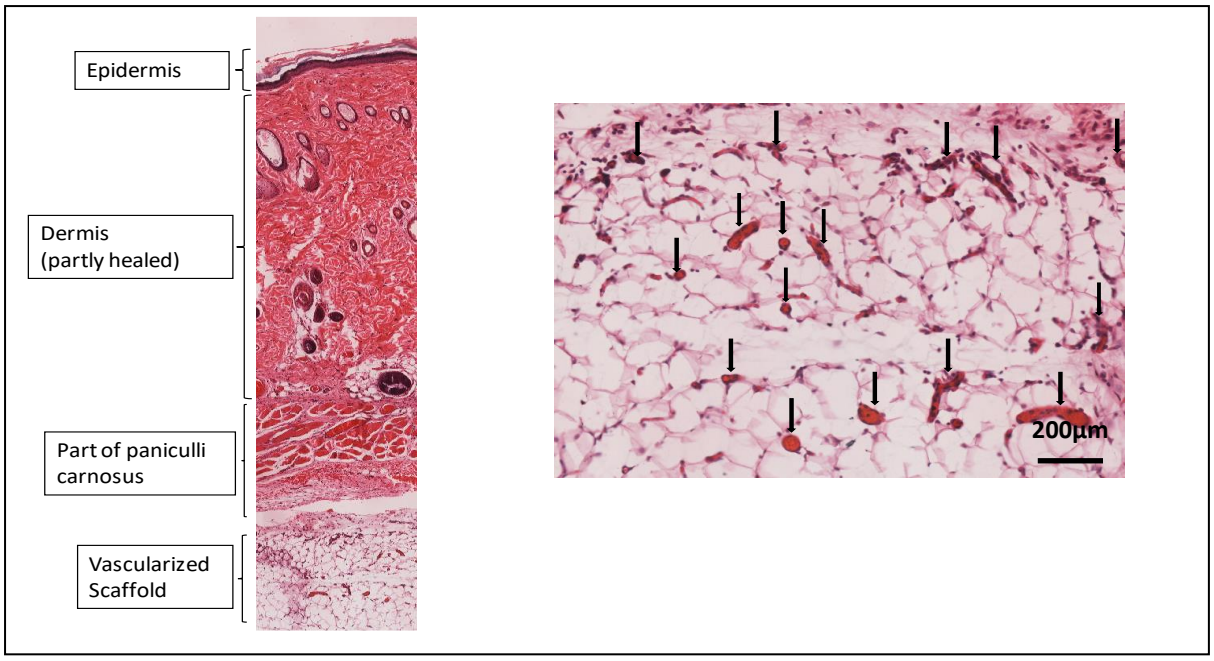


Figure 5-9 Day 14 biopsy of EmDerm-C (abraded). There is increased vascularization of the wound site as shown by the arrows and scaffolds have been remodelled/integrated into the wounds.

EmDerm-CF

There was evidence of residual inflammation in the tissue around the scaffold. There is evidence of vascularization of the scaffold, with some collagen matrix deposition and remodelling. There was also regeneration of the dermal layer but no evidence of regeneration of the paniculli carnosus layer.

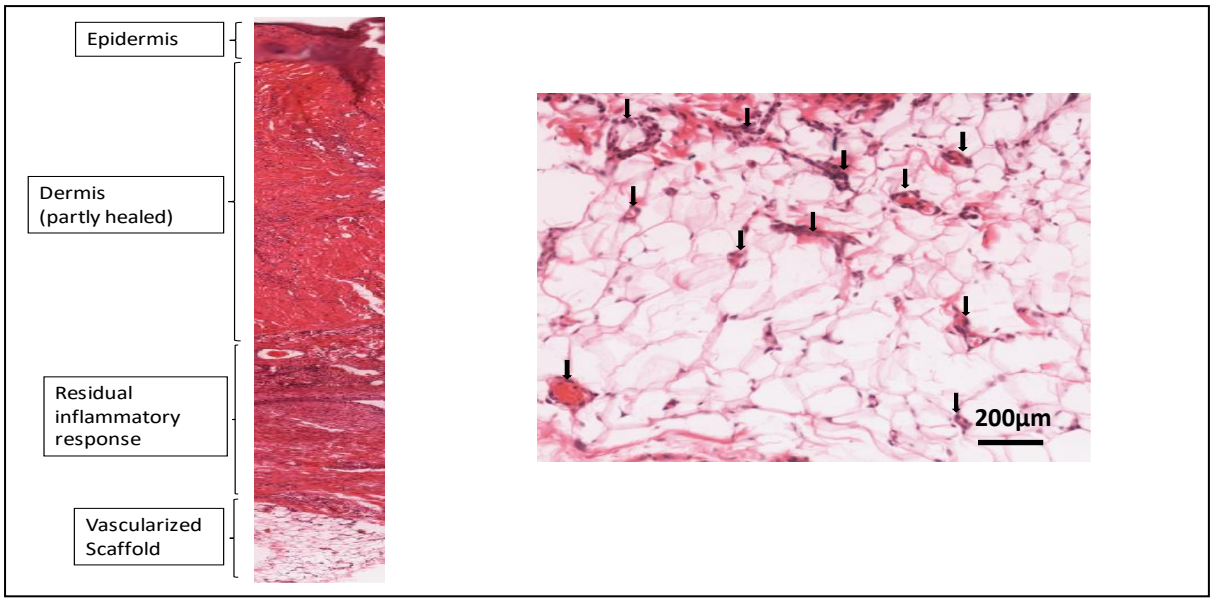


Figure 5-10 Day 14 biopsy of EmDerm-CF (abraded). There is increased vascularization of the wound site as shown by the arrows and scaffolds have been remodelled/integrated into the wounds. However, there is some residual inflammatory response and increased deposition of ECM in the dermal layer.

EmDerm-F

There is minimal inflammation in the tissue surrounding the scaffold. There is evidence of vascularization of the scaffold with increased collagen matrix deposition and scaffold remodelling. The dermal layer has almost completely healed, however there is no regeneration of the paniculli carnosus, which is similar to the EmDerm-CF scaffold.

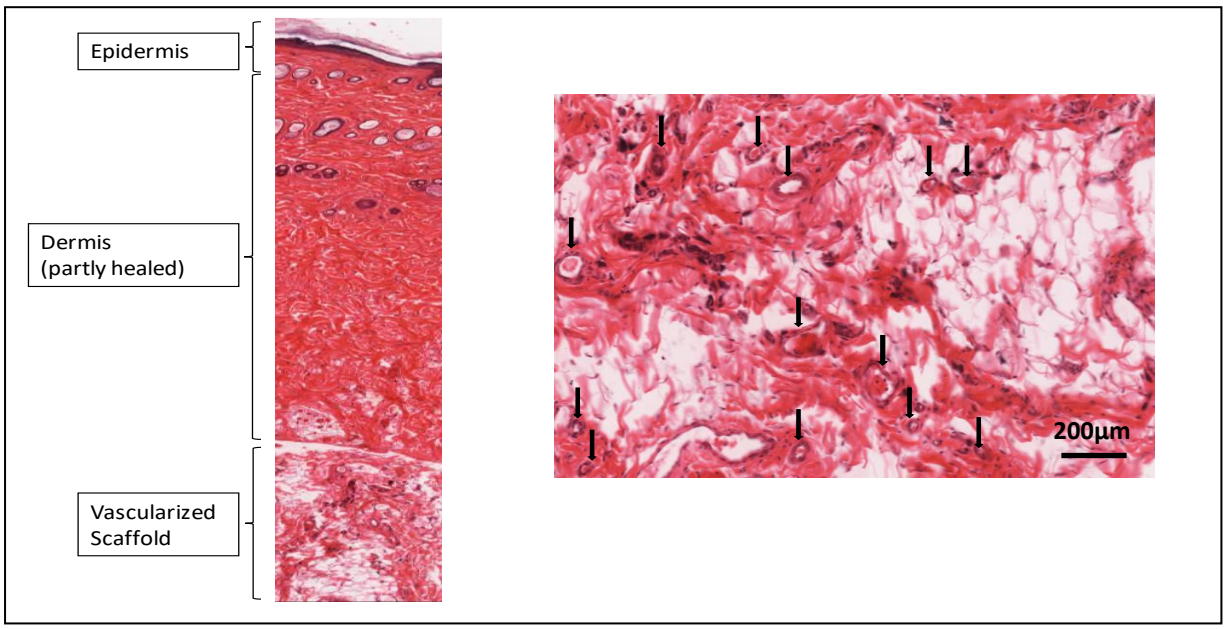


Figure 5-11 Day 14 biopsy of EmDerm-F (abraded). There is increased vascularization of the wound (as shown by arrows) and significant deposition of ECM material within the wound site and dermal layer.

Non-abraded wounds

EmDerm-C

At Week 2, the non-abraded wounds with EmDerm-C implanted showed minimal inflammatory response within and surrounding the scaffold. There is excellent vascularization of the scaffold and matrix remodelling as well.

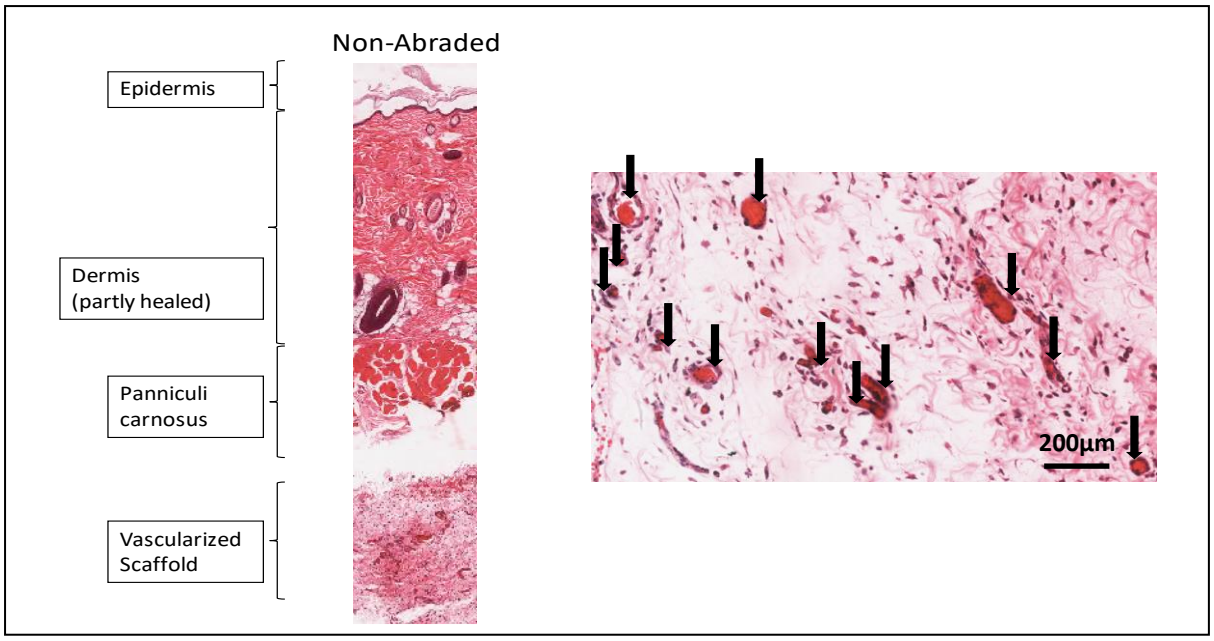


Figure 5-12 Day 14 biopsy of EmDerm-C (non-abraded). There is minimal inflammatory response and most of the scaffold has been remodelled with ingrowth of vascular structure (see arrows).

EmDerm-CF

EmDerm-CF scaffolds in the non-abraded wounds also showed minimal inflammatory response around and within the scaffolds. There is formation of vasculature within and around the scaffolds and much of the original scaffold has been degraded and remodelled into connective tissue.

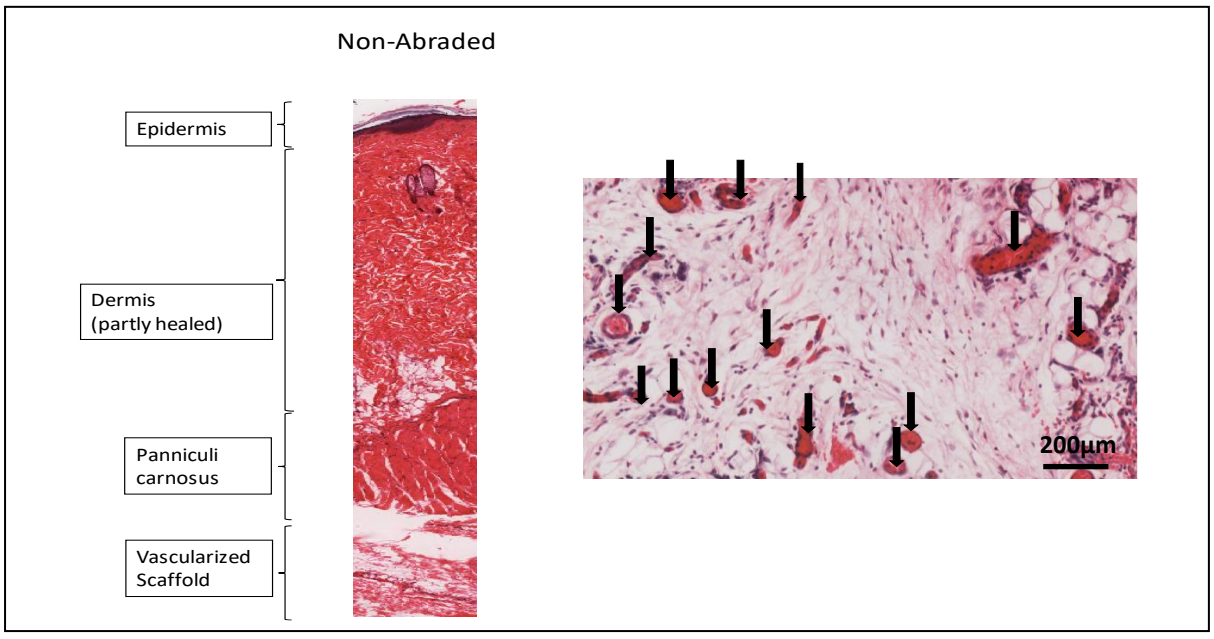


Figure 5-13 Day 14 biopsy of EmDerm-CF (non-abraded). There is minimal inflammatory response and most of the scaffold has been remodelled with ingrowth of vascular structure (see arrows).

EmDerm-F

EmDerm-F scaffolds demonstrated the least degree of vascularization and some residual inflammatory response. The scaffold itself is mostly entirely degraded. However, there is also greater deposition of extracellular matrix compared to the other two scaffolds, indicating some degree of fibrosis present. The new matrix laid down appear to be disorganized fibrils with no obvious form or structure within it.

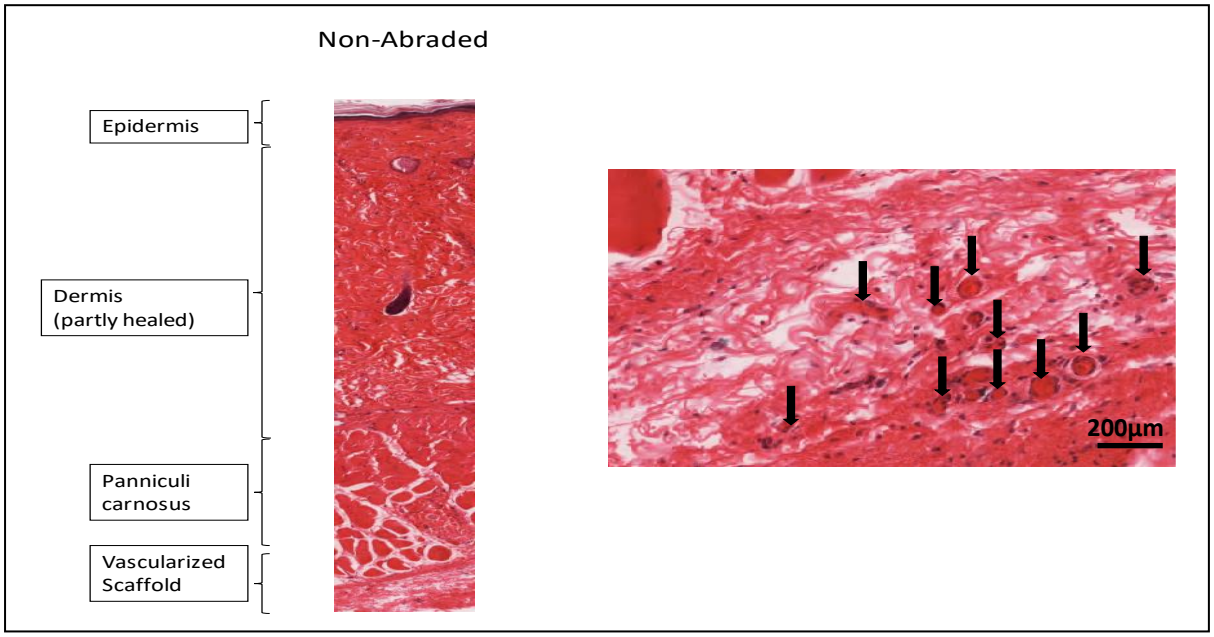


Figure 5-14 Day 14 biopsy of EmDerm-F (non-abraded). There is minimal inflammatory response and most of the scaffold has been remodelled with ingrowth of vascular structure (see arrows). There is significant deposition of ECM as well.

Quantification of vascularization

Mean number of vessels in EmDerm-C scaffolds (mean 6.5 ± 2.3) was significantly higher compared to the EmDerm-F scaffolds in the abraded and non-abraded wound model (mean 3.7 ± 1.6 and 1.9 ± 1.6 respectively). EmDerm-CF scaffolds resulted in intermediate degree of vascularization compared to EmDerm-C and EmDerm-F in both the abraded and non-abraded wounds (mean 4.7 ± 2.0 and 3.2 ± 1.0 respectively). However, this result is not statistically significant.

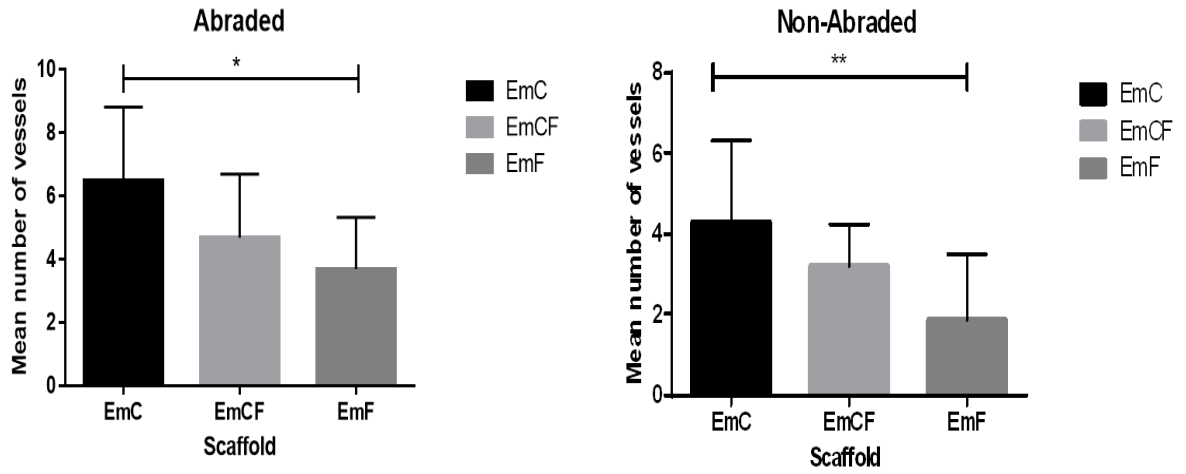


Figure 5-15 Mean number of blood vessels in biopsy samples of EmDerms implanted subcutaneously in rats. In both the abraded and non-abraded wounds, there is higher mean number of vascular structures in wounds treated with EmDerm-C ($p<0.05$ for abraded model and $p<0.01$ for non-abraded model). (mean ± SD, n=2)

Quantification of local inflammatory response

Inflammatory grade was lowest in EmDerm-C (mean 1.5 ± 0.48) scaffolds compared to EmDerm-CF (mean 3.1 ± 0.81) and EmDerm-F (mean 3.3 ± 0.67) scaffolds in the abraded wound model. Mean inflammatory grade was also lowest in EmDerm-C (mean 1.5 ± 0.52) compared to EmDerm-CF (mean 3.1 ± 0.74) and EmDerm-F (mean 3.4 ± 0.7). There was no significant difference in inflammatory response between EmDerm-CF and EmDerm-F scaffolds.

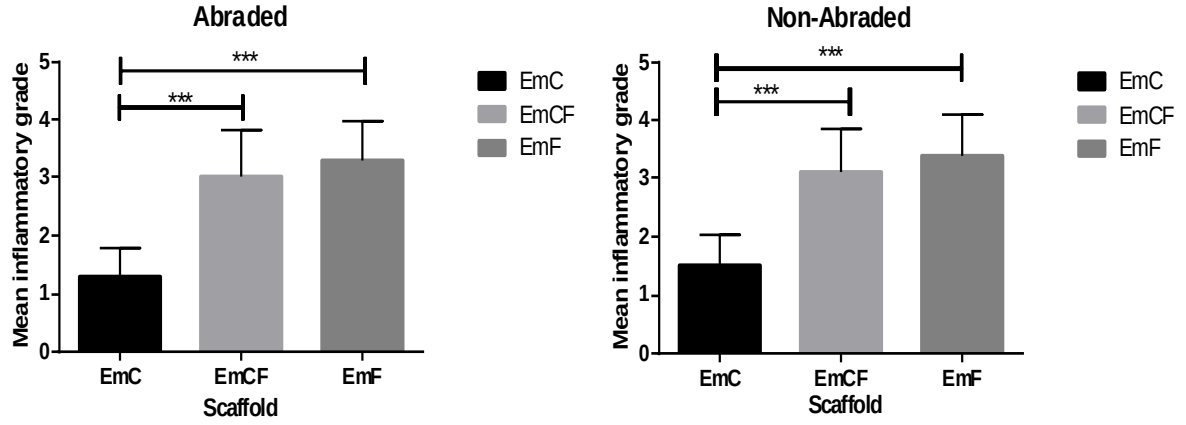


Figure 5-16 Mean grade of inflammation in biopsy samples of EmDerms implanted subcutaneously in rats.. In both the abraded and non-abraded wounds, there is significantly higher degree of inflammation in EmDerm-F scaffolds, followed by EmDerm-CF then EmDerm-C ($p<0.001$). (mean ± SD, n=2)

5.4. Discussion

The aim of this pilot study was to characterize the in vivo effect of emulsion-templated collagen, collagen-fibrin and fibrin scaffolds to evaluate for biocompatibility and efficacy. One of the key limitations of this project is a small sample size (only three rats were used to test the EmDerm scaffolds). This was mainly due to funding issues as there were plans to conduct a larger scale study on completion of this pilot study. There was also a need to determine if the EmDerm scaffolds were themselves toxic (as they have never been tested in vivo before) and thus a small sample size would reduce the number of rats exposed to any scaffold toxicity effect.

In this study, a classical chamber model was not used as the main objective of this initial pilot study was to determine if the surfactants and breakdown products from the EmDerm scaffolds exert a toxic effect on wound healing physiology. The non-abraded wound model was designed to test for presence of any localized reaction to scaffold implantation and degradation. The abraded wound model simulates a partial thickness skin graft where part of the lower dermis is removed, and the scaffold is implanted under the remaining dermis to test for wound healing and revascularization of the wound in a minimally invasive manner. The subcutaneous implantation wound model has been validated as a wound healing model in several studies (185,186)

One of the other reasons for using a subcutaneous implantation model was to embrace the 3R's principle of human animal research, particularly refining the initial experimental question to focus on bio-compatibility, rather than the more complex physiology of open wound healing. Our secondary objective was to explore the effect of an acute wound model on scaffold integration and degradation through histological evaluation. A subcutaneous implantation model was hypothesized to permit a less invasive assessment of dermal scaffold integration without interference from external factors e.g. types of dressings, sheared off scaffolds, infection, wound contracture and wound chambers/flanges. The classical chamber model would be useful in the next phase in vivo work in determining effect of scaffold

implantation which is more akin to the clinical setting of applying a dermal skin substitute over a partial thickness wound. However, the license for the study was still pending at the time of writing this thesis.

Additionally, many rodent wound healing studies focus on closure as an end-point and measure rate of wound contraction as an indicator of healing. However, dermal scaffolds aim to reduce contraction by providing a matrix structure of cellular ingress and neovascularization. Therefore, the subcutaneous implantation model would allow for a more objective measure of regenerative wound healing, rather than using wound contraction as an outcome measure. This wound healing model also involves removal of the paniculli carnosus which is the main cause of wound contraction in rodent wound healing models, thus enabling better assessment of scaffold engraftment and integration.

A time point of two weeks was selected to examine the effect of the scaffold on early revascularization. This concurs with other comparative studies of dermal scaffolds on rodent wound healing models. (187,188) This duration of time would allow for the inflammatory response from the wound creation and initial injury to settle down and formation of a neodermis. Ideally, wound beds should be ready for epidermal engraftment by Day 14, which was another reason for selecting this time point. On Day 7, all three EmDerm scaffolds were noted to have minimal angiogenesis and vasculogenesis and had varying inflammatory responses. Therefore, a longer time-point was needed to assess vascular ingrowth and resolution of inflammation.

A differential effect was noted across all three EmDerm scaffolds over the two-week period as well. EmDerm-C scaffolds had the highest number of vascular structures on Day 14 compared to other EmDerm scaffolds. This is comparable to Integra, one of the gold standard skin substitutes. Vascular ingrowth of Integra in a rodent wound healing model was previously evaluated by King et al and around 70% of the animals had developed evidence of angiogenesis by Day 14. (189) However, the wound

healing model used to test for efficacy of Matriderm and Integra were different and thus a different inflammatory reaction profile is to be expected. (190)

Overall, EmDerm-C scaffolds appear to be the most biocompatible with least inflammatory response and highest rate of vascularization of the scaffold. This may be due to the fact that collagen is an abundantly found extracellular matrix which allows for good cellular attachment and migration. This could also be due to the added nanofibrillar surface of EmDerm-C scaffolds, resulting in greater surface area for cell adhesion and proliferation.

EmDerm-F scaffolds appear to be the least biocompatible, with the greatest inflammatory response within 7 days and lowest rate of vascularization at 14 days. This finding is interesting as fibrin scaffolds have previously been shown to be more pro-angiogenic than Integra and Matriderm. (191) The emulsion-templated fibrin-based scaffolds were initially hypothesized to promote faster revascularization as fibrin itself is pro-angiogenic. However, this does not seem to be the case for EmDerm-F scaffolds, compared the other scaffolds.

Although there was no obvious systemic inflammatory response in the animals to the scaffolds, there was a notable local inflammatory effect at Day 7 post-implantation in both the abraded and non-abraded wound models. This is rather unsurprising as inflammation is part of the wound healing response. Nevertheless, the inflammatory response appears to resolve by Day 14. This is in contrast to Matriderm and Integra where the inflammatory response persists beyond Day 14 in a full-thickness defect rat wound healing model. (187) The inflammatory phase is followed by a rather rapid vascularization and remodelling of the neodermis by Day 14. Also, extracellular matrix deposition was more pronounced in EmDerm-F compared to the other two scaffolds. This effect can be explained by the increased production and secretion of growth factors, collagen production and degradation enzymes, as described in Chapter 4.

Interestingly, the degree of local inflammatory response and vascularization was not significantly affected by type of wound (abraded vs non-abraded) but rather, the type of material the scaffolds were made of. The release of fibrin degradation products in EmDerm-CF and EmDerm-F may have resulted in a greater inflammatory response compared to EmDerm-C scaffolds. (192) This may be due to poorer stability with EDC/NHS cross-linking for the fibrin scaffolds, which degraded rapidly compared to collagen scaffolds (see Chapter 3).

Another explanation is that the slightly higher endotoxin levels in EmDerm-CF and EmDerm-F scaffolds could have triggered the local inflammatory response due to incomplete washout of residual during scaffold hydration and preparation. However, the endotoxin levels were minimal according to the LAL assay across all three scaffolds and is within the acceptable endotoxin level limits. There may also be incomplete washout of the residual surfactants (Tween 20 and Span 20) which may have resulted in a degree of inflammation around and within the scaffold post-implantation. This may be because the EmDerm-CF and EmDerm-F scaffolds were slightly thicker than EmDerm-C scaffolds and more surfactant molecules may be trapped within the scaffolds even after washing. However, this is unlikely as the in vitro assays demonstrate good cell proliferation in all scaffolds.

Overall, the degree of inflammation noted for EmDerm scaffolds is minimal and transient. Most of the inflammatory cells (e.g. polymorphonuclear cells) are seen in Day 7 biopsies but resolve by Day 14. The degree of inflammatory response correlate somewhat to the endotoxin levels and enzymatic stability of the EmDerm scaffolds with EmDerm-C having the lowest endotoxin levels and slowest degradation rate, while EmDerm-F has the highest endotoxin levels and fastest degradation rate.

It is also interesting to note that there were notable differences in extracellular matrix remodelling between the various EmDerm scaffolds when implanted in vivo, despite using the same emulsion-templating manufacturing methods. This suggests that the type of material used to create the scaffolds significantly influences the cell behaviour in the acute wound environment. This is especially apparent for EmDerm-F scaffolds where higher amounts of extracellular matrix is laid down, compared to other EmDerm scaffolds.

5.5. Summary

In conclusion, in vivo results suggest that EmDerm scaffolds are biocompatible and promote wound healing and vascularization over a two-week period. There is a mild-to-moderate inflammatory response around and within the scaffolds on Day 7, but this effect is transient and resolves by Day 14. EmDerm-C had the least inflammatory response and highest degree of vascularization of the neodermis. The outcomes of this study are encouraging as they demonstrate that EmDerm scaffolds integrate well into wounds. However, there is a need to further validate the results from this study to other wound healing models such as porcine wound healing models and chronic wound healing models before translation into clinical trials.

Chapter 6 Electrospun Membranes as Epidermal Skin Substitute

6.1. Introduction

The culture of keratinocytes was first introduced by Rheinwald and Green using a feeder layer of irradiated fibroblasts. (193) Since then, cultured epithelial autografts (CEA) have been introduced to replace the epidermal layer in patients with large surface area burns or wounds. (194) However, the disadvantages of CEA is that there is a delay between cell harvesting and culturing the keratinocytes into sheets, the risks of infection, poor engraftment and high costs which limits the clinical application of CEAs. (194) Use of cultured epidermal allografts have also been gradually declining due to inherent problems such as blistering and tearing of the fragile epidermal layer during treatment, necessitating further regrafting surgeries. (195)

Subconfluent keratinocytes grown on a delivery system have been developed to circumnavigate the problem of long culture times and use of enzymatic dissociation to separate the confluent sheets of keratinocytes from the feeder layers. (196) One such example is LaserSkin which is made up of autologous keratinocytes grown on a hyaluronic acid laser-perforated matrix. (197) This obviates the need for harvesting split-thickness skin grafts, the current gold standard for replacing areas of skin loss.

Spray-based delivery of keratinocytes have also been developed such as ReCell and MySkin. However, there is still a need for an epidermal carrier system for delivery of keratinocytes as the spray-based technique is inefficient and associated with high loss of non-adherent cells. It also does not allow for cell expansion and lacks the physical properties of the epidermal layer which acts as a barrier to prevent excessive heat and water loss. (39)

One approach for managing such extensive areas of skin loss is to use a bioengineered epidermal skin substitute, which is not only capable of integrating into the wound bed, but also acts as a substrate for

supporting cell attachment and proliferation. More recently, synthetic polymers such as poly DL-lactide and ε-caprolactone copolymer have been used to develop an epidermal skin substitutes (e.g. Suprathel) which recapitulate the functions of the epidermis. (48,198) However, it does not integrate into the wound nor support growth of keratinocytes on the matrix itself.

Various tissue-engineering approaches have been employed to create skin substitutes to replace and restore the function of skin. The native architecture of skin is made up of various extracellular matrix (ECM) components, which form a fibrillar meshwork for cellular attachment and proliferation. (199,200) Electrospinning is a method of generating fine fibres by applying a high voltage to polymer solutions. (201) The structure of these fine fibres mimics the native extracellular matrix of the epidermal and dermal skin layers, which may provide surface topographical cues guiding cellular migration and proliferation. (202)

Electrospinning can be done with either natural materials such as gelatin and collagen or synthetic materials such as polycaprolactone, poly-L-lactide and poly (lactic-co-glycolic acid). Synthetic polymers have desirable mechanical properties while gelatin, which is produced from partially denatured collagen, is itself highly biocompatible as it has cell-binding motifs which provides recognition sites for cells to bind. (14)

Polycaprolactone (PCL) is an FDA-approved, biodegradable, biocompatible polyester which is commonly used to make medical devices e.g. sutures (Monocryl), implants and wound dressings. (203) It's degradation product – caproic acid, can be metabolized and excreted by the body renally. Depending on the molecular weight (MW) of the polymer, the degradation of PCL can take up to one to two years, which limits its use for wound healing purposes. (204) They are also known to be rather hydrophobic which makes it difficult for cells to be seeded on PCL-based materials.

Poly-L-lactic acid (PLLA) is another FDA-approved, biodegradable, biocompatible polyester which is commonly used for three-dimensional (3D) printing and disposable packaging. It can be broken down into lactic acid which is non-toxic and also renally excreted. PLLA is commonly used in bone tissue engineering due to its high tensile strength (205) and is medically approved for use as an injectable filler in cheek atrophy. (206)

Poly (lactic-co-glycolic acid) (PLGA) is yet another FDA-approved, biodegradable, biocompatible polyester which can be metabolized into lactic acid and glycolic acid which are by-products naturally eliminated by the body. Degradation of PLGA depends on the ratio of lactide to glycolide in the polymer itself and can range from 2 to 6 months. (207) They are commonly used to make biomedical devices such as sutures, prosthesis and implantable drug delivery devices. (208)

In this study, several candidate pure polymer and hybrid gelatin/polymer solutions, which are FDA approved, biodegradable and biocompatible have been chosen for evaluation as electrospun epidermal constructs. The objective of this research is to develop an epidermal carrier which supports keratinocyte growth by acting as a pseudo-basement membrane and integrates into the wound surface itself.

6.2. Materials and Methods

Materials

Polymers used for electrospinning are as follows: polycaprolactone (PCL) M_w 85 000 purchased from Sigma, poly (lactic-co-glycolic acid) (PLGA) 75:25 (Resomer RG 756) M_W 56 000 purchased from Sigma, poly-L-lactide (PLLA) (Purasorb PL 32) obtained from Corbion Purac. Gelatin from porcine skin Type A, Bloom 300 was purchased from Sigma and hexafluoroisopropanol (HFIP) was purchased from Apollo Scientific. Dulbecco's phosphate buffered saline (DPBS) and Trypsin-EDTA 1X was purchased from Gibco. Live/Dead and MTT 3-(4,5-dimethythiazol-2-yl)-2,5-diphenyltetrazolium

bromide assays were purchased from ThermoFisher Scientific. Human epidermal keratinocytes (HEK) cells were purchased from Invitrogen while Human Keratinocyte Growth Supplement (HKGS) and EpiLife media were purchased from Life Technologies.

Preparation of solutions

Polymer solutions were prepared by dissolving the polymer or polymer/gelatin mixture in HFIP overnight at room temperature. The following standardized compositions were used: 8% w/v of PCL, 8% w/v of PCL/gelatin (at 3:1 v/v ratio), 8% w/v of PLLA, 8% w/v of PLLA/gelatin (at 3:1 v/v ratio), 12% w/v of PLGA, 12% w/v of PLGA/gelatin (at 3:1 v/v ratio).

Experimental Setup

Each polymer solution was loaded into a 5ml syringe connected to a 21G blunt needle, driven through 3 feet of PTFE tubing using a syringe pump (Harvard USA). The opposite end of the tubing was connected to a custom-made copper head and the desired voltage was applied using a high voltage power supply (Genvolt, UK, Model 73030). The distance between the positively charged copper head and negatively charge collecting plate was set to 13.5cm. The voltage and pump rate for each polymer solution or mixture was varied until a stable Taylor's cone was observed and a mat of fibres were visible on the collecting plate.

Settings optimized for each of the polymer solutions or mixtures are as follows: 11.5kV at 1ml/hr for 8% PCL, 8% PCL/gelatin, 8% PLLA, 8% PLLA/gelatin, 12% PLGA and 12% PLGA/gelatin. All electrospinning experiments were done under 1 bar of nitrogen at room temperature for approximately 20 minutes. All electrospun fibre mats were kept under the fume hood overnight to ensure residual HFIP solvent was completely removed.

Characterization of electrospun membranes

Fibre morphology and diameter

The morphology and diameter of the electrospun fibres were determined by scanning electron microscopy (SEM). Samples were sputter coated with gold for 60 seconds before imaging under SEM. Images at five different positions were taken for each sample. Mean and standard deviation of diameters of 50 randomly selected fibres per frame were calculated using Image J (NIH, USA).

Membrane porosity

Porosity is an important determinant for migration of cells through scaffolds as well as biodegradability. The porosity of electrospun membranes was estimated using the following formula (209):

$$Porosity\ (\%) = 100 \times [1 - (apparent\ density / material\ density)]$$

whereby apparent density is calculated using the formula:

$$Apparent\ density = mass\ of\ scaffold / (area \times thickness\ of\ scaffold).$$

Mechanical properties

The mechanical properties of each electrospun membrane were measured using a universal testing machine (Instron, USA). The samples were cut into rectangular strips measuring 40mm x 2mm x T (where T represents a variable thickness, depending on type of electrospun membrane used). A uniaxial force was applied at a rate of 10 mm/min using a 100g load cell. Stress-strain curves were plotted using force-displacement data obtained. From the stress-strain curves, ultimate tensile strength and Young's modulus of each membrane was obtained.

Membrane degradation

Membrane degradation was determined by change in mass of the electrospun membranes after incubation in 0.25% Trypsin-EDTA solution for 7 days at 37 °C at 5% CO_2. At Day 1, 3 and 7, the

membranes were removed, washed with PBS, vacuum-dried and weighed. Percentage original mass (%) was calculated using the formula below:

Percentage original mass (%) = measured mass / original mass x 100%

Membrane contraction

Each electrospun membrane was cut into rectangular strips measuring 30mm x 10mm and incubated in Dulbecco's phosphate buffered saline (DPBS) for 30 days at 37°C at 5% CO_2. After 30 days, the membranes were removed from DPBS and air-dried overnight. Change in area of the electrospun membranes was measured and percentage membrane shrinkage was calculated as shown below:

Percentage membrane shrinkage (%) = (initial area – measured area) / initial area x 100%

Biocompatibility of the electrospun membranes

Cell viability (Live/Dead assay)

Cell viability of human epidermal keratinocytes seeded was determined using the Live/Dead assay on Day 7 and 14. The assay discriminates live from dead cells by staining live cells with green-fluorescent calcein-AM to indicate intracellular esterase activity and dead cells with red-fluorescent ethidium homodimer-1 due to loss of plasma membrane integrity. Each electrospun membrane was cut into 10 mm x 10 mm squares and placed in a 24 well plate. The membranes were sterilized under UV light and soaked in PBS for 1 hour prior to cell seeding. Human epidermal keratinocytes in Epilife media + Human Keratinocyte Growth Factor (HKGS) + Penicillin/Streptomycin/Amphotericin were seeded at 1 x 10^4 cells/ml cell density and media was changed every alternate day. Live/Dead solution was added on Day 7 and 14 after removal of cell media and cells were imaged using Nikon Confocal Microscope whereby live cells were green and dead cells were red. The percentage of live cells was quantified for each membrane. Each experiment was done in triplicates.

Cell proliferation

Cell proliferation of seeded keratinocytes was measured by the colorimetric MTT 3-(4,5-dimethythiazol-2-yl)-2,5-diphenyltetrazolium bromide assay on Days 3, 7 and 14. Each electrospun membrane was cut into 10 mm x 10 mm squares and placed in a 48 well plate. The membranes were sterilized under UV light and soaked in PBS for 1 hour prior to cell seeding. Human epidermal keratinocytes in Epilife media + Human Keratinocyte Growth Factor (HKGS) + Penicillin/Streptomycin/Amphotericin were seeded at 1 x 10^3 cells/ml cell density and media was changed every alternate day. 20µl of 12mM of MTT solution (or 5mg/ml) was added on Day 3, 7 and 14 after removal of cell media and formazan was solubilized using 100µl Dimethyl sulfoxide (DMSO). The resulting solution was transferred to a 96 well plate and the optical density (OD) was read at 540nm wavelength on a multiplate reader (Tecan Life Science, Switzerland) in triplicates.

Immunohistochemistry

Each electrospun membrane was cut into 10 mm x 10 mm squares and placed in a 24 well plate. The membranes were sterilized under UV light and soaked in PBS for 1 hour prior to cell seeding. Human epidermal keratinocytes in Epilife media + Human Keratinocyte Growth Factor (HKGS) + Penicillin/Streptomycin/Amphotericin were seeded at 1 x 10^4 cells/ml cell density and media was changed every alternate day. At Day 10, the seeded membranes were fixed using 4% paraformaldehyde at 4 °C overnight. Each membrane was then washed with PBS for 5 minutes twice. Following that, each scaffold was permeabilized with 0.25% Triton-X for 10 minutes, before rinsing twice with PBS again. 5% bovine serum albumin was added and allowed to incubate for 30 minutes to reduce non-specific binding. Phalloidin (50 µg/ml) was then added to stain actin filaments and left for 1 hour at room temperature and then removed. Finally, Hoescht solution was added for 5 minutes to stain the nuclei and then removed. Each scaffold was further washed with PBS twice and imaged using Nikon Confocal Microscope at 10x magnification.

Statistical analysis

All data are expressed as mean ± SD. Results were analysed using one-way analysis of variance (ANOVA) to evaluate statistical significance between comparisons with post-hoc Tukey test. Repeated measures ANOVA was used for the values which were measured repeatedly at different time points. A value of $p<0.05$ was considered to be statistically significant. Where applicable, * denotes a p–value of <0.05, ** denotes a p–value of <0.01 and *** denotes a p-value of <0.001. All statistical analysis was performed using GraphPad Prism Version 4.0 for Windows.

6.3. Results

Fibre morphology and diameter

Figure 6-1 shows the morphology of each of the electrospun fibre mats. 8% PCL, 8% PCL/gelatin, 8% PLLA, 8% PLLA/gelatin, 12% PLGA and 12% PLGA/gelatin solutions all formed smooth fibrous mats. The mean fibre diameter for PCL and PCL/gelatin is approximately 2 microns thick by SEM (see Table 6-1). Addition of gelatin resulted in a small decrease in mean fibre diameter for each polymer solution with the effect being most pronounced for PLLA. A concentration of 12% PLGA and 12% PLGA/gelatin was used instead of 8% as beaded fibres were obtained when 8% solutions were used for PLGA and PLGA/gelatin solutions.

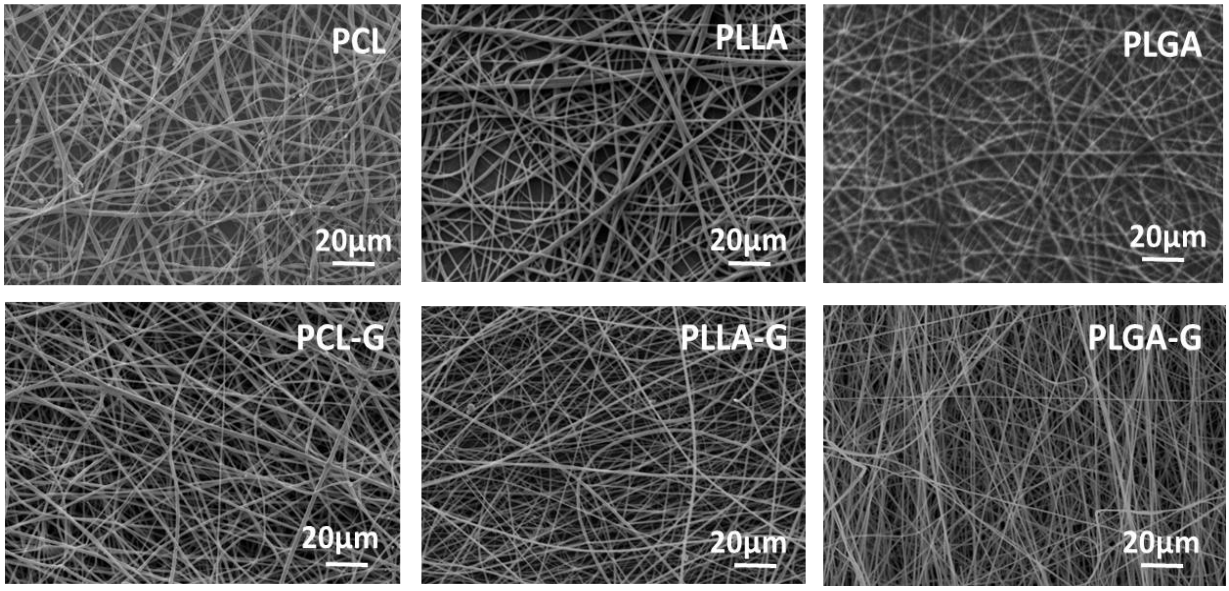


Figure 6-1 Scanning electron microscopy (SEM) images of all electrospun scaffolds. (scale bar = 20 µm, n=3)

Material	Fibre diameter (µm) Mean ± SD
PCL	2.02 ± 0.75
PLLA	1.95 ± 0.52
PLGA	1.20 ± 0.51
PCL/gel	1.89 ± 0.64
PLLA/gel	1.51 ± 0.51
PLGA/gel	1.12 ± 0.38

Table 6-1 Summary of fibre diameter of all electrospun membranes (mean ± SD, n=3).

Membrane porosity

Using the formula as stated earlier, PCL/gelatin and PLGA/gelatin appeared to be least porous at porosity of about 58% and 75% respectively. PLLA and PLLA/gelatin appeared to be most porous achieving porosities of about 87% and 85% respectively. Addition of gelatin to polymer solutions appears to have resulted in a decrease in porosity of electrospun scaffolds. This may be due to smaller mean diameter of fibres, which result in a higher fibre density per cross-sectional area of the scaffolds. A porosity of more than 80% is considered to be ideal for allowing cell infiltration into scaffolds. This was achieved for all electrospun scaffolds apart from PCL/gelatin and PLGA/gelatin (Table 6-2).

Material	Porosity (%) Mean ± SD
PCL	81.95 ± 1.79
PLLA	87.16 ± 1.67
PLGA	83.86 ± 1.41
PCL/gel	58.27 ± 2.96
PLLA/gel	85.81 ± 0.05
PLGA/gel	75.60 ± 0.97

Table 6-2 Summary of porosity results of all electrospun membranes (mean ± SD, n=3).

Mechanical properties of the membranes

Electrospun PCL membranes were rather brittle and was least elastic with a Young's modulus of 10.9 MPa and least strong with a tensile strength of 2.56 MPa. Addition of gelatin appeared to improve the elasticity and tensile strength of PCL. However, addition of gelatin resulted in decrease in Young's modulus and tensile strength of PLLA and PLGA. PLLA electrospun membranes appeared to be most

elastic with a Young's modulus of 162.1 ± 61.3 MPa and had the highest tensile strength (8.08 ± 1.04 MPa). A summary of the results is shown below in Table 6-3.

Material	Young's modulus (MPa) Mean ± SD	Tensile strength (MPa) Mean ± SD
PCL	10.9 ± 5.61	2.56 ± 0.53
PLLA	162.1 ± 61.3	8.08 ± 1.04
PLGA	152.1 ± 20.7	5.41 ± 1.63
PCL/gel	52.4 ± 13.9	5.35 ± 0.46
PLLA/gel	126.8 ± 24.0	6.07 ± 0.50
PLGA/gel	145.5 ± 33.6	5.10 ± 0.48

Table 6-3 Summary of mechanical properties of all electrospun membranes by tensile testing (mean ± SD, n=3).

Membrane degradation

Figure 6-2 shows the degradation profile of each pair of pure polymer and gelatin-polymer electrospun membrane. Addition of gelatin did not appear to significantly alter the degradation rate of electrospun PCL or PLGA membranes. However, PLLA/gelatin membranes appear to degrade significantly faster than pure PLLA electrospun membranes. This may be attributed to a variety of reasons. Addition of gelatin to PLLA may have resulted in increased hydrophilicity of the PLLA/gelatin electrospun membrane and increase in surface area as gelatin is degraded by trypsin.

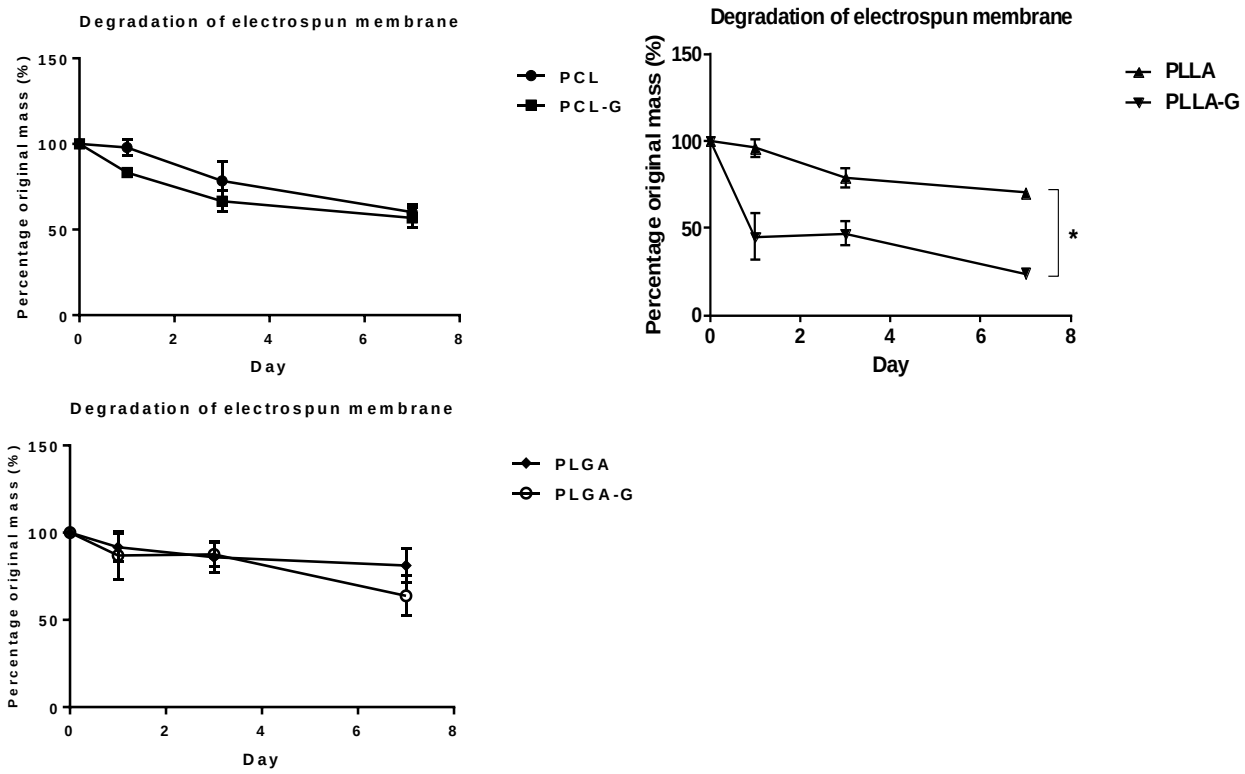


Figure 6-2 Hydrolytic degradation profiles of electrospun membranes incubated in DPBS on Day 1, 3 and 7 showing greatest reduction in percentage original mass of PLLA/gelatin over 7 days ($p < 0.05$, $n=3$)..

Membrane contraction

PLGA and PLGA/gelatin membrane contracted to a greater extent compared to other membranes. As shown in Figure 6-3, PLGA and PLGA/gelatin membranes shrank by about 70 – 80% compared to the original size of the membranes. Reduction in area of membrane was least for PCL and PCL/gelatin membranes. Addition of gelatin appears to increase the degree of contraction of the electrospun membrane, however this effect was only significant for PCL-G. The contraction of electrospun scaffolds may be due to reorganization or partial degradation of electrospun fibres and appear to be most for PLGA based electrospun materials, followed by PLLA and PCL based membranes. It may also be an effect of fibre shrinkage upon hydration of these electrospun membranes.

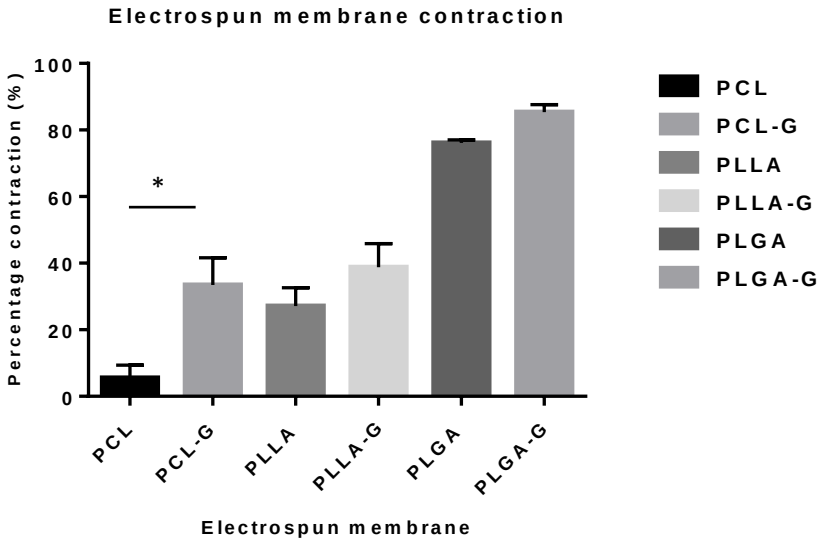


Figure 6-3 Electrospun membranes were hydrated in DPBS for 30 days. Reduction in mean area of electrospun scaffolds were greatest for PLGA and PLGA/gelatin scaffolds and least for PCL and PLLA scaffolds. There was significant increase in membrane contraction in PCL-G membranes compared to PCL membranes ($p<0.05$, $n=3$).

Membrane biocompatibility

All keratinocytes seeded on the electrospun scaffolds showed cell viability of above 70%. Hybrid gelatin-polymer membranes had improved cell viability at Day 7 and Day 14, compared to pure polymer membranes, however this was not statistically significant (Figure 6-4). The MTT assay demonstrated that keratinocytes seeded on PCL/gelatin, PLLA/gelatin and PLGA/gelatin had the higher proliferation rate as measured by absorbance on Day 7 and Day 14, compared to pure polymer electrospun membranes (Figure 6-5). Metabolic activity as measured by the MTT assay was significantly higher on Day 14 compared to Day 3 or Day 7 across all electrospun scaffolds. These results are consistent with the cell viability assays. In terms of morphology of cells, the keratinocytes appear to adopt a more flattened and stretched out morphology on hybrid scaffolds compared to pure polymer scaffolds, indicating greater cell attachment and migration (Figure 6-5). Thus, addition of gelatin to polymer solutions appears to increase the biocompatibility of the electrospun membranes.

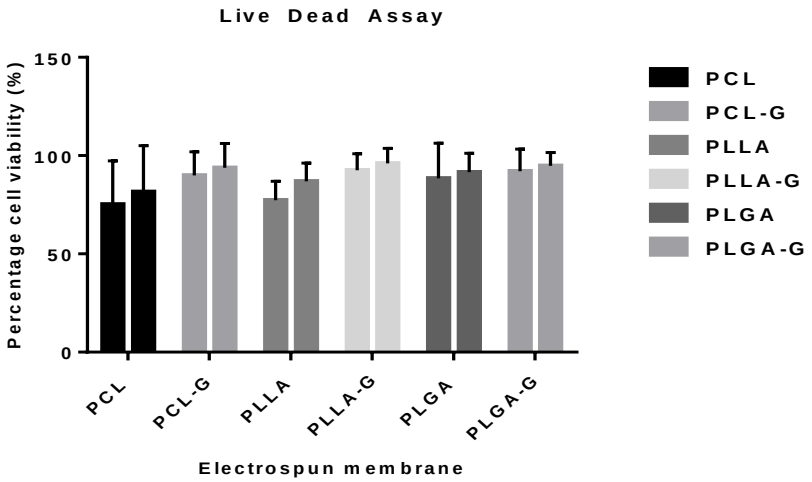


Figure 6-4 Live/Dead assay of human epidermal keratinocytes on electrospun membranes on Day 7 and Day 14 showing high cell viability (>70%) across all electrospun scaffolds. Hybrid scaffolds had higher mean percentage cell viability compared to pure polymer scaffolds but was not statistically significant ($p>0.05$, $n=3$).

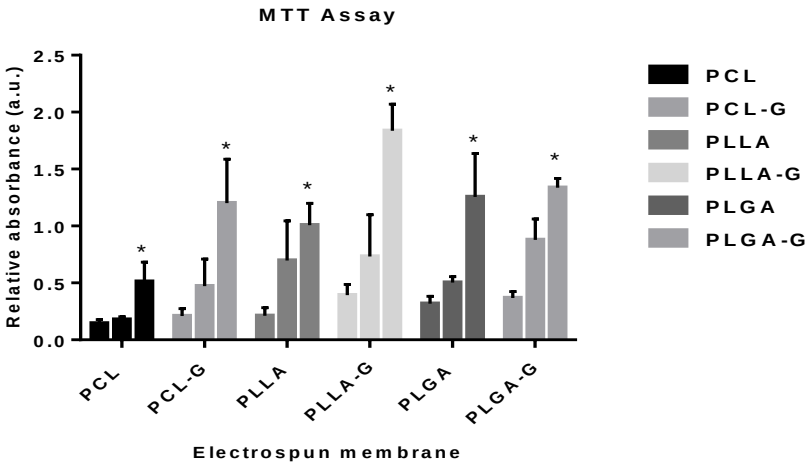


Figure 6-5 Cell proliferation (MTT) assay of human epidermal keratinocytes on electrospun membrane on Day 3,7 and 14 showing significant increase cell proliferation in all electrospun membranes by Day 14, as compared to Day 3. The effect is more pronounced in hybrid scaffolds compared to pure polymer scaffolds but was not statistically significant ($p>0.05$, $n=3$).

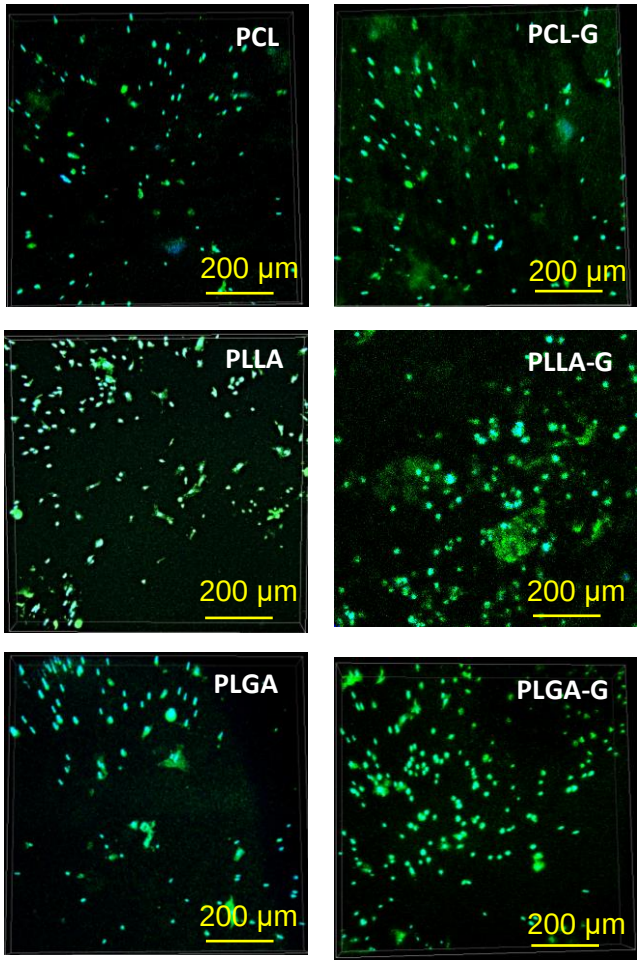


Figure 6-6 Confocal microscopy of keratinocytes cultured on electrospun membranes stained with Phalloidin and Hoescht. Keratinocytes on hybrid membranes appear to have a more flattened, spread-out morphology (especially on PLLA-G) compared to polymer only membranes at 10x magnification (scale bar = 200 µm, n=3)

6.4. Discussion

Effect of gelatin on fibre density and porosity of electrospun scaffolds

Addition of gelatin resulted in thinner fibre diameters of electrospun scaffolds. This may be due to change in the dielectric properties of the blended polymer solution, resulting in finer fibres. The amino acid side chains of gelatin may become protonated or deprotonated depending on local pH, thus affecting the conductivity of the polymer solution during electrospinning process. (210) There has been a lot of debate with regards to the ideal size of fibre diameter for tissue engineering purposes. Although nanofibres are thought to be mimic the fibrillar nature of collagen (about 300 nm wide), dense nanofibers often result in smaller pore sizes and thus, prohibit cellular ingress and scaffold

integration.(211,212) According to literature, the preferred porosity range of scaffolds for infiltration of cells ranges from 60% - 90%. (213)

Larger microfibers with diameters of one to two microns were found to facilitate cell adhesion and proliferation whilst mimicking the fibrous architecture of native extracellular matrix. (214,215) The increase in fibre size also resulted in greater interfibre distances, which contributed to greater porosity of the electrospun scaffolds. Additionally, the electrospun membranes were not cross-linked to preserve porosity and elasticity of the membranes. In this study, the electrospun membranes developed from polymer-gelatin blends all had fibre diameters between one to two microns and PLLA/gelatin had a porosity of >80% which makes it ideal for cell attachment, proliferation and migration.

Effect of gelatin on mechanical properties of electrospun scaffolds

Addition of gelatin to PLLA and PLGA appears to reduce elasticity and tensile strength of the electrospun membranes. Interestingly, the opposite was found to be true for PCL. This may be related to the decrease in porosity of PCL/gelatin scaffolds, resulting in a higher fibre density per cross-sectional area and therefore improved mechanical properties of the membrane. As mean tensile strength of skin is approximately 3 - 20 MPa and the average Young's modulus of skin is about 100 - 150 MPa (216), all the electrospun hybrid and pure polyer scaffolds, apart from PCL, fall into this range making them ideal as skin substitutes in terms of mechanical properties.

The considerable contraction of PLGA and PLGA/gelatin scaffolds upon hydration makes them less suitable as epidermal carriers. This phenomenon may be due to the fibre shrinkage and molecular realignment of PLGA and PLGA/gelatin fibres which have partially degraded, resulting in compromise of its structural integrity. Light microscopy of partially hydrolyzed PLGA and PLGA/gelatin membranes showed patchy areas of defects, which may account for the significant contraction of these

membranes. This poses a disadvantage for PLGA-based materials as skin scaffolds as shrinkage of the material would inhibit cell infiltration and may cause significant scarring.

PLGA is known to degrade the most rapidly out of all three polymers selected and its degradation rate can be altered by changing the ratio of glycolic acid to lactic acid of PLGA. (207,208) It is also known to crystallize when heated which may affect its glass transition temperature, resulting in shrinkage as well. (217) In contrast, PCL/gelatin, PLLA/gelatin, PCL and PLLA appear to contract to a lesser extent which is comparable to the degree of contraction of native skin (approximately 20%). (218)

Effect of gelatin on biocompatibility of electrospun scaffolds

Addition of gelatin appears to improve the biocompatibility and biodegradability of the electrospun scaffolds. Gelatin is derived from denatured collagen, which is a major structural protein in biological tissues with cell binding motifs. This provides topographical cues for cell attachment, migration and proliferation. (219) This corresponds with our findings of improved cell viability and proliferation for hybrid membranes compared to pure polymer membranes. However, this did not reach statistical significance, as the polymers were themselves highly biocompatible.

Addition of gelatin also resulted in improved biodegradability of PLLA/gelatin scaffolds, but not PCL/gelatin or PLGA/gelatin scaffolds. This may be due to increase in hydrophilicity of PLLA/gelatin scaffolds which allows for greater hydrolysis of PLLA/gelatin fibres. Also, as gelatin is digested by trypsin, it leaves behind cavities which exposes a greater surface area to volume ratio of PLLA exposed for hydrolytic degradation. This effect may be less pronounced for PCL/gelatin and PLGA/gelatin as PCL and PLGA are less hydrophobic than PLLA.

6.5. Summary

Addition of gelatin to polymer solutions resulted in electrospun fibrous mats with good mechanical properties, biocompatibility and biodegradability. In general, hybrid membranes performed much better in terms of biocompatibility and biodegradability compared to pure polymer electrospun membranes. However, PCL/gelatin membranes were least porous (<60%) and PLGA/gelatin membranes had significant contraction. Thus, by process of elimination, electrospun PLLA/gelatin membranes appear to be most suitable as epidermal skin substitutes due to its superior mechanical properties, greater porosity and biocompatibility compared to other electrospun membranes.

Chapter 7 Conclusion and Future Work

7.1. Conclusions

In this thesis, a novel bio-engineered skin substitute for the dermal and epidermal layers comprising of an emulsion-templated dermal scaffold and an electrospun epidermal membrane was developed for clinical application in partial and full-thickness wounds. To do so, protein behaviour in emulsions were studied using various techniques such as confocal microscopy to examine protein localization in emulsions, circular dichroism and tryptophan fluorescence to investigate changes in protein conformation after exposure to the emulsions, as well as lactate dehydrogenase enzyme assay to quantify changes in protein function after incubation in emulsions.

Using data from the above experiments, a biocompatible emulsion system was proposed using a non-ionic surfactant blend, inert oil phase and an aqueous buffer. This biocompatible emulsion system was used to develop three types of emulsion-templated scaffolds (EmDerm) using collagen, collagen-fibrin and fibrin. Parameters for control of emulsion droplet sizes were investigated which allowed for control of scaffold porosity. A range of excipients and freeze-drying parameters were tested to examine their effects on nanostructure of the scaffolds using scanning electron microscopy.

The EmDerm scaffolds were tested for biocompatibility using in vitro assays and in vivo experiments using rat wound healing models. The mechanical properties and degradation rate of both EmDerm scaffolds and electrospun membranes were also tested in vitro.

The main conclusions from this body of work are:

1) **Non-ionic surfactants protect proteins from denaturation in oil-in-water emulsion systems**. Surfactants are necessary to stabilize the oil-water interface and to create minute droplets in emulsion systems. These droplets act as porogens to create emulsion-templated scaffolds with tuneable pore sizes. Non-ionic surfactants were found to reduce denaturation of proteins in

emulsion systems. The mechanism by which this occurs is likely through competitive adsorption. Non-ionic surfactants preferentially adsorb onto the interfacial boundaries, thus preventing protein molecules from adsorption which alters their native conformation. This keeps the proteins in the bulk aqueous phase where they remain functionally intact. This effect is dependent on concentration of surfactants available, as there needs to be sufficient surfactants to completely cover the interfacial regions but not excessively so such that the surfactants bind to protein molecules and cause aggregation and hindrance to the active site of enzyme proteins.

2) **Emulsion-templating can be used to template native protein hydrogels to create microporous protein scaffolds.**

Emulsions have been used to template polymers, polysaccharides and a limited range of proteins e.g. BSA, gelatin. Using a non-denaturing biocompatible emulsion system, both an enzymatic reaction between thrombin and fibrinogen and thermal gelation of collagen was found to be preserved. Moreover, size of emulsion droplets corresponded closely with size of pores of the resulting scaffolds which can be tuned according to the desired function of the scaffold.

3) **Choice of excipients and freeze-drying parameters affect the fibrillar nanostructure of emulsion-templated scaffolds.**

A range of excipients were tested to examine the effect of freeze-drying to preserve the nanostructure of emulsion-templated scaffolds. P68, a polaxamer with a central hydrophobic chain flanked by two hydrophilic chains, was found to best preserve the nanostructure of EmDerm scaffolds. Rate of warming during freeze-drying was found to affect the fibrillar nanostructure of the scaffolds. A slower rate of 0.3°C/min and a freezing temperature (T_f) of below -30°C was found to prevent melt-back during the drying phase.

4) **Emulsion-templated scaffolds are biocompatible and promote cell proliferation in both monoculture and co-culture experiments.**

EmDerm scaffolds were all biocompatible and supported cell proliferation of human epidermal keratinocytes, human dermal endothelial cells, human dermal fibroblasts and human bone-marrow derived mesenchymal stem cells. There was also good cellular ingress into EmDerms when co-cultured with HEK/HDF, HDF/HDE and MSC/HDE. In particular, co-culture of HDFs and HDEs in EmDerm-C scaffolds appear to promote formation of tubule-like vascular structures in vitro.

5) **Emulsion templated scaffolds result in localized inflammation in the first week of the wound healing process while vascularization and matrix remodelling occur after the initial inflammatory phase**.

   In vivo results suggest that there is an initial local inflammatory response associated with implantation of EmDerm scaffolds which initiates a later vascularization phase and matrix remodelling. This may be due to mechanical forces, residual surfactant molecules or endotoxin presence which have not been completely washed out of the scaffolds. Vascularization and matrix remodelling occur due to secretion of growth factors, degradative enzymes and structural proteins as described in Chapter 4.

6) **Electrospun membranes act as a suitable carrier for keratinocytes, as an epidermal substitute**.

   Electrospun membranes support keratinocyte proliferation, which can be overlaid on top of the dermal layer to reconstitute a bilayer skin construct. The PLLA/gelatin electrospun membrane had ideal mechanical properties and biocompatibility for keratinocyte growth. This allows autologous keratinocytes to be harvested and grown separately whilst the dermal substitute revascularizes for a two-stage reconstruction procedure.

7.2. Future Work

Studying effect of buffers on protein-surfactant interaction

The nature of protein-surfactant interaction is affected not only by the type and concentration of protein and surfactant, but also the effect of aqueous buffer on protein charge and surfactant charge. There may

also be an effect of temperature and presence of other molecules or excipients present within the system. Protein functionality is dependent on pH and thus, conformation changes may occur depending on type of buffers used as well.

In our emulsion system, only MES/NaCl buffers were used. Other potential buffer systems include phosphate buffers, citrate buffers, acetate buffers, Tris buffers, HEPES buffers and more. The choice of buffer depends on the pKa of the buffers as there is a trade-off between buffering capacity and ionic charge present in the aqueous system.

Formulation of other biocompatible emulsion systems

The results of this study show that emulsion-templating is a technique which can be applied to create any gellable protein hydrogel scaffold using a non-ionic surfactant. In this thesis, only Tween 20/Span 20 surfactants were used. Thus, it is reasonable to extend the range of surfactants to other types of non-ionic surfactants e.g. Triton family, Brij family and more. These surfactants may confer better stability and less toxicity to cells compared to surfactants from the Span and Tween family.

In our study, a higher concentration of Tween/Span resulted in decreased biocompatibility of emulsion-templated scaffolds which may be due to smaller pore sizes and surfactant residues remaining in the scaffold. There is also a limit for reducing the concentration of Tween/Span surfactant mix as the emulsions formed may become unstable and coalesce. Therefore, alternative non-ionic surfactants may be needed to achieve both emulsion stability and biocompatibility.

Manufacture of other emulsion-templated protein scaffolds

In this study, only two native proteins were tested – collagen and fibrin. The range of emulsion-templated protein scaffolds can be extended to include other extracellular matrix such as hyaluronan, heparan sulfate, chondroitin sulfate, elastin, fibronectin and laminin. The range of EmDerm scaffolds

can also be expanded by including biodegradable polymers to the protein scaffolds to improve mechanical properties and degradation profile of the scaffolds such as polyvinyl alcohol, polydioxanone, polyglactin, poliglecaprone and more.

In our lab, emulsion-templated collagen-hyaluronic acid, collagen-chondroitin sulfate and collagen-elastin have been developed using the Tween 20/Span 20 emulsion system. However, the pore sizes were rather non-uniform and the protein-emulsion system was unstable. In a separate study, fibrin-PVA emulsion templated scaffolds appear to have improved mechanical properties and was shown to be biocompatible as well. This could be extrapolated to other polymers as well.

Optimization of manufacturing process for batch consistency

It was also noted that there was some batch-to-batch differences in some of the scaffolds manufactured in our lab despite using the same manufacturing steps and parameters. This may be due to need for further optimization of lyophilization parameters e.g. rate of cooling and heating ramp, duration of primary and secondary drying, need for a more consistent mixing technique and choice of excipients e.g. other salts, sugars and polymers. There may also be batch-to-batch differences in quality of collagen and fibrinogen obtained from commercial suppliers which are not medical-grade materials. Therefore, sourcing of materials is another factor which needs to be taken into consideration for commercialization of EmDerm scaffolds.

Combining the electrospun membrane and emulsion-templated scaffold to create a bilayer

In this study, the emulsion-templated scaffold and electrospun membrane are manufactured and for use in a two-stage reconstruction. However, there may be potential for combining both to create a bilayer construct for use in single stage reconstruction. The electrospun membrane can act as a biocompatible semi-permeable membrane overlying the emulsion-templated scaffold which integrates into the wound.

However, the harvesting of sufficient skin cells for immediate implantation would remain an issue, especially in large surface area burns. There would still need to be a period of time for expansion of keratinocytes for seeding autologous cells onto the electrospun membrane and fibroblasts onto the emulsion-templated scaffolds. An alternative is to use the bilayer scaffold to create a seeded epidermal-dermal skin substitute using allogenic cells for application in extensive burns and wounds which is similar to Apligraf.

Further in vivo testing and clinical trials

Although initial in vivo work to ensure biocompatibility of the EmDerm scaffolds has been performed, there is still a need to further test the scaffolds for efficacy in animal models for full-thickness burns and chronic wound models. Currently, animal study protocols have been written up for murine and porcine burns wound healing model and a delayed burn wound healing model where tangential excision is performed a week after initial burn injury using a heated iron rod. Scaffolds are then implanted onto the wounds and biopsies taken every other week up to 6 weeks.

There is also a need to investigate the nature of the initial inflammatory phase response when these scaffolds are seeded and to minimize this if possible. Immunohistochemistry staining for neutrophils, lymphocytes, regulatory T cells in biopsy samples could give a better idea of types of inflammatory response occurring locally. Meanwhile, flow cytometry to look for inflammatory cells present in blood samples could also give further insight into haematological changes occurring due to implantation of emulsion-templated scaffolds.

Lastly, the emulsion-templated scaffolds will also require testing in randomized controlled trials and be compared to ‘gold standard’ established commercial scaffolds such as Integra, to determine if there is any added benefit for using EmDerm scaffolds. Such RCTs could involve various types of wounds

including burns, donor site wounds, diabetic foot ulcers, venous leg ulcers, pressure ulcers and other surgical wounds.

7.3. Contributions to the Field

Over the past few decades, various skin substitutes have been developed with the aim of improving wound healing outcomes in acute and chronic wounds. Some have developed cell-based therapies e.g. fetal stem cell delivery on temporary scaffolds to promote 'scarless' healing (220) while others have developed biologically active matrices with impregnated growth factors to modify the wound environment for closure of hard-to-heal ulcers. (221) Emerging rapid-prototyping techniques for print-on skin and directly-sprayed electrospun dressings have also been developed as new promising biomedical engineering technologies that are being translated into the healthcare setting. (222,223)

In this thesis, a two-stage reconstruction method is explored using an emulsion-templated dermal scaffold and electrospun epidermal membrane. In an ideal setting, a one-stage reconstruction method would be preferred as it negates the need for a second operation. However, this would require a concurrent split-thickness skin graft to be applied onto the scaffold. This may not be possible in patients with large surface area burns. The benefits of a two-stage reconstruction is that it gives sufficient time for the dermal scaffold to engraft, whilst autologous keratinocytes are harvested and expanded to meet clinical needs. An example of this approach is the use of Hyalomatrix as a dermal template and Laserskin as a delivery system for cultured autologous keratinocytes (CAK). Use of Hyalomatrix appears to cause a dose dependent increase in take rate of CAK. (224)

Emulsion-templated scaffolds or EmDerms have been developed using a non-denaturing biocompatible emulsions system which allows for manufacture of a nanofibrous and microporous protein scaffold derived from extracellular matrix (e.g. collagen and fibrin). As the non-ionic surfactants prevent the protein hydrogel from denaturing, they retain their native fibrillar structure. The preservation of cell

binding motifs of native proteins such as collagen and its fibrillar nanostructure gives these scaffolds an added advantage as there is greater surface area for cellular attachment, migration and proliferation.

One of the key contributions of emulsion-templated scaffolds is that they appear to facilitate cellular ingress, integrate into the wound rapidly and vascularize within the two-week window. Although further in vivo testing is needed to substantiate this, the preliminary results for EmDerm scaffolds are promising. The use of electrospun membranes also enables subconfluent keratinocytes to be applied directly onto the vascularized EmDerm scaffold at two-weeks, as these membranes are biocompatible and biodegradable. However, further experiments to optimize seeding densities, degradation rate and scale-up of production of electrospun membranes are still needed.

Emulsion-templating is also comparable with other rapid-manufacturing techniques and cost-effective. It allows for pore sizes and type of material to be tuned according to clinical need, depending on type of tissues replaced. Electrospinning is also a highly efficient and reproducible method of generating nanofibrous mats for tissue engineering purposes as long as environmental conditions and equipment settings are optimized. Other manufacturing techniques such as freeze-drying, gas foaming or salt-leaching are less ideal as they are expensive, results in inconsistent pore sizes with variable interconnectivity and may not be amenable for rapid production and industrial scale-up.

In conclusion, a novel bottom-up manufacturing method was developed for dermal scaffolds which has favourable biological properties and appears to rapidly integrate in acute wound environments. An electrospun epidermal carrier for keratinocytes was also developed for a two-stage reconstruction process which obviates the need for harvesting split-thickness skin grafts from patients with large surface area burns. This may potentially improve outcomes for such patients in the future.

References

(1) Peck MD. Epidemiology of burns throughout the world. Part I: Distribution and risk factors. Burns 2011;37(7):1087-1100.

(2) Pham C, Greenwood J, Cleland H, Woodruff P, Maddern G. Bioengineered skin substitutes for the management of burns: a systematic review. Burns 2007;33(8):946-957.

(3) Halim AS, Khoo TL, Mohd Yussof SJ. Biologic and synthetic skin substitutes: An overview. Indian J Plast Surg 2010 Sep;43(Suppl):S23-8.

(4) MacNeil S. Biomaterials for tissue engineering of skin. Materials today 2008;11(5):26-35.

(5) MacNeil S. Biomaterials for tissue engineering of skin. Materials today 2008;11(5):26-35.

(6) Oltulu P, Ince B, Kokbudak N, Findik S, Kilinc F. Measurement of epidermis, dermis, and total skin thicknesses from six different body regions with a new ethical histometric technique. Turkish Journal of Plastic Surgery 2018;26(2):56.

(7) Kolarsick PA, Kolarsick MA, Goodwin C. Anatomy and physiology of the skin. Journal of the Dermatology Nurses' Association 2011;3(4):203-213.

(8) Werner S, Krieg T, Smola H. Keratinocyte–fibroblast interactions in wound healing. J Invest Dermatol 2007;127(5):998-1008.

(9) Tiwari VK. Burn wound: How it differs from other wounds? Indian J Plast Surg 2012 May;45(2):364-373.

(10) Young A, McNaught C. The physiology of wound healing. Surgery (Oxford) 2011;29(10):475-479.

(11) Thornton JF. Skin grafts and skin substitutes. Selected Readings in Plastic Surgery 2004;10(1):1-24.

(12) Davison-Kotler E, Sharma V, Kang NV, García-Gareta E. A Universal Classification System of Skin Substitutes Inspired by Factorial Design. Tissue Engineering Part B: Reviews 2018;24(4):279-288.

(13) Debels H, Hamdi M, Abberton K, Morrison W. Dermal matrices and bioengineered skin substitutes: a critical review of current options. Plastic and Reconstructive Surgery Global Open 2015;3(1).

(14) Stevens MM, George JH. Exploring and engineering the cell surface interface. Science 2005 Nov 18;310(5751):1135-1138.

(15) Silverstein MS. Emulsion-templated porous polymers: A retrospective perspective. Polymer 2014;55(1):304-320.

(16) Kim H, Decker E, McClements D. Impact of protein surface denaturation on droplet flocculation in hexadecane oil-in-water emulsions stabilized by β-lactoglobulin. J Agric Food Chem 2002;50(24):7131-7137.

(17) Jeschke MG, Pinto R, Kraft R, Nathens AB, Finnerty CC, Gamelli RL, et al. Morbidity and survival probability in burn patients in modern burn care. Crit Care Med 2015 Apr;43(4):808-815.

(18) Widjaja W, Tan J, Maitz PK. Efficacy of dermal substitute on deep dermal to full thickness burn injury: a systematic review. ANZ J Surg 2017;87(6):446-452.

(19) Andonovska D, Dzokic G, Spasevska L, Trajkovska T, Popovska K, Todorov I, et al. The advantages of the application of amnion membrane in the treatment of burns. Prilozi 2008 Jul;29(1):183-198.

(20) Gerding RL, Emerman CL, Effron D, Lukens T, Imbembo AL, Fratianne RB. Outpatient management of partial-thickness burns: Biobrane® versus 1% silver sulfadiazine. Ann Emerg Med 1990;19(2):121-124.

(21) Lagus H., SarlomoRikala M., Bohling T., Vuola J. Prospective study on burns treated with Integra, a cellulose sponge and split thickness skin graft: Comparative clinical and histological study - Randomized controlled trial. Burns 2013 December 2013;39(8):1577-1587.

(22) Vloemans A, Soesman A, Suijker M, Kreis R, Middelkoop E. A randomised clinical trial comparing a hydrocolloid-derived dressing and glycerol preserved allograft skin in the management of partial thickness burns. Burns 2003;29(7):702-710.

(23) Keck M, Selig H, Lumenta D, Kamolz L, Mittlböck M, Frey M. The use of Suprathel® in deep dermal burns: first results of a prospective study. Burns 2012;38(3):388-395.

(24) Adly O, Moghazy A, Abbas A, Ellabban A, Ali O, Mohamed B. Assessment of amniotic and polyurethane membrane dressings in the treatment of burns. Burns 2010;36(5):703-710.

(25) Branski LK, Herndon DN, Celis MM, Norbury WB, Masters OE, Jeschke MG. Amnion in the treatment of pediatric partial-thickness facial burns. Burns 2008;34(3):393-399.

(26) Barret JP, Dziewulski P, Ramzy PI, Wolf SE, Desai MH, Herndon DN. Biobrane versus 1% silver sulfadiazine in second-degree pediatric burns. Plast Reconstr Surg 2000 Jan;105(1):62-65.

(27) Cassidy C, Peter SDS, Lacey S, Beery M, Ward-Smith P, Sharp RJ, et al. Biobrane versus duoderm for the treatment of intermediate thickness burns in children: a prospective, randomized trial. Burns 2005;31(7):890-893.

(28) Demling RH, DeSanti L. Management of partial thickness facial burns (comparison of topical antibiotics and bio-engineered skin substitutes). Burns 1999;25(3):256-261.

(29) Noordenbos J, Doré C, Hansbrough JF. Safety and Efficacy of TransCyte* for the Treatment of Partial-Thickness Burns. Journal of Burn Care & Research 1999;20(4):275-281.

(30) Heimbach D, Luterman A, Burke J, Cram A, Herndon D, Hunt J, et al. Artificial dermis for major burns. A multi-center randomized clinical trial. Ann Surg 1988 Sep;208(3):313-320.

(31) Mohammadi AA, Johari HG, Eskandari S. Effect of amniotic membrane on graft take in extremity burns. Burns 2013;39(6):1137-1141.

(32) Boyce ST, Kagan RJ, Greenhalgh DG, Warner P, Yakuboff KP, Palmieri T, et al. Cultured skin substitutes reduce requirements for harvesting of skin autograft for closure of excised, full-thickness burns. J Trauma 2006 Apr;60(4):821-829.

(33) Gardien KL, Marck RE, Bloemen MC, Waaijman T, Gibbs S, Ulrich MM, et al. Outcome of burns treated with autologous cultured proliferating epidermal cells: a prospective randomized multicenter intrapatient comparative trial. Cell Transplant 2016;25(3):437-448.

(34) Munster AM, Smith-Meek M, Shalom A. Acellular allograft dermal matrix: immediate or delayed epidermal coverage? Burns 2001;27(2):150-153.

(35) Branski LK, Herndon DN, Pereira C, Mlcak RP, Celis MM, Lee JO, et al. Longitudinal assessment of Integra in primary burn management: a randomized pediatric clinical trial. Crit Care Med 2007 Nov;35(11):2615-2623.

(36) Gravante G, Di Fede M, Araco A, Grimaldi M, De Angelis B, Arpino A, et al. A randomized trial comparing ReCell® system of epidermal cells delivery versus classic skin grafts for the treatment of deep partial thickness burns. Burns 2007;33(8):966-972.

(37) Kumar RJ, Kimble RM, Boots R, Pegg SP. Treatment of partial-thickness burns: a prospective, randomized trial using TranscyteTM. ANZ J Surg 2004;74(8):622-626.

(38) Purdue GF, Hunt JL, Still Jr JM, Law EJ, Herndon DN, Goldfarb IW, et al. A multicenter clinical trial of a biosynthetic skin replacement, Dermagraft-TC, compared with cryopreserved human cadaver skin for temporary coverage of excised burn wounds. Journal of Burn Care & Research 1997;18(1):52-57.

(39) Wood F, Martin L, Lewis D, Rawlins J, McWilliams T, Burrows S, et al. A prospective randomised clinical pilot study to compare the effectiveness of Biobrane® synthetic wound dressing, with or without autologous cell suspension, to the local standard treatment regimen in paediatric scald injuries. Burns 2012;38(6):830-839.

(40) Hosseini SN, Karimian A, Mousavinasab SN, Rahmanpour H, Yamini M, Zahmatkesh SH. Xenoderm versus 1% silver sulfadiazine in partial-thickness burns. Asian Journal of Surgery 2009;32(4):234-239.

(41) Lal S, Barrow RE, Wolf SE, Chinkes DL, Hart DW, Heggers JP, et al. BIOBRANE (R) IMPROVES WOUND HEALING IN BURNED CHILDREN WITHOUT INCREASED RISK OF INFECTION. Shock 2000;14(3):314-319.

(42) Horch RE, Jeschke MG, Spilker G, Herndon DN, Kopp J. Treatment of second degree facial burns with allografts—preliminary results. Burns 2005;31(5):597-602.

(43) Boyce ST, Kagan RJ, Yakuboff KP, Meyer NA, Rieman MT, Greenhalgh DG, et al. Cultured skin substitutes reduce donor skin harvesting for closure of excised, full-thickness burns. Ann Surg 2002;235(2):269-279.

(44) Gerding RL, Imbembo AL, Fratianne RB. Biosynthetic skin substitute vs. 1% silver sulfadiazine for treatment of inpatient partial-thickness thermal burns. Journal of Trauma and Acute Care Surgery 1988;28(8):1265-1269.

(45) Mohammadi A.A., Seyed Jafari S.M., Kiasat M., Tavakkolian A.R., Imani M.T., Ayaz M., et al. Effect of fresh human amniotic membrane dressing on graft take in patients with chronic burn wounds compared with conventional methods. Burns 2013 March 2013;39(2):349-353.

(46) Ryssel H, Gazyakan E, Germann G, Öhlbauer M. The use of MatriDerm® in early excision and simultaneous autologous skin grafting in burns—a pilot study. Burns 2008;34(1):93-97.

(47) Selig HF, Keck M, Lumenta DB, Mittlböck M, Kamolz LP. The use of a polylactide-based copolymer as a temporary skin substitute in deep dermal burns: 1-year follow-up results of a prospective clinical noninferiority trial. Wound Repair and Regeneration 2013;21(3):402-409.

(48) Uhlig C, Rapp M, Hartmann B, Hierlemann H, Planck H, Dittel K. Suprathel®—An innovative, resorbable skin substitute for the treatment of burn victims. Burns 2007;33(2):221-229.

(49) Waymack P, Duff RG, Sabolinski M, Apligraf T, of the Apligraf, Burn Study Group2Members, Hansbrough J, et al. The effect of a tissue engineered bilayered living skin analog, over meshed split-thickness autografts on the healing of excised burn wounds. Burns 2000;26(7):609-619.

(50) Yi JW, Kim JK. Prospective randomized comparison of scar appearances between cograft of acellular dermal matrix with autologous split-thickness skin and autologous split-thickness skin graft alone for full-thickness skin defects of the extremities. Plast Reconstr Surg 2015;135(3):609e-616e.

(51) Bayat A, Bock O, Mrowietz U, Ollier WE, Ferguson MW. Genetic susceptibility to keloid disease and hypertrophic scarring: transforming growth factor beta1 common polymorphisms and plasma levels. Plast Reconstr Surg 2003 Feb;111(2):535-43; discussion 544-6.

(52) Sen CK, Gordillo GM, Roy S, Kirsner R, Lambert L, Hunt TK, et al. Human skin wounds: a major and snowballing threat to public health and the economy. Wound repair and regeneration 2009;17(6):763-771.

(53) Alexiadou K, Doupis J. Management of diabetic foot ulcers. Diabetes Therapy 2012;3(1):4.

(54) Guest M, Smith J, Sira M, Madden P, Greenhalgh R, Davies A. Venous ulcer healing by four-layer compression bandaging is not influenced by the pattern of venous incompetence. Br J Surg 1999;86(11):1437-1440.

(55) Brigido SA. The use of an acellular dermal regenerative tissue matrix in the treatment of lower extremity wounds: a prospective 16-week pilot study. International wound journal 2006;3(3):181-187.

(56) Reyzelman A, Crews RT, Moore JC, Moore L, Mukker JS, Offutt S, et al. Clinical effectiveness of an acellular dermal regenerative tissue matrix compared to standard wound management in healing diabetic foot ulcers: a prospective, randomised, multicentre study. International wound journal 2009;6(3):196-208.

(57) Driver VR, Lavery LA, Reyzelman AM, Dutra TG, Dove CR, Kotsis SV, et al. A clinical trial of Integra Template for diabetic foot ulcer treatment. Wound Repair and Regeneration 2015;23(6):891-900.

(58) Edmonds M, European and Australian Apligraf Diabetic Foot Ulcer Study Group. Apligraf in the treatment of neuropathic diabetic foot ulcers. The international journal of lower extremity wounds 2009;8(1):11-18.

(59) Veves A, Falanga V, Armstrong DG, Sabolinski ML, Apligraf Diabetic Foot Ulcer Study. Graftskin, a human skin equivalent, is effective in the management of noninfected neuropathic diabetic foot ulcers: a prospective randomized multicenter clinical trial. Diabetes Care 2001 Feb;24(2):290-295.

(60) Zelen CM, Gould L, Serena TE, Carter MJ, Keller J, Li WW. A prospective, randomised, controlled, multi-centre comparative effectiveness study of healing using dehydrated human

amnion/chorion membrane allograft, bioengineered skin substitute or standard of care for treatment of chronic lower extremity diabetic ulcers. International wound journal 2015;12(6):724-732.

(61) Naughton G, Mansbridge J, Gentzkow G. A metabolically active human dermal replacement for the treatment of diabetic foot ulcers. Artif Organs 1997;21(11):1203-1210.

(62) Gentzkow GD, Iwasaki SD, Hershon KS, Mengel M, Prendergast JJ, Ricotta JJ, et al. Use of dermagraft, a cultured human dermis, to treat diabetic foot ulcers. Diabetes Care 1996 Apr;19(4):350-354.

(63) Hanft JR, Surprenant MS. Healing of chronic foot ulcers in diabetic patients treated with a human fibroblast-derived dermis. J Foot Ankle Surg 2002 Sep-Oct;41(5):291-299.

(64) Marston WA, Hanft J, Norwood P, Pollak R, Dermagraft Diabetic Foot Ulcer Study Group. The efficacy and safety of Dermagraft in improving the healing of chronic diabetic foot ulcers: results of a prospective randomized trial. Diabetes Care 2003 Jun;26(6):1701-1705.

(65) Hu Z, Chen D, Guo D, Liang Y, Zhang J, Zhu J, et al. Randomized clinical trial of autologous skin cell suspension combined with skin grafting for chronic wounds. Br J Surg 2015;102(2):e117-e123.

(66) Lavery LA, Fulmer J, Shebetka KA, Regulski M, Vayser D, Fried D, et al. The efficacy and safety of Grafix® for the treatment of chronic diabetic foot ulcers: results of a multi-centre, controlled, randomised, blinded, clinical trial. International wound journal 2014;11(5):554-560.

(67) You H, Han S, Rhie J. Randomised controlled clinical trial for autologous fibroblast-hyaluronic acid complex in treating diabetic foot ulcers. J Wound Care 2014;23(11):521-530.

(68) Zelen CM, Serena TE, Denoziere G, Fetterolf DE. A prospective randomised comparative parallel study of amniotic membrane wound graft in the management of diabetic foot ulcers. International wound journal 2013;10(5):502-507.

(69) Uccioli L, Giurato L, Ruotolo V, Ciavarella A, Grimaldi MS, Piaggesi A, et al. Two-step autologous grafting using HYAFF scaffolds in treating difficult diabetic foot ulcers: Results of a multicenter, randomized controlled clinical trial with long-term follow-up. International Journal of Lower Extremity Wounds 2011;10(2):80-85.

(70) You H.J., Han S.K., Rhie JW. Randomised controlled clinical trial for autologous fibroblast-hyaluronic acid complex in treating diabetic foot ulcers. J Wound Care 2014 01 Nov 2014;23(11):521-2, 524, 526-30.

(71) Puttirutvong P. Meshed skin graft versus split thickness skin graft in diabetic ulcer coverage. J Med Assoc Thai 2004 Jan;87(1):66-72.

(72) Abbruzzese L, Rizzo L, Fanelli G, Tedeschi A, Scatena A, Goretti C, et al. Effectiveness and safety of a novel gel dressing in the management of neuropathic leg ulcers in diabetic patients: a prospective double-blind randomized trial. The international journal of lower extremity wounds 2009;8(3):134-140.

(73) Caravaggi C, De Giglio R, Pritelli C, Sommaria M, Dalla Noce S, Faglia E, et al. HYAFF 11-based autologous dermal and epidermal grafts in the treatment of noninfected diabetic plantar and dorsal foot ulcers: a prospective, multicenter, controlled, randomized clinical trial. Diabetes Care 2003 Oct;26(10):2853-2859.

(74) Uccioli L, Giurato L, Ruotolo V, Ciavarella A, Grimaldi MS, Piaggesi A, et al. Two-step autologous grafting using HYAFF scaffolds in treating difficult diabetic foot ulcers: results of a multicenter, randomized controlled clinical trial with long-term follow-up. The international journal of lower extremity wounds 2011;10(2):80-85.

(75) You H, Han S, Rhie J. Randomised controlled clinical trial for autologous fibroblast-hyaluronic acid complex in treating diabetic foot ulcers. J Wound Care 2014;23(11):521-530.

(76) Zelen CM, Serena TE, Snyder RJ. A prospective, randomised comparative study of weekly versus biweekly application of dehydrated human amnion/chorion membrane allograft in the management of diabetic foot ulcers. International wound journal 2014;11(2):122-128.

(77) You H, Han S, Lee J, Chang H. Treatment of diabetic foot ulcers using cultured allogeneic keratinocytes—a pilot study. Wound Repair and Regeneration 2012;20(4):491-499.

(78) Lawrence DiDomenico D, Emch KJ, Landsman AR, Adam Landsman D. A Prospective Comparison of Dia-betic Foot Ulcers Treated With Either a Cryopreserved Skin Allograft or a Bioengineered Skin Substitute. Wounds 2011;23(7):184-189.

(79) Landsman A, Roukis TS, DeFronzo DJ, Agnew P, Petranto RD, Surprenant M. ???? Living cells or collagen matrix: which is more beneficial in the treatment of diabetic foot ulcers? Wounds: a compendium of clinical research and practice 2008;20(5):111-116.

(80) Niezgoda JA, Van Gils CC, Frykberg RG, Hodde JP, OASIS Diabetic Ulcer Study Group. Randomized clinical trial comparing OASIS Wound Matrix to Regranex Gel for diabetic ulcers. Adv Skin Wound Care 2005;18(5):258-266.

(81) Sanders L, Landsman AS, Landsman A, Keller N, Cook J, Cook E, et al. A prospective, multicenter, randomized, controlled clinical trial comparing a bioengineered skin substitute to a human skin allograft. Ostomy Wound Manage 2014 Sep;60(9):26-38.

(82) Zelen CM, Serena TE, Gould L, Le L, Carter MJ, Keller J, et al. Treatment of chronic diabetic lower extremity ulcers with advanced therapies: a prospective, randomised, controlled, multi-centre comparative study examining clinical efficacy and cost. International wound journal 2016;13(2):272-282.

(83) Blume P, Driver VR, Tallis AJ, Kirsner RS, Kroeker R, Payne WG, et al. Formulated collagen gel accelerates healing rate immediately after application in patients with diabetic neuropathic foot ulcers. Wound Repair and Regeneration 2011;19(3):302-308.

(84) Brigido SA, Boc SF, Lopez RC. Effective management of major lower extremity wounds using an acellular regenerative tissue matrix: a pilot study. Orthopedics 2004;27(1):S145-S149.

(85) Hu Z, Zhu J, Cao X, Chen C, Li S, Guo D, et al. Composite skin grafting with human acellular dermal matrix scaffold for treatment of diabetic foot ulcers: a randomized controlled trial. J Am Coll Surg 2016;222(6):1171-1179.

(86) Lipkin S, Chaikof E, Isseroff Z, Silverstein P. Effectiveness of bilayered cellular matrix in healing of neuropathic diabetic foot ulcers: results of a multicenter pilot trial. Wounds-a Compendium of Clinical Research and Practice 2003;15(7):230-236.

(87) Sams HH, Chen J, King LE. Graftskin treatment of difficult to heal diabetic foot ulcers: one center's experience. Dermatologic surgery 2002;28(8):698-703.

(88) Veves A, Sheehan P, Pham HT. A randomized, controlled trial of Promogran (a collagen/oxidized regenerated cellulose dressing) vs standard treatment in the management of diabetic foot ulcers. Archives of surgery 2002;137(7):822-827.

(89) Tadros TF. Emulsion formation and stability. : John Wiley & Sons; 2013.

(90) Kale SN, Deore SL. Emulsion micro emulsion and nano emulsion: A review. Systematic Reviews in Pharmacy 2017;8(1):39.

(91) Mishra M, Muthuprasanna P, Prabha KS, Rani PS, Satish IA, Ch IS, et al. Basics and potential applications of surfactants-a review. 2009.

(92) Maldonado-Valderrama J, Patino JMR. Interfacial rheology of protein–surfactant mixtures. Current Opinion in Colloid & Interface Science 2010;15(4):271-282.

(93) Kim H, Decker E, McClements D. Influence of protein concentration and order of addition on thermal stability of β-lactoglobulin stabilized n-hexadecane oil-in-water emulsions at neutral pH. Langmuir 2005;21(1):134-139.

(94) Fainerman V, Zholob S, Leser M, Michel M, Miller R. Competitive adsorption from mixed nonionic surfactant/protein solutions. J Colloid Interface Sci 2004;274(2):496-501.

(95) Courthaudon J, Dickinson E, Dalgleish DG. Competitive adsorption of β-casein and nonionic surfactants in oil-in-water emulsions. J Colloid Interface Sci 1991;145(2):390-395.

(96) Mehan S, Aswal VK, Kohlbrecher J. Tuning of protein-surfactant interaction to modify the resultant structure. Physical Review E 2015;92(3):032713.

(97) Griffin WC. Calculation of HLB values of non-ionic surfactants. J.Soc.Cosmet.Chem. 1954;5:249-256.

(98) Griffin W. Hydrophilic-lipophilic balance. J Soc Cosmet Chem 1949;1:311-326.

(99) Alderborn G, Aulton M. Pharmaceutics the science of dosage form design. Pharm Sci Dos Form Des 2002.

(100) Horiuchi S, Winter G. CMC determination of nonionic surfactants in protein formulations using ultrasonic resonance technology. European Journal of Pharmaceutics and Biopharmaceutics 2015;92:8-14.

(101) Goddard ED. Interactions of Surfactants with Polymers and Proteins: 0. : CRC press; 2017.

(102) Otzen D. Protein–surfactant interactions: a tale of many states. Biochimica et Biophysica Acta (BBA)-Proteins and Proteomics 2011;1814(5):562-591.

(103) Owen R, Sherborne C, Paterson T, Green NH, Reilly GC, Claeyssens F. Emulsion templated scaffolds with tunable mechanical properties for bone tissue engineering. Journal of the mechanical behavior of biomedical materials 2016;54:159-172.

(104) Li Z, Xiao M, Wang J, Ngai T. Pure protein scaffolds from pickering high internal phase emulsion template. Macromolecular rapid communications 2013;34(2):169-174.

(105) Patel AR, Cludts N, Bin Sintang MD, Lewille B, Lesaffer A, Dewettinck K. Polysaccharide-based oleogels prepared with an emulsion-templated approach. ChemPhysChem 2014;15(16):3435-3439.

(106) Barbetta A, Massimi M, Di Rosario B, Nardecchia S, De Colli M, Devirgiliis LC, et al. Emulsion templated scaffolds that include gelatin and glycosaminoglycans. Biomacromolecules 2008;9(10):2844-2856.

(107) Janik H, Marzec M. A review: Fabrication of porous polyurethane scaffolds. Materials Science and Engineering: C 2015;48:586-591.

(108) Whang K, Healy K, Elenz D, Nam E, Tsai D, Thomas C, et al. Engineering bone regeneration with bioabsorbable scaffolds with novel microarchitecture. Tissue Eng 1999;5(1):35-51.

(109) Druecke D, Langer S, Lamme E, Pieper J, Ugarkovic M, Steinau HU, et al. Neovascularization of poly (ether ester) block-copolymer scaffolds in vivo: Long-term investigations using intravital fluorescent microscopy. Journal of Biomedical Materials Research Part A 2004;68(1):10-18.

(110) Dalgleish DG. Adsorption of protein and the stability of emulsions. Trends Food Sci Technol 1997;8(1):1-6.

(111) Chen J, Dickinson E, Iveson G. Interfacial interactions, competitive adsorption and emulsion stability. Food Structure 1993;12(2):1.

(112) Dickinson E. Proteins at interfaces and in emulsions stability, rheology and interactions. Journal of the Chemical Society, Faraday Transactions 1998;94(12):1657-1669.

(113) McClements DJ. Protein-stabilized emulsions. Current opinion in colloid & interface science 2004;9(5):305-313.

(114) Ahmed TA, Dare EV, Hincke M. Fibrin: a versatile scaffold for tissue engineering applications. Tissue Engineering Part B: Reviews 2008;14(2):199-215.

(115) James-Smith MA, Alford K, Shah DO. A novel method to quantify the amount of surfactant at the oil/water interface and to determine total interfacial area of emulsions. J Colloid Interface Sci 2007;310(2):590-598.

(116) Kundu P, Agrawal A, Mateen H, Mishra IM. Stability of oil-in-water macro-emulsion with anionic surfactant: Effect of electrolytes and temperature. Chemical Engineering Science 2013;102:176-185.

(117) Rudin J, Bernard C, Wasan DT. Effect of added surfactant on interfacial-tension and spontaneous emulsification in alkali/acidic oil systems. Ind Eng Chem Res 1994;33(5):1150-1158.

(118) Boyd J, Parkinson C, Sherman P. Factors affecting emulsion stability, and the HLB concept. J Colloid Interface Sci 1972;41(2):359-370.

(119) Wilde P, Mackie A, Husband F, Gunning P, Morris V. Proteins and emulsifiers at liquid interfaces. Adv Colloid Interface Sci 2004;108:63-71.

(120) Khan TA, Mahler H, Kishore RS. Key interactions of surfactants in therapeutic protein formulations: A review. European Journal of Pharmaceutics and Biopharmaceutics 2015;97:60-67.

(121) Lim X, Potter M, Cui Z, Dye JF. Manufacture and characterisation of EmDerm—novel hierarchically structured bio-active scaffolds for tissue regeneration. J Mater Sci Mater Med 2018;29(6):79.

(122) TAKAMURA A, MINOWA T, NORO S, KUBO T. Effects of Tween and Span group emulsifiers on the stability of o/w emulsions. Chemical and Pharmaceutical Bulletin 1979;27(12):2921-2926.

(123) Shinoda K, Yoneyama T, Tsutsumi H. Evaluation of emulsifier blending. J Dispersion Sci Technol 1980;1(1):1-12.

(124) Anderson JE, Kim BR, Mueller SA, Lofton TV. Composition and analysis of mineral oils and other organic compounds in metalworking and hydraulic fluids. 2003.

(125) Sajjadi S, Zerfa M, Brooks B. Phase inversion in p-xylene/water emulsions with the non-ionic surfactant pair sorbitan monolaurate/polyoxyethylene sorbitan monolaurate (Span 20/Tween 20). Colloids Surf Physicochem Eng Aspects 2003;218(1):241-254.

(126) Kim C, Hsieh Y. Wetting and absorbency of nonionic surfactant solutions on cotton fabrics. Colloids Surf Physicochem Eng Aspects 2001;187:385-397.

(127) Tcholakova S, Denkov ND, Danner T. Role of surfactant type and concentration for the mean drop size during emulsification in turbulent flow. Langmuir 2004;20(18):7444-7458.

(128) Ruckenstein E. The origin of thermodynamic stability of microemulsions. Chemical Physics Letters 1978;57(4):517-521.

(129) Walstra P. Principles of emulsion formation. Chemical Engineering Science 1993;48(2):333-349.

(130) li Zhai J, Day L, Aguilar M, Wooster TJ. Protein folding at emulsion oil/water interfaces. Current opinion in colloid & interface science 2013;18(4):257-271.

(131) Bhuyan AK. On the mechanism of SDS-induced protein denaturation. Biopolymers 2010;93(2):186-199.

(132) Chen J, Dickinson E. Time-dependent competitive adsorption of milk proteins and surfactants in oil-in-water emulsions. J Sci Food Agric 1993;62(3):283-289.

(133) Cameron NR. High internal phase emulsion templating as a route to well-defined porous polymers. Polymer 2005;46(5):1439-1449.

(134) Whang K, Thomas C, Healy K, Nuber G. A novel method to fabricate bioabsorbable scaffolds. Polymer 1995;36(4):837-842.

(135) Ho H, Hsiao C, Chen C, Sokoloski TD, Sheu M. Fibrin-based drug delivery systems. II. The preparation and characterization of microbeads. Drug Dev Ind Pharm 1994;20(4):535-546.

(136) Whang K, Goldstick TK, Healy KE. A biodegradable polymer scaffold for delivery of osteotropic factors. Biomaterials 2000;21(24):2545-2551.

(137) Franks GV, Moss B, Phelan D. Chitosan tissue scaffolds by emulsion templating. Journal of Biomaterials Science, Polymer Edition 2006;17(12):1439-1450.

(138) Murphy CM, O'Brien FJ. Understanding the effect of mean pore size on cell activity in collagen-glycosaminoglycan scaffolds. Cell adhesion & migration 2010;4(3):377-381.

(139) Loh QL, Choong C. Three-dimensional scaffolds for tissue engineering applications: role of porosity and pore size. Tissue Engineering Part B: Reviews 2013;19(6):485-502.

(140) Bružauskaitė I, Bironaitė D, Bagdonas E, Bernotienė E. Scaffolds and cells for tissue regeneration: different scaffold pore sizes—different cell effects. Cytotechnology 2016;68(3):355-369.

(141) Dagalakis N, Flink J, Stasikelis P, Burke J, Yannas I. Design of an artificial skin. Part III. Control of pore structure. Journal of Biomedical Materials Research Part A 1980;14(4):511-528.

(142) Murphy CM, Haugh MG, O'Brien FJ. The effect of mean pore size on cell attachment, proliferation and migration in collagen–glycosaminoglycan scaffolds for bone tissue engineering. Biomaterials 2010;31(3):461-466.

(143) O'brien FJ. Biomaterials & scaffolds for tissue engineering. Materials today 2011;14(3):88-95.

(144) Velasco MA, Narvaez-Tovar CA, Garzon-Alvarado DA. Design, materials, and mechanobiology of biodegradable scaffolds for bone tissue engineering. Biomed Res Int 2015;2015:729076.

(145) Santos MI, Tuzlakoglu K, Fuchs S, Gomes ME, Peters K, Unger RE, et al. Endothelial cell colonization and angiogenic potential of combined nano-and micro-fibrous scaffolds for bone tissue engineering. Biomaterials 2008;29(32):4306-4313.

(146) Beachley V, Wen X. Polymer nanofibrous structures: Fabrication, biofunctionalization, and cell interactions. Progress in polymer science 2010;35(7):868-892.

(147) Jones JR, Lee PD, Hench LL. Hierarchical porous materials for tissue engineering. Philos Trans A Math Phys Eng Sci 2006 Jan 15;364(1838):263-281.

(148) Johnson KE, Wilgus TA. Vascular endothelial growth factor and angiogenesis in the regulation of cutaneous wound repair. Advances in wound care 2014;3(10):647-661.

(149) Shibuya M. Vascular endothelial growth factor (VEGF) and its receptor (VEGFR) signaling in angiogenesis: a crucial target for anti-and pro-angiogenic therapies. Genes & cancer 2011;2(12):1097-1105.

(150) Pepper M, Ferrara N, Orci L, Montesano R. Potent synergism between vascular endothelial growth factor and basic fibroblast growth factor in the induction of angiogenesis in vitro. Biochem Biophys Res Commun 1992;189(2):824-831.

(151) Kaga T, Kawano H, Sakaguchi M, Nakazawa T, Taniyama Y, Morishita R. Hepatocyte growth factor stimulated angiogenesis without inflammation: differential actions between hepatocyte growth factor, vascular endothelial growth factor and basic fibroblast growth factor. Vascular pharmacology 2012;57(1):3-9.

(152) Koblizek TI, Weiss C, Yancopoulos GD, Deutsch U, Risau W. Angiopoietin-1 induces sprouting angiogenesis in vitro. Current Biology 1998;8(9):529-532.

(153) Fagiani E, Christofori G. Angiopoietins in angiogenesis. Cancer Lett 2013;328(1):18-26.

(154) Nicosia RF, Bonanno E, Smith M. Fibronectin promotes the elongation of microvessels during angiogenesis in vitro. J Cell Physiol 1993;154(3):654-661.

(155) Mongiat M, Andreuzzi E, Tarticchio G, Paulitti A. Extracellular matrix, a hard player in angiogenesis. International journal of molecular sciences 2016;17(11):1822.

(156) Starke RD, Ferraro F, Paschalaki KE, Dryden NH, McKinnon TA, Sutton RE, et al. Endothelial von Willebrand factor regulates angiogenesis. Blood 2011 Jan 20;117(3):1071-1080.

(157) Ning Y, Manegold PC, Hong YK, Zhang W, Pohl A, Lurje G, et al. Interleukin-8 is associated with proliferation, migration, angiogenesis and chemosensitivity in vitro and in vivo in colon cancer cell line models. International Journal of Cancer 2011;128(9):2038-2049.

(158) Shepherd D, Shepherd J, Ghose S, Kew S, Cameron RE, Best S. The process of EDC-NHS cross-linking of reconstituted collagen fibres increases collagen fibrillar order and alignment. APL materials 2015;3(1):014902.

(159) Potter MJ, Linge C, Cussons P, Dye JF, Sanders R. An investigation to optimize angiogenesis within potential dermal replacements. Plast Reconstr Surg 2006 May;117(6):1876-1885.

(160) Wahl EA, Fierro FA, Peavy TR, Hopfner U, Dye JF, Machens H, et al. In vitro evaluation of scaffolds for the delivery of mesenchymal stem cells to wounds. BioMed research international 2015;2015.

(161) Ahmed TA, Dare EV, Hincke M. Fibrin: a versatile scaffold for tissue engineering applications. Tissue Engineering Part B: Reviews 2008;14(2):199-215.

(162) Caiado F, Carvalho T, Silva F, Castro C, Clode N, Dye JF, et al. The role of fibrin E on the modulation of endothelial progenitors adhesion, differentiation and angiogenic growth factor production and the promotion of wound healing. Biomaterials 2011;32(29):7096-7105.

(163) Sheikh FA, Ju HW, Lee JM, Moon BM, Park HJ, Lee OJ, et al. 3D electrospun silk fibroin nanofibers for fabrication of artificial skin. Nanomedicine: Nanotechnology, Biology, and Medicine 2015;11(3):681-691.

(164) García-Gareta E, Ravindran N, Sharma V, Samizadeh S, Dye JF. A novel multiparameter in vitro model of three-dimensional cell ingress into scaffolds for dermal reconstruction to predict in vivo outcome. BioResearch open access 2013;2(6):412-420.

(165) Reinertsen E, Skinner M, Wu B, Tawil B. Concentration of fibrin and presence of plasminogen affect proliferation, fibrinolytic activity, and morphology of human fibroblasts and keratinocytes in 3D fibrin constructs. Tissue Engineering Part A 2014;20(21-22):2860-2869.

(166) Nayak S, Kundu SC. Sericin-carboxymethyl cellulose porous matrices as cellular wound dressing material. Journal of Biomedical Materials Research - Part A 2014;102(6):1928-1940.

(167) Kubo M, Norris DA, Howell SE, Ryan SR, Clark RA. Human keratinocytes synthesize, secrete, and deposit fibronectin in the pericellular matrix. J Invest Dermatol 1984;82(6):580-586.

(168) Halaban R, Langdon R, Birchall N, Cuono C, Baird A, Scott G, et al. Basic fibroblast growth factor from human keratinocytes is a natural mitogen for melanocytes. J Cell Biol 1988;107(4):1611-1619.

(169) Barker JN, Jones ML, Mitra RS, Crockett-Torabe E, Fantone JC, Kunkel SL, et al. Modulation of keratinocyte-derived interleukin-8 which is chemotactic for neutrophils and T lymphocytes. Am J Pathol 1991 Oct;139(4):869-876.

(170) O'toole E. Extracellular matrix and keratinocyte migration. Clin Exp Dermatol 2001;26(6):525-530.

(171) Harrison C, Gossiel F, Bullock A, Sun T, Blumsohn A, Mac Neil S. Investigation of keratinocyte regulation of collagen I synthesis by dermal fibroblasts in a simple in vitro model. Br J Dermatol 2006;154(3):401-410.

(172) Kubo K, Kuroyanagi Y. A study of cytokines released from fibroblasts in cultured dermal substitute. Artif Organs 2005;29(10):845-849.

(173) Mansbridge JN, Liu K, Pinney RE, Patch R, Ratcliffe A, Naughton GK. Growth factors secreted by fibroblasts: role in healing diabetic foot ulcers. Diabetes, Obesity and Metabolism 1999;1(5):265-279.

(174) Nickel W. The unconventional secretory machinery of fibroblast growth factor 2. Traffic 2011;12(7):799-805.

(175) Li A, Dubey S, Varney ML, Dave BJ, Singh RK. IL-8 directly enhanced endothelial cell survival, proliferation, and matrix metalloproteinases production and regulated angiogenesis. J Immunol 2003 Mar 15;170(6):3369-3376.

(176) Monti M, Donnini S, Morbidelli L, Giachetti A, Mochly-Rosen D, Mignatti P, et al. PKCε activation promotes FGF-2 exocytosis and induces endothelial cell proliferation and sprouting. J Mol Cell Cardiol 2013;63:107-117.

(177) Bahramsoltani M, Slosarek I, De Spiegelaere W, Plendl J. Angiogenesis and collagen type IV expression in different endothelial cell culture systems. Anat Histol Embryol 2014;43(2):103-115.

(178) Alessandro R, Masiero L, Lapidos K, Spoonster J, Kohn EC. Endothelial cell spreading on type IV collagen and spreading-induced FAK phosphorylation is regulated by Ca2 influx. Biochem Biophys Res Commun 1998;248(3):635-640.

(179) Stewart Jr JA, West TA, Lucchesi PA. Nitric Oxide-induced Collagen IV Expression and Angiogenesis: FAK or Fiction? American Journal of Physiology-Cell Physiology 2011.

(180) Ma S, Xie N, Li W, Yuan B, Shi Y, Wang Y. Immunobiology of mesenchymal stem cells. Cell Death Differ 2014;21(2):216.

(181) Pankajakshan D, Agrawal DK. Mesenchymal Stem Cell Paracrine Factors in Vascular Repair and Regeneration. J Biomed Technol Res 2014;1(1):10.19104/jbtr.2014.107. Epub 2014 Aug 28.

(182) Leuning DG, Beijer NR, Fossé NA, Vermeulen S, Lievers E, Kooten C, et al. The cytokine secretion profile of mesenchymal stromal cells is determined by surface structure of the microenvironment. Scientific reports 2018;8(1):7716.

(183) Thin Luu N, Mcgettrick HM, Buckley CD, Newsome PN, Ed Rainger G, Frampton J, et al. Crosstalk between mesenchymal stem cells and endothelial cells leads to downregulation of cytokine-induced leukocyte recruitment. Stem Cells 2013;31(12):2690-2702.

(184) Williams KL. Endotoxin as a Standard. Endotoxins: CRC Press; 2007. p. 187-210.

(185) Diegelmann RF, Lindblad WJ, Cohen IK. A subcutaneous implant for wound healing studies in humans. J Surg Res 1986;40(3):229-237.

(186) Socarras TO, Vasconcelos AC, Campos PP, Pereira NB, Souza JP, Andrade SP. Foreign body response to subcutaneous implants in diabetic rats. PloS one 2014;9(11):e110945.

(187) Böttcher-Haberzeth S, Biedermann T, Schiestl C, Hartmann-Fritsch F, Schneider J, Reichmann E, et al. Matriderm® 1 mm versus Integra® Single Layer 1.3 mm for one-step closure of full thickness skin defects: a comparative experimental study in rats. Pediatr Surg Int 2012;28(2):171-177.

(188) Wosgrau ACC, da Silva Jeremias T, Leonardi DF, Pereima MJ, Di Giunta G, Trentin AG. Comparative experimental study of wound healing in mice: pelnac versus integra. PloS one 2015;10(3):e0120322.

(189) King W, Lam P, Liew C, Ho W, Lil A. Evaluation of artificial skin (Integra) in a rodent model. Burns 1997;23:S30-S32.

(190) Böttcher-Haberzeth S, Biedermann T, Schiestl C, Hartmann-Fritsch F, Schneider J, Reichmann E, et al. Matriderm® 1 mm versus Integra® Single Layer 1.3 mm for one-step closure of full thickness skin defects: a comparative experimental study in rats. Pediatr Surg Int 2012;28(2):171-177.

(191) Bootle-Wilbraham C, Tazzyman S, Thompson W, Stirk C, Lewis C. Fibrin fragment E stimulates the proliferation, migration and differentiation of human microvascular endothelial cells in vitro. Angiogenesis 2001;4(4):269-275.

(192) Jennewein C, Tran N, Paulus P, Ellinghaus P, Eble JA, Zacharowski K. Novel aspects of fibrin (ogen) fragments during inflammation. Molecular medicine 2011;17(5-6):568-573.

(193) Rheinwatd JG, Green H. Seria cultivation of strains of human epidemal keratinocytes: the formation keratinizin colonies from single cell is. Cell 1975;6(3):331-343.

(194) Atiyeh BS, Costagliola M. Cultured epithelial autograft (CEA) in burn treatment: three decades later. Burns 2007;33(4):405-413.

(195) Barret JP, Wolf SE, Desai MH, Herndon DN. Cost-efficacy of cultured epidermal autografts in massive pediatric burns. Ann Surg 2000;231(6):869-876.

(196) Chester D, Balderson D, Papini R. A review of keratinocyte delivery to the wound bed. J Burn Care Rehabil 2004;25(3):266-275.

(197) Chan ES, Lam P, Liew C, Lau HC, Yen RS, King WW. A new technique to resurface wounds with composite biocompatible epidermal graft and artificial skin. Journal of Trauma and Acute Care Surgery 2001;50(2):358-362.

(198) Schwarze H, Küntscher M, Uhlig C, Hierlemann H, Prantl L, Noack N, et al. Suprathel®, a new skin substitute, in the management of donor sites of split-thickness skin grafts: Results of a clinical study. Burns 2007;33(7):850-854.

(199) Elbe-Bürger A. Skin architecture and function. Handbook of Burns: Springer; 2012. p. 29-46.

(200) Gauglitz GG, Schauber J. Skin: architecture and Function. Dermal Replacements in General, Burn, and Plastic Surgery: Springer; 2013. p. 1-11.

(201) Bhardwaj N, Kundu SC. Electrospinning: a fascinating fiber fabrication technique. Biotechnol Adv 2010;28(3):325-347.

(202) Wang X, Ding B, Li B. Biomimetic electrospun nanofibrous structures for tissue engineering. Materials Today 2013;16(6):229-241.

(203) Sun H, Mei L, Song C, Cui X, Wang P. The in vivo degradation, absorption and excretion of PCL-based implant. Biomaterials 2006;27(9):1735-1740.

(204) Lam CX, Teoh SH, Hutmacher DW. Comparison of the degradation of polycaprolactone and polycaprolactone–(β-tricalcium phosphate) scaffolds in alkaline medium. Polym Int 2007;56(6):718-728.

(205) Wang Z, Wang Y, Ito Y, Zhang P, Chen X. A comparative study on the in vivo degradation of poly(L-lactide) based composite implants for bone fracture fixation. Sci Rep 2016 Feb 9;6:20770.

(206) Zollino I, Carinci F. The use of poly-L-lactic acid filler in facial volume restoration: A review.

(207) Gentile P, Chiono V, Carmagnola I, Hatton PV. An overview of poly (lactic-co-glycolic) acid (PLGA)-based biomaterials for bone tissue engineering. International journal of molecular sciences 2014;15(3):3640-3659.

(208) Makadia HK, Siegel SJ. Poly lactic-co-glycolic acid (PLGA) as biodegradable controlled drug delivery carrier. Polymers 2011;3(3):1377-1397.

(209) Wang N, Burugapalli K, Song W, Halls J, Moussy F, Zheng Y, et al. Tailored fibro-porous structure of electrospun polyurethane membranes, their size-dependent properties and trans-membrane glucose diffusion. J Membr Sci 2013;427:207-217.

(210) Erencia M, Cano F, Tornero JA, Fernandes MM, Tzanov T, Macanás J, et al. Electrospinning of gelatin fibers using solutions with low acetic acid concentration: Effect of solvent composition on both diameter of electrospun fibers and cytotoxicity. J Appl Polym Sci 2015;132(25).

(211) Sun T, Norton D, Ryan A, MacNeil S, Haycock J. Investigation of fibroblast and keratinocyte cell-scaffold interactions using a novel 3D cell culture system. J Mater Sci Mater Med 2007;18(2):321-328.

(212) Lowery JL, Datta N, Rutledge GC. Effect of fiber diameter, pore size and seeding method on growth of human dermal fibroblasts in electrospun poly (ε-caprolactone) fibrous mats. Biomaterials 2010;31(3):491-504.

(213) Kumbar S, James R, Nukavarapu S, Laurencin C. Electrospun nanofiber scaffolds: engineering soft tissues. Biomedical Materials 2008;3(3):034002.

(214) Wanasekara N, Chen M, Chalivendra V, Bhowmick S. Investigation of the Young's Modulus of Fibers in an Electrospun PCL Scaffold Using AFM and its Correlation to cell Attachment. MEMS and Nanotechnology, Volume 2: Springer; 2011. p. 157-162.

(215) Doyle AD, Carvajal N, Jin A, Matsumoto K, Yamada KM. Local 3D matrix microenvironment regulates cell migration through spatiotemporal dynamics of contractility-dependent adhesions. Nature communications 2015;6.

(216) Dynamic tensile properties of human skin. IRCOBI Conference 2012, 12-14 September 2012, Dublin (Ireland): International Research Council on the Biomechanics of Injury; 2012.

(217) Tseng L, Mather PT, Henderson JH. Shape-memory-actuated change in scaffold fiber alignment directs stem cell morphology. Acta biomaterialia 2013;9(11):8790-8801.

(218) Ru C, Wang F, Pang M, Sun L, Chen R, Sun Y. Suspended, Shrinkage-Free, Electrospun PLGA Nanofibrous Scaffold for Skin Tissue Engineering. ACS applied materials & interfaces 2015;7(20):10872-10877.

(219) Davidenko N, Schuster CF, Bax DV, Farndale RW, Hamaia S, Best SM, et al. Evaluation of cell binding to collagen and gelatin: a study of the effect of 2D and 3D architecture and surface chemistry. J Mater Sci Mater Med 2016;27(10):148.

(220) Hirt-Burri N, Ramelet A, Raffoul W, de Buys Roessingh A, Scaletta C, Pioletti D, et al. Biologicals and fetal cell therapy for wound and scar management. ISRN dermatology 2011;2011.

(221) Park J, Hwang S, Yoon I. Advanced growth factor delivery systems in wound management and skin regeneration. Molecules 2017;22(8):1259.

(222) Hakimi N, Cheng R, Leng L, Sotoudehfar M, Ba PQ, Bakhtyar N, et al. Handheld skin printer: in situ formation of planar biomaterials and tissues. Lab on a Chip 2018;18(10):1440-1451.

(223) Haik J, Kornhaber R, Blal B, Harats M. The feasibility of a handheld electrospinning device for the application of nanofibrous wound dressings. Advances in wound care 2017;6(5):166-174.

(224) Myers SR, Partha VN, Soranzo C, Price RD, Navsaria HA. Hyalomatrix: a temporary epidermal barrier, hyaluronan delivery, and neodermis induction system for keratinocyte stem cell therapy. Tissue Eng 2007;13(11):2733-2741.